MAGMATIC VOLATILES:
A melt inclusion study of Taupo Volcanic Zone rhyolites, New Zealand

Florence Bégué

A thesis submitted in partial fulfilment of the requirements for the degree of

DOCTOR OF PHILOSOPHY

in the

Department of Geological Sciences of the

UNIVERSITY OF CANTERBURY

March, 2014

Abstract

The central segment of the Taupo Volcanic Zone (TVZ) is one of the world's most productive areas of silicic volcanism and geothermal activity. Rhyolites largely predominate the eruptive output in the central TVZ, with only minor basalts, andesites and dacites. The rhyolites show diversity in composition, and form a compositional continuum between two end-member types (R1 and R2), as suggested in previous studies. In this thesis I present results from a quartz- (and rare plagioclase-) hosted melt inclusions study, focussing on the volatile concentration (i.e. H_2O, Cl, F, CO_2) and their relative distribution between R1 and R2 rhyolites. The main objective is to add further constraints on the magmatic systems with regard to their contribution to the hydrothermal systems in the central TVZ.

A comparative study between R1 and R2 melt inclusions show distinct volatile, fluid-mobile, and highly incompatible element compositions. Differences in the bulk volatile concentration of the parental magmas (i.e. basalts intruding the lower crust) are suggested to be at the origin of these volatile disparities. Further analysis on the volatile exsolution of R1 and R2 melts lead to the observation that the two rhyolite types exsolve a volatile phase at different stages in their magmatic history. From Cl and H_2O concentrations, it is suggested that R1 magmas exsolve a vapour phase first, whereas R2 rhyolites more likely exsolve a hydrosaline fluid phase. These results have considerable implications for the magmatic contribution into the hydrothermal systems in the central TVZ, as differences in the composition of the resulting volatile phase may be expected.

The hydrothermal systems in the central TVZ are subdivided into two groups based on their gas and fluid chemistry; and the current model suggests that there are two distinct contributions: a typical 'arc' system, with geochemical affinity with andesitic fluids, located along the eastern margin of the TVZ, and a typical 'rift' system, with geochemical affinity with rhyolitic/basaltic

fluids, located along the central and/or western region of the TVZ. The addition of the new data on the rhyolitic melt inclusions, leads to a re-evaluation of the magmatic contribution into the hydrothermal systems, with a particular focus on B and Cl. The results indicate a more diverse variety of contributions to the meteoric water in the hydrothermal systems, and also show that the east-west distribution of 'arc' and 'rift' fluids is not a viable model for the central TVZ. This work emphasises that melt inclusion data and their volatile degassing history cannot be underestimated when characterising and quantifying the magmatic component in hydrothermal fluids.

The melt inclusion data also provide further insight into the pre-eruptive magmatic plumbing systems and are particularly important from a hazard perspective. Included in the thesis is a detailed petrological analysis of rhyolite melt inclusions across the central TVZ and an interpretation that large silicic magma systems (in the TVZ) are typically comprised of multiple batches of magma emplaced at some of the shallowest depths on Earth. Tectonic activity is suggested to play an important role in triggering large caldera-forming eruptions as the evacuation of one magma batch could cause a regional-scale readjustment that is sufficient enough to trigger and allow simultaneous eruption of an adjacent melt batch.

Acknowledgements

A huge thank you…

- Dr. Darren Gravley, Dr. Ben Kennedy, Dr. Chad Deering, and Dr. Isabelle Chambefort for being such a great supervisory team. Thank you for all the time you invested and the knowledge you shared with me!
- Darren for taking me on board on the Source to Surface project, for the trust you had in me and for being so supportive and open to the different things I wanted to explore during this PhD;
- Chad for your guidance, for challenging me to think more critically, for the numerous skype sessions which always left me very motivated to get the work done. I also appreciated you being so fast with returning feedback;
- Ben for your 'outside the box' thinking and your enthusiasm, which is contagious, and also for giving me the opportunity to do some teaching;
- Isabelle for always bringing a different perspective into the research. I really enjoyed the stimulating discussions around your whiteboard;
- Prof. Jim Cole for always having the door open for discussion, great advice and support during these 3 years!
- The great researchers helping me out with analytical work, and giving me the opportunity to work in such amazing labs; Dr. Scott Kuehner (University of Washington), Dr. Richard Hervig and Dr. Lynda Williams (Arizona State University), Dr. Frank Tepley (Oregon State University), Dr. Paul Wallace (University of Oregon), and Dr. Kerry Swanson and Mike Flaws (University of Canterbury). I would not have such a great dataset to present here without your help;
- The staff and lecturers at the department of Geological Sciences at the University of Canterbury. It was great to be a part of this department and being given the opportunity to be involved in demonstrating labs and field trips;
- Rob Spiers for sharing his knowledge on sample preparation and polishing; Sacha Baldwin-Cunningham, Cathy Higgins, and Chris Grimshaw for helping me out with field supplies and microscopes; Kerry Swanson for the help at the SEM; Pat Roberts, John Southward and Janet Warburton for all your help making this thesis run smoothly;
- Dr. Olivier Bachmann for the contribution to my research through stimulating discussions;
- Dr. Guilherme Gualda for the valued discussions and the opportunity to work on the rhyolite-MELTS manuscript together;

- Dr. Mark Ghiorso for your help with Rhyolite-MELTS and with the processing of all the data;
- Ayla Pamukcu (soon to be Dr.) for the additional analyses on the Oruanui glass and great discussion (scientific and non-scientific);
- Dr. Nick Mortimer from GNS for kindly giving some greywacke powders;
- Timberlands Limited and Hancock Forest Management for granting access to the Kaingaroa and Kinleith forests;
- Staff at GNS Wairakei for letting me work there on a few occasions, and helping me out with the microthermometry;
- Keith Gordon and Geoffrey Smith from Otago University for running some tests on my samples with the Raman spectroscopy;
- Dr. Samuele Agostini for advice on the boron isotopes;
- Jonathan, Ayla, Darren, Chad and Guil for being the best at pumice sampling;
- Sarah, Chad and Heather, and Isa and Jamil for your hospitality during my stays in Seattle and Taupo;
- Paul and Jonathan for being such awesome office mates and friends; it was great to have you guys around, especially during the last few months of thesis writing craziness!
- All the postgraduate students I had the pleasure demonstrating, having a beer, and/or a chat with in the hallway of the 4th floor. Thanks Hamish, Sarah, Carolyn, Alison, Latasha, James, Nick, Narges, Tom, Matt …
- Eva, Jackie, Kris, Felix, Paul A., Paul S., Jonathan, Marie-Claude, Johnny, Theo, Penelopi, Lauriane, Louise, Josh, Greer, Bruce for all the fun nights and week-ends, the great hikes, climbing etc…hope there will be many more in NZ or elsewhere!
- My family for being so wonderful and supportive of my decisions, even if it means to be so far apart;
- Seba for so many different reasons…in particular for always encouraging me to take on new challenges! I wouldn't be here if it wasn't for you…

Finally, none of this could have been possible without funding! I am very grateful to Mighty River Power Company Ltd. for establishing the Source to Surface geothermal research programme with the University of Canterbury and the aid of a University of Canterbury doctoral scholarship. I also received additional funding from the Mason Trust Fund to go overseas for a conference and lab work, and additional financial support from the Luxembourg's Minster of Higher Education and Research through CEDIES, for which I am also thankful.

List of Publications

The main chapters in this thesis (Chapter 2 to 5) are written in publication format. Here is an overview of the manuscripts that have been submitted as peer-reviewed articles or are currently under preparation. All of these are based on the work I did during my doctoral degree. I am the lead author on all these papers, and I contributed to (1) field and laboratory work, (2) results analysis and discussion, and (3) writing of the manuscripts, in all cases. Details on the co-author's contribution on these publications are listed on the co-authorship forms in Appendix A.

- Bégué, F., Deering, C. D., Gravley, D. M., Kennedy, B. M., Chambefort, I., Gualda, G. A. R. & Bachmann, O. (in press): Extraction, storage and eruption of multiple isolated magma batches in the paired Mamaku and Ohakuri eruption, Taupo Volcanic Zone, New Zealand. Journal of Petrology. **(Chapter 2)**
- Bégué, F., Gravley, D.M., Chambefort, I., Deering, C.D & Kennedy, B.M (in press): Magmatic volatile distribution in rhyolites as recorded by melt inclusions in the Taupo Volcanic Zone, New Zealand. In: The Role of Volatiles in the Genesis, Evolution and Eruption of Arc Magmas, Special Publication, Geological Society of London. **(Chapter 3)**
- Bégué, F., Gualda, G. A. R., Ghiorso, M. S., Pamukcu, A. S., Kennedy, B. M., Gravley, D. M., Deering, C. D. & Chambefort, I. (in review): Phase-equilibrium geobarometers for silicic rocks based on rhyolite-MELTS. Part 2: Application to Taupo Volcanic Zone rhyolites. Contributions to Mineralogy and Petrology. **(Chapter 4)**
- Bégué, F., Chambefort, I., Deering, C.D., Gravley, D.M. & Kennedy, B.M. (in prep.): Magmatic degassing and link with hydrothermal systems: Taupo Volcanic Zone, New Zealand **(Chapter 5)**

The following proceedings paper has been included as an appendix to this thesis. It will eventually be submitted as a peer-reviewed publication once I have all the results.

- Bégué, F., Deering, C., Gravley, D., Kennedy, B. & Chambefort, I. (2012): Volatile transfer from magma sources in the Taupo Volcanic Zone: A quartz-hosted melt inclusion study in rhyolites. New Zealand Geothermal Workshop 2012 Proceedings **(Appendix E).**

Table of Contents

List of Figures

List of Tables

Chapter 1

Introduction

Geothermal energy is a primary energy resource for New Zealand, and accounts for ~14% of the electricity production (in 2012; source: Ministry of Economic Development). The majority of this energy is sourced from the Taupo Volcanic Zone (TVZ), which has an extraordinary heat flux (4200±500 MW e.g. Bibby et al. 1995; Hochstein et al., 1995). The central segment of the TVZ hosts 23 hydrothermal fields regularly distributed; 6 of which are production fields that are currently generating electriciy (~750 MWe total; source: New Zealand Geothermal Association). It is generally accepted that large scale fluid convective systems in the upper crust, dominated by meteoric water, are driven by an underlying magmatic heat source (e.g. Bibby et al., 1995; Hochstein, 1995); in several geothermal fields a magmatic geochemical signature has also been identified (e.g. Giggenbach 1995; Christenson 2002). A variety of secondary processes, amongst them boiling, dilution, mixing and/or fluid-rock interaction, occur in hydrothermal systems and make it very difficult to recover the original composition of the magmatic source. The central TVZ is not only known for its spectacular geothermal manifestation, but is also one of the world's most productive region for silicic volcanism during the past ~2 Ma.

The main objective in this thesis is to better understand the magmatic source of these hydrothermal systems, and attempt to characterise this magmatic contribution. With this aim in mind, I will present here a melt inclusion study of the central TVZ that focuses on magmatic volatile compositions in an attempt to address some key and poorly understood aspects with respect to the rhyolitic magmatism.

1.1. Taupo Volcanic Zone

1.1.1. Tectonic setting and crustal structure

The TVZ has evolved over the past ~2Ma and during that time it has proved to be one of the world's most silicically active volcanic regions (Houghton et al., 1995; Wilson, 2006). This is thought to be a consequence of its very unique tectonic setting whereby the volcanic arc, related to the northwest-directed subduction of the Pacific Plate (including the 17km thick Hikurangi Plateau) beneath the North Island, is being rifted apart. The rifted TVZ arc can be subdivided into three segments (Fig. 1.1), with andesitic cone volcanoes, typical of continental arcs, dominating the northern and the southern segments, and explosive caldera-forming eruptions and effusive domes of rhyolitic composition dominating the 125 x 60 km central segment (Wilson et al., 1995; 2009). More than 6,000 km^3 of rhyolitic magma has erupted over a period of ~2 Ma, with minor dacites, andesites and basalts (Fig. 1.1; e.g. Wilson et al. 1995; 2009). A close relationship between rifting and accumulation and evacuation of these large rhyolitic magma bodies has been inferred (e.g. Rowland et al. 2010). Many studies show that the regional extensional regime partly controls caldera structures and geometry (e.g. Cole et al. 2010; Seebeck et al. 2010; Spinks et al. 2005), and it may also play an important role in magma migration in the upper crust and eruptive processes (Gravley et al. 2007; Allan et al. 2012).

1.1.2. Magmatism and volcanism

Current models on the petrogenesis of rhyolitic melts invoke a two-stage process with, in the first place, intrusions of basalt into the lower crust. The resulting melt from assimilation and fractional crystallisation (AFC processes) is extracted into an intermediate mush zone in the mid- to upper-crust (e.g. Jackson et al., 2003; Annen and Sparks, 2002; Annen et al., 2006). Within this crystal-rich intermediate mush zone, rhyolitic melts are suggested to be generated by equilibrium crystallization and batch extraction (e.g. Bachamnn & Bergantz, 2004).

Similar models have been used to explain the voluminous rhyolite production in the TVZ from a parental mafic magma (e.g. McCulloch et al., 1994; Graham et al., 1995; Price et al., 2005; Deering et al., 2011-a). A strong presence of mantle component in the silicic magmas has been suggested, with only minor assimilation (<25 %) in the lower crustal region (e.g. McCulloch et al., 1994; Deering et al., 2008). A recent study on the bulk-rock geochemistry of the rare basalts that made it to the surface in the central TVZ has provided a potential link between the variability seen in the rhyolites and distinct mafic parents (Rooney & Deering, 2014). Ewart et al. (1975) first suggested this variability in the central TVZ rhyolites. With detailed petrological and petrographical studies along with better geochronological constraints, Deering et al. (2008: 2010) suggested a compositional range between two end-member rhyolite compositions: R1 and R2. These types can be distinguished based on their mineral assemblage, with hydrous mineral phases (hornblende ± cummingtonite ± biotite) only present in R1 rhyolites, their crystal content and bulk-rock trace-element composition. These differences are suggested to reflect changes in the initial conditions in the lower crust (fO_2 and fH_2O), dictated by slab-derived fluids from the subduction zone (Deering et al. 2010). This interpretation has been reinforced through the link with the basalt composition, which also suggests different sources for the primitive melt generation, with variable contribution from the subducting slab (Rooney & Deering, 2014).

The eruptive deposits that have been studied in this thesis are listed in Table 1.1; further background information on specific volcanic centres are given in each chapter.

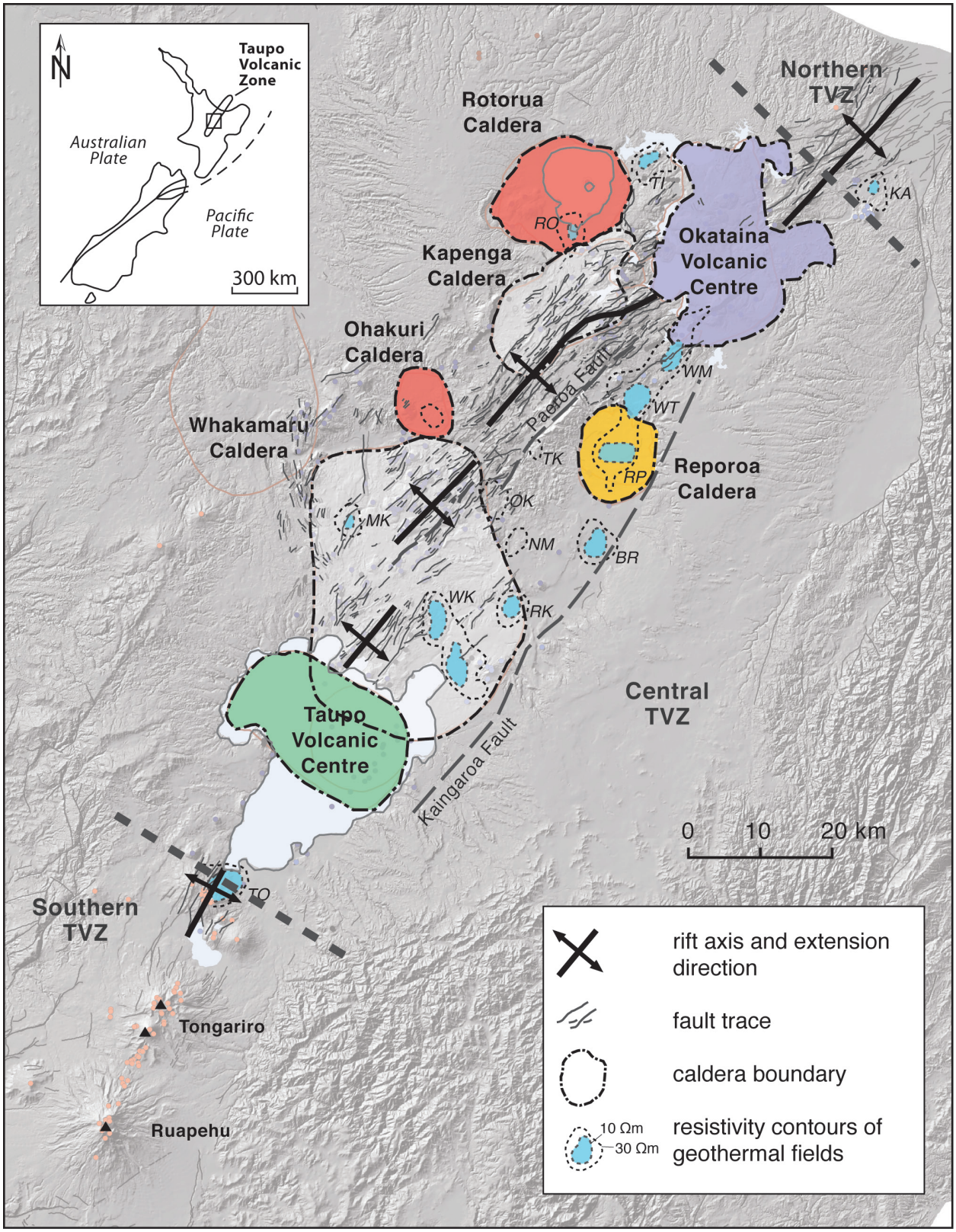

Figure 1.1: Map of the TVZ, New Zealand. Caldera boundaries and structures after Rowland et al., (2010), resistivity contours and geothermal fields after Bibby et al., (1995). Abbreviations geothermal fields: TO-Tokaanu, WK-Wairakei, RK-Rotokawa, MK-Mokai, NM-Ngatamariki, BR-Broadlands Ohaaki, OK-Orakei Korako, RP-Reporoa, TK-Te Kopia, WT-Waiotapu, WM-Waimangu, RO-Rotorua, TI-Tikitere, KA-Kawerau.

Table 1.1: Summary of ignimbrites from the central TVZ, analysed in this study.

Source Caldera		Eruption Name	Age (ka)	Volume (km3)	Mineral Assemblage	Crystallinity (%)	Rhyolite type	No of analyzed pumice clasts	
Taupo	**TVC**	Taupo	~ 1.8	35	plg + opx ± qtz	< 5	R2	5	*Chapt. 3, 4 and 5*
		Oruanui	~ 26.5	~ 530	qtz + plg + hbl+ opx	< 5	R1 + R2	5	*Chapt. 3, 4 and 5*
Reporoa	-	Kaingaroa	230 ± 10	>100	plg + opx	~ 5	R2	9	*Chapt. 3*
Ohakuri	**RoOhVC**	Ohakuri	240 ± 10	> 100	qtz + plg + opx	< 10	R2	14	*Chapt. 2, 3, 4 and 5*
Rotorua		Mamaku	240 ± 10	> 145	qtz + plg + opx ± hbl	< 10	R2	9	*Chapt. 2, 3, 4 and 5*
Okataina	**OVC**	Kaharoa	0.7 ± 0.012	~ 5	qtz + plg + bt ± hbl ± cum	~ 10	R1	6	*Chapt. 3, 4 and 5*
		Rotoiti	~ 61	~ 100	qtz + plg + cum + hbl + opx ± bt	< 30	R1	5	*Chapt. 3, 4 and 5*
		Matahina	322 ± 7	> 160	qtz + plg + opx ± bt ± hbl	< 15	R1 + R2	6	*Chapt. 3, 4 and 5*

bt-biotite; cum-cumingtonite; hbl-hornblende; opx-orthopyroxene; plg-plagioclase; qtz-quartz; san-sanidine Compilation from the following sources: Beresford (1997), Cole at al. (2010), Deering et al. (2008; 2010), Gravley (2004), Gravley et al. (2007), Leonard et al., 2010; Milner et al. (2003), Nairn et al. (2004), Schmitz & Smith (2004), Smith et al. (2005), Sutton et al. (1995), Wilson et al. (2006, 2009).

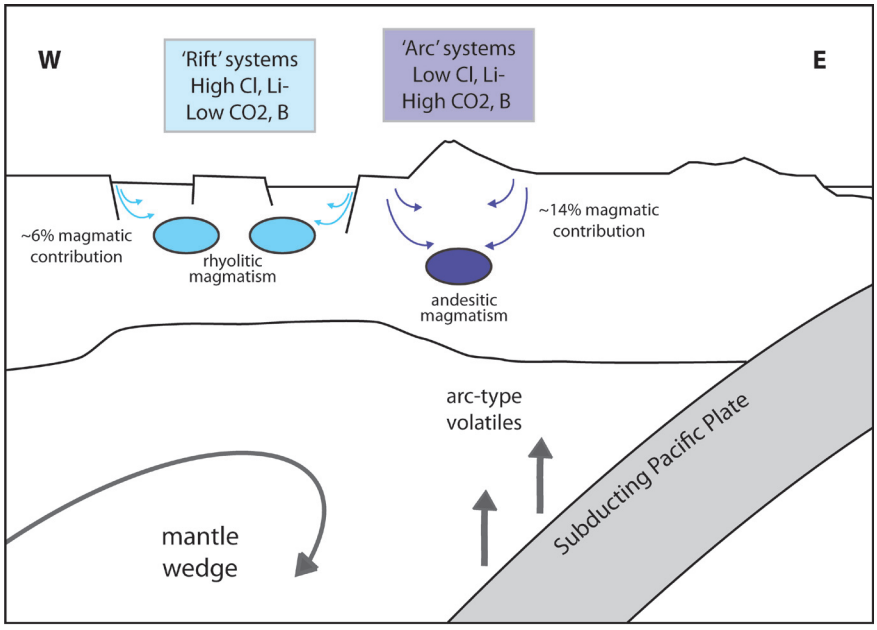

Figure 1.2: Schematic representation of the current model of the hydrothermal fluid distribution in the central TVZ (modified after Giggenbach, 1995; Bernal et al., 2014). Arc vs. back-arc (or 'rift') distribution is suggested to be related to andesitic and rhyolitic magmatic systems.

1.1.3. Geothermal systems and deep reservoir fluids

The central TVZ has a natural heat output of 4200±500 MW (estimated using the principle of chloride ion conservation; Bibby et al. 1995), with 23 geothermal fields and two extinct ones that are regularly distributed with an average spacing of 10-15 km, but the heat flux seems nevertheless more concentrated along the eastern margin. No variation in their position has been recorded for at least the past 200 ka, even major volcanic eruptions have not significantly perturbed them (e.g. Bibby et al. 1995). Thus, a large-scale convective system with very stable deep plumes is the generally accepted model for geothermal reservoirs in the central TVZ (Bibby et al. 1995; Heise et al. 2007). The depth reached by the convective cell of the geothermal systems is unknown, but the circulation of fluids below the brittle-ductile transition is not likely (~ 6-7 km; e.g. Bibby et al. 1995; Heise et al., 2007).

There is general agreement that magmatic bodies beneath a large part of the TVZ are responsible for the stable convective geothermal activity. Reyners et al. (2006) suggested that the anomalous subduction zone geometry to explain the extraordinarily high heat flow and the massive generation of rhyolitic magma. They suggested that the subduction of the Hikurangi Plateau, which is twice as thick as a normal oceanic crust (17 km), causes more dehydration and releasing of water into the mantle wedge. From this, a larger amount of mantle melting and basalt, and therefore heat, generation occurs.

Surface springs, fumaroles and geothermal well fluid compositions in the central TVZ have been the topic of many studies (e.g. Giggenbach, 1995). The hydrothermal systems are in general very diluted by meteoric water (~90 %); from the stable isotope signatures of these hydrothermal fluids, a contribution of magmatic fluids between 6 and 14 ± 4 % has been suggested (e.g. Giggenbach 1995). Giggenbach (1995) studied discharge water of six different fields in the central TVZ that led to a distinction of two types of deep supply fluids: (1) a high gas and CO_2 content, and high B/Cl, Li/Cs, CO_2/He and N_2/Ar ratios, suggested to have geochemical affinities similar to andesitic

magmatism; this fluid is mostly present in the geothermal systems along the eastern boundary of the TVZ, and (2) a low gas and CO_2 content, but high Cl, with compositional affinities more likely corresponding to leaching or degassing of rhyolitic material; this second fluid type being fairly widespread across the arc, away from the eastern boundary (Fig. 1.2). Similar conclusions have been drawn form other big picture fluid distribution studies of the reservoir fluids, with the recent study of Bernal et al. (2014), based on fluid composition and isotopic signature (i.e. $\delta^{7}Li$, $\delta^{37}Cl$, $\delta^{18}O$ and δD).

1.2. Magmatic volatiles

1.2.1. Degassing

Volatiles are omnipresent in subduction zones, and play an important role in the generation and behaviour of magmas at depth and the style of volcanic eruptions, and they are integral to the development of magmatic-derived hydrothermal systems. Volatile studies are, therefore, essential in identifying volcanic and geologic processes. In arc volcanic systems, the major volatile species are H, C, S and Cl (e.g. Symonds et al., 1994; Giggenbach, 1996; Fischer, 2008). These volatile species largely originate from the mantle wedge, the subducted altered oceanic crust and its overlying sediments, with some small contribution from the continental crust (e.g. Wallace, 2005; Hilton et al., 2002; Bindeman et al., 2004; Zelenski & Taran, 2011; Chambefort et al., 2013-a). Subduction zone processes are essential in the recycling of aqueous fluids (and fluid-mobile elements) from the surface environment, producing a distinct arc signature associated with this tectonic setting (e.g. Kay, 1980; Hawkesworth & Ellam, 1989; McCulloch & Gamble, 1991).

Several authors have attempted to quantify the degassing and volatile flux at arc volcanoes worldwide (e.g. Wallace & Gerlach, 1994; Wallace et al., 1995; Johnson et al., 2010; Zelenski & Taran, 2011; Wallace, 2005) either through monitoring of gas flux at the surface (e.g. Taran et al., 1991; Giggenbach, 1996; Aiuppa et al., 2002; Edmonds et al., 2009; Zelenski & Taran, 2011) or

by assessing volatile concentrations in mineral-hosted melt inclusions and volcanic glass from eruptive deposits (e.g. Anderson et al., 1989; Wallace & Gerlach, 1994; Wallace et al., 1995; Métrich & Wallace, 2008; Johnson et al., 2010; 2011; Reubi et al., 2013). There are different approaches to determine the volatile fluxes; one is based on actual surface flux measurements on and near primary volcanic vents. Some workers also use ratios of CO_2 with noble gas isotopes (Hilton et al. 2002; Fischer & Marty 2005). Problems with this method are that some diffusive degassing or degassing along fractures may occur away from the main vent and won't be taken into account in the global balance, or near-surface secondary processes like boiling, mixing or fluid-rock interaction could mask the original magmatic composition of the fluid. In general it is, therefore, very difficult to measure the total discharge compositions (Fischer & Marty 2005; Johnson et al. 2011).

Another approach is to determine the flux by combining melt inclusion data with vapour-melt partitioning models of the major volatile species (e.g. London et al., 1988; Webster et al., 1989; Shinohara, 1994; Schatz et al., 2004), or using coexisting fluid inclusions if these are present (e.g. Zajacz et al., 2008). This allows the composition of the exsolved volatile phase to be estimated. In comparison to surface measurements, this approach may enable identification of secondary processes altering the primary magmatic fluids, like unmixing or fluid-rock interactions (e.g. Johnson et al. 2010). However, there are large uncertainties related to the volatile measurements, which may represent already partially degassed melts prior to melt inclusion entrapment, which means assumptions have to be made to estimate the degassing and flux. This is particularly relevant for CO_2, which, because of its low solubility (Lowenstern, 2001), is likely to partition into a vapour phase prior to magmatic crystallization. Some authors have applied a combination of these two approaches (e.g. Wardell et al. 2001; Edmonds et al. 2003) to constrain the degassing behaviour especially of SO_2 and the eruption pattern of active volcanoes. Degassing of magmatic systems has also largely been investigated in the context of porphyry and epithermal deposits, as

the metal partitioning in these exsolved volatile phases likely plays a role in the genesis of ore deposits (e.g. Hedenquist & Lowenstern, 1994; Lowenstern, 1994; Dilles et al., 2000; Sillitoe & Hedenquist, 2003, Heinrich et al., 2004; Simmons et al., 2005; Williams-Jones & Heinrich, 2005; Chambefort et al., 2008, 2013-a; Tosdal et al., 2009).

The heat and mass transfer to hydrothermal systems and hydrothermal alteration will also be highly dependent on volatile release, which drive hydrothermal convection cells around magmatic systems (e.g. Lindgren, 1907; Elder, 1966; Norton & Knight, 1977). For decades, studies have focused on volatile exsolution during crystallisation prior to ascent and eruption of magma, and showed that evolved melts in most cases already reached volatile saturation while at low crystallinity before ascent and eruption (e.g. Anderson et al., 1989; Lowenstern et al., 1991; Lowenstern, 1993, 1994; Wallace & Gerlach, 1994; Wallace et al., 1995; Johnson et al., 2011). As such, volatile exsolution can play a significant role at different evolutionary stages within a given magmatic system.

Degassing of volatiles is complex because of large variations of solubilities and vapour-melt partitioning coefficients; therefore, more data are required on magmatic volatiles and their partitioning during magma storage, crystallization and degassing. However, it constitutes a good starting point to understand the heat and mass transfer to overlying geothermal systems.

1.2.2. Methodology

For this thesis, I will focus on examining volatiles dissolved in the melt prior to eruption, by analysing the composition of mostly quartz-hosted (rare plagioclase-hosted) melt inclusions in rhyolites (Fig. 1.3). The eruptive deposits have been chosen based on their: (1) composition (R1 and R2 rhyolites), (2) age (~320 to 0.7 ka), (3) melt inclusion appearance, and (4) location of the related volcanic centre. The aim is to cover a wide range of distinct eruptive deposits, to fully explore large-scale differences in the magmatic systems. Only unaltered pumice clasts from pyroclastic flows and fall deposits are used for this research; a summary of the main characteristics of the rhyolitic eruptive deposits used for this thesis are detailed in table 1.1.

In comparison to volcanic glass (e.g. pumice matrix, obsidian), melt inclusions have the advantage that they are less affected by degassing during eruptive processes or secondary alteration. The mineral-host entrapping the little pocket of melt can potentially shield the inclusion from decompression and other post-entrapment changes (e.g. Schiano & Bourdon 1999) preserving the original composition of the melt and fluid at the time of crystallization. However, experimental studies show that inclusion glass may also be affected by post-entrapment alteration, for instance through dissolution and re-precipitation on melt inclusion walls or diffusion of material through cracks within crystals (e.g. Bucholz et al. 2013; Gaetani et al. 2000; Severs et al. 2007; Steele-McInnis et al. 2011; Zajacz et al. 2009). Thus a methodical and careful approach is necessary in the choice of melt inclusions that will be used for analysis. For this research, only 100% glassy, and fully enclosed (i.e. no hourglass inclusions or re-entrants) have been used (Fig. 1.3). Melt inclusions were also correlated to the growth history of their host mineral using cathodoluminescence imaging (Fig. 1.4). To obtain the chemical composition of individual melt inclusions, advanced micro-analytical techniques (e.g. Electron microprobe; Secondary ion mass spectrometry, Fourier transform infrared spectroscopy) have been used. Detailed sample preparation, analytical conditions and analytical errors are given in chapter 2 and 3. Pressure estimates of the analysed eruptive

deposits have been obtained with the rhyolite-MELTS geobarometer, which is a new method developed by Gualda & Ghiorso (revised). Further information on this method is given in chapter 4.

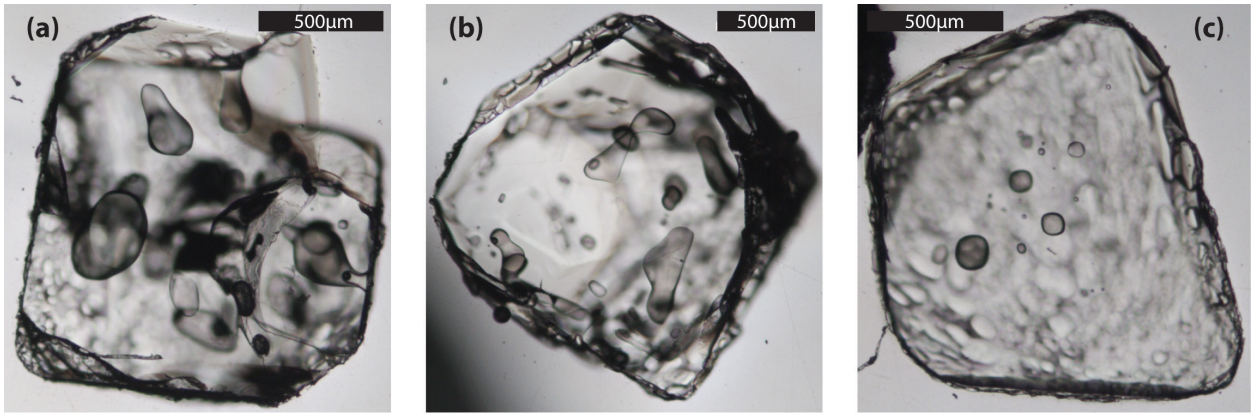

Figure 1.3: Photomicrograph of quartz crystals extracted from rhyolites from the central TVZ, with melt inclusions. Multiple glassy melt inclusions in each quartz crystal (a-c). Hourglass inclusions and re-entrants in (a) and (b), some with small vapour bubbles. These melt inclusions have not been analysed in this study.

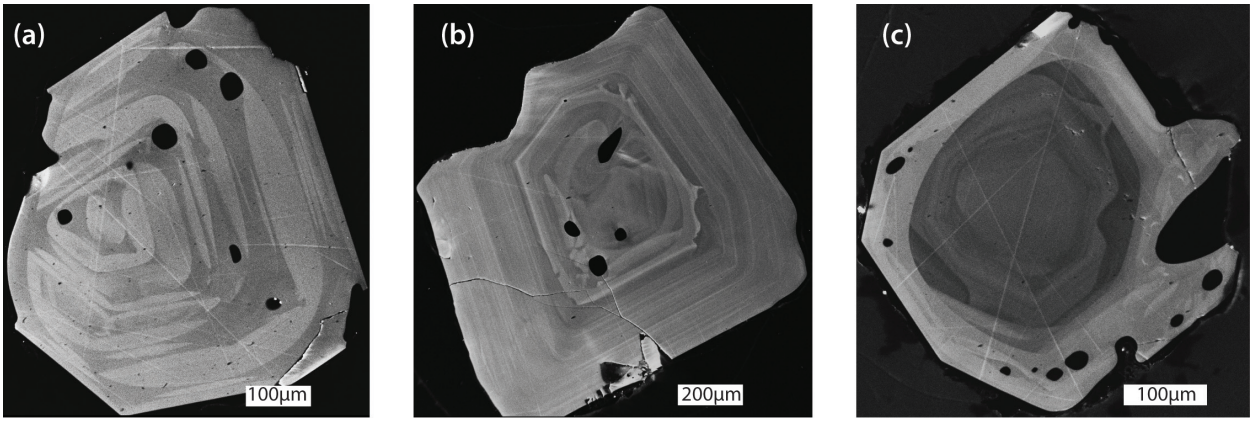

Figure 1.4: Cathodoluminescence (CL) imaging of quartz crystals. Melt inclusions don't have a CL signal and represent the black blobs in the crystals; (a) oscillatory and skeletal CL zoning; (b) and (c) distinct core zone showing one partial dissolution event; (c) bright CL rim indicating a change in composition (and temperature) of the magma.

1.3. Research objectives

The main goal of this thesis is to gain knowledge on the magmatic volatile composition to examine their degassing history and their contribution to the TVZ hydrothermal systems. In order to better understand the role of volatile exsolution in magmatic-hydrothermal systems, questions and/or uncertainties associated with the composition and concentrations of the magmatic fluid phase need to be resolved. These key and poorly understood aspects have to be addressed first, before the link between magmatic and hydrothermal systems can be accurately assessed. This thesis presents an analysis on the magmatic volatile and major, and trace element composition distribution in rhyolitic eruptive deposits, dated between ~320 ka to 0.7 ka, from five different volcanic centres (Fig. 1.1; Table1.1).

- **Composition of the magmatic systems – focus on R2 rhyolites:**

  Numerous studies on melt inclusions and volatiles address the R1 rhyolite type, with the Okataina Volcanic Centre (OVC) and the Taupo Volcanic Centre (TVC; Fig. 1.1; Table 1.1; e.g. Liu et al., 2006; Shane et al., 2007; Smith et al., 2010; Johnson et al., 2011), mainly because they represent the two main active eruptive loci of the modern TVZ (61 ka to present). However, in order to do a comparative study of the different rhyolites, it is essential to collect more data on the R2 rhyolite type. Here, we focus on the Rotorua and Ohakuri Volcanic Centres (RoOhVC) located along the western boundary of the TVZ (Fig. 1.1), which both evacuated R2 rhyolites during a multi-ignimbrite-forming eruption (after Deering et al., 2008). Furthermore a detailed understanding of the pre-eruptive conditions of the Rotorua and Ohakuri magmas provides a unique view into the inter-relationship between regional tectonics, magmatism and eruptive processes associated with a complex eruption sequence involving the coincidental collapse of two calderas (Gravley et al., 2007; Chapter 2).

- **Comparative study of volatile concentration among the TVZ rhyolites:**

  Volatile concentrations (i.e. H_2O, Cl, F, CO_2, S) from a representative range of rhyolites are compared in order to identify a spatial variability across the central TVZ. Some research questions that I attempt to address are: can we assume that most evolved magmatic systems in the same tectonic environment will have similar volatile concentrations and saturation? Do these magmas exsolve similar volatile compositions? What is the origin of the variability in volatile concentration?

- **Comparative study of the reservoir depth for silicic magmas across the central TVZ:**

  Many studies have focussed on determining the residence depth of evolved silicic magma bodies in the upper crust for a specific eruption or eruptive centre using diverse geobarometers. However, to date there is no comparative study between R1 and R2 rhyolites in the TVZ. Here, a geobarometry study is conducted to address depth variations among the TVZ volcanic centres, and also among different magmatic systems within the same volcanic centre. Resolving the residence depth of the magmatic systems is essential in order to understand the exsolution of volatile phase(s) from these magmas, as depth (pressure) is a major control on the solubility of the volatiles.

With the gained knowledge from these studies, correlations between the magmatic and surface/well fluid compositions can be attempted. As described above, current models on the hydrothermal discharge fluids suggest that there is an East-West distribution of the hydrothermal systems characterised by either an ‘arc’ or a ‘rift’ signature (Giggenbach, 1995; Bernal et al., 2014). The objective here is to build on this model for hydrothermal fluid distribution in the TVZ with the volatile data from the rhyolites, and to address some of the many remaining questions on the contribution of the heat source:

- What is the composition of the magmatic source associated to the hydrothermal systems? Is the magmatic signature measured at geothermal systems related to the most recently erupted magma or a deeper magma with a different composition?
- Why do some hydrothermal systems along the eastern border of the TVZ have a 'rift' (or rhyolite) related signature and not (arc) as suggested by the current model?
- Why would the large amount of erupted rhyolite not leave a magmatic signature relative to the supposed andesites that do not make it to the surface along the eastern TVZ margin?

1.4. Thesis organisation

This thesis is written in manuscript format, with each of the central chapters (Chapter 2 to 5) corresponding to a manuscript that has either been submitted or is to be submitted.

- **Chapter 2** focuses on the Rotorua and Ohakuri volcanic centres (RoOhVC), located on the western boundary of the central TVZ (Fig. 1.1). The aim of this chapter is to gain further insight into the magmatic plumbing system of these eruptions that occurred simultaneously from two distinct caldera centres ~30 km apart. Trace and major element composition from quartz-hosted melt inclusions are used, and combined with bulk-rock and mineral compositions from previous studies (Milner et al., 2003; Gravley, 2007; Deering et al., 2008). Current models of rhyolite petrogenesis for the central TVZ are discussed, and the influence of regional tectonics on magma transport and eruptive processes is explored. This chapter has been submitted, reviewed, modified and re-submitted to Journal of Petrology.
- **Chapter 3** builds onto the conclusions of chapter 2, to further discuss differences in volatile concentrations and expands the discussion to the entire central TVZ. It addresses volatile concentrations of some of the main eruptive deposits in the central TVZ (Table 1.1), and provides a comparison in volatiles between R1 and R2 rhyolite melt inclusions. I discuss the origin of volatiles in the TVZ magmas and their solubilities in silicic magmatism. The

importance of volatile exsolution is examined and different approaches are used to establish the presence of a coexisting volatile phase prior to eruption. This Chapter represents an important milestone for further analyses of the magmatic volatiles and is an important contribution to later discussions on the link between the magmatic and hydrothermal systems in Chapter 5. This chapter has been accepted for publication in a Special Publication of the Geological Society of London, entitled: "The Role of Volatiles in the Genesis, Evolution and Eruption of Arc Magmas".

- **Chapter 4** is another comparative study of the TVZ rhyolitic systems, which addresses the residence depth of the silicic magma bodies. Differences among the eruptive centres, but also among the eruptions within the same volcanic centre, are discussed. Another purpose of this study is to discuss the utility of the rhyolite-MELTS geobarometer – a new method to estimate pressures developed by Gualda & Ghiorso (revised). This new geobarometer is compared to existing pressure estimates on TVZ rhyolites from the literature, obtained with different geobarometers. This study proves to be very important as the same geobaromater can be used for R1 and R2 rhyolites, and it is independent of volatile concentrations and saturation. This is particularly important because, from the results of Chapter 3, volatile saturation cannot be assumed in all TVZ rhyolites. This will be submitted to Contributions to Mineralogy and Petrology.
- **Chapter 5** explores ideas on the link between the magmatic and hydrothermal systems. The three previous chapters are used to set up the discussion in this final chapter, which aims to examine and answer some of the fundamental questions that originally lead to this research. The gained knowledge on the volatile distribution, composition and depth of the magmatic systems is used to build on the current model on the compositional distribution of the geothermal systems, originally proposed by Giggenbach (1995; Fig. 1.2).

- To further explore the link between the magmatic and hydrothermal systems, I analysed boron isotopes in rhyolitic melt inclusions. Boron isotopes may be a useful tracer of the magmatic input into the hydrothermal systems, and if coupled with the other trace elements and isotopes, they may provide further constraints on the contribution of slab-derived fluids in the magmatic systems. Preliminary results are presented in a short conference proceeding, presented at the 2012 New Zealand Geothermal Workshop (Appendix E).

Chapter 2

Extraction, storage and eruption of multiple isolated magma batches in the paired Mamaku and Ohakuri eruption, Taupo Volcanic Zone, New Zealand

2.1. Abstract

The Taupo Volcanic Zone (TVZ) is well known for its extraordinary rate of rhyolitic magma generation and caldera-forming eruptions. Less is known about how large volumes of rhyolitic magma are extracted and stored prior to eruption, and the role tectonics might be playing in the process of melt extraction and control of caldera eruption(s). Here we present a new model for the extraction, storage and simultaneous eruption of the >245 km^3 paired Mamaku and Ohakuri magmas sourced from calderas centred ~30 km apart (the Rotorua and Ohakuri calderas, respectively) in the central TVZ. The Mamaku and Ohakuri ignimbrites share a similar bulk pumice composition and the same phenocryst assemblage; however, bulk-rock compositions suggest several poorly mixed magma types in each erupted volume, which are randomly distributed throughout the eruptive deposits. In order to refine models of the pre-eruptive geometry of the magmatic system and discuss a possible origin for triggering of each eruption, we present an expanded database of matrix glass and quartz-hosted melt inclusion compositions along with the existing bulk-rock and mineral compositions. Major and trace element compositions show that the region produced five different magma batches, extracted from the same source region, and a continuous intermediate mush zone beneath the Mamaku-Ohakuri region is suggested here. These magma batches were most likely juxtaposed and isolated from each other in the upper crust and evolved separately until eruption. The observed geochemical differences in the batches are likely to be generated by different extraction conditions of the rhyolitic melt from a slightly heterogeneous mush. The lack of

evidence for more mafic recharge prior to eruption (for example there are no bright cathodoluminescence (CL) rims on quartz crystals), suggests that a magmatic input is unlikely to be an eruption trigger. However, tectonic activity could be an efficient way to trigger the eruption of isolated magma batches with the evacuation of one magma batch causing a disturbance to the local stress field and activating regionally linked faults, which then lead to the eruption of additional magma batches and associated caldera subsidence. In addition, the extensional tectonic regime coupled to a high heat flux could be the controlling factor in the emplacement of some of the shallowest and most SiO_2-rich magmas on Earth.

2.2. Introduction

Caldera-forming volcanic events commonly evacuate large volumes of silicic magma characterised by multiple pumice types with heterogeneous composition (e.g. Smith & Bailey, 1966, Lipman, 1967, Hildreth, 1981). How these different silicic magma types are generated, how they are stored, and what triggers their eruption are essential questions in understanding the magmatic processes associated with these large and potentially catastrophic events. The traditional model invoked to explain chemical heterogeneities within a large eruption is to have one large chemically layered magma chamber, which fractionates in-situ (e.g. Bacon & Druitt, 1988; Hildreth, 1981, Brown et al., 1998-a). However, an increasing number of studies suggest that an incrementally built reservoir, with the potential presence of discrete magma batches, may better explain these heterogeneities in certain systems, with in-situ differentiation still playing an important role (e.g. Cambray et al., 1995; Hildreth & Wilson, 2007; Lipman, 2007; Shane et al., 2007; Miller et al., 2011). These discrete batches may or may not interact prior to eruption, and may have unique magmatic histories (e.g. Reubi & Nicholls, 2005). In high-silica rhyolites, the differences between multiple magma batches can be challenging to detect because evidence based on mineral, glass and bulk chemistry is often subtle (e.g. Gualda & Ghiorso, 2013-b). The ‘mush model’ for

the petrogenesis of rhyolites involves interstitial melt extraction from upper crustal crystalline mush zones (e.g. Bachmann & Bergantz, 2004; Hildreth, 2004; Hildreth & Wilson, 2007), forming shallow cupolas of highly eruptible rhyolitic melt. Timescales related to crystal-melt segregation from a mush zone are important, and it is essential to distinguish between the time necessary to assemble and extract the rhyolitic melt from the mush (i.e. time to generate the melt and physically segregate it from the crystal mush), with the residence and crystallisation time of that segregated melt until eruption. Finally, another important, and still poorly understood aspect in terms of hazard assessment is the trigger(s) of these very explosive eruptions. The critical overpressure for eruption may not be reached by volatile exsolution alone, and an input of more mafic magma in the chamber has been suggested by many authors as another way to increase the internal pressure in the chamber, possibly leading to an eruption (e.g. Sparks et al., 1977; Blake, 1981; Pallister et al., 1992; Folch & Marti, 1998). A less frequently invoked model suggests tectonic eruption trigger (e.g. Gravley et al., 2007; Allan et al., 2012); however the relationship between regional tectonics and large ignimbrite eruptions is not well understood.

The central Taupo Volcanic Zone (TVZ) in New Zealand is a rifted-arc where rhyolitic volcanism has been linked to extensional tectonics (Wilson et al., 2009). During an ignimbrite flare-up (~340-240 ka; Gravley et al., 2009; D. Gravley et al., in preparation) seven distinct volcanic centres evacuated more than 3000 km^3 of high-silica rhyolites, and, although being generally quite homogeneous (Dunbar et al., 1989-a), small chemical heterogeneities have been identified in most of the produced ignimbrites. The high-resolution chronostratigraphy and spatial distribution of ignimbrites in the TVZ present an ideal opportunity to study the origin of these heterogeneities and further decipher the relationship between magma emplacement, tectonics and volcanism. Paired eruptions are not uncommon in the central TVZ, and the ~60 ka Rotoiti and Earthquake Flat event is one well-documented example (Charlier et al., 2003), where regional tectonics is implicated in back-to-back eruptions from two different vent sites, with a magma system composed of

independent and unconnected magma bodies (Charlier et al., 2003). Here we will focus on another paired eruption sequence: the 240 ka Mamaku and Ohakuri eruptions that together evacuated more than 245 km3 of rhyolitic magma (Milner et al., 2003; Gravley et al., 2007), and generated two separate caldera collapses 30 km apart. Both eruptive events produced heterogeneous bulk pumice compositions (i.e. three distinct magma types in each ignimbrite), but, remarkably, each of the recognized types can be found in both the Mamaku and Ohakuri ignimbrites (Milner et al., 2003; Gravley et al., 2007). This paper presents a geochemical study of these ignimbrites in order to reconstruct their magmatic history and understand how the various magma types were assembled prior to their almost simultaneous eruption, and to identify potential eruption triggers. Here we show that, not only did the Mamaku and Ohakuri eruptions evacuate multiple, chemically distinct, magma batches extracted from the same mush zone, but also that these batches evolved in isolation, despite being stored in reservoirs just a few kilometres apart.

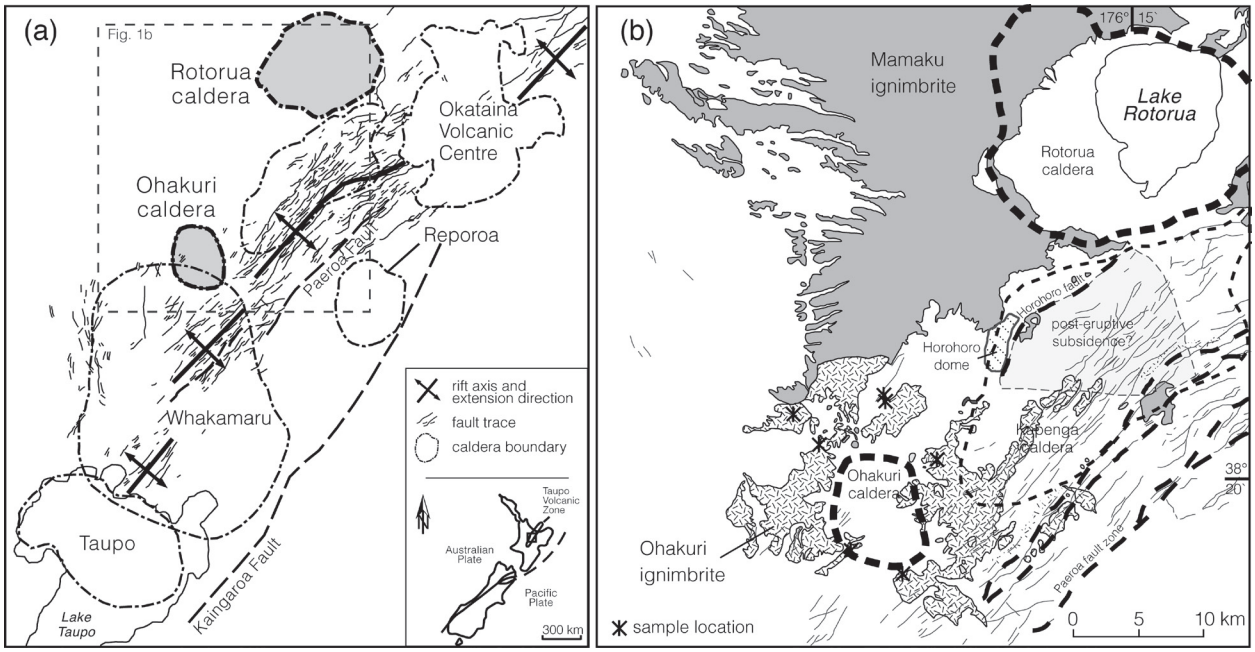

Figure 2.1: (a) Map of the Taupo Volcanic Zone (TVZ), New Zealand. Caldera boundaries and structures after Rowland et al. (2010) (b) Geological map of the Ohakuri-Rotorua region and outline of the suggested post-eruptive subsidence area after Gravley et al. (2007); sample locations are marked with an asterisk.

2.3. Geological Background

The TVZ is a rifted-arc and reflects the subduction of the Pacific Plate beneath the North Island of New Zealand, which is currently subject to a NW-SE extension of 5-15mm/yr from SW to NE (Wallace et al., 2004). The TVZ can be subdivided into three segments, with the northern and the southern segments dominated by andesitic volcanism typical of continental arcs. The 125 x 60 km central segment is dominated by explosive caldera-forming rhyolitic volcanism, with only minor dacites and basalts erupted (Wilson et al., 1995; 2009). More than 6,000 km^3 of rhyolites erupted over a period of ~1.6 Ma (andesitic activity started ~2 Ma ago; Houghton et al., 1995; Wilson et al., 1995). Rifting in the central TVZ started accelerating approx. 0.9 Ma (Wilson et al., 1995), and is responsible for thinning of the crust and a heavily intruded lower crustal region from ~16 to 30 km depth (i.e. Harrison & White, 2006). Rifting has also lead to several extension-related graben structures segmented along the length of the central zone, where a close relationship between tectonics, magmatism, and volcanism has been inferred from detailed field studies (Wilson et al., 2009; Rowland et al., 2010). The onset of accelerated rifting preceded or directly coincided with a transition to dominantly silicic volcanism (Wilson et al., 1995, Deering et al., 2012), and caldera structures and their geometry are partially controlled by this regional extensional regime (Fig. 2.1a; i.e. the Okataina Volcanic Centre; Cole et al., 2010, Seebeck et al., 2010). Two different types of rhyolites have been identified in the central TVZ, starting with the early work of Ewart (1965) and Ewart et al. (1975). Improved geochronology and more detailed bulk-rock and mineral chemistry have refined the chemical distinction, and a spatio-temporal distribution between 'wet-oxidizing' [rhyolite R1; crystal-rich (up to 45 vol.%); dominantly hydrous mineral phases (hornblende ± cummingtonite ± biotite); high fO_2 (ΔQFM = 1-2)] and 'dry-reducing' [rhyolite R2; crystal-poor (<10 vol.%); dominantly anhydrous mineral phases (orthopyroxene ± clinopyroxene); low fO_2 (ΔQFM = 0-1)] rhyolite types has been proposed (Deering et al., 2008; 2010). It has been suggested that the origin of these two end-member rhyolite types is related to subduction

zone processes, with distinct slab-derived fluid flux through time and space (Deering et al., 2010; Rooney & Deering, 2014).

An abrupt change in magmatism, volcanism and tectonics occurred ~340 ka, with an ignimbrite flare-up event that lasted until ~240 ka (Gravley et al., 2009; D. Gravley et al., in preparation). During this flare-up more than 3,000 km^3 of magma (almost half of the total erupted ignimbrite volume from the TVZ) erupted from at least seven different calderas in the central TVZ (Gravley et al., 2009). The Mamaku (>145 km^3; Milner et al., 2003) and Ohakuri (>100 km^3; Gravley et al., 2007) erupted during the last pulse of this flare-up, approximately 240 ka (Gravley et al., 2007). The Mamaku and Ohakuri ignimbrites are sourced from the Rotorua and Ohakuri calderas, respectively, which are located on the western side of the central TVZ (Fig. 2.1). Interbedding of eruptive deposits, a lack of soil development and most importantly no trace of significant erosion between the Mamaku and Ohakuri deposits led Gravley et al. (2007) to suggest that the two eruptions occurred simultaneously. The eruption sequence began with the Ohakuri fall deposit (Unit 2 in Gravley et al., 2007), which was the first to be deposited; its vent location, identified by isopleth maps for maximum pumice and lithic clast size, is nearby or within the Ohakuri caldera (Gravley et al., 2007). This fall deposit is interbedded with the Mamaku ignimbrite, which erupted from the Rotorua caldera ~30 km to the northeast. No paleosol nor deep erosion are observed at the top of the Mamaku ignimbrite, suggesting a time break of only days to weeks before the emplacement of the Ohakuri ignimbrite. Field evidence provides a more accurate picture than the $^{40}Ar/^{39}Ar$ dates for both eruptions (240±11 ka for the Mamaku ignimbrite and 244±10 ka for the Ohakuri ignimbrite; Gravley et al., 2007). Furthermore, a close relationship between caldera structures and rift tectonics has been identified. Paleogeomorphic reconstruction demonstrates that collateral subsidence occurred as part of the eruption sequence (Gravley et al., 2007). The asymmetric geometry of the Rotorua caldera, which deepens considerably towards the southwest (Milner et al., 2002), and the prominent Horohoro fault scarp and associated depression (Fig. 2.1) provide

morphological evidence of the relationship between volcanism and faulting between the Ohakuri and Rotorua calderas (Gravley et al., 2007). The Horohoro fault runs through the Horohoro rhyolitic dome, situated on the inferred western margin of the Kapenga caldera (Fig. 2.1b). Field relationships show that the Mamaku ignimbrite was deposited around that dome, without over-topping it, demonstrating that the dome predates the Mamaku eruption (Milner, 2001). Part of the dome and the Mamaku ignimbrite have been displaced along the Horohoro fault, and field evidence supports syn-eruptive and/or immediately post-eruptive faulting, as the Ohakuri ignimbrite is thicker on the eastern side of the fault scarp (Gravley et al., 2007). The subsidence of a ~40 km^2 area adjacent to the Horohoro dome (Fig. 2.1b) is suggested to be related to lateral migration of magma towards the Ohakuri caldera (Gravley et al., 2007). Lateral magma withdrawal may be a more common process in the rifting central TVZ than previously thought, as it has recently been invoked for the Oruanui eruption from the Taupo Volcanic Centre (Allan et al., 2012).

An important age constraint for magmatic processes related to the Ohakuri and Mamaku ignimbrites is the Pokai ignimbrite (~275±10 ka, ~100 km^3; Wilson et al., 2009). This ignimbrite, sourced from a composite structure known as the Kapenga caldera (Rogan, 1982, Wilson et al., 1984, Karhunen, 1993), is separated from the Ohakuri and Mamaku deposits by a >30 cm thick, dark organic paleosol. The inferred boundary of the Kapenga caldera overlaps with the Ohakuri caldera to the south and incorporates the area of collateral subsidence between the Rotorua and Ohakuri calderas (Fig. 2.1), suggesting that the locations of the Pokai and the Mamaku-Ohakuri magmatic systems coincided. The time between these two events (~275 to 240 ka) was also marked by a dome-building event (i.e. the Horohoro dome, located on the inferred western margin of the Kapenga caldera, Fig. 2.1b).

The Mamaku ignimbrite is physically very homogeneous (Milner, 2001; Milner et al., 2003). The main sequence is predominantly massive, and it has been subdivided into three major units, with a non-welded, unconsolidated and pumiceous lower unit (lMI), through a largely welded

middle unit (mMI), and to an intensely vapour-phase altered upper unit (uMI; Milner, 2001; Milner et al., 2003). In contrast, Ohakuri is a non-welded, largely vitric ignimbrite, and presents complex stratigraphic depositional units with dune bedding, mantling deposition, and energetic flows (Gravley, 2004; Gravley et al., 2007). Three different magma types have been identified in the Mamaku and Ohakuri deposits based on their bulk-rock compositions (Milner, 2001; Milner et al., 2003; Gravley, 2004; Gravley et al., 2007). Those different magma (pumice) types are found together at the same stratigraphic levels throughout the eruptive deposits and have the same lateral distribution, suggesting simultaneous eruption of all magma types (Milner et al., 2003; Gravley, 2004). Strong chemical similarities between the Mamaku and Ohakuri rhyolites have been identified (Gravley, 2004; Gravley et al., 2007), and will be further explored in this study.

2.4. Analytical Methods

2.4.1. Sample preparation

We cleaned, oven-dried (50°C), and crushed 28 individual pumice clasts from the Ohakuri fall deposit and ignimbrite, and the Mamaku ignimbrite. As there is a lack of chemical stratification for both ignimbrites, no specific unit was targeted for pumice sampling (grid references of the sample locations are given in Appendix B-1). In order to avoid the extensive vapour phase alteration (VPA) and devitrification that affects the middle and upper Mamaku ignimbrite (mMI and uMI; Milner et al., 2003), only samples from the lower Mamaku ignimbrite were analysed. The various pumice types are very similar macro- and microscopically, and they can only be identified through chemical analysis. Therefore, samples have been chosen based on the appearance of the pumice glass and degree of weathering, and only fresh and pristine pumice clasts were selected for analysis.

Quartz crystals were handpicked and mounted on one-inch epoxy mounts. To identify quartz-hosted melt inclusions we used immersion oil (refractive index 1.54) and chose only fully

enclosed and glassy melt inclusions for analysis, which are larger than 50 μm to avoid boundary layer effects (Roedder, 1984). Rare Mamaku and Ohakuri melt inclusions had a vapour bubble; these inclusions were avoided for analyses.

2.4.2. Bulk-rock and mineral geochemistry

Bulk-rock and mineral chemistry presented here is a compilation from published work (Milner et al., 2003; Deering et al., 2008; 2010) and PhD Theses (Milner, 2001; Gravley, 2004). Bulk-rock analyses have been acquired for 175 samples with X-ray fluorescence spectrometry (XRF) at the University of Canterbury (157 samples; Milner et al., 2003; Gravley, 2001) and Michigan State University (18 samples; Deering et al., 2008). Inductively coupled plasma (ICP) mass spectrometry was used to analyze Nb, Eu, Gd, Tb, Dy, Ho, Er, Yb, Lu, Hf, Ta, Y, Ba and Pb for 18 bulk-rock samples at Michigan State University (Deering et al., 2008). Core and rim mineral composition was acquired using an electron microprobe (EPMA) at the University of Michigan (Cameca SX100; Deering et al., 2008; 2010) and Victoria University of Wellington (JEOL Superprobe 733; Milner, 2001; Milner et al., 2003).

2.4.3. Major elements compositions of matrix glass and quartz-hosted melt inclusions

Major element compositions of glass shards from 28 individual pumice clasts and 157 quartz-hosted melt inclusions (in some cases multiple melt inclusions within the same quartz crystal) were acquired with an electron microprobe (JEOL 733 Superprobe) at the University of Washington (UW). We used an acceleration voltage of 15kV, a beam current of 5 nA, a defocused beam of 10 μm in diameter, and we measured Na first in the routine to minimise Na migration, although it can still occur at these conditions (Morgan & London, 1996). Counting times were 20 sec. for Si and P, and 40 sec. for the other major elements. The rhyolite glass VG 568 was used as a standard (Jarosewich et al., 1980), and has been used to establish the standard error (reported in Tables 2.4 and 2.5). Matrix glass analyses with totals lower than 95 wt.% were discarded from this study. For melt inclusions, average totals were ~95 wt.% (93-97.5 wt.%). All reported results are normalised

to anhydrous conditions. Analytical errors were <1 % for SiO_2 and Al_2O_3, <3 % for Na_2O and K_2O, and <7 % for FeO and CaO. Titanium and manganese were below detection limit, which was 0.13 wt.% for TiO_2, and 0.07 wt.% for MnO.

2.4.4. Trace elements in quartz-hosted melt inclusions

We used the secondary ion mass spectrometer IMS Cameca 6f at Arizona State University (ASU) to analyse trace elements (Li, Rb, Sr, Y, Cs, Ba, La, Ce, Pr, Nd, Sm, Th and U) in 64 melt inclusions on gold coated epoxy mounts. The primary O- beam intensity was set at 10 nA, and was focussed to a spot of 10-20 μm in diameter. The NIST 610 glass was used as a standard, being measured several times during each session. The composition of the standard was used to convert the measured trace element (relative to Si ratios) in concentrations (ppm). The analytical error was less than 3 % for all elements, except for the Th and U for which the error was 10 %.

2.4.5. Quartz Cathodoluminescence

Quartz cathodoluminescence (CL) imaging was performed after the EMPA and SIMS analyses with a Gatan CL detector on the JEOL JSM-7000F scanning electron microscope at the University of Canterbury. The acceleration voltage was set at 15 kV, with a beam current ranging from 15 to 18 nA and a working distance of 11 mm.

2.5. Geochemical Results

2.5.1. Bulk-rock Geochemistry

Average major and trace element compositions of individual pumice clasts are presented in Table 2.1. These data are combined with XRF bulk-rock composition from previously published work (Milner et al., 2003) and unpublished theses (Milner, 2001; Gravley, 2004). The composition of pumice lapilli from the Ohakuri fall deposit could not be acquired due to the small size (<2 cm) of the samples.

We use the same terminology as previous authors for the different magma types for the Mamaku (Milner, 2001) and Ohakuri ignimbrites (Gravley, 2004); Type 3 represents the least evolved magma (65-72 wt.% SiO_2), followed by Type 2 (70-75 wt.% SiO_2), and finally the most evolved Type 1 (74-78 wt.% SiO_2; Table 2.1). As reported by previous authors, the Type 1 and 2 of the Ohakuri ignimbrite overlap in composition with the Type 1, 2 and 3 of the Mamaku ignimbrite; Ohakuri Type 3 is distinct and less evolved (Gravley et al., 2007). The Rb versus Sr compositions of the bulk pumice is shown here to illustrate the different magma types (Fig. 2.2), which plot along different linear trend-lines, and are separated by a compositional gap.

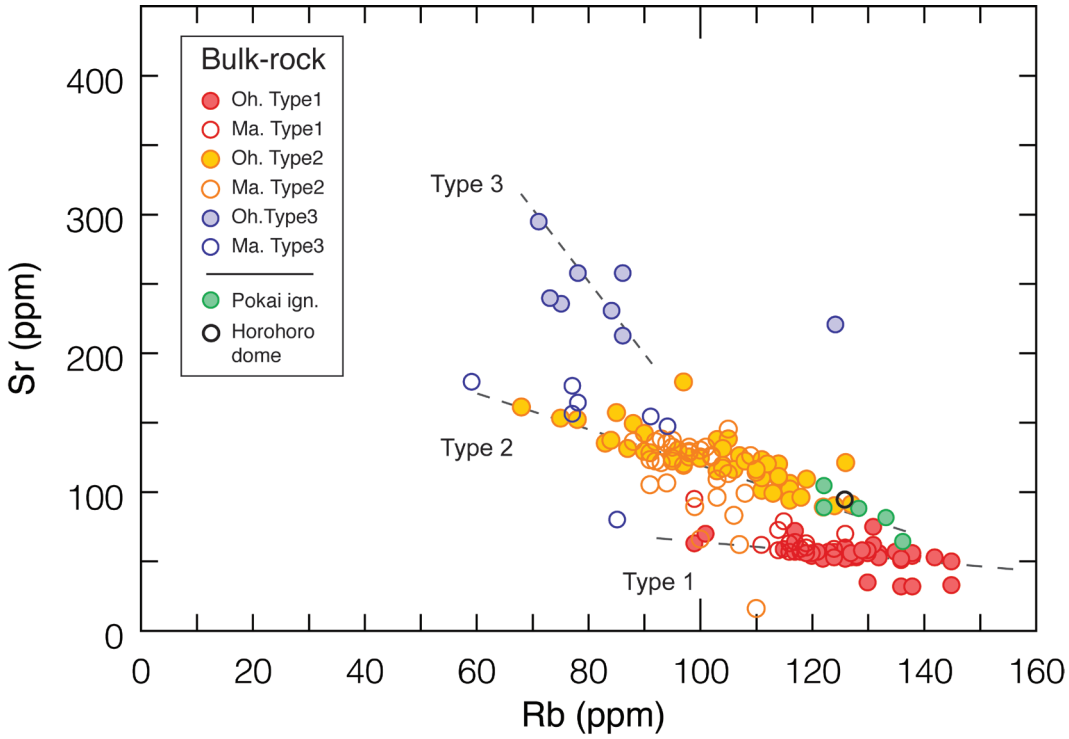

Figure 2.2: Rb vs. Sr from single-clast pumice bulk rock analyses from the Mamaku (open symbols) and Ohakuri (filled symbols) deposits; data from Milner et al. (2003), Gravley (2004), Deering et al. (2008).

2.5.2. Mineral Compositions

The Mamaku and Ohakuri rhyolites have the same phenocryst assemblage, which is predominantly plagioclase, quartz, orthopyroxene, and Fe-Ti oxides (Table 2.2). The representative composition is summarised in Table 2.3.

2.5.2.1. Plagioclase

Plagioclase is the most abundant mineral phase in the Mamaku and Ohakuri deposits. It occurs as euhedral to subhedral tabular crystals, and forms individual phenocrysts as well as glomerocrysts with orthopyroxene and oxides. Mamaku plagioclase is normally zoned in all magma types (An_{31-17} for Type 1, An_{47-15} for Type 2, and An_{43-20} for Type 3; Milner et al., 2003). Ohakuri plagioclase has a very similar range, with An_{40-21} for Type 1, An_{38-22} for Type 2, and An_{46-20} for Type 3 (Fig. 2.3a). Ohakuri plagioclase overall appears to be slightly less potassic and encompass a smaller CaO range (Fig. 2.3b). In general, the Mamaku and Ohakuri plagioclase have a lower An content than other documented TVZ plagioclase from rhyolites (Fig. 2.3a, Schmitz & Smith, 2004; Deering et al., 2008; Smith et al., 2010).

2.5.2.2. Orthopyroxene

Orthopyroxene is found in every pumice type from the Mamaku and Ohakuri ignimbrites, and mostly has a stubby prism habit. It contains numerous mineral inclusions, which are frequently oxides and apatite, but rare clinopyroxene inclusions also occur. The En content [Mg/(Mg+Ca+Fe)] in the pyroxenes of the Mamaku and Ohakuri pumice clasts overlap from En_{40-54}, although the Mamaku has a second, smaller population of pyroxene with compositions of En_{58-64} (Fig. 2.4).

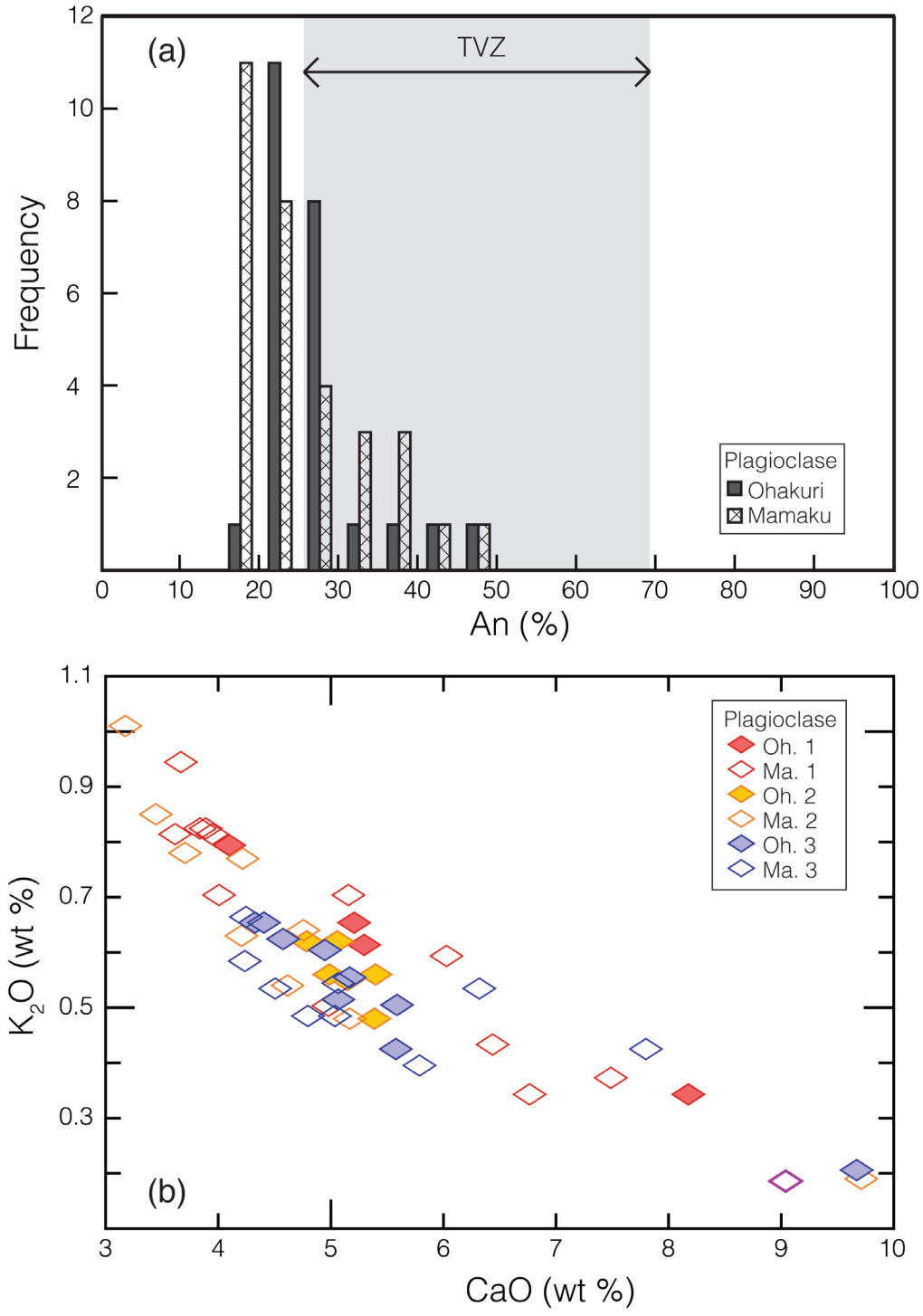

Figure 2.3: Mamaku and Ohakuri plagioclase compositions; (a) An (%) vs. frequency. Grey fields represent the An range for plagioclase in TVZ rhyolites (after Schmitz & Smith, 2004; Wilson et al., 2006; Deering et al., 2008; Smith et al., 2010); (b) CaO vs. K_2O for the Mamaku (open symbols) and Ohakuri (filled symbols) eruptions; data from Milner (2001), Deering et al. (2008; 2010).

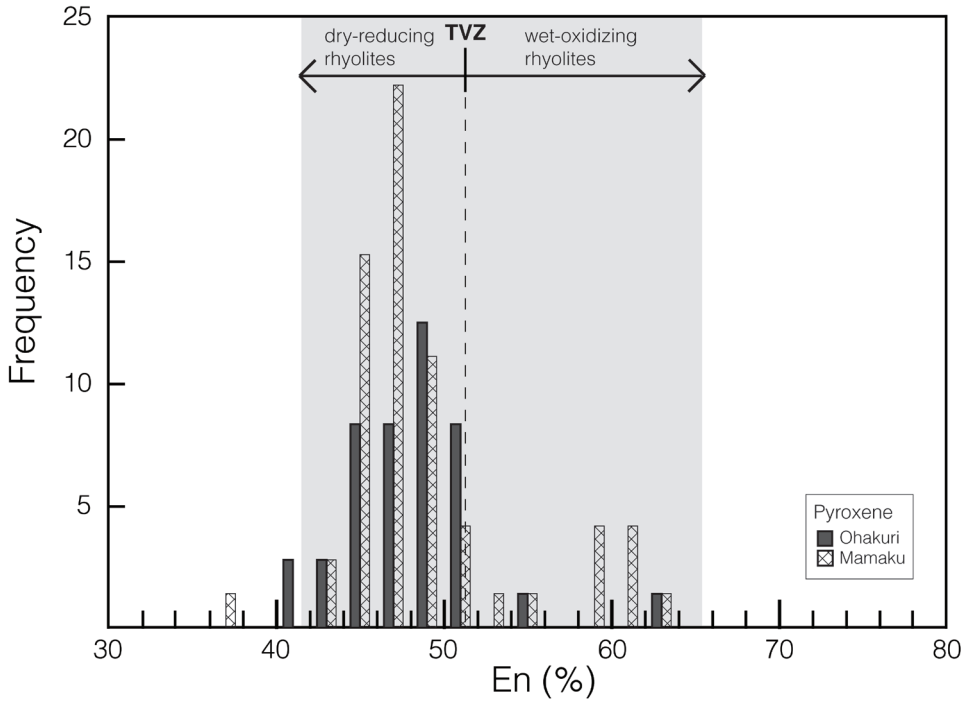

Figure 2.4: Mamaku and Ohakuri pyroxene compositions; En vs. frequency. Grey field represents the En range for all central TVZ pyroxenes (after Deering et al., 2008).

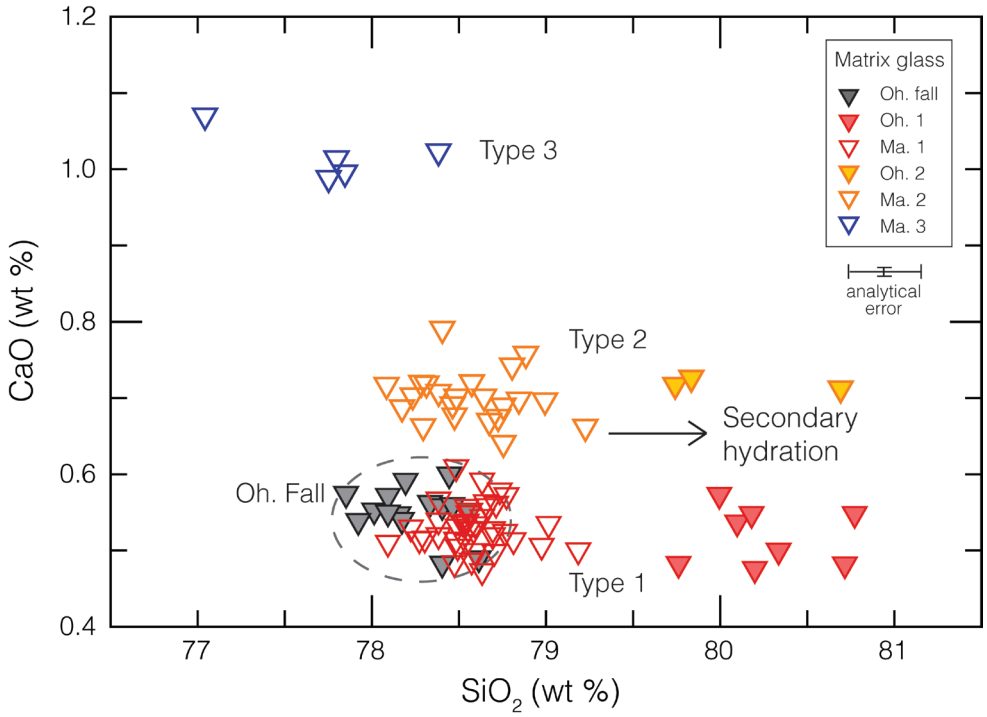

Figure 2.5: Major element composition of the matrix glass in the Mamaku (open symbols) and Ohakuri (filled symbols) ignimbrites and fall deposit , normalised to anhydrous conditions (analysis totals > 95 wt.%). Alkali loss due to secondary hydration affects the normalisation, thus the high SiO_2 content.

2.5.3. Glass Geochemistry

2.5.3.1. Matrix glass

Matrix glass of the Mamaku (Ma) and Ohakuri (Oh) pumice clasts shows typical high-silica rhyolite compositions, with SiO_2 contents ranging from 77 to 78.5 wt.% for Mamaku Type 3, and from 78 to 80 wt.% for Mamaku and Ohakuri Type 1, 2, and fall deposit (Fig. 2.5). Analyses with totals below 95 wt.% were discarded assuming secondary hydration and breakdown of the glass to clays. This criterion forced us to exclude all of the data for Ohakuri Type 3 pumice. Average glass compositions and standard deviations are given in Table 2.4 (extended dataset is available in Appendix B-2).

The glass compositions of Type 3, 2 and 1 plot within three distinct CaO ranges, decreasing from Type 3 to 1 (Fig. 2.5). Type 2 pumices in the Mamaku and Ohakuri are indistinguishable in terms of CaO. Likewise the Type 1 pumice CaO glass compositions in the Mamaku and Ohakuri are similar and together plot close to the Ohakuri fall matrix glass. However, the SiO_2 of Type 1 and 2 magmas shows a similar range (Fig. 2.5-2.6). Na_2O and K_2O produce similar groupings as CaO (Fig. 2.6a and c), suggesting a trend towards more evolved compositions from Type 3 to 1. Within each individual pumice type, there is a strong decrease in Na_2O, and, to a smaller degree, in K_2O with increasing SiO_2 (Fig. 2.6).

This alkali loss (Fig. 2.6a-c) may be the result of two distinct processes (aside from Na loss during analytical procedures): 1) secondary hydration of the matrix glass, which will favour alkali migration (Cerling et al., 1985), and 2) plagioclase crystallisation and fractionation. One way to test the influence of either process is to compare the melt inclusion composition with the matrix glass. We observe lower Na_2O and K_2O content in the matrix glass (Fig. 2.6a-c); however, Al_2O_3 is higher in the matrix glass than in the melt inclusions (Fig. 2.6b). If plagioclase crystallisation caused the alkali variability, Al_2O_3 would also be consumed by the reaction, and it should be lower in the matrix glass compared to the melt inclusions. Therefore, secondary hydration seems to be a

more plausible explanation, and the high SiO_2 and Al_2O_3 contents are thus an effect of the normalisation, as they are the most abundant oxides. This is corroborated by the low analytical totals, especially for the Ohakuri matrix glass, which seems to be more affected than the Mamaku matrix glass. We also confirmed this by renormalising the matrix glass composition using the same Na_2O and K_2O content as in the melt inclusions, which eliminated the effect of the higher Al_2O_3 content in the matrix glass compared to the melt inclusions. For this reason, the matrix glass composition is only used for distinguishing between the different magma types and to discuss magma mixing in this study, and it will not be included in the establishment of the petrogenetic model.

2.5.3.2. Quartz-hosted melt inclusions

Average melt inclusion compositions are given in Table 2.5 and 2.6 (extended dataset in Appendix B-3). Analysed melt inclusions are all high-silica rhyolite in composition, with SiO_2 contents ranging from 77.5 to 79.5 wt.% (Fig. 2.6-2.7). The melt inclusion analyses are subdivided into their respective magma types, according to the results of the matrix glass from the host pumice of each quartz grain. Mamaku Type 3 melt inclusions examined in this study were all devitrified and, therefore, were not analysed. In contrast to the matrix glass, it is not possible to separate the magma types using the melt inclusion CaO content alone (Fig. 2.7a, c), but Figure 2.7a and c show distinct negative trends within individual magma types. Individual magma types have a small range (2 wt.%) in silica contents and these overlap between the different types. The Ohakuri fall deposit and most of the Mamaku Type 1 analyses plot on the lower SiO_2 end. Furthermore, Type 1 melt inclusions for the Mamaku and Ohakuri have less SiO_2 than the Type 2, and the Ohakuri Type3. The Ohakuri Type 3 has the least evolved bulk pumice chemistry, yet melt inclusions with the highest SiO2 content. In contrast to SiO_2, K_2O contents are higher in the Type 1 melt inclusions (Fig. 2.7b, d), and, aside from a few outliers, Type 1 and Type 2 clearly plot into two different potassium fields. Ohakuri Type 3 plots within the potassium field of the Type 2 inclusions, and the Ohakuri fall inclusions plot with Type 1.

In Figure 2.7 (b, d) we observe a few outliers; melt inclusions from sample Ma21 (Mamaku pumice with a Type 1 matrix glass chemistry) plot with the Type 2 population (i.e. lower K_2O content; Fig. 2.7d); these four outliers represent analyses from 3 different quartz crystals from the same pumice, but all other melt inclusions from that pumice plot with the Type 1 population. Equally, four data-points for pumice Ma22 and one for pumice Ma25 (both have a Type 2 matrix glass composition) plot with the Type 1 population (i.e. high K_2O content in the melt inclusions; Fig. 2.7d). In Figure 2.7b we observe two outliers of Type 2 pumice (sample Oh3 and D160) that have higher K_2O content and plot with Type 1 population; all other analysed melt inclusions from these two samples have K_2O concentrations consistent with Type 2. Water contents of the magma can be estimated using the water by difference (WBD) method for the analysed melt inclusion compositions. Average WBD results (Table 2.5) range between 3.8 wt.% and 5.6 wt.%, with errors of ±1 wt.%.

The most notable variations in melt inclusion composition between the magma types from the Mamaku and the Ohakuri lie in the trace elements. The Rb/Sr ratio ranges from 3 to 8, and plots along a positive trend with SiO_2 for each pumice type (Fig. 2.8a). The trends are steep and distinct, but parallel for Type 1 Mamaku, Ohakuri, and Ohakuri fall deposit. In contrast, Type 2 magmas have a low Rb/Sr ratio and a shallow slope (except for a few outliers). Type 3 Ohakuri has the same range in Rb/Sr ratio as Type 1 pumice. The observed outliers (predominantly Mamaku samples), displaying high Rb/Sr ratio and high SiO_2, each represent a melt inclusion from a different pumice clast.

Mamaku and Ohakuri can be distinguished by distinct U contents in the melt inclusions, with values below 1 ppm for all Mamaku types, and values between 2 and 3.5 ppm for all Ohakuri types, including the fall deposit (Fig. 2.8b). Cs contents are higher in Mamaku melt inclusions (4-7 ppm) than in Ohakuri types 1, 2 and 3 (2.5-5.5 ppm; Fig. 2.8b-c). Cs contents in the Ohakuri fall deposit (5-6 ppm) overlaps with Mamaku inclusions. Li behaves similarly to Cs, with a higher

content in the Mamaku melt inclusions and Ohakuri fall deposit (Li values from 60-90 ppm), and values that plot below 60 ppm for the Ohakuri melt inclusions (Fig. 2.8c).

Bulk-pumice and melt inclusion compositions are compared in Figure 2.9 a-d. For the Mamaku and Ohakuri Type 1 bulk-pumice compositions are very similar to melt inclusions, with some overlapping data-points (Fig. 2.9 a-b), which is consistent with the low crystallinity in the Type 1 (Table 2.2). In contrast, the bulk pumice and melt inclusion compositions for Ohakuri Type 2 and 3 and for Mamaku Type 2 plot as distinct clusters (Fig. 2.9 c-d). Melt inclusion compositions are more evolved than the bulk pumice, which is shown by the selected elements in Fig. 2.9, with lower MgO and Sr in the melt inclusions.

2.5.4. Cathodoluminescence (CL)

Cathodoluminescence images were obtained for 92 quartz grains: 48 from Ohakuri pumice, including the fall deposit, and 44 from Mamaku pumice; almost all imaged quartz is surrounded by glass, indicating that the observed crystal habits are primary. These CL images are essential to understanding quartz growth history and changes in conditions experienced by quartz crystals. The intensities of the CL zones are related to chemical impurities in the quartz lattice (e.g. Peppard et al., 2001; Landtwing & Pettke, 2005). For volcanic quartz, some CL zones have been shown to correlate well with the Ti concentration, which in turn reflects the formation temperature and Ti activity of the melt (Wark & Watson, 2006), pressure (Thomas et al., 2010), and growth rate (Huang & Audétat, 2012), and therefore, can provide valuable information on magma chamber processes (e.g. Matthews et al., 2011; Wilcock et al., 2012).

The imaged quartz crystals are overall euhedral to subhedral, with slight embayments on some of the pyramidal faces (Fig. 2.10a, e-n). Large variation in CL patterns is observed between quartz crystals. A core zone is present in more than 95% of the imaged quartz and we distinguish among different cores: 1) rounded cores (~40 grains), overall slightly brighter, often display oscillatory zoning (Fig. 2.10 g, m, o-r) that is truncated by the next CL zone; 2) jagged cores (~20

grains) with very irregular boundaries (Fig. 2.10 f, i, l), often displaying oscillatory zoning, some cores are very bright (~10 grains; Fig. 2.10 q, s); and 3) skeletal cores (~15 grains) with generally darker CL intensities (Fig. 2.10 e, k). A dark CL zone almost always surrounds these cores, filling the irregularities and forming an outline that parallels the crystal face (Fig. 2.10 f, h, j, o-p, r).

The jagged boundaries of the core and the discordant zoning with the surrounding zones suggest a partial melting event. Oscillatory concentric zoning is ubiquitous throughout the quartz crystals (e.g. Fig. 2.10 q), with an alternation between bright and dark CL zones, parallel to each other. Bright rims (50-150 μm) can be observed on a few of the crystals (~7 grains; Fig. 2.10 h, j, n, t). These rims are either concordant with the previous zone (Fig. 2.10 j), or surround rounded core zones (Fig. 2.10 j, n). Late stage skeletal growth, which is presumably related to rapid growth, is present on ~6 grains (Fig. 2.10 m, t). The bright rims and late stage skeletal growth patterns have not been observed in the imaged quartz from the Ohakuri Type 1 and fall deposit. Rare crystals (3 grains) have a thin bright rim (<10 μm), but only partially present on one face of the crystal (Fig. 2.10s). However, it is important to note here that the presence of the bright rims is not pervasive throughout the same pumice clast (i.e. quartz crystals that are presumably located close to each other in the magma chamber just prior to eruption do not all record the same event in their outermost zones). Mamaku samples generally have more complex zoning than Ohakuri, with sometimes more than one partially resorbed horizon (~8 grains; Fig. 2.10 l, t). The frequency of these CL zoning patterns for each pumice type is summarised in Figure 2.11.

Melt inclusions are nearly always found in the dark CL zones surrounding the core zone, which has also been observed in the quartz crystals from the Oruanui eruption (Taupo Volcanic Centre, Liu et al., 2006). The ones present in the vicinity of the crystal rims are mostly re-entrants (Fig. 2.10 a-c, m). Melt inclusions have mostly irregular or rounded shapes, while some of the smaller inclusions are faceted (e.g. Fig. 2.10d).

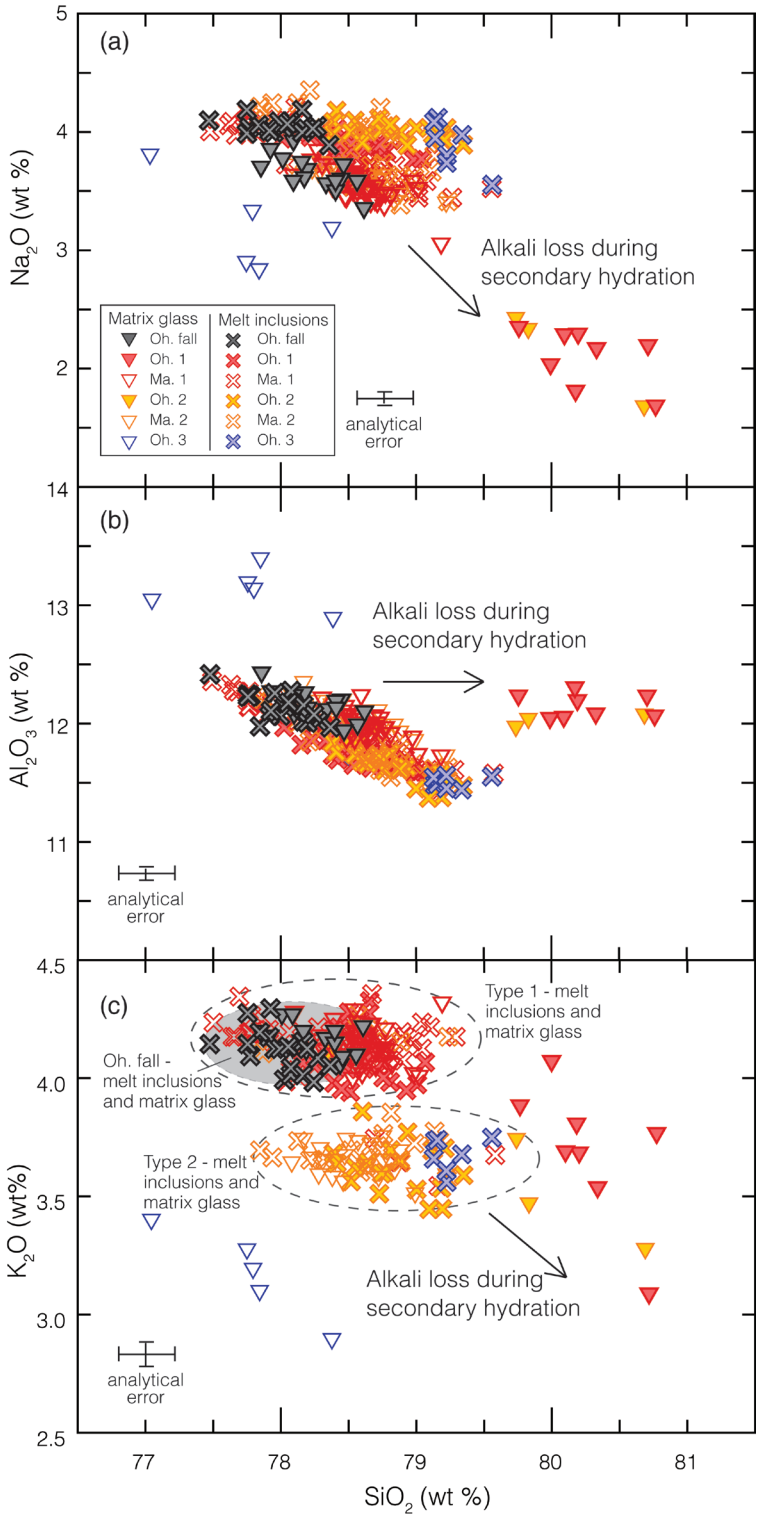

Figure 2.6: Major element composition of the matrix glass and the melt inclusions in the Mamaku (open symbols) and Ohakuri (filled symbols) ignimbrites and fall deposit, all data normalised to anhydrous conditions; (a) less Na_2O in the matrix glass compared to the melt inclusions; (b) higher Al_2O_3 content in the matrix glass than in the melt inclusions. Alkali loss due to secondary hydration affects the normalisation, thus the high SiO_2 and Al_2O_3 contents; (c) K_2O loss in the matrix glass compared to the melt inclusions. Few melt inclusion outliers with more than 80 wt.% SiO_2 were removed.

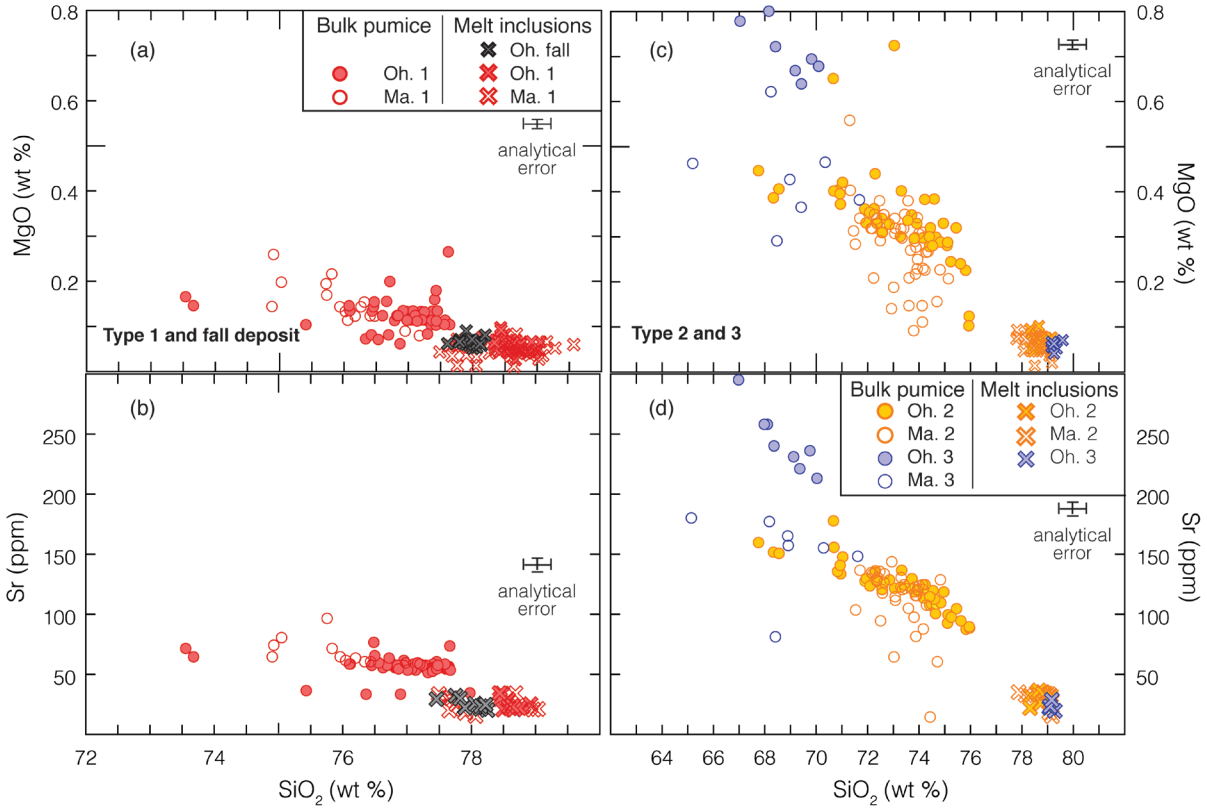

Figure 2.7: Major element composition of the melt inclusions in the Ohakuri ignimbrite and fall deposit (a-b) and Mamaku ignimbrite (c-d).

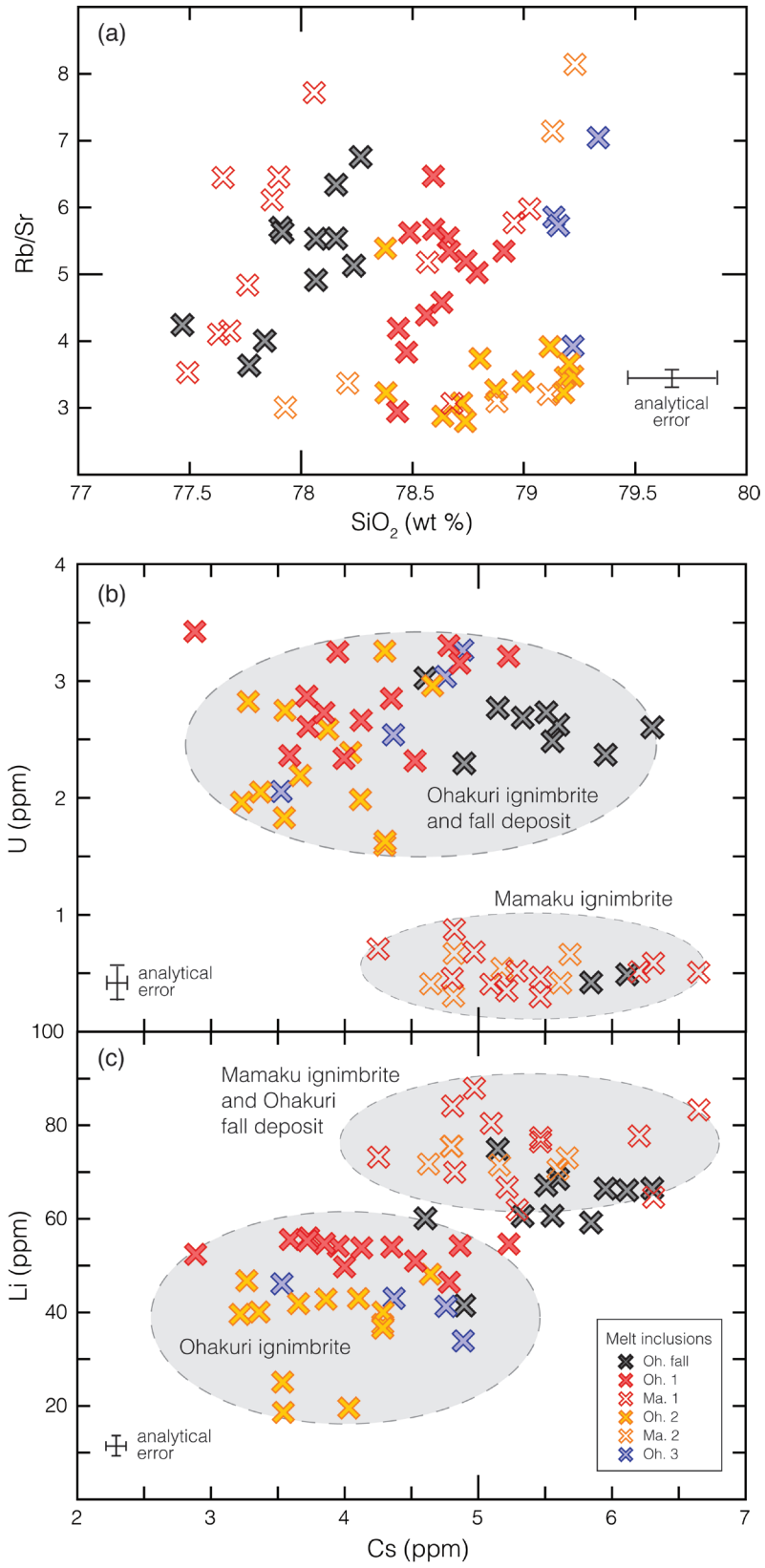

Figure 2.8: Trace element composition of the melt inclusions in the Mamaku (open symbols), Ohakuri (filled symbols) ignimbrites and Ohakuri fall deposit; (a) SiO_2 vs. Rb/Sr; (b) Cs vs. U; (c) Cs vs. Li.

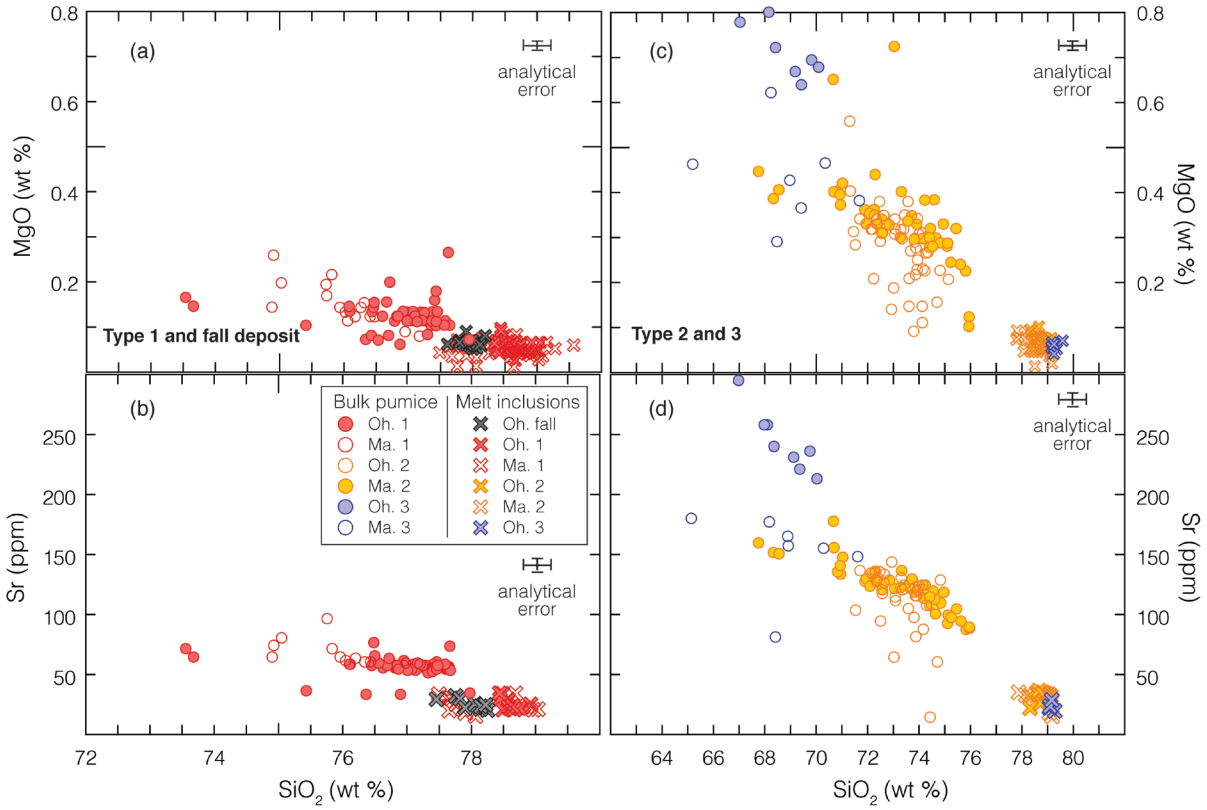

Figure 2.9: Major element composition of melt inclusions compared with the bulk pumice chemistry (Gravley, 2004; Milner, 2001) for Type 1 and Ohakuri fall deposit (a and b), and Type 2 and 3 (c and d); Mamaku (open symbols) and Ohakuri (filled symbols).

2.5.5. Intensive Parameters

Temperature and oxygen fugacity (Table 2.3) have been determined using the Fe-Ti oxide geothermobarometer from Ghiorso & Evans (2008); however, we discarded the oxide pairs that failed to meet the equilibrium criteria proposed by Bacon & Hirschmann (1988).

The calculated temperature for the Mamaku and Ohakuri oxide pairs is between 740°C and 820 °C; log fO_2 (NNO) range from -0.6 to 0.2, and plots along a positive trend with temperature (Fig. 2.12). In comparison to the other TVZ volcanic systems (Fig. 2.12), the Mamaku and Ohakuri mostly follow the trend of the 'dry and reduced' rhyolite types as characterised by Deering et al. (2010).

2.5.6. Crystallisation conditions

The residence depth of these magma batches is essential to understanding their crystallisation conditions, and the pre-eruptive reservoir geometry. We project the melt inclusions and bulk-rock compositions in the haplogranite Qz-Ab-Or ternary (Tuttle & Bowen, 1958; Holtz et al., 1992). Data are corrected for their anorthite content using the method described in Blundy & Cashman (2001), and analyses with >1 % normative corundum have been excluded (Fig. 2.13).

The projected melt inclusion and bulk pumice compositions for the Ohakuri Type 1 (Fig. 2.13a) overlap in the Qz-Ab-Or ternary, and plot in a very narrow range, indicating quasi-isobaric, nearly invariant (i.e. eutectoid) quartz-saturated crystallisation under pressures around 50 MPa. It is noteworthy that the crystallinity in the Type 1 magma is <1 vol% (Table 2.2). In contrast, Ohakuri Type 2 bulk compositions have lower normative quartz (Fig. 2.13a), and form an array toward the projected melt inclusion compositions. The compositional gap between the average bulk-rock and the melt inclusion composition is consistent with initial crystallization on the feldspar side (at quartz-undersaturated conditions), and may indicate late crystallisation of quartz. The projected Mamaku melt inclusion compositions for Type 1 and 2 form an array in the Qz-Ab-Or ternary (Fig. 2.13b). This is intriguing as it shows that even under conditions where quartz is saturated, the

compositions evolve towards the Qz apex, suggestive of polybaric evolution. Similar glass evolutions have been described as decompression crystallisation (Blundy & Cashman, 2001), implying that magma decompression is slow enough for crystallisation to continue.

To better constrain crystallisation pressures we employed phase equilibria calculations using Rhyolite-MELTS (Gualda et al., 2012-a) to model crystallisation pressures (G. Gualda & M. Ghiorso, revised). Because melt inclusions represent melt in equilibrium with both quartz and plagioclase (+ orthopyroxene and Fe-Ti oxides), they need to be saturated in both phases at their liquidus; given that the pressure effect on the slope of saturation temperature is different for quartz and plagioclase, there is a cross-over in pressure versus temperature space that corresponds to the crystallisation conditions. In practice, the method consists of searching within a plausible range of pressures for the pressure at which the liquidus assemblage consists of quartz + plagioclase (G. Gualda & M. Ghiorso, revised; Gualda & Ghiorso, 2013-b). We use the melt inclusion compositions as input in Rhyolite-MELTS and run simulations at pressures of 25-400 MPa, in intervals of 25 MPa, under water-saturated conditions and fugacity fixed at NNO. Importantly, the resulting pressure estimates are insensitive to the assumption of water-saturation (G. Gualda & M. Ghiorso, revised; Gualda & Ghiorso, 2013-b). Details on the application of this geobarometer on TVZ rhyolites is beyond the scope of this paper, and will be the topic of a separate study (Chapter 4).

Application of the method above leads to estimated pressures that range from 60 to 130 MPa for the Mamaku ignimbrite (Fig. 2.14). These results are fairly homogeneous and do not seem to suggest polybaric crystallisation of the Mamaku magma, at least within the level of uncertainty (~50 MPa, 2σ) as seems to be indicated by the Qz-Ab-Or ternary diagrams (Fig. 2.13b). Rhyolite-MELTS calculations for Ohakuri rhyolites yield lower pressure estimates, with values ranging between 30-50 (Fig. 2.14). However, these calculations do not seem to be reliable, and only 9 out of 65 melt inclusion analyses for the Ohakuri melts have a solution in the phase equilibria calculations, and should be treated as absolute minimum pressures. Nevertheless, the pressure

range resulting from the rhyolite-MELTS geobarometer seems to agree reasonably well with the estimates in figure 2.13. The very high SiO_2 content (77-80 wt.%) and the low An content of plagioclase (Fig. 2.3a) are also consistent with shallow storage pressures (Blundy & Cashman, 2001; Gualda & Ghiorso, 2013-a). The estimated pressures are also in agreement with the pressures that have been suggested for other TVZ rhyolites based on H_2O-CO_2 solubilities in melt inclusions, with 50-200 MPa for the OVC (Smith et al., 2010; Johnson et al., 2011), and 90-190 MPa for the Oruanui rhyolite (Liu et al., 2006), although the lower end of their pressure range are considered to be related to degassing of the melt. These results reinforce the fact that the central TVZ magmas are stored in some of the shallowest reservoirs on Earth, which is suggested to be related to an exceptionally high heat flux from depth (Bibby et al., 1995), and the extensional tectonic regime.

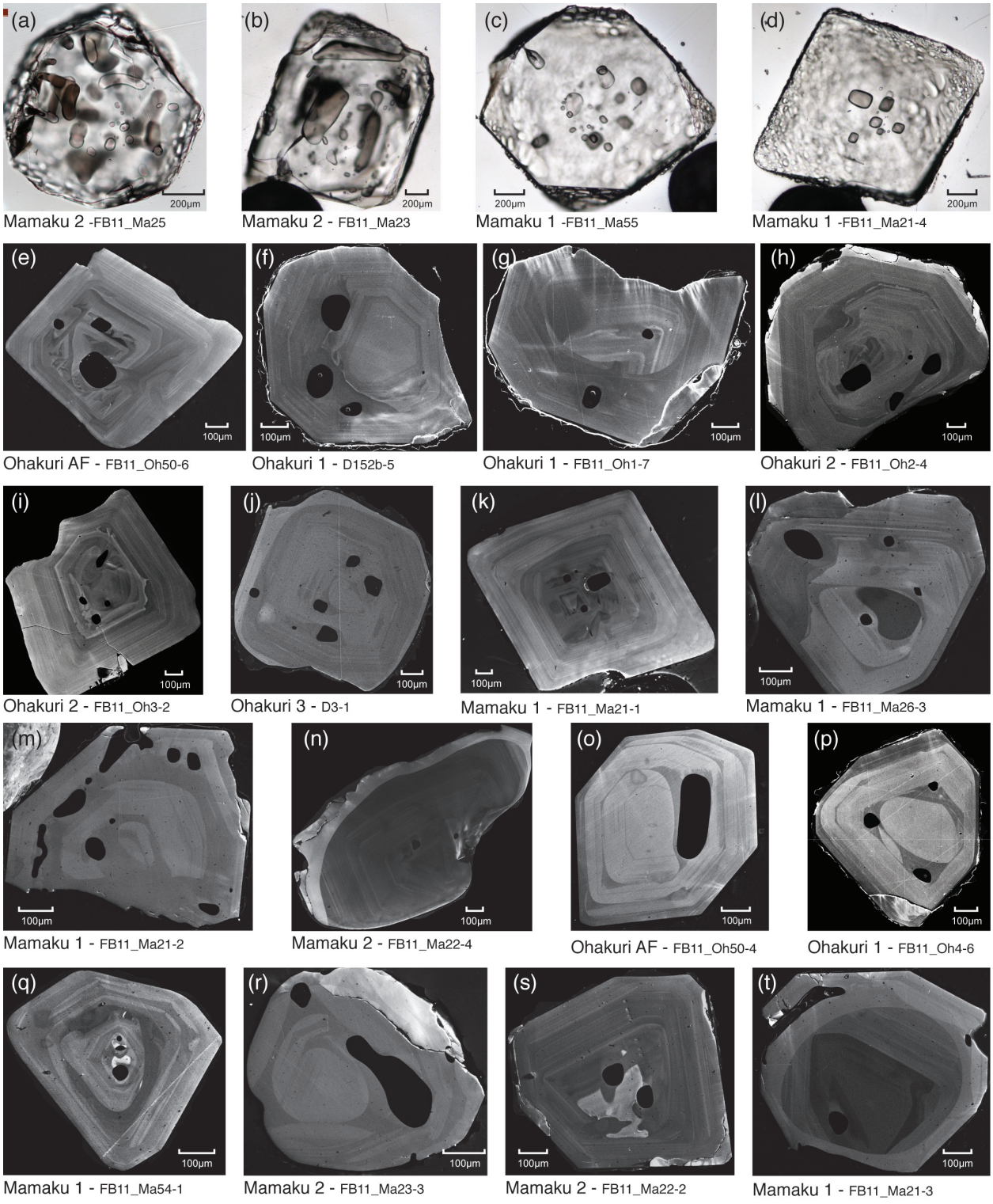

Figure 2.10: (a) to (d): Photomicrograph in transmission light of selected quartz crystals; (e) to (t): representative CL images of quartz crystals. Rounded core zones truncated by the next CL zone in (g), (m) and (o)-(r); jagged cores in (f), (i) and (l); bright core zones in (q) and (s); skeletal cores in (e) and (k). Oscillatory concentric zoning in (q). Late stage skeletal growth in (m) and (t). Bright rims in (h), (j), (n) and (t). Thin bright rim in (s).

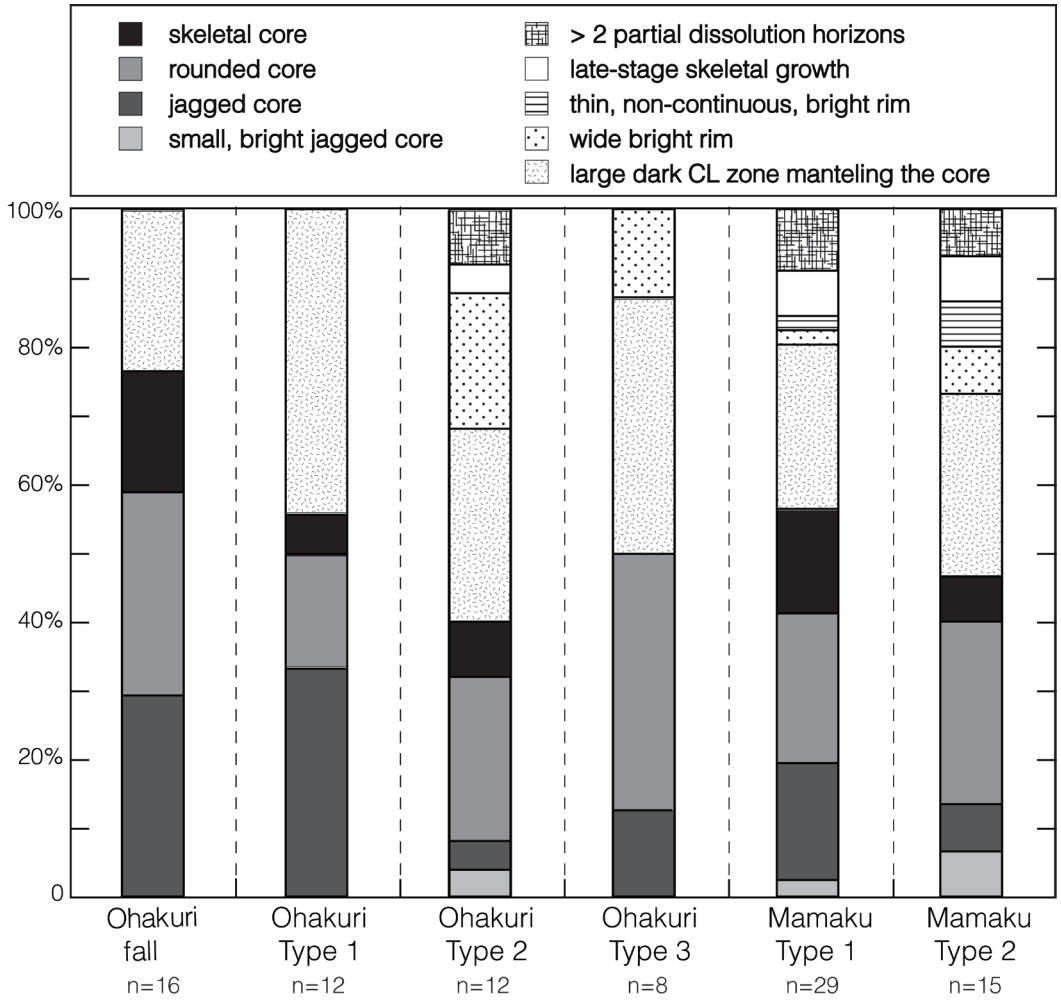

Figure 2.11: Frequency of the CL zoning types for quartz phenocrysts identified for each pumice type of the Mamaku, Ohakuri ignimbrites and Ohakuri fall deposit. See text for description of the zoning patterns.

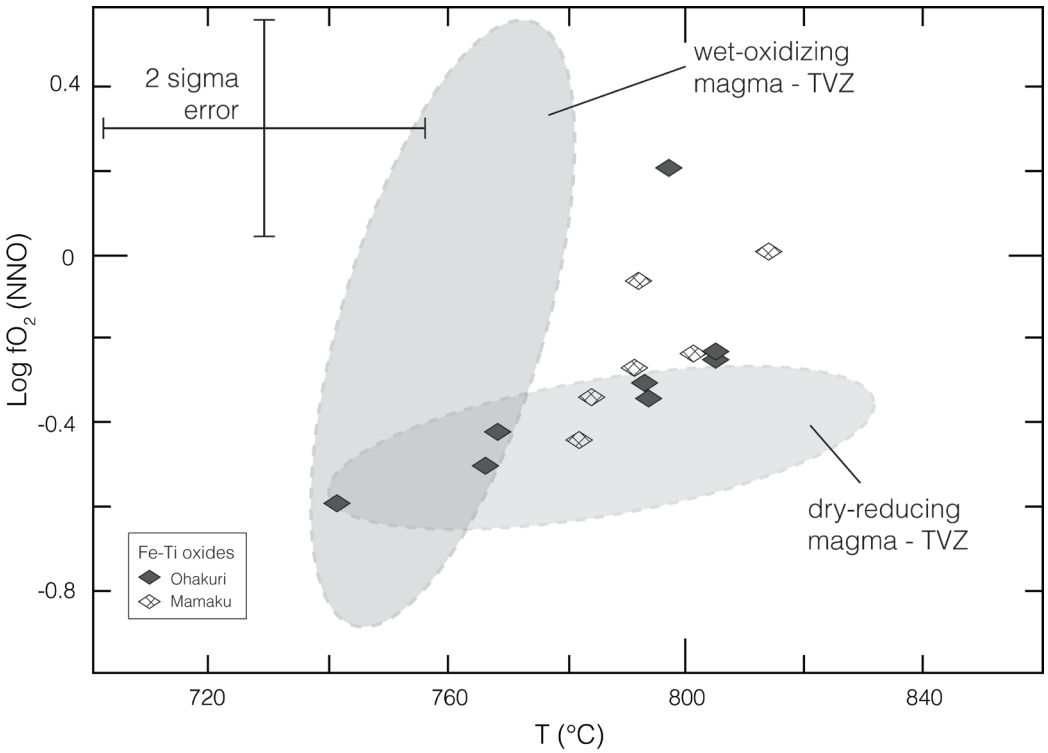

Figure 2.12: Temperature vs. fO_2 calculated for the Mamaku (open symbols) and Ohakuri (filled symbols), error bars represent ±2σ, grey shaded area represent data for the 'dry-reducing' and the 'wet-oxidising' rhyolites in the TVZ (after Deering et al., 2010).

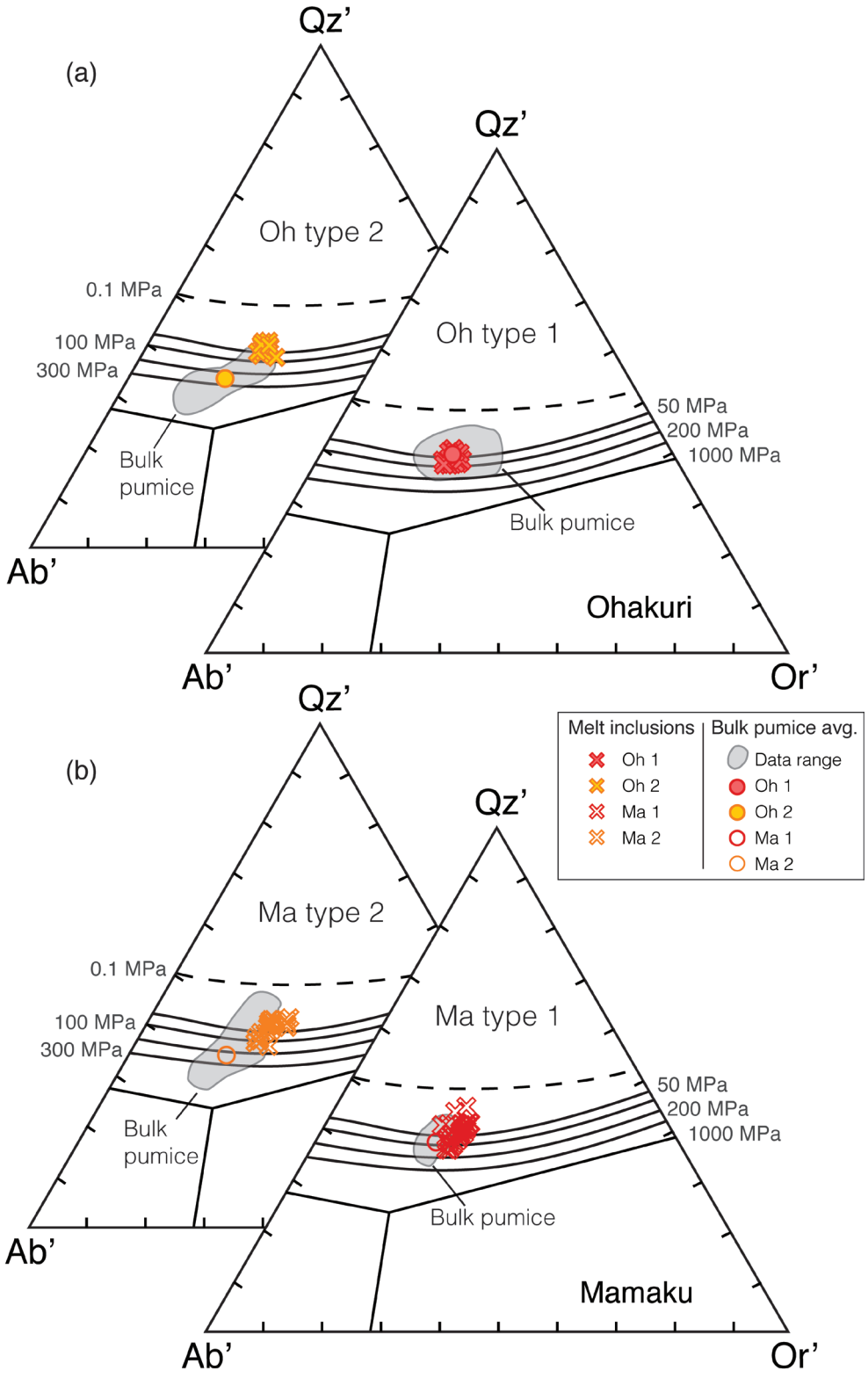

Figure 2.13: Projection of melt inclusion and average bulk pumice compositions onto the haplogranite Qz-Ab-Or ternary; correction for anorthite content after Cashman & Blundy (2001); a) Ohakuri ignimbrite, Type 2 and 1; b) Mamaku ignimbrite, Type 2 and 1 (grey shaded area represents bulk pumice data range). Ohakuri Type 3 data are not included here, as the melt inclusions are not in equilibrium with the bulk melt composition.

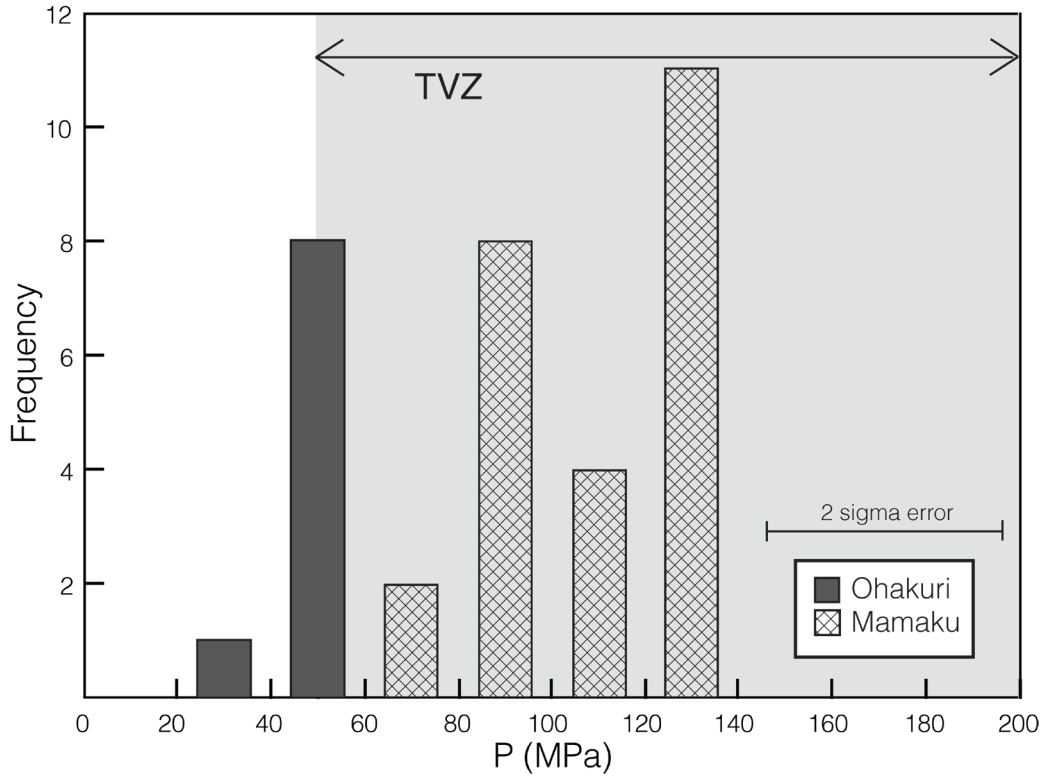

Figure 2.14: Pressure vs. frequency diagram for the Mamaku and Ohakuri ignimbrite showing the distribution of the phase equilibria calculations in Rhyolite-MELTS using the composition of quartz-hosted melt inclusions (method after G. Gualda & M. Ghiorso, revised). These results represent absolute minimum pressures. Grey field represents the pressure range calculated after H_2O-CO_2 solubilities for the Oruanui ignimbrite and the Okataina Volcanic Centre (after Liu et al., 2006; Smith et al., 2010; Johnson et al., 2011).

2.6. Discussion

This dataset of new and compiled compositions of bulk-rock, minerals, matrix glass and melt inclusions allows us to reconstruct the evolution of the different magma types of the Mamaku and Ohakuri magmatic system from the parent magma source to the simultaneous eruptions. For the following discussion we will use the terminology as described in Miller et al. (2011) to distinguish between the magma chamber (i.e. continuous zone where eruptible magma is present), the magma reservoir (i.e. all of the melt-bearing region, including magma chambers and the crystal-rich non eruptible magma/mush), and the magmatic system (i.e. encompasses the magma chamber and reservoir, as well as the solidified portion representing an active zone of magma transfer and storage).

2.6.1. Rhyolite petrogenesis and magma reservoir geometry

Multiple stages of crustal assimilation and fractional crystallisation processes (AFC) from a basaltic parent have been suggested in many studies to explain the origin of evolved magma compositions (e.g. Bachmann & Bergantz, 2004; Annen et al., 2006; Hildreth & Wilson, 2007). To explain the presence of large volumes of crystal-poor silicic magma in the upper crust, current models appeal to the presence of a crystal-rich intermediate mush-zone in the mid- to upper crust, which can be up to a few kilometres thick (Hildreth & Fierstein, 2000; Bachmann & Bergantz, 2004; Hildreth, 2004; Hildreth & Wilson, 2007; Deering et al., 2011-a). The interstitial melt from this crystalline mush represents the rhyolitic melt, and is extracted by a combination of processes (mainly hindered settling and/or compaction) to form crystal-poor high-silica chambers in the upper parts of the reservoirs (Bachmann & Bergantz, 2004). The optimal crystallinity window for an efficient melt extraction from the mush is likely between ~50-70 % crystals (Dufek & Bachmann, 2010). The longevity of the mush system in the upper crust is maintained thermally by episodic heat and mass input from recharge of intermediate magma into the mush-zone (Bachmann & Bergantz, 2004; Hildreth, 2004; Annen et al., 2006; Hildreth & Wilson, 2007; Gelman et al., 2013).

The 240 ka Mamaku and Ohakuri rhyolites are both 'dry-reducing' magmas (R2 rhyolite type, after Deering et al., 2008; 2010), and present many similarities in their bulk-rock geochemistry, mineral assemblage (Table 2.2) and heterogeneity of pumice composition in their pyroclastic deposits. They also have similar ranges of oxygen fugacity and temperatures (Fig. 2.12). Despite these similarities, there are also some differences. Orthopyroxene compositions of the Mamaku ignimbrite also encompass a broader range compared to Ohakuri (Fig. 2.4). In comparison with a larger TVZ mineral dataset (Deering et al., 2010), the Ohakuri and most of the Mamaku pyroxenes plot in the range of the dry-reducing pyroxenes, as expected, but the high-En population of the Mamaku overlaps with the wet-oxidising rhyolite end-member compositions. In the melt inclusion compositions, small differences in fluid-mobile elements are observed, with the Mamaku melt inclusions having less U, and higher Cs and Li content (Fig. 2.8b-c). Other differences between the Mamaku and Ohakuri eruptives have been previously observed (Gravley et al., 2007), with differences in their plagioclase to quartz ratios (Table 2.2), bulk Zr concentration for the Type 2 magma that has a broader range of variation in the Mamaku ignimbrite (i.e. overlaps with the Type 3 magma), and also Rb/Sr ratio, more variable in Ohakuri Type 1 (Gravley et al., 2007).

Despite these subtle compositional differences, the predominant geochemical similarities suggest that at a broader scale, Ohakuri and Mamaku magmas are derived from a very similar source. Considering the current model for rhyolite petrogenesis, consisting of a mid-crustal mush zone, we infer extraction of Mamaku and Ohakuri magmas from a common intermediate crystalline mush-zone, extending between and beneath the Rotorua and Ohakuri calderas (Fig. 2.1). The low-crystallinity nature of these rhyolites and the absence of co-erupted intermediate magma composition are in agreement with the presence of a crystal mush, which is relatively non-eruptible. Only rare andesitic 'blebs' have been found in the Mamaku and Ohakuri eruptive products, and no mingled or mixed composition pumices have been reported (Milner et al., 2003; Gravley et al., 2007). Considering the ~450 km^2 horizontal span of the aforementioned common mush (~45 x 10

km; Fig. 2.1), hindered settling by ~500 m would be sufficient to extract ~225 km^3 of rhyolitic melt (after Bachmann & Bergantz, 2004), regardless of the total mush thickness and the melt segregation process. This rough estimate of total melt produced is consistent with the suggested minimum erupted volume from the Mamaku and Ohakuri eruptions, but would also require the presence of magma beneath the area in between the Rotorua and Ohakuri volcanic centres (Kapenga area). This has been suggested based on field evidence for the Ohakuri system, with magma (referred to as the Kapenga magma; Gravley, 2004) residing underneath the Kapenga area (Fig. 2.1), which migrated southwest to the current location of the Ohakuri caldera (Gravley et al., 2007).

This crystal mush can remain near the eutectic for extended periods of time (Huber et al., 2010), especially if thermal rejuvenation by recharge occurs periodically (e.g. Bachmann & Bergantz, 2004; Annen, 2009; Gelman et al., 2013). This is a likely scenario in the central TVZ during the period in question, as high a sustained heat source, likely to be upper mantle, is required to sustain magmatism associated with the ~340-240 ka ignimbrite flare-up event (c.f. Best & Christiansen, 1991; de Silva & Gosnold, 2007; Gravley et al., 2009; D. Gravley et al., in preparation). A long-lived subterranean crystal mush, perturbed by episodic rejuvenation, has also been identified at other central TVZ magmatic systems, as evidenced by recent zircon geochronology work on rhyolites from the Okataina Volcanic Centre (Fig. 2.1a; Storm et al., 2011). Local, minor heterogeneities in this mush-zone likely persist due to the high but slightly variable crystallinities and lack of large-scale convective homogenisation (Dufek & Bachmann, 2010), and the melt extraction efficiency may vary along a horizontally extensive mush. Local mush heterogeneities have also been suggested as the cause for geochemical differences for the smaller Okareka eruption (Okataina Volcanic Centre; Shane et al., 2008-a). Similarly, we conclude that the compositional differences between the Mamaku and Ohakuri magmas are related to heterogeneities in the mush-zone.

2.6.2. Rhyolite magma batches

In the scenario proposed above, Mamaku and Ohakuri magmas have been extracted from the same locally heterogeneous source reservoir, and they both are characterised by very similar variations in their pumice chemistry; in fact, we observe larger chemical disparities between the magma types at a single centre than between the Ohakuri and Rotorua centres. Three distinct magma types are present in their respective ignimbrites with a less evolved dacitic to rhyodacitic Type 3 melt to two evolved high silica rhyolites, Type 2 and 1. In addition, the melt inclusions from these magma types also have distinct compositions (Fig. 2.7-2.8a); however, they show a narrow range of SiO2, which suggests similar crystallisation conditions (Gualda & Ghiorso, 2013-a). The bulk rock and melt inclusion chemistry from Type 1 and 2 (Mamaku and Ohakuri) plot along a similar liquid line of descent (Fig. 2.9), suggesting that the melt inclusions are in equilibrium with their respective bulk magma type. The lower MgO content in the melt inclusions compared to the bulk-rock chemistry indicates that their entrapment occurred after the crystallisation of some mafic minerals (Fig. 2.9 a and c). The presence of a compositional gap between the bulk-rock and melt inclusion compositions for the Type 2 and 3 of the Ohakuri and Type 2 for the Mamaku ignimbrites (Fig. 2.9 c-d) further emphasises that melt inclusions were entrapped late (i.e. quartz crystallised relatively late in the pre-eruptive history). For the Ohakuri ignimbrite, we also observe that Type 1 melt inclusions are only present in Type 1 pumice, and the same applies to Type 2 (Fig. 2.6c). This indicates that no discernable mixing between these two magma types occurred prior to eruption. For the Mamaku ignimbrite, some melt inclusions with Type 1 matrix glass have compositions similar to Type 2 magma and vice-versa (Fig. 2.7d). However, this does not apply to all of the analysed melt inclusions from the same pumice, and the matrix glass compositions from the pumice clasts in question do not indicate any mixing prior to eruption.

In the most recent model proposed to explain the co-eruption of these chemically distinct bulk magma compositions for the Mamaku ignimbrite (Milner et al., 2003), Type 3 magma represents

the parental magma for the generation of Type 2, and consequently Type 1 magma through plagioclase fractionation. This result favours a single, vertically zoned magma chamber, geochemically layered, with Type 3 magma being the deepest layer in the chamber and Type 1 the shallowest (Milner et al., 2003). Similar models of magma chambers fractionating in situ have been used in the past to explain heterogeneous pumice chemistry [e.g. Grizzly Peak Tuff, Colorado, US (Fridrich & Mahood, 1987); Whakamaru ignimbrite, TVZ (Brown et al., 1998-a)]. However, both the bulk-pumice and melt inclusion compositions for the Mamaku and Ohakuri ignimbrites are in disagreement with this model. Major and trace element compositions of the Type 2 and 1 melt inclusions plot along divergent trends (Fig. 2.7-2.8a), and compositional gaps are often observed between the types; therefore, crystal fractionation is ruled out as a dominant process for the generation of Type 1 magma from Type 2 compositions. A similar argument has been made using Ohakuri bulk rock compositions, which show that Rb and Sr in Type 2 and 1 plot along divergent linear trends (Fig. 2.2; Gravley et al., 2007).

A model depicting separate and chemically distinct magma batches has been suggested as an alternative to the layered magma chamber model at large silicic systems elsewhere (e.g. Cambray et al., 1995; Shane et al., 2007; 2008-a; Gualda & Ghiorso, 2013-b). In this model, the melt is extracted incrementally from the mush zone, and may or may not amalgamate in a large magma chamber. This model accounts well for the distinct compositions between the Ohakuri Type 1 and 2, as each melt batch is extracted separately. Moreover, it seems that very limited mixing between the magma types occurred, which would be indicative of a lack of direct interaction among the distinct magma batches. The coincidence of the different magma types at the same stratigraphic level is considered to reflect simultaneous eruption of all magma batches, which would have to be very close to each other in the upper crust. A similar model of isolated magma batches has also been proposed for other systems [e.g. Rotoiti - Earthquake Flat, OVC (Charlier et al., 2003); Batur Volcanic Field, Indonesia (Reubi & Nicholls, 2005); Snake River Plain, USA (Ellis & Wolff,

2012)]. The evidence for multiple magma batches is less obvious in the bulk compositions of the Mamaku ignimbrite (Fig. 2.2), but the melt inclusion compositions support separate batches (Fig. 2.7-2.8a). The outliers among the Mamaku melt inclusions are not indicative of mixing between Type 1 and 2, as the compositional differences are not consistent throughout all analysed elements, and throughout the pumice clasts. These outliers could represent quartz grains of xeno- or ante-crystic origin, as relicts of the magmatic reservoir that fed older eruptions from the overlapping Kapenga caldera (Fig. 2.1; i.e. ~275 ka Pokai ignimbrite) or assimilation of largely crystallised margins of the reservoir. From the CL images, we identify a distinct core zone in the majority of the quartz grains (Fig. 2.10-2.11). With the available data, we cannot assign an origin to these cores; however, an inherited origin is consistent with the variability in CL-zoning of quartz cores in crystals from the same pumice clast.

Type 3 melt inclusions from the Ohakuri ignimbrite are the most evolved (up to ~80 wt.% SiO_2), contrary to the bulk composition, which is the least evolved (~68 wt.% SiO_2). This melt type represents only a very small volume compared to Type 1 and 2, and it also has the highest crystallinity, with ~15 vol.% (Table 2.1), which could be indicative of a crystal accumulation zone. However there is no chemical evidence that would directly support this, as bulk concentrations of chemical tracers for accumulation zones [i.e. Zr, Rb, and Ba (Table 2.1); Kennedy & Stix, 2007; Deering & Bachmann, 2010] are similar for Types 2 and 3 magmas. Regarding the differences in SiO_2 content between the bulk pumice and melt inclusions and the crystallinity, it is also very unlikely that the quartz is in equilibrium with the melt, suggesting that they could be of antecrystic origin. Incorporation of crystallised margins of the reservoir (see Brown et al., 1998-b for a number of examples of plutonic lithics; Shane et al., 2012) could account for the presence of quartz crystals with high-silica rhyolite melt inclusions, as co-erupted granodiorite lithics are found within the Ohakuri ignimbrite (D. Gravley, pers. comm. 2012). Another plausible explanation for the presence of these high-silica melt inclusions in the Type 3 quartz is mixing of a

rhyodacitic magma with a rhyolitic melt. The Type 3 melt inclusions are chemically very similar to the Type 2 inclusions, which could indicate some degree of interaction with the Type 2 melt batch. However, the distinct Rb/Sr ratio of the Type 3 melt inclusions compared to the Type 2 (Fig. 2.8a), and the absence of a clear mixing line in the bulk-rock chemistry (Gravley et al., 2007) between those two types suggest that interaction with a different rhyolitic melt is more likely (i.e. a melt that was not erupted with the Ohakuri).

The Ohakuri fall deposit, sourced from or adjacent to the Ohakuri caldera (Gravley et al., 2007), is the first eruptive unit, and its melt inclusion chemistry is very similar to a Type 1 magma (Fig. 2.7 and 2.8). However, it seems to share more geochemical characteristics with a Mamaku melt, and shows the same enrichment in Cs and Li (Fig. 2.8b-c). Enrichment in fluid-mobile elements is common in early-erupted material like the Ohakuri fall deposit, due to volatile fluxing from degassing magma (e.g. Berlo et al., 2004). However, here we have evidence to suggest that the fall deposit is a separate batch from the other Ohakuri magmas, as differences in other trace elements apart from the fluid-mobile elements can be observed, and from pressure estimates the melts from the fall deposit seem to reside at slightly greater depth compared to the Ohakuri magmas (Chapter 3 and 4). The relationship between the Ohakuri fall deposit and the Mamaku and Ohakuri magmas is not well understood and remains to be explored. From the current knowledge of the Mamaku-Ohakuri, and other central TVZ magma systems, however, tapping into a magma chamber that is tens of kilometres away from the vent location and lateral magma movements may be a plausible explanation for these chemical similarities between the Ohakuri fall deposit and the Mamaku magmas. With the so far available data, this remains speculative, and for now the fall deposit is represented as a separate magma batch residing close to the Ohakuri centre. Further work will be focussed around this problematic.

2.6.3. Pre-eruptive magmatic system

A schematic model for the Mamaku and Ohakuri magmatic system takes into consideration all the above observations in the geochemical data and volcano-tectonic events described in Gravley et al. (2007) (Fig. 2.15). A continuous intermediate mush-zone, which extends beneath the Ohakuri and Rotorua area, is the source of the distinct magma batches involved in the paired eruption. Of the multiple magma batches, at least four are spatially isolated, as no mixing is observed between the Type 1 and Type 2 of Ohakuri and Mamaku magmas. The much smaller Ohakuri Type 3 and fall deposit batches are represented as well, although their magmatic history is not well constrained. As suggested above, the Type 3 magma composition may have involved mixing of a rhyodacite with a rhyolite or some previously emplaced granitic material, indicated by the melt composition trapped in the quartz crystals.

The extensional regime of the central TVZ, with a profound inter-relationship between magmatism, tectonics, and volcanism (Wilson et al., 2009; Rowland et al., 2010) is probably not the most favourable environment for the establishment of longer-lived magma chambers. Lateral magma migration has been described in the literature as a result of this unstable crustal environment for the Oruanui eruption (Allan et al., 2012), and is also suggested here for the Ohakuri eruption. Field evidence (Gravley et al., 2007) show that syn-eruptive subsidence of a 40 km^2 area in the Kapenga region and formation of the Horohoro fault scarp (Fig. 2.1b) occurred during the Ohakuri eruption, which is suggested to reflect magma residing underneath the Kapenga area and migrating southwest to the current location of the Ohakuri caldera (Gravley et al., 2007). The discrete magma batch model suggested here is in agreement with the structural evidence of lateral magma migration, as one of the magma batches may have resided beneath the Kapenga area. Another line of evidence is the compositional and isotopic similarities between the Ohakuri rhyolite and the Horohoro dome (Fig. 2.2; Deering et al., 2008), which is located on the western margin of the Kapenga caldera (Fig. 2.1b). This dome erupted prior to and was subsequently faulted

in response to lateral migration of magma that fed the Ohakuri ignimbrite eruption (Gravley et al., 2007). However, there is currently not enough geologic evidence to identify which magma type laterally migrated from beneath the Kapenga area to its eruption site. The random distribution of the magma types throughout the eruptive deposits is indicative of simultaneous evacuation of the magma batches during eruption, and may be associated to eruptive processes and styles of caldera collapse (e.g. Kennedy et al., 2008). The estimated pressures yield similar results (within the error) for the different magma types, corresponding to a depth of ~4 km (using a crustal density of 2.7 g/cm^3), which would be concordant with a model of laterally juxtaposed magma batches in the upper crust.

A unique aspect of the Rotorua-Ohakuri magmatic system is that almost chemically identical Type 1 and Type 2 magmas have been extracted at two different locations. Timing of melt extraction from the common crystal mush may play an important role in producing the same rhyolites beneath the Rotorua and the Ohakuri volcanic centres, and Type 1 and Type 2 magmas could represent the product of two distinct extraction events. This raises the important question on the driving mechanism for melt extraction and the available time frame to assemble >245 km^3 of crystal poor rhyolitic melt.

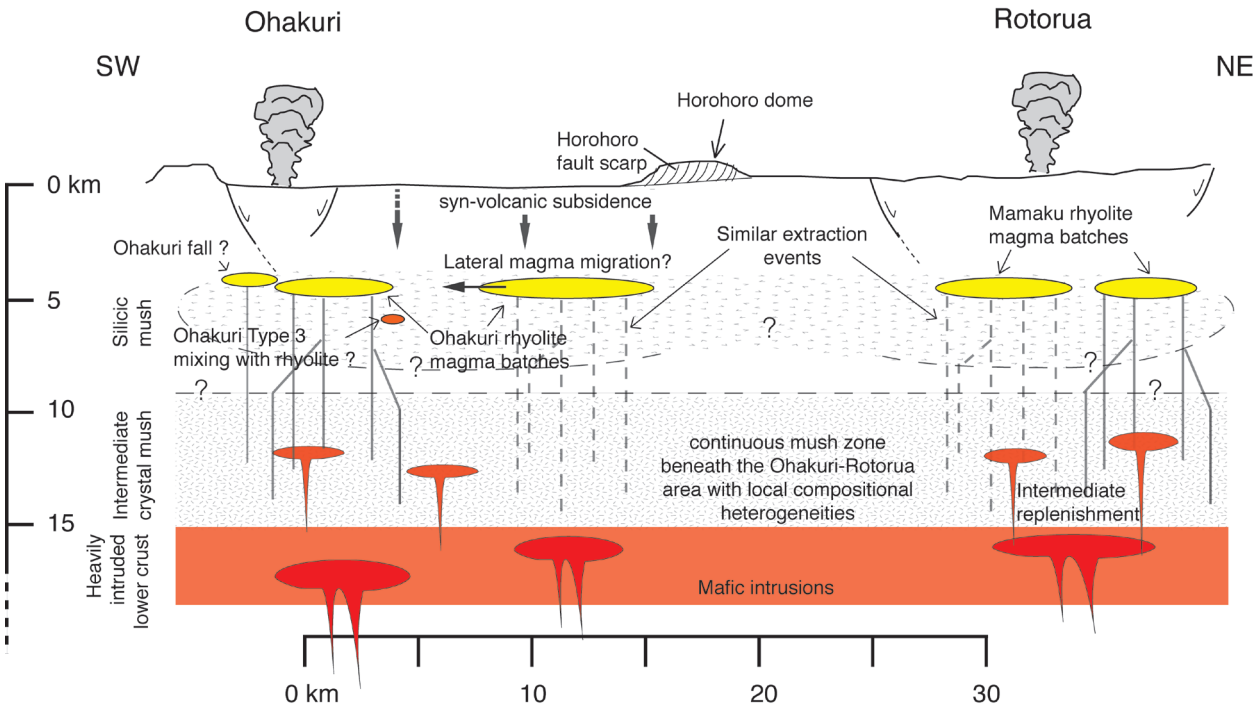

Figure 2.15: Schematic model of the Rotorua and Ohakuri magma systems based on inferred pre-eruptive conditions (this paper) and geomorphic reconstructions (Gravley et al., 2007). Heterogeneous pumice clast chemistry in the eruptives is suggested to reflect multiple magma batches extracted from the same source (i.e. intermediate mush-zone). Extraction conditions for the magma Type 1 is suggested to be very similar between the two eruptive centre (same for the Type 2 magma); no mixing of these batches occurred prior to eruption(scale and relative volumes are approximate).

2.6.4. Extraction timescales and processes

The timescales for rhyolitic melt extraction and crystallisation within the extracted melt have been estimated to be faster (e.g. Wilson & Charlier, 2009; Gualda et al., 2012-b) than suggested by models of melt segregation from intermediate mush by hindered settling (e.g. Bachmann & Bergantz, 2004). The ~275±10 ka Pokai ignimbrite (Gravley et al., 2007) is stratigraphically beneath the Ohakuri and the Mamaku ignimbrites, with a well-developed paleosol separating the units (Gravley et al., 2007). The Pokai magma is sourced from the Kapenga caldera (Fig. 2.1; Karhunen, 1993), within the same area where later, during the paired Mamaku-Ohakuri event, synvolcanic subsidence occurred (Fig. 2.1 and 2.15). This subsidence suggests the presence of magma during the ~240 ka event in the same region that the Pokai magma resided (Gravley et al., 2007), which leaves between ~15-55 ka (35 ± 20 ka) to generate/extract the crystal-poor rhyolite erupted during the Mamaku and Ohakuri events in the region of the Kapenga caldera. The rhyolites feeding these eruptions likely shared the same intermediate mush. This inference is supported by that fact that the Pokai rhyolite is geochemically very similar to the Mamaku and Ohakuri magmas; it is a 'dry-reducing' magma (Deering et al., 2008), it has the same anhydrous mineral assemblage and similar bulk-rock compositions (Fig. 2.2; Karhunen, 1993; Gravley, 2004), which is supportive of a common mush zone.

After eruption of the Pokai ignimbrite, rejuvenation (reheating, remelting and melt extraction) of the residual intermediate mush zone occurred, and extraction could resume and form new pockets of crystal-poor melt in this area to form the Mamaku and Ohakuri magma batches. The presence of antecrysts in the Mamaku and Ohakuri melts has been suggested to explain the compositional outliers in the melt inclusion data, and the lack of equilibrium between melt inclusion and bulk-rock compositions for the Type 3. Furthermore, CL imaging revealed the presence of inherited cores in most of the crystals. These aspects are evidence for the process of reheating, remelting and melt extraction, which likely remobilises some pre-existing melt and crystals. Crystal-melt

segregation and extraction mechanisms are suggested to be a combination of hindered settling, micro-settling and compaction of crystals in the mush zone; however, grain size and porosity will be the important parameters dictating the segregation timescales (Bachmann & Bergantz, 2004). These timescales can be relatively fast, especially if hindered settling is the dominant process, and have been suggested to be 10^4-10^5 years for the extraction of ~500 km^3 of rhyolite (Bachmann & Bergantz, 2004). Wilson & Charlier (2009) show evidence for much shorter timescales around ~3000 years associated to melt accumulation of the ~530 km^3 Oruanui magma (TVZ), which is in line with findings by Gualda et al. (2012-b) on the Bishop Tuff. These timescales for melt accumulation are within the available timeframe for the Mamaku and Ohakuri rhyolites. However, if we consider that the Type 1 and Type 2 represent two temporally distinct melt extraction episodes, these would have to be closely timed, suggesting very efficient melt extraction from the crystal mush, and, consequently, efficient rejuvenation of this mush. In the central TVZ where tectonism and magmatism are understood to be closely linked (Wilson et al., 2009, Rowland et al., 2010) it is possible that regional-scale tectonism may have played an important role as an additional mechanism accelerating the melt extraction process from the crystal mush. The short time window to extract the melt could also be one of the reasons for the isolated magma batches, suggesting that there was not enough time for amalgamation of the different batches into either a single large magma body or as two separate magma chambers located below the Rotorua and Ohakuri centres.

2.6.5. Eruption Triggers

The Mamaku and Ohakuri eruptive events are thought to have occurred over the course of several days or weeks (Gravley et al., 2007). The initial event resulted in the fall deposit sourced from the Ohakuri region, followed by the Mamaku pyroclastic flows, and the Ohakuri flows each containing three distinct magma types (Gravley et al., 2007). This leads to the question as to what triggered this sequence of eruptive events and allowed the almost synchronous eruption of several distinct magma types. The quest to understand triggers of such large, silicic ignimbrite-forming

eruptions is frequently addressed in the literature (e.g. Sparks et al., 1977; Pallister et al., 1992; Manga & Brodsky, 2006; da Silva et al., 2008). It is often suggested that destabilisation of the magma chamber is induced by overpressurisation, either by magmatic input into the chamber, or by applying an external trigger (i.e. depressurisation, or change of regional stress regime). A magmatic intrusion can increase the internal pressure of a magma chamber by either directly increasing the volume by liquid mass addition, or indirectly by increasing the volatile contents as a more mafic magma quenches and exsolves a vapour phase (e.g. Sparks et al., 1977; Blake, 1981; Pallister et al., 1992; Folch & Marty, 1998).

Quartz CL has been used in a number of recent studies to identify the involvement of mafic and felsic replenishment where direct evidence of mass addition is otherwise cryptic (e.g. Matthews et al., 2011; Wilcock et al., 2012). The CL zoning is used as a proxy for variations in Ti concentration in quartz (Wark & Spear, 2005), and crystallisation temperature by virtue of the Ti-in-quartz thermometer (Wark & Watson, 2006). This mafic or felsic input is suggested to be responsible for the occurrence of bright rims that form sharp contacts along, or truncate, interior zones in these quartz crystals (i.e. increase in Ti and temperature; Wark et al., 2007; Wiebe et al., 2007). Quartz CL in the Mamaku and Ohakuri eruptive products does not record crystallisation of quartz crystals at uniformly higher temperature conditions prior to eruption. Bright CL rims are present in less than 10% of the imaged quartz (Fig. 2.11), and furthermore, these bright rims are not systematically present throughout the investigated pumice clasts (i.e. quartz in single pumice do not all have bright rims). In a crystal-poor magmatic system such as the Ohakuri-Mamaku, the heat transfer through individual batches would have been rapid and be recorded in a high proportion of quartz phenocrysts. The origin of the rare bright CL rims is, however, unclear, other than that they may represent relicts from a magmatic reservoir that fed a previous eruption.

In contrast to the quartz zoning, plagioclase crystals only present normal zoning with regard to An, which indicates that they do not record an addition of a less evolved magma, nor an increase

in temperature during its crystallisation history. Despite the presence of rare mafic blebs described in Milner et al. (2003) and Gravley et al. (2007), no basalt co-erupted with either the Mamaku or Ohakuri eruptions, unlike in other central TVZ eruptions where mafic input is the suggested trigger. For these eruptions basaltic clasts and/or mingling and mixing has been directly observed in the pyroclastic deposits (e.g. Kaharoa eruption, Leonard et al., 2002; Whakamaru eruption, Brown et al., 1998-a; Matthews et al., 2011; Matahina eruption, Deering et al., 2011-b). Consequently, we consider a shallow mafic injection trigger unlikely for the Mamaku-Ohakuri eruptions.

Another way to trigger an eruption is to externally induce eruption by depressurisation of the magma chamber or by changing the orientation of stress (i.e. tectonic control). Close relationships between volcanic eruptions and tectonics are a controversial topic, even though there are examples of recent eruptions directly following large earthquakes [e.g. the 1960 fissure eruption after a large M 9.5 earthquake in Chile (Lara et al., 2004); the 2004-2005 M >8.5 earthquake series preceding the eruption of the Talang volcano, Indonesia (Walter & Amelung, 2007)]. An external, tectonic trigger has also been suggested for the ~5 Ma Atana eruption, Central Andes, as indicated by geochemistry, caldera geometry and regional faulting (Lindsay et al., 2001). Conversely, volcanic eruption can reactivate regional faults (e.g. the 6.5 ka Kikai caldera eruption triggered two large earthquakes in southern Kyushu, Japan; Naruo & Kobayashi, 2002). These examples are all in subduction-related volcanic arc settings; however, for the TVZ, which is a 'rifted' arc, it may be appropriate to also compare with examples from volcanic regions undergoing high rates of extension.

In other continental rift settings, close associations between regional tectonism and volcanism have frequently been observed [e.g. coupled earthquake swarm and volcanism during the 2007 Oldoinyo Lengai eruption in the East African Rift (Baer et al., 2008)], and silicic volcanism has also been suggested to be a precursor event for rift segment propagation events (Afar triple point; Lahitte et al., 2003). In the TVZ several studies describe that close relationship, as well as important

controls exerted by the regional tectonics on caldera structure and geometry (e.g. Cole et al., 2010, Seebeck et al., 2010). Furthermore, it has been suggested that the extensional regime is related to the lateral magma movements in the shallow crust for the Oruanui super-eruption (Taupo Volcanic Centre; Allan et al., 2012). The paired Rotoiti and Earthquake Flat eruption is another example in the TVZ, where regional tectonic adjustments related to the caldera collapse from the Rotoiti eruption potentially triggered the Earthquake Flat eruption (Charlier et al., 2003).

For the Mamaku and Ohakuri paired event, a structural link between the two calderas has been established, and the caldera geometries are related to regional faults (Milner et al., 2002, Gravley et al., 2007; Ashwell et al., 2013). The Rotorua caldera shows a complex geometry where regional faults and magma withdrawal have interacted to generate complex collapse-style morphologies (down-sag, trapdoor and piecemeal; Milner et al., 2002; Ashwell et al., 2013). In the Ohakuri – Rotorua area, linked eruption-related regional faulting has also been identified (Gravley et al., 2007), and the lateral magma withdrawal associated with the Ohakuri eruption is linked to collateral subsidence of a large area (Gravley et al., 2007). Furthermore, the Mamaku and Ohakuri ignimbrite represents the last pulse of the ignimbrite flare-up (~340-240 ka), and this is suggested to coincide with a period of accelerated rifting (Gravley et al., 2009; D. Gravley et al., in preparation). Therefore, in the absence of evidence for mafic injections, an external tectonic eruption trigger is possible and this may in turn have set off a cascading sequence of subsurface magma batch linkage and eruption. We suggest here that reactivation and amalgamation of fault segments were associated with the evacuation of >245 km^3 of rhyolitic magma from two different locations, lateral migration of magma, formation of calderas and a collateral volcano-tectonic depression, all in a very short time period.

2.7. Conclusions

New melt inclusion and matrix glass data are combined with existing bulk-rock and mineral data, to retrace the evolution of the Mamaku and Ohakuri magmatic systems associated with the paired eruption and two caldera collapses in the central TVZ. Both volcanic centres erupted chemically distinct magma types, with the types being very similar between the two centres. Based on this comprehensive geochemical analysis, we show that:

1. The Rotorua-Ohakuri region included at least five different magma batches, extractedfrom the same source reservoir (i.e. a continuous intermediate mush zone beneath that area);
2. At least four of these magma batches were isolated from each other in the upper crust and evolved separately until eruption, as no mixing and mingling between these magma types has been identified;
3. Minor geochemical differences in the batches are likely associated with different extraction conditions of the rhyolitic melt from a slightly heterogeneous intermediate mush zone;
4. The similar magma types at the Ohakuri and the Rotorua caldera centres could be linked to parallel extraction conditions, and regional tectonics may have accelerated the extraction mechanism;
5. Lack of evidence in melt compositions for mafic recharge prior to eruption, and from quartz-cathodoluminescence imaging, suggest that a magmatic input is unlikely to be an eruption trigger. However, tectonic activity, which was previously suggested as a potential trigger (Gravley et al., 2007), could be an efficient way to activate these isolated magma batches. The evacuation of one magma batch could adjust regional tectonics sufficiently to trigger and allow simultaneous eruption of an adjacent melt batch;
6. Collateral subsidence features between the calderas, identified by detailed surface mapping (Gravley et al., 2007), suggest lateral magma withdrawal, which is in good agreement with the model of juxtaposed small magma chambers in the upper crust.

Recent studies of major caldera-forming eruptions in the central TVZ have appealed to a model of multiple magma batches, which seems to work well with the dynamic extensional regime. It is noteworthy here that the TVZ presents exceptional spatial/temporal resolution, enabling good correlation between surface features, geochemistry, and geochronology of the deposits. Without detailed fieldwork and a comprehensive geochemical evaluation at the crystal scale, the Mamaku and Ohakuri events might have been regarded as a single, large eruption associated with a caldera collapse encompassing the Rotorua, Kapenga and Ohakuri area [approximately 450 km^2; i.e. Valles Caldera, 434±2 km^2 and Long Valley, 350±5 km^2 (e.g. Geyer & Marti, 2008)]. From this study, we suggest that the tectonically triggered eruption of a single, small magma chamber can in turn trigger additional eruptions through fault linkages between one or more small magma chambers, and lead to an otherwise unexpected, more catastrophic event. These results have important implications for hazard identification and risk assessment in active volcanic regions that host large calderas. In addition, the evidence for these rhyolitic magma batches being especially shallow could be important to volcanic monitoring and recognizing signs of caldera unrest.

Table 2.1: Mamaku and Ohakuri average bulk pumice compositions.

	Ohakuri						Mamaku					
	Type 1		Type 2		Type 3		Type 1		Type 2		Type 3	
	XRF (n=46) ICP-MS (n=4)		XRF (n=46) ICP-MS (n=4)		XRF (n=8)		XRF (n=17) ICP-MS (n=4)		XRF (n=50) ICP-MS (n=6)		XRF (n=8)	
Bulk pumice	**Avg.**	**1 σ**	**Avg.**	**1 σ**	**Avg.**	**1 σ**	**Avg.**	**1 σ**	**Avg.**	**1 σ**	**Avg.**	**1 σ**
SiO_2	77.30	0.40	74.28	1.38	68.75	1.03	76.20	1.07	73.85	0.29	68.89	1.87
TiO_2	0.15	0.01	0.28	0.03	0.51	0.04	0.18	0.03	0.29	0.03	0.37	0.06
Al_2O_3	12.45	0.23	14.02	1.23	16.15	0.58	13.56	0.90	14.64	0.42	18.99	2.15
Fe_2O_3	1.46	0.05	2.32	0.27	3.60	0.39	1.57	0.23	2.29	0.21	3.07	0.38
MnO	0.05	0.00	0.07	0.01	0.12	0.02	0.06	0.01	0.07	0.02	0.09	0.02
MgO	0.20	0.05	0.35	0.06	0.72	0.06	0.15	0.08	0.30	0.06	0.38	0.17
CaO	0.73	0.03	1.39	0.16	2.80	0.26	0.83	0.17	1.24	0.22	1.70	0.31
Na_2O	3.67	0.23	3.81	0.44	4.75	0.33	3.79	0.12	4.06	0.13	4.09	0.35
K_2O	3.98	0.11	3.46	0.18	2.51	0.29	3.66	0.19	3.24	0.13	2.39	0.34
P_2O_5	0.01	0.01	0.03	0.01	0.08	0.04	0.01	0.01	0.02	0.01	0.02	0.01
LOI	4.40	1.13	3.55	0.48			4.97		3.16	0.28	4.17	1.42
Total	95.48	1.12	96.32	0.48			96.19	0.87	96.52	0.24		
Quartz (Q)	38.9	1.4	35.5	0.9	24.7	2.3	38.2	0.9	34.8	0.8	31.8	2.2
Orthoclase (Or)	23.5	0.6	20.4	1.1	14.9	1.7	21.6	1.1	19.1	0.8	14.1	2.0
Albite (Ab)	31.0	2.0	32.2	3.7	40.2	2.8	32.0	1.0	34.4	1.1	34.6	2.9
Anorthite (An)	3.6	0.1	6.7	0.8	13.4	1.5	4.0	0.8	6.0	1.0	8.3	1.6
Rb	125	7	108	9	85	17	111	8	94	3	70	30
Sr	58	2	121	13	244	26	72	18	114	14	133	62
Y	*27.92*	*4.79*	*27.03*	*4.94*	26	2	*37.66*	*4.05*	*34.75*	*3.88*	36	2
Ba	*837.03*	*68.65*	*822.20*	*22.63*	634	17	*791.63*	*73.61*	*761.10*	*52.65*	784	96
La	*25.64*	*5.05*	*25.00*	*7.24*	24	5	*30.60*	*4.83*	*23.26*	*5.38*	28	4
Ce	*70.05*	*15.72*	*63.73*	*15.51*	61	18	*63.73*	*15.51*	*64.26*	*9.35*	76	4
Pr	*6.87*	*0.20*	*6.23*	*0.83*			*7.03*	*0.16*	*6.70*	*0.44*		
Nd	*26.00*	*0.26*	*23.51*	*4.01*	38		*26.17*	*0.23*	*25.06*	*2.12*	29	8
Sm	*5.53*	*0.20*	*5.07*	*1.04*			*5.70*	*0.10*	*5.37*	*0.49*		
Th	*15.08*	*3.06*	12	1	17	5	14	1	13	2	13	2
U	*4.21*	*0.34*	3	0			4	0	3	0		
V	*3.29*	*1.39*	*12*	*4*	3	0	*5*	*1*	*8*	*5*	3	1
Cr	*3.85*	*1.21*	*3*	*1*	3	1	*4*	*1*	*3*	*1*	3	1
Ni	*16.33*	*0.58*	16	0			18		16	0		
Cu	3	2	7	4	72	4	1		27	17	76	35
Zn	40	2	47	5	14	2	71		56	4	17	3
Zr	167	9	250	7	181	48	190	28	279	27	218	69
Nb	*12.84*	*1.30*	*13.07*	*1.60*	9	1	*12.70*	*1.57*	*13.26*	*1.57*	11	2
Eu	*0.83*	*0.08*	*1.15*	*0.19*			*0.96*	*0.10*	*1.06*	*0.22*		
Gd	*6.07*	*0.28*	*5.45*	*1.21*			*6.14*	*0.32*	*5.69*	*0.34*		
Tb	*0.92*	*0.03*	*0.83*	*0.15*			*0.97*	*0.04*	*0.91*	*0.07*		
Dy	*5.40*	*0.09*	*4.94*	*1.13*			*5.74*	*0.20*	*5.21*	*0.46*		
Ho	*1.12*	*0.06*	*1.02*	*0.25*			*1.23*	*0.03*	*1.10*	*0.13*		
Er	*3.40*	*0.11*	*3.04*	*0.64*			*3.80*	*0.08*	*3.37*	*0.43*		
Yb	*3.73*	*0.16*	*3.42*	*0.73*			*3.94*	*0.26*	*3.58*	*0.32*		
Lu	*0.59*	*0.02*	*0.54*	*0.11*			*0.61*	*0.05*	*0.55*	*0.04*		
Hf	*4.87*	*0.16*	*6.06*	*0.13*			*5.19*	*0.99*	*6.31*	*0.55*		
Ta	*2.04*	*0.20*	*1.50*	*0.05*			*1.58*	*0.44*	*1.49*	*0.55*		
Pb	*39.07*	*3.14*	*28.51*	*2.54*	12	2	*42.01*	*8.45*	*36.56*	*6.93*	22	11

Major elements are given in wt% and trace elements in ppm. Compilation from published work (Milner et al., 2003; 2001; Gravley, 2004); XRF (University of Canterbury and Michigan State University); ICP-MS (Michigan State University) for the analysis in *italics*.

Q, Or, Ab and An values are CIPW normative minerals.

Table 2.2: Summary of the Mamaku and Ohakuri magma types.

	Crystal content	**Mineral assemblage**	**plg : qtz ratio**
Ohakuri Type 1	< 1 vol % [1]	plg + qtz + opx + Fe/Ti ox [1]	~ 1 [1]
Ohakuri Type 2	< 3-5 vol % [1]	plg + qtz + opx + Fe/Ti ox [1]	~ 2 [1]
Ohakuri Type 3	10-15 vol % [1]	plg + qtz + opx + Fe/Ti ox ± *hbl* [1]	~ 4 [1]
Ohakuri fall deposit	--	plg + qtz + opx + Fe/Ti ox [1]	--
Mamaku Type 1	6-7 vol % [1, 2]	plg + qtz + opx + Fe/Ti ox ± *augite* ± *hbl* [2]	~ 2 [1]
Mamaku Type 2	6-7 vol % [1] ; 5-7 vol % [2]	plg + qtz + opx + Fe/Ti ox ± *augite* [2]	~ 2 [1]
Mamaku Type 3	4-5 vol % [2]	plg + opx + Fe/Ti ox ± qtz ± *augite* ± *hbl* [2]	~ 8 [2]

[1]Gravley, 2004; [2] Milner, 2001
plg - plagioclase; qtz - quartz; opx - orthopyroxene; ox - oxide
minerals *in italic* - only trace amount present

Table 2.3: Mamaku and Ohakuri representative mineral chemistry.

	Eruption	Magma type	SiO_2	TiO_2	Al_2O_3	FeO	MnO	MgO	CaO	Na_2O	K_2O	Total	Ab%	An%	Or%	Mg#	En%	fO_2 (ΔNNO)	T (°C)
Plagioclase																			
D-90_plag1core	Ohakuri	Type 1	62.06		24.37	0.22			5.19	8.35	0.65	100.84	71.7	24.6	3.7				
D-90_plag1rim	Ohakuri	Type 1	62.18		25.00	0.23			5.28	8.33	0.61	101.63	71.5	25.0	3.4				
D-60_plag3core	Ohakuri	Type 2	61.15		24.37	0.23			5.39	8.34	0.48	99.95	71.7	25.6	2.7				
D-60_plag3rim	Ohakuri	Type 2	62.18		23.97	0.26			4.99	8.08	0.56	100.05	72.1	24.6	3.3				
D-87_plag2core	Ohakuri	Type 3	61.55		24.55	0.22			5.58	8.12	0.43	100.44	70.7	26.9	2.5				
D-87_plag2rim	Ohakuri	Type 3	61.88		24.02	0.23			4.95	8.35	0.61	100.04	72.7	23.8	3.5				
MKP35-1core	Mamaku	Type 1	62.55	-	23.17	0.33	0.06	-	4.96	8.51	0.50	100.16	73.5	23.7	2.8				
MKP35-1rim	Mamaku	Type 1	60.31		24.89	0.39	0.22	0.01	6.42	7.71	0.43	100.51	66.8	30.7	2.5				
MKP116-3core	Mamaku	Type 2	62.87	0.09	23.24	0.24	0.07	0.03	4.76	8.83	0.64	101.01	74.3	22.1	3.5				
MKP116-3rim	Mamaku	Type 2	63.31	0.10	22.99	0.34	0.04	0.04	4.21	8.85	0.63	100.51	76.4	20.1	3.6				
MPK29-1core	Mamaku	Type 3	63.65	0.06	24.67	0.31	0.04	0.03	5.79	5.66	0.40	100.69	62.0	35.1	2.9				
MPK29-1rim	Mamaku	Type 3	61.98	0.01	23.60	0.15		-	5.04	7.31	0.49	98.68	70.2	26.7	3.1				
Orthopyroxene																			
D-90_opx2core	Ohakuri	Type 1	49.96	0.08	0.16	34.43	2.37	12.95	0.98			100.92				40.1	39.3		
D-90_opx2rim	Ohakuri	Type 1	49.52	0.09	0.18	32.98	2.18	13.98	1.04			99.97				43.0	42.1		
D-60_opx2core	Ohakuri	Type 2	50.82	0.09	0.26	30.76	1.95	15.48	1.24			100.60				47.3	46.0		
D-60_opx2rim	Ohakuri	Type 2	51.08	0.17	0.53	28.77	1.56	16.72	1.30			100.14				50.9	49.5		
D-87_opx1core	Ohakuri	Type 3	52.48	0.18	0.74	23.45	1.25	21.56	1.12			100.77				62.1	60.7		
D-87_opx1rim	Ohakuri	Type 3	51.07	0.09	0.21	30.65	1.96	15.34	1.16			100.48				47.2	46.0		
MKP3-1core	Mamaku	Type 1	51.69	0.16	0.37	27.01	1.64	18.28	1.28			100.53				54.7	53.2		
MKP35-1rim	Mamaku	Type 1	50.46	0.12	0.26	30.48	2.47	15.50	1.17			100.53				47.6	46.4		
MKP116-1core	Mamaku	Type 2	49.72	0.21	0.33	31.80	2.07	14.79	1.14			100.10				45.3	44.2		
MKP116-1rim	Mamaku	Type 2	49.99	0.14	0.34	32.51	2.30	14.26	1.20			101.02				43.9	42.7		
MKP29-1core	Mamaku	Type 3	50.95	0.15	0.36	30.82	2.24	15.56	1.23			101.38				47.4	46.1		
MKP29-1rim	Mamaku	Type 3	51.30	0.10	0.27	31.01	2.27	15.04	1.23			101.40				46.4	45.1		

After Gravley (2004); Milner (2001); Deering et al. (2008).

Table 2.3: Mamaku and Ohakuri representative mineral chemistry (cont.).

	Eruption	Magma type	SiO_2	TiO_2	Al_2O_3	FeO	MnO	MgO	CaO	Na_2O	K_2O	Total	Ab%	An%	Or%	Mg#	En%	fO_2 (ΔNNO)	T (°C)
Oxides																			
D-90_ox mt	Ohakuri	Type 1	0.11	10.97	0.97	80.51	0.70	0.43	0.02			93.72						-0.5	768
D-90_ox1ilm	Ohakuri	Type 1	0.04	47.61	-	47.28	1.47	1.05	0.00			97.45							
UC1204mt	Ohakuri	Type 2	0.10	11.65	1.09	81.43	0.78	0.54	0.00			95.70						-0.34	796
UC1204ilm	Ohakuri	Type 2	0.02	47.31	0.05	47.78	1.33	1.17	-			97.85							
D-87_ox1mt	Ohakuri	Type 3	0.06	11.04	1.17	80.86	0.76	0.58	0.03			94.50						0.21	799
D-87_ox2ilm	Ohakuri	Type 3	0.09	47.07	0.09	47.96	1.28	1.33	-			97.83							
UC1185mt	Mamaku	Type 1	0.06	11.37	1.11	79.98	0.77	0.56	0.02			94.25						-0.44	784
UC1185ilm	Mamaku	Type 1	0.01	47.55	0.06	47.41	1.30	1.24	0.01			97.78							
UC1176mt	Mamaku	Type 2	0.09	11.29	0.99	82.22	0.80	0.46	0.04			96.03						-0.27	793
UC1176ilm	Mamaku	Type 2	0.04	47.31	0.05	48.37	1.41	0.96	0.18			98.33							

Major elements are given in wt%.
Data after Gravley (2004); Milner (2001); Deering et al. (2008).
Fe-Ti oxide geothermometry after Ghiorso & Evans (2008) for oxygen fugacity ($fO2$) and temperature (T) calculations.
Core and rim mineral chemistry was acquired using an electon microprobe analyser (EPMA) at the University of Michigan (Cameca SX100; Deering et al., 2008; 2010) and Victoria University of Wellington (JEOL Superprobe 733; Milner, 2001; Milner et al., 2003).

Table 2.4: Mamaku and Ohakuri average matrix glass compositions.

	Ohakuri Fall deposit		**Ohakuri Type 1**		**Ohakuri Type 2**		**Mamaku Type 1**		**Mamaku Type 2**		**Mamaku Type 3**		**SE**[a] VG 568
Matrix glass	avg.	1 σ	avg.	1 σ	avg.	1 σ	avg.	1 σ	avg.	1 σ	avg.	1 σ	*n=35*
SiO_2	78.24	0.23	80.25	0.34	80.08	0.52	78.58	0.21	78.56	0.29	77.76	0.48	*0.148*
TiO_2	0.08	0.05	0.09	0.05	0.16	0.05	0.07	0.05	0.11	0.06	0.17	0.08	*0.011*
Al_2O_3	12.16	0.12	12.17	0.10	12.04	0.05	12.03	0.11	12.04	0.16	13.15	0.19	*0.137*
FeO	1.07	0.05	1.09	0.07	1.24	0.07	1.03	0.05	1.23	0.06	1.39	0.10	*0.117*
MgO	0.06	0.01	0.06	0.01	0.10	0.00	0.06	0.01	0.08	0.01	0.13	0.03	*0.006*
CaO	0.55	0.03	0.52	0.04	0.72	0.01	0.53	0.03	0.70	0.03	1.02	0.03	*0.002*
Na_2O	3.66	0.14	2.11	0.24	2.15	0.41	3.54	0.13	3.61	0.10	3.21	0.39	*0.006*
K_2O	4.17	0.06	3.70	0.29	3.50	0.23	4.15	0.08	3.66	0.07	3.17	0.19	*0.091*
Total	95.47	0.33	95.40	0.32	96.34	0.67	95.96	0.51	95.80	0.47	96.44	1.26	*0.026*
Quartz (Q)	38.9		51.8		51.5		40.1		41.0		43.5		
Orthoclase (Or)	24.6		21.9		20.7		24.5		21.6		18.7		
Albite (Ab)	31.0		17.8		18.2		30.0		30.5		27.1		
Anorthite (An)	2.7		2.6		3.6		2.6		3.5		5.0		

Major elements are given in wt%. Analyses are normalised to anhydrous conditions.
Total number of analysed pumice clasts: 28.
Major element compositions determined by the electron microprobe (JEOL 733 Superprobe) at the University of Washington (UW). Analytical conditions: acceleration voltage 15kV, beam current 5 nA, and 10 μm in diameter beam; Counting times 20 sec. for Si and P; 40 sec. for all the other elements.
[a] Standard error = standard deviation divided by the square root of the number of samples.
Analytical errors: <1 % for SiO_2 and Al_2O_3, <3 % for Na_2O and K_2O, and <7 % for FeO and CaO.

Table 2.5: Average major element composition for Mamaku and Ohakuri quartz-hosted melt inclusions.

	Ohakuri Fall deposit *n=19*		**Ohakuri Type 1** *n=35*		**Ohakuri Type 2** *n=22*		**Ohakuri Type 3** *n=8*		**Mamaku Type 1** *n=43*		**Mamaku Type 2** *n=21*		**SE**[a] VG 568 *n=35*
	from 5 clasts, 16 quartz crystals		*from 4 clasts, 25 quartz crystals*		*from 4 clasts, 20 quartz crystals*		*from 1 clast, 4 quartz crystals*		*from 6 clasts, 30 quartz crystals*		*from 3 clasts, 13 quartz crystals*		
Melt inclusions	avg.	1 σ	avg.	1 σ	avg.	1 σ	avg.	1 σ	avg.	1 σ	avg.	1 σ	
SiO_2	78.00	0.21	78.55	0.22	78.85	0.30	79.47	0.59	78.54	0.69	78.59	0.40	*0.148*
TiO_2	0.08	0.04	0.10	0.05	0.12	0.05	0.14	0.06	0.13	0.08	0.13	0.06	*0.011*
Al_2O_3	12.14	0.12	11.77	0.10	11.63	0.14	11.37	0.36	11.86	0.33	11.80	0.21	*0.137*
FeO	0.94	0.07	1.01	0.09	1.09	0.11	0.96	0.09	0.98	0.08	1.06	0.07	*0.117*
MnO	0.05	0.02	0.04	0.02	0.04	0.03	0.03	0.01	0.04	0.03	0.06	0.02	*0.006*
MgO	0.06	0.01	0.06	0.01	0.07	0.02	0.05	0.02	0.05	0.02	0.06	0.02	*0.002*
CaO	0.55	0.05	0.54	0.06	0.61	0.05	0.54	0.05	0.53	0.07	0.61	0.08	*0.006*
Na_2O	4.05	0.07	3.88	0.07	4.01	0.07	3.87	0.18	3.73	0.30	3.87	0.29	*0.091*
K_2O	4.12	0.08	4.10	0.10	3.65	0.14	3.61	0.18	4.13	0.17	3.82	0.21	*0.026*
Total	94.11	0.37	95.26	0.35	95.52	0.64	95.98	0.48	94.56	0.82	94.80	0.60	
WBD	5.65	0.40	4.55	0.39	4.21	0.72	3.81	0.44	5.31	0.80	5.02	0.66	
Quartz (Q)	36.7	0.7	38.3	0.6	39.4	0.9	41.2	1.9	39.1	2.6	39.2	1.8	
Orthoclase(Or)	24.3	0.5	24.2	0.6	21.6	0.8	21.3	1.1	24.4	1.0	22.6	1.3	
Albite(Ab)	34.3	0.6	32.8	0.6	33.9	0.6	32.7	1.5	31.6	2.6	32.8	2.5	
Anorthite(An)	2.6	0.3	2.5	0.3	2.8	0.2	2.5	0.4	2.5	0.4	2.9	0.5	

Major elements are given in wt%; Analyses are normalised to anhydrous conditions.
Major element compositions determined by electron microprobe (JEOL 733 Superprobe) at the University of
WBD - water by difference.
Washington (UW). Analytical conditions: acceleration voltage 15kV, beam current 5 nA, and 10 μm in
diameter beam; Counting times 20 sec. for Si and P; 40 sec. for all the other elements.
[a] Standard error = standard deviation divided by the square root of the number of samples.
Analytical errors: <1 % for SiO_2 and Al_2O_3, <3 % for Na_2O and K_2O, and <7 % for FeO and CaO.
Ti and Mn were below detection limit (0.13 wt% for TiO_2, and 0.07 wt% for MnO).

Table 2.6: Average trace element composition for Mamaku and Ohakuri quartz-hosted melt inclusions.

	Ohakuri Fall deposit *n=11*		**Ohakuri Type 1** *n=14*		**Ohakuri Type 2** *n=13*		**Ohakuri Type 3** *n=4*		**Mamaku Type 1** *n=12*		**Mamaku Type 2** *n=6*		**SE**[a] NIST 610 *n=13*
	from 5 clasts, 9 quartz crystals		*from 4 clasts, 12 quartz crystals*		*from 4 clasts, 12 quartz crystals*		*from 1 clast, 2 quartz crystals*		*from 6 clasts, 9 quartz crystals*		*from 3 clasts, 5 quartz crystals*		
Melt inclusions	avg.	1 σ	avg.	1 σ	avg.	1 σ	avg.	1 σ	avg.	1 σ	avg.	1 σ	
Li	63	8	53	3	37	9	41	4	75	8	73	2	*3*
Rb	123	5	122	11	106	8	132	10	122	7	115	10	*7*
Sr	24	4	25	5	31	4	24	3	25	6	29	8	*6*
Y	30	1	30	1	28	2	30	1	30	1	29	0	*4*
Cs	6	0	4	1	4	0	4	1	5	1	5	0	*6*
Ba	619	10	610	30	576	24	616	29	624	23	577	12	*6*
La	23	1	23	1	22	2	23	1	23	1	22	1	*7*
Ce	48	2	49	2	45	3	49	2	49	2	46	1	*3*
Pr	5	0	5	0	5	0	5	1	6	0	5	0	*5*
Nd	19	1	19	1	17	2	19	1	20	1	18	0	*5*
Sm	4	1	4	1	4	1	4	0	5	0	4	0	*29*
Th	11	1	11	1	10	1	10	1	11	1	10	1	*11*
U	2	1	3	0	2	1	3	0	1	0	1	0	*11*

Trace elements are given in ppm.
SIMS analyses with a IMS Cameca 6f (Arizona State University); 10 nA beam intensity, 10-20 μm spot size.
[a] Standard error = standard deviation divided by the square root of the number of samples.
Analytical error: < 3 % for all elements, and ~10 % for Th and U.

Chapter 3

Magmatic volatile distribution as recorded by rhyolitic melt inclusions in the Taupo Volcanic Zone, New Zealand

3.1. Abstract

The central Taupo Volcanic Zone (TVZ) is an actively rifting continental arc and is well known for its exceptionally high rate of rhyolitic magma generation and frequent caldera-forming eruptions. Two end-member types of rhyolites (R1 and R2) have been previously identified, based on differences in their bulk-rock chemistry and mineral assemblage, with hydrous phases crystallizing in the R1 type, which are not present or only rare in R2 rhyolites. Here we present new trace element and volatile data from rhyolitic melt inclusions measured in several representative eruptive deposits (R1 and R2 rhyolites) from the central TVZ to examine their volatile concentrations and origin. R1 and R2 show very distinct Cl concentrations, with R2 rhyolites being enriched in Cl by ~1000 ppm. H_2O is slightly higher in the R1 rhyolites, whereas CO_2 concentrations are similar between the two end-member types. The origin of these volatile disparities between R1 and R2 melts is attributed to differences in the initial bulk volatile content of the parental magma, possibly associated with distinct input of fluids from the subduction zone. These disparities in bulk volatile concentrations can lead to variations in relative timing of exsolution of volatile phase(s) - prior to melt inclusion entrapment.

3.2. Introduction

Volatiles play an important role in the behaviour of magmas at depth and the style of volcanic eruptions, and they are integral to the development of magmatic-derived hydrothermal systems. The major volatile species in arc volcanic systems are H, C, S and Cl (e.g. Symonds et al., 1994; Giggenbach, 1996; Fischer, 2008), and they largely originate from the mantle wedge, the subducted altered oceanic crust and its overlying sediments – possibly with some additional contribution from the continental crust (e.g. Wallace, 2005; Hilton et al., 2002; Bindeman et al., 2004; Zelenski & Taran, 2011; Chambefort et al., 2013-a). These components of subduction zones play an important role in the recycling of aqueous fluids (and fluid-mobile elements) from the surface environment, producing the distinct arc signature associated with subduction zone volcanism (e.g. Kay, 1980; Hawkesworth & Ellam, 1989; McCulloch & Gamble, 1991). However, the composition and quantity of volatiles transported to the surface by the magmas are governed by saturation state and timing of exsolution, which will strongly depend on pressure, temperature, and composition of the melt and coexisting fluid (e.g. McMillan & Holloway, 1987; Webster & Holloway, 1988; Métrich & Rutherford, 1992; Webster, 1992; Carroll & Webster, 1994; Student & Bodnar, 1999; Newman & Lowenstern, 2002; Burnham, 1994; Aiuppa et al., 2009).

Magmatic degassing has been documented in many studies, and plays a significant role in eruptive processes and styles. Degassing has been quantified at many arc volcanoes by either monitoring of gas flux at the surface (e.g. Taran et al., 1991; Giggenbach, 1996; Aiuppa et al., 2002; Edmonds et al., 2009; Zelenski & Taran, 2011) or by assessing volatile concentrations in mineral-hosted melt inclusions and volcanic glass from eruptive deposits (e.g. Anderson et al., 1989; Wallace & Gerlach, 1994; Wallace et al., 1995; Métrich & Wallace, 2008; Johnson et al., 2010; 2011; Reubi et al., 2013). Crystallisation driven exsolution of fluid phases (i.e. second boiling) has also been investigated in the context of porphyry and epithermal deposits, as the metal partitioning in these exsolved volatile phases likely plays a role in the genesis of ore deposits (e.g. Hedenquist

& Lowenstern, 1994; Lowenstern, 1994; Dilles et al., 2000; Sillitoe & Hedenquist, 2003, Heinrich et al., 2004; Simmons et al., 2005; Williams-Jones & Heinrich, 2005; Chambefort et al., 2008, 2013-a; Tosdal et al., 2009). The heat and mass transfer to hydrothermal systems and hydrothermal alteration will also be highly dependent on volatile release, which drive hydrothermal convection cells around magmatic systems (e.g. Lindgren, 1907; Elder, 1966; Norton & Knight, 1977). For decades, studies have focused on volatile exsolution during crystallisation prior to ascent and eruption of magma, and showed that evolved melts in most cases already reached volatile saturation while at low crystallinity before ascent and eruption (e.g. Anderson et al., 1989; Lowenstern et al., 1991; Lowenstern, 1993, 1994; Wallace & Gerlach, 1994; Wallace et al., 1995; Johnson et al., 2011). As such, volatile exsolution can play a significant role at different evolutionary stages within a given magmatic system. In order to better understand the role of volatile exsolution in magmatic-hydrothermal systems, questions and/or uncertainties associated with the composition and concentrations of the magmatic fluid phase need to be resolved. For instance, can we assume that most evolved magmatic systems in the same tectonic environment will have similar volatile content and saturation, and exsolve similar fluid compositions? These are important questions that should be considered when assessing heat and mass transfer in active volcanic regions.

The actively rifting central Taupo Volcanic Zone (TVZ) is well known for its exceptionally high rate of rhyolitic magma generation and frequent caldera-forming eruptions (e.g. Wilson, 1996), and the extensive petro-chemical research in the TVZ make it an ideal setting to study the diversity of volatile exsolution and fluid compositions. Heterogeneities in bulk-rock geochemistry and petrology have been identified among the erupted rhyolites (e.g. Ewart 1975; Deering et al., 2008), forming a compositional range between two end-member types (rhyolite R1 and R2; Deering et al., 2008; 2010). This diversity in rhyolite types is suggested to be related to a range in volatile compositions within their respective magmatic systems (Deering et al., 2008; 2010); however, little comparative work focussing on characterising dissolved volatile compositions

has been done (c.f. Smith et al., 2005; Liu et al., 2006; Johnson et al., 2011). Here, we have directly measured pre-eruptive volatile compositions dissolved in the melts trapped in quartz- and plagioclase-hosted melt inclusions from seven major TVZ ignimbrites and associated fall deposits erupted between ~320 and 0.7 ka, sourced from four distinct volcanic centres (Fig. 3.1; Table 3.1). Volatile and trace element concentrations are compared among the volcanic centres, to assess the main factors responsible for their distribution. We particularly focus on addressing the R2 rhyolite type with the Rotorua and Ohakuri volcanic centres, as they are less well studied compared to the R1 type and fewer data exist in the literature. The volatile species, origins, concentrations and saturation are discussed with respect to the depth of magmatic systems, and their spatial distribution.

3.3. Geological Background

The TVZ is a rifted-arc currently subject to a NW-SE extension of 5-15mm/yr, from SW to NE (Darby & Meertens, 1995; Wallace et al., 2004). It is volcanically and structurally segmented, with its northern and southern segments dominated by andesitic cone-building eruptions (Wilson et al., 1995). The 125 x 60 km central segment has been active for at least 1.8 Ma and is characterised by explosive rhyolitic caldera-forming eruptions and effusive lava dome building events, with comparatively minor andesites, dacites and basalts erupted (Houghton et al., 1995; Wilson et al., 1995; 2009; Eastwood et al., 2013). More than 6,000 km^3 of rhyolite magma has been explosively erupted from at least eight different caldera centres (Wilson et al., 2009). Rifting in the central TVZ is believed to have accelerated approximately 0.9 Ma (Wilson et al., 1995; 2009), and has led to the thinning of the crust, accompanied by voluminous basaltic magmatism intruding the lower crustal region from ~16 to 30 km depth (Harrison & White 2006, and references therein). Interrelationships between rifting, and accumulation and evacuation of large rhyolitic magma bodies are recognised (Rowland et al., 2010), and regional tectonic architecture partially controls the location and geometry of caldera structures (i.e. Okataina Volcanic Centre; Cole et al., 2010, Seebeck et

al., 2010), suggesting a close relationship between tectonics, magmatism, and volcanism (Wilson et al., 2009).

The origin of silicic magmatism through multiple stages of crustal assimilation and fractional crystallisation processes (AFC) from a basaltic parent has been highlighted in many studies (e.g. Bachmann & Bergantz, 2004; Annen et al., 2006). Evidence for AFC processes in the central TVZ have been presented (McCulloch et al., 1994; Deering et al., 2008; 2010), and even if basalts form <1 vol.% of erupted rocks, they must play an important role in the petrogenesis of the rhyolites, and their plutonic equivalents could make up a significant volume of the lower- to middle-crust.

For this study, we focus on some major eruptive deposits dated between ~320 ka and 0.7 ka, that provide a good representation of rhyolitic volcanism in the central TVZ in time, space and composition. These eruptive deposits are sourced from the Okataina Volcanic Centre (OVC), the Taupo Volcanic Centre (TVC) and the Rotorua and Ohakuri Volcanic Centres (RoOhVC) as outlined in Figure 3.1. Essential information of the analysed deposits are summarized in Table 3.1, and detailed information on the individual eruptive centres can be found in Wilson et al. (1995; 2009) and Cole & Spinks (2009) amongst others.

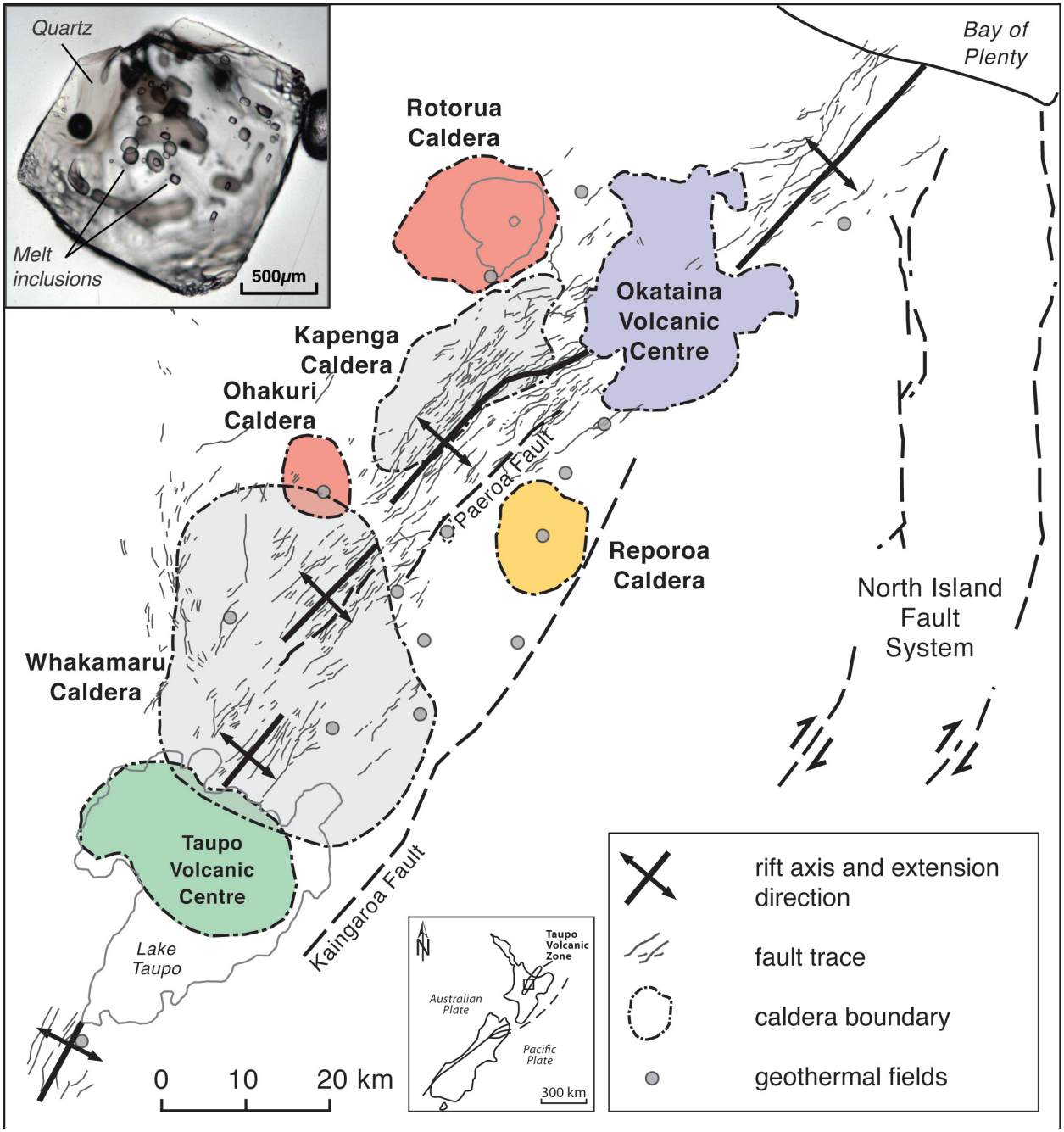

Figure 3.1: Map of the central TVZ, New Zealand. Caldera boundaries and structures after Rowland et al. (2010). Upper left inset shows a photomicrograph of a quartz crystal with melt inclusions from the Ohakuri ignimbrite.

3.4. Methodology

3.4.1. Sample preparation

We cleaned, oven-dried (50°C), and crushed 64 individual pumices from ten different fall deposits (for Matahina, Ohakuri, Oruanui, Taupo and Kaharoa eruptive deposits) and ignimbrites (Matahina, Ohakuri, Mamaku, Rotoiti and Oruanui eruptive deposits) from the central TVZ, as listed in Table 3.1. Quartz and plagioclase crystals were handpicked and melt inclusions were identified using immersion oil (refractive index 1.54). We chose only fully enclosed and glassy melt inclusions and most crystals had multiple inclusions. To avoid boundary layer effects, we selected only >50 μm melt inclusions for analysis (Roedder, 1984). For electron microprobe microanalysis (EMPA) and secondary ion mass spectrometry (SIMS), we prepared single-polished one-inch epoxy mounts, where multiple crystals (with similar size) were mounted, and specific melt inclusions present at the same level were targeted for exposure. Fourier transform infrared (FTIR) spectroscopy was performed on double-polished crystal wafers, which were different samples than the ones used for EMPA and SIMS analysis. Notes on melt inclusion appearance and on the potential presence of bubbles were taken before exposure of the targeted inclusions, and a clear distinction in the results section is made between melt inclusions hosting a bubble (open symbols) and the ones that were not (closed symbols). Melt inclusions for most of the Taupo and all of the Kaingaroa samples were plagioclase-hosted, although the Kaingaroa melt inclusions were too small for trace element analysis, and only volatile and major elements are presented here. The Whakamaru ignimbrite did not have any glassy melt inclusions and, therefore, the results were not included in this study.

3.4.2. Electron Microprobe Microanalysis (EMPA)

Major element compositions of 235 quartz-hosted and 15 plagioclase-hosted melt inclusions (some within the same crystal) were determined by electron microprobe (EPMA) at the University of Washington (UW, JEOL 733 Superprobe) and Oregon State University (OSU, Cameca SX100). We applied standard analytical conditions with an acceleration voltage of 15 kV, a beam current of 5 nA, a defocused beam of 10 μm in diameter, and measured Na first in the routine to minimise Na migration, although it can still occur at these conditions (Morgan & London 1996). All displayed results are normalised to anhydrous conditions.

Volatile compositions (Cl, F, and S) were also analysed with the same EPMA, using two distinct techniques. With the JEOL 733 Superprobe at UW, volatiles were analysed using a beam blanking technique described in Witter & Kuehner (2004), with an acceleration voltage of 10 kV, a beam current of ~100 nA, and a defocused beam of 10 μm in diameter. With the Cameca SX100 at OSU, volatiles were measured simultaneously with the major elements. We used some of the unknown samples as an internal standard between the two different electron microprobes, and no discrepancies in volatile content were observed. Two sigma (2σ) analytical error was very similar between both electron microprobes, with <3 % for Cl, and ~10 % for F. Using the beam blanking technique on the JEOL 733 Superprobe, the detection limit for Cl and F was lower with an average of 30 ppm for Cl and 70 for F. Detection limits with the Cameca SX100 was on average 80 ppm for Cl and 110 for F. Sulfur contents did not exceed the detection limit, which was ~35 ppm using the beam blanking technique on the JEOL 733 Superprobe and ~95 ppm with the Cameca SX100.

3.4.3. Secondary Ion Mass Spectrometer (SIMS)

We used the secondary ion mass spectrometer IMS Cameca 6f at Arizona State University (ASU) to analyse trace elements (Li, B, Rb, Sr, Y, Cs, Ba, La, Ce, Pr, Nd, Sm, Th and U) in 142 melt inclusions on gold-coated epoxy mounts. The primary O- beam intensity was set at 10 nA, and we used the composition of the standard NIST 610, that was measured several times during

each session, to convert the measured trace element relative to Si ratios in concentrations (ppm). 2σ analytical error was <5 % for most of the trace elements, except for Cs and Sm for which the 2σ error was 10 %, and 15 % for U.

3.4.4. Fourier Transform Infrared (FTIR) Spectroscopy

3.4.4.1. Transmission FTIR

Melt inclusions from 22 quartz crystals from 12 pumices from the Mamaku and Ohakuri ignimbrites and Ohakuri fall deposit (RoOhVC) were doubly intersected and measured by transmission FTIR at the University of Oregon. None of the analysed melt inclusions had a vapour bubble.

In most samples, total water concentrations were calculated using the near IR peaks at 5200 cm^{-1} and 4500 cm^{-1}, using calibrations and parameters after Zhang et al. (1997). For some samples we used the total OH peak at 3500 cm^{-1} to calculate the water concentration, using Beer's Law ($c=MA/\varrho d\varepsilon$, where M is the molecular weight, A is the measured absorbance, ϱ is the glass density, d is the thickness of the melt inclusion and ε is the molar absorption coefficient; Stolper 1982). CO_2 concentrations were calculated using the 2350 cm^{-1} peak and Beer's law, using a molar absorption coefficient of 1214 $Lmol^{-1}cm^{-1}$ (Behrens et al. 2004). Melt inclusion thickness was measured by interference fringes after Wysoczanski & Tani (2006). Uncertainties in measuring inclusion thickness and fitting the background are typically <0.3 wt.% for H_20 and <5 % of the amount present for CO_2.

3.4.4.2. Reflectance FTIR

We measured water content in 40 melt inclusions of the Ohakuri and Mamaku eruptive deposits (RoOhVC) by FTIR reflectance spectroscopy at the University of Oregon using the reflectance technique after the method of Hervig et al. (2003). These data were acquired on the same mounts used for EMPA and SIMS analyses. We calculated the amplitude of the ~3650 cm^{-1} peak (caused by O-H resonance) by subtracting the measured reflectance with the reflectance at

3200 cm^{-1} (corresponding to the background), and normalized this value to a reflectance taken at 4000 cm^{-1} to account for instrumental variability (Hervig et al., 2003). To calculate the water contents, we used the calibration of Johnson et al. (2011), which is based on the same rhyolitic glass standards used by (Hervig et al., 2003). Only melt inclusions with a diameter >100 μm were analysed to ensure a good signal to noise ratio; and with these analytical conditions, the estimated error was ±0.5 wt.%. We found good correlation for H_2O values between transmission and reflectance FTIR (Appendix C-3).

3.5. Results

The average major element composition of melt inclusions from the analysed eruptive deposits is presented in Table 3.2, and plotted in Figure 3.2. Quartz-hosted melt inclusions have a SiO_2 content of 75-80 wt.%, and plot on the high SiO_2 end of the bulk-rock composition of the TVZ rhyolites (after Beresford, 1997; Brown et al., 1998-a; Deering et al., 2008; Gravley, 2004; Karhunen, 1993; Milner et al., 2003; Nairn et al., 2004; Schmitz & Smith, 2004; Shane et al., 2007; Smith et al., 2002; 2004) (Fig. 3.2). The plagioclase-hosted melt inclusions (Kaingaroa and most of the Taupo analyses) include some slightly less-evolved melt relative to those that are quartz-hosted, with SiO_2 contents ranging from 73-77 wt.% (Fig. 3.2). In general, the major element composition in the melt inclusions of the analysed TVZ rhyolites is fairly homogeneous.

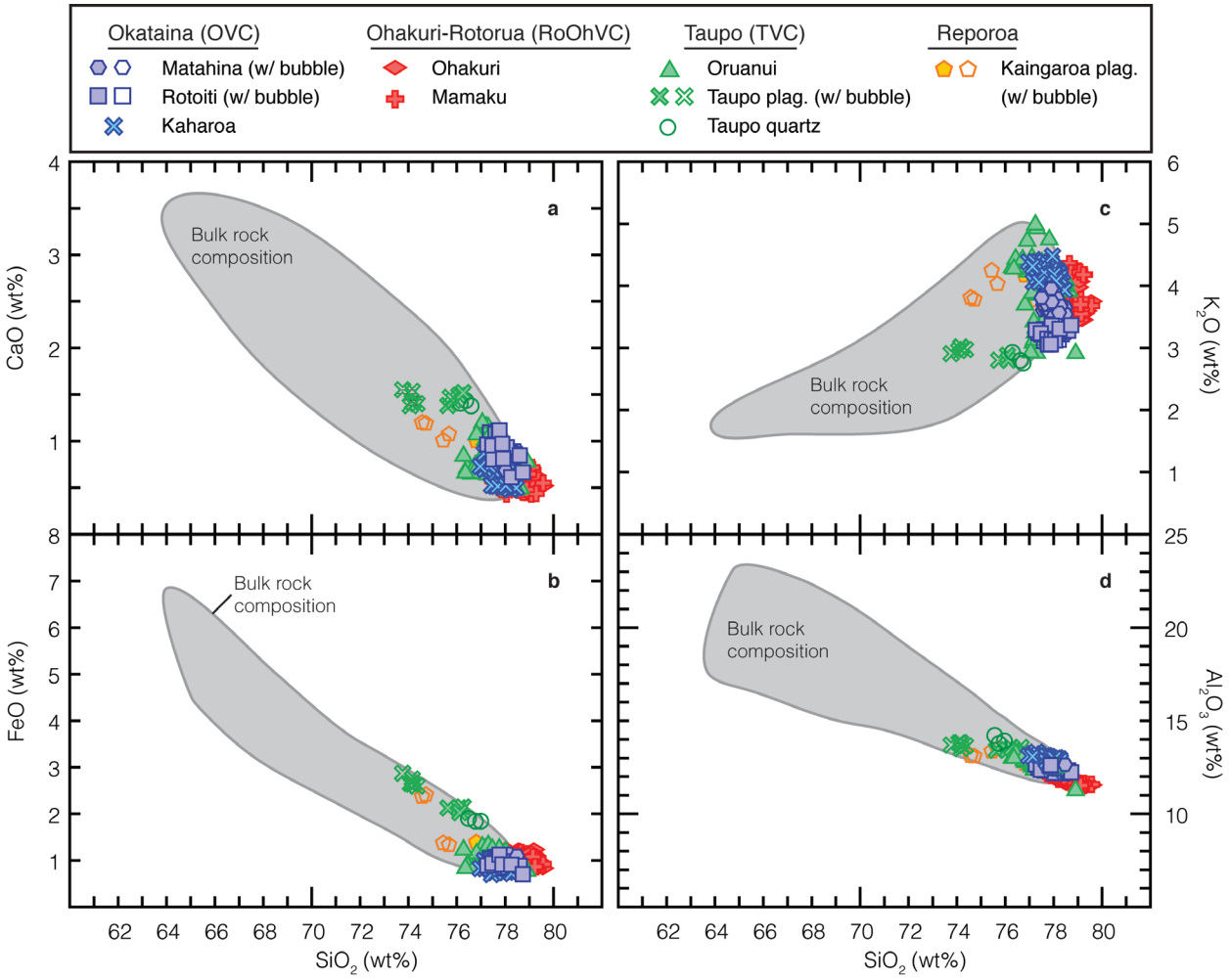

Figure 3.2: (a)-(d) Major element composition of analysed rhyolitic melt inclusions from the central TVZ, open symbols correspond to melt inclusions containing a vapour bubble. Analytical error is smaller than the size of the symbol. Grey field corresponds to bulk-rock composition after Beresford (1997); Brown et al., (1998a); Deering et al., (2008); Gravley (2004); Karhunen (1993); Milner et al., (2003); Nairn et al., (2004); Schmitz & Smith (2004); Shane et al., (2007); Smith et al., (2004).

3.5.1. Rotorua and Ohakuri Volcanic Centres (RoOhVC)

The Rotorua and Ohakuri Volcanic Centres (RoOhVC) produced R2 rhyolites (Deering et al., 2008), but prior to this study there were no volatile data available for these melts, hence we have focused on analysing melt inclusions from these magmatic systems. The Mamaku and Ohakuri eruptions both produced slightly heterogeneous magma types in their bulk composition (Gravley et al., 2007; Milner et al., 2003) and, therefore, it is useful to identify the volatile concentration with respect to their different magma types. Major and trace element data for these ignimbrites are discussed in Chapter 2- here we focus on the volatile distribution of the different magma types. The same terminology for the different magma types is used as in Milner et al. (2003) and Gravley (2004) based on the bulk magma composition, with a more evolved rhyolitic Type 1 (74-78 wt% SiO_2) and Type 2 (70-75 wt% SiO_2) for the Ohakuri and Mamaku ignimbrites, a rhyodacitic Type 3 65-72 wt% SiO_2) for the Ohakuri ignimbrite, and a rhyolitic fall deposit from the Ohakuri eruption.

Average volatile compositions are presented in Table 3.2. The Ohakuri ignimbrite melt inclusions have between 3.5 and 5 wt.% H_2O, but CO_2 is almost undetectable, with a measured maximum of 7 ppm (Fig. 3.3a). However, the data from the Ohakuri fall deposit encompass a larger range of H_2O (3.5-6 wt.%) and CO_2 (20-90 ppm) concentrations along a positive linear correlation (Fig. 3.3a). The Mamaku melt inclusions have a similar range in H_2O content as Ohakuri, but all measured Mamaku melt inclusions have some CO_2 contents ranging between 20-70 ppm (Fig. 3.3a). The data from the two Mamaku magma types plot separately, with the Mamaku Type 1 having a slightly higher H_2O-CO_2 concentration. Cl contents are high in the Mamaku and Ohakuri magmas and range from 0.25 to 0.35 wt.% for all types. No correlations are recognisable between the H_2O and Cl content for the individual magma types (Fig. 3.3b); however, a weak positive correlation exists between Cl and Y (ranging from 24 to 33 ppm) for some of the Mamaku and Ohakuri magma types (Fig. 3.4).

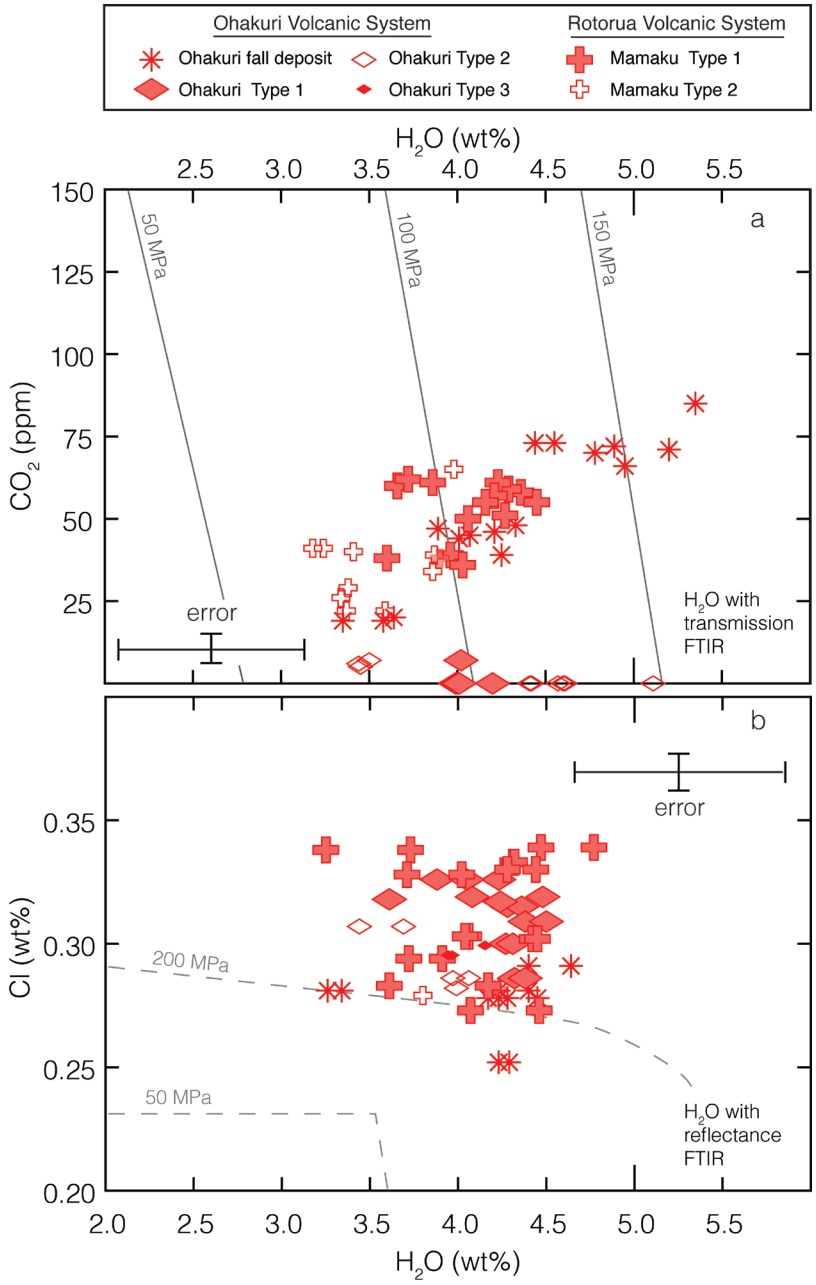

Figure 3.3: Volatile variations for the different magma types from the Rotorua and Ohakuri volcanic centres (RoOhVC). (a) CO_2 (ppm) and (b) Cl (wt.%) as a function of H_2O (wt.%); Vapour saturation isobars for 50, 100, 150 and 200 MPa at 760°C in (a) were calculated using VolatileCalc (Newman & Lowenstern, 2002), isobars of 50 and 200 MPa in (b) are from Wallace (2005), based on experimental data from Webster et al. (1999). None of the selected melt inclusions for analysis from these units have a vapour bubble. Type 1 and 2 for the Mamaku and Ohakuri ignimbrite correspond to different magma batches (Chapter 2), and the same terminology for the different magma types is used as in Milner et al. (2003) and Gravley (2004) based on the bulk magma composition. Reflectance and transmission FTIR analyses were not undertaken on the same samples.

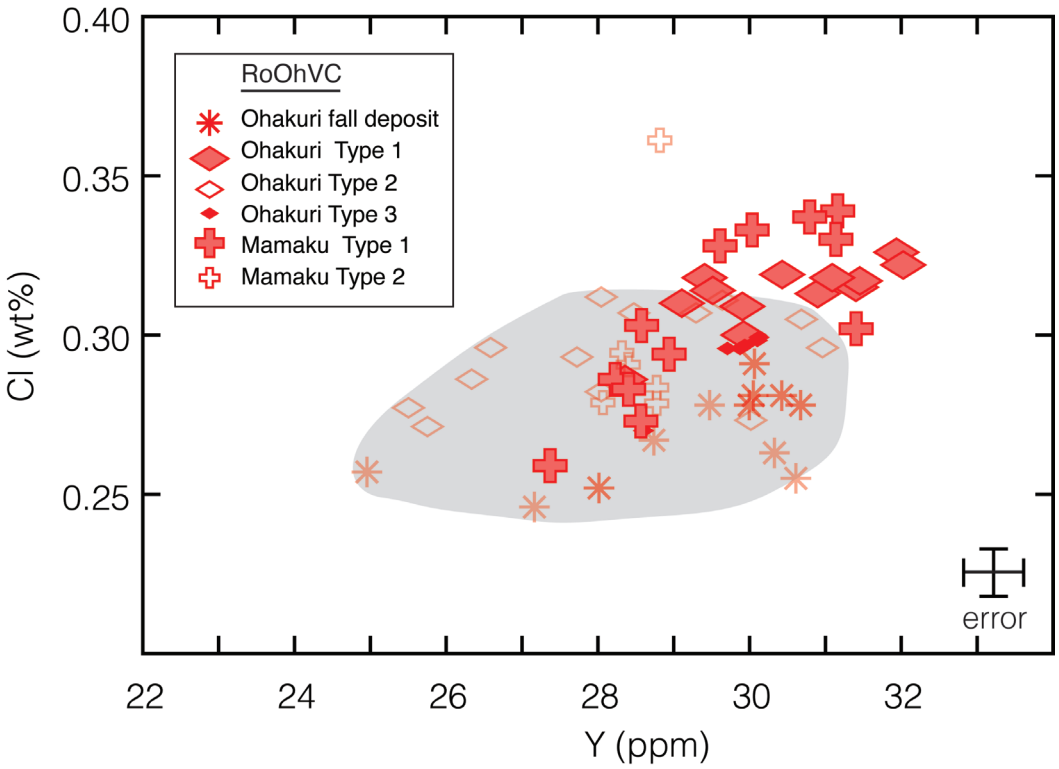

Figure 3.4: Volatile variations for the different magma types from the Rotorua and Ohakuri volcanic centres (RoOhVC); Cl (wt.%) as a function of Y (ppm). None of the selected melt inclusions for analysis from these units have a vapour bubble. Type 1 and 2 for the Mamaku and Ohakuri ignimbrite correspond to different magma batches (Chapter 2), and the same terminology for the different magma types is used as in Milner et al. (2003) and Gravley (2004) based on the bulk magma composition. For most of the magma type, the data are scattered (grey field), but there is a positive correlation between Cl and Y for the Ohakuri Type 1 and 3 and Mamaku Type 1.

3.5.2. Comparison of volatiles and trace elements among the TVZ volcanic centres

Average volatile contents of the analysed melt inclusions are also presented in Table 3.2. Chlorine contents span a large range (Fig. 3.5-3.6) and form two distinct groups; 1) the Rotorua-Ohakuri Volcanic Centres (RoOhVC), which have the highest Cl contents ranging from 0.25 to 0.35 wt.%, and 2) the Okataina Volcanic Centre (OVC) and the Taupo Volcanic Centre (TVC), which cluster within a much smaller range from 0.15 to 0.22 wt.%. The Oruanui and Taupo eruptive deposits, both from the TVC, have a few outliers, with Cl contents up to 0.28 wt.%. Fluorine contents also span a large range from almost 0 to 0.08 wt.% (Fig. 3.5b and 3.6a). Melt inclusions from the RoOhVC generally have higher F contents with a relatively small range (0.04-0.08 wt.%) (Fig. 3.5b and 3.6a). The water content in the RoOhVC melt inclusions ranges from 3.2 to 5.5 wt.% (average of 4.2 wt.%). This range of water contents is similar to the OVC and TVC values, ranging from 3 to 6 wt.% (average of 4.8 wt.% for the OVC and 4.4 wt.% for the TVC; Fig. 3.6b and c; data from Dunbar et al., 1989-b; Liu et al., 2006; Johnson et al., 2011). TVZ rhyolites have in general a low CO_2 content (Fig. 3.6c); the RoOhVC melt inclusions have between 0-90 ppm CO_2 (average ~35 ppm), which is similar to the OVC data ranging between 0-150 ppm (average ~20 ppm, Johnson et al., 2011). The Oruanui magma from the TVC has CO_2 contents ranging between 0 and 200 ppm (average ~100 ppm), and a few outliers have concentrations of ~300 ppm (Fig. 3.6c; Liu et al., 2006).

The average trace element data from the melt inclusions is presented in Table 3.3. In general, similar to the volatile data, the trace element compositions separate the RoOhVC from the OVC and TVC. The Rb/Sr ratio ranges between 3-8 for the RoOhVC and is higher than the OVC and TVC melt inclusions (0.5-3; Fig. 3.5b-c). Figure 3.7 shows selected ratios of trace elements, arranged chronologically (Fig. 3.7 a-d) and spatially (i.e. depth of the Wadati Benioff Zone; Fig. 3.7e-h). The RoOhVC is characterised by lower Th/Y and Ba/Y ratios, and higher Li/Cs and B/Cl ratios compared to the OVC. The TVC data lie in between the RoOhVC and the OVC, and the

Taupo eruption has, like the RoOhVC, low Th/Y and Ba/Y ratios. In general, Ba content ranges from 400 to 850 ppm, and La content from 7 to 28 ppm Ba and La are positively correlated for individual volcanic centres, with a linear increase of Ba with increasing La (Fig. 3.8). We observe two distinct trends, almost parallel to each other, with the OVC having the highest Ba/La ratio and the RoOhVC the lowest. The TVC data lie in between the OVC and RoOhVC, but Taupo products again do not fit with the trend of the Oruanui eruptive deposits (Fig. 3.8).

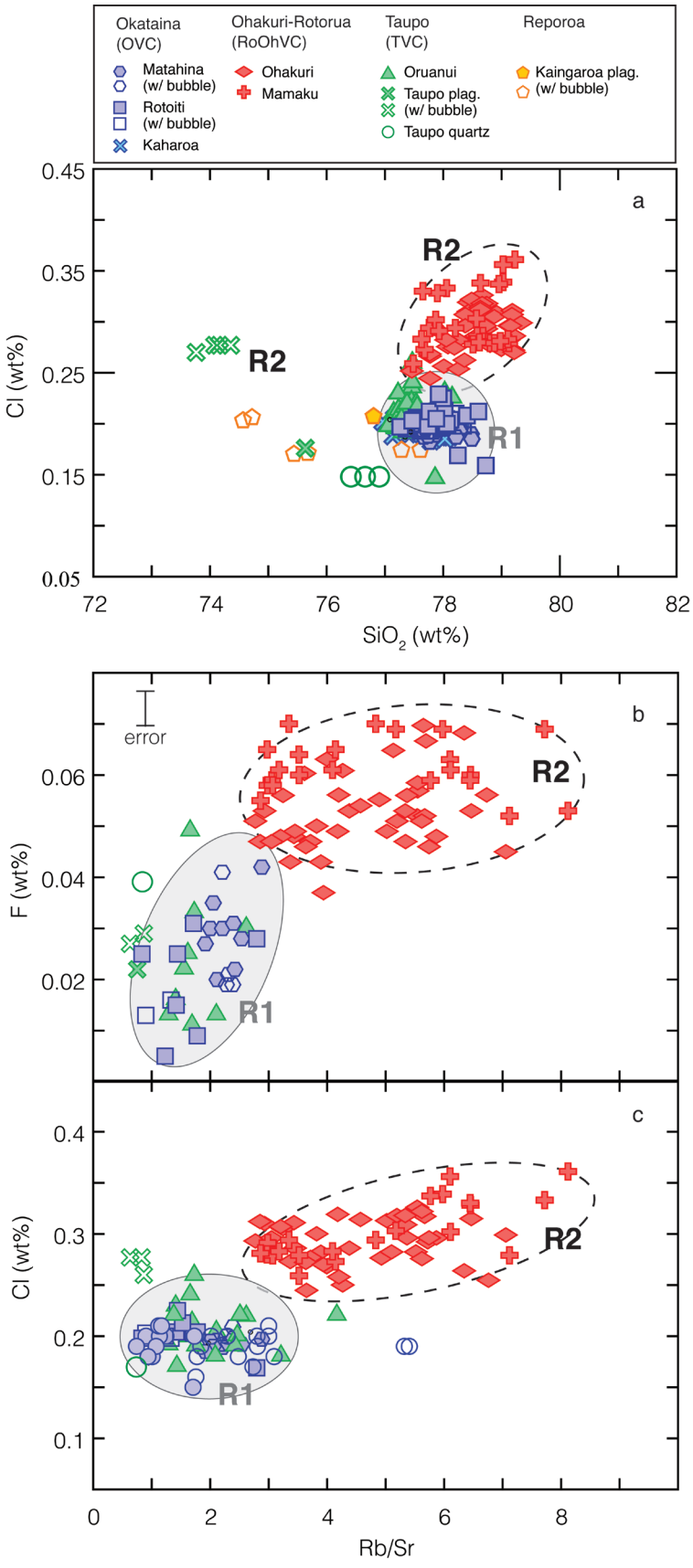

Figure 3.5: (a) Cl (wt.%) as a function of SiO_2 (wt.%), (b) Cl (wt.%), and (c) F (wt.%) as a function of Rb/Sr ratio in analysed rhyolitic melt inclusions from the central TVZ, open symbols correspond to melt inclusions containing a vapour bubble. Analytical errors for Cl and Rb/Sr ratio are smaller than the size of the symbol.

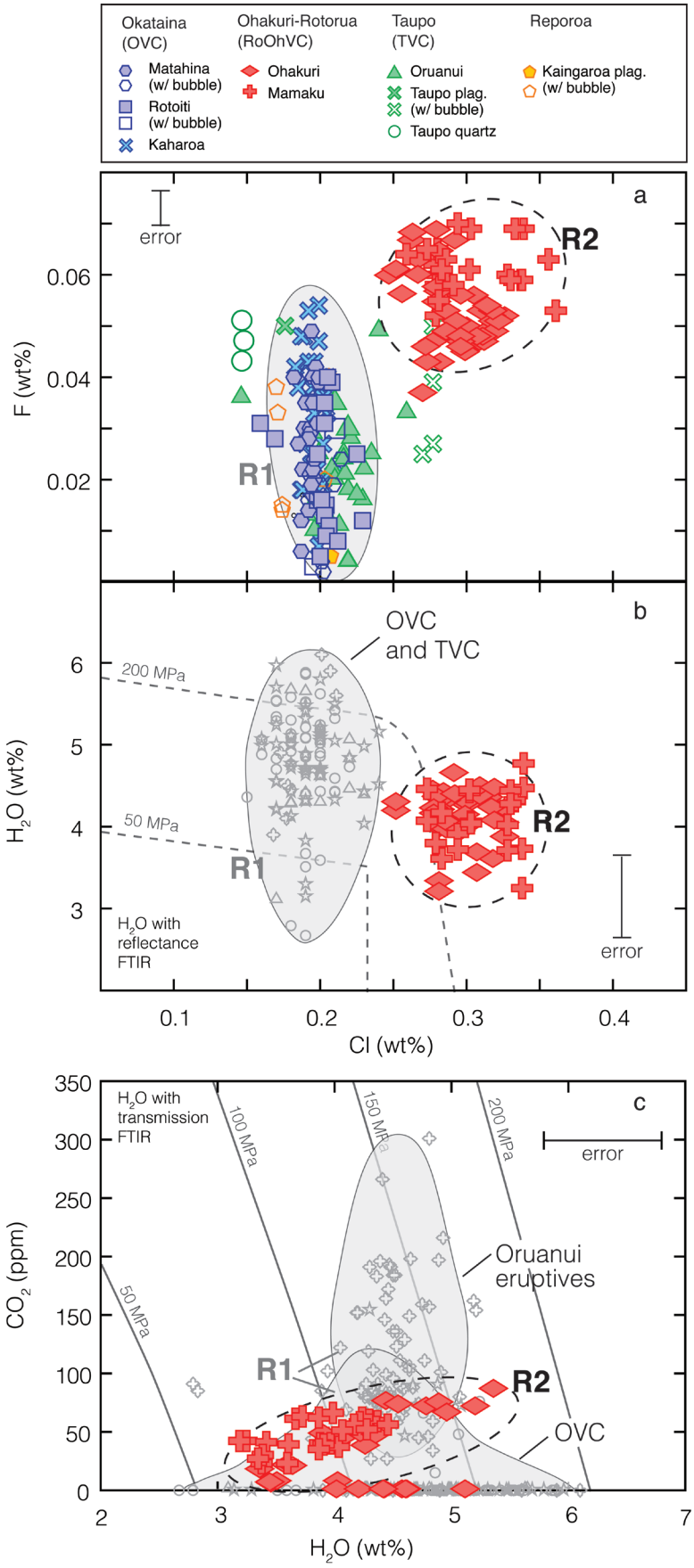

Figure 3.6: (a) F (wt.%), (b) H_2O (wt.%) as a function of Cl (wt.%); and (c) CO_2 (ppm) as a function of H_2O (wt.%) in analysed rhyolitic melt inclusions from the central TVZ, open symbols correspond to melt inclusions containing a vapour bubble. Grey field in (b) and (c) represent melt inclusion data for the OVC and the Taupo eruption (after Dunbar et al., 1989-b; Liu et al., 2006; Johnson et al., 2011). Isobars of 50 and 200 MPa in (b) are from Wallace (2005), based on experimental data from Webster et al. (1999); vapour saturation isobars for 50, 100, 150 and 200 MPa at 760°C in (c) were calculated using VolatileCalc (Newman & Lowenstern, 2002). Analytical errors for Cl are smaller than the size of the symbol.

3.6. Discussion

3.6.1. Disparities in volatile exsolution among the TVZ rhyolites

The TVZ rhyolites form a continuum in compositions between R1 and R2 rhyolites (Deering et al., 2008; 2010). The major differences between these end-member rhyolite types are their mineral assemblage, with hydrous mineral phases (hornblende ± cummingtonite ± biotite) only present in R1 rhyolites, their crystal content and bulk-rock trace-element composition. Deering et al. (2008; 2010) have interpreted these differences between R1 ad R2 to be related to changes in fH_2O, fO_2, and P-T conditions in the lower- to mid-crust (15-30 km), where the evolved magmas are generated through fractionation from repeated basalt intrusions. This led the authors of these studies to refer to the R1 and R2 types as 'cold-wet-oxidising' and 'hot-dry-reducing' rhyolites, respectively (Deering et al., 2010). Eruption temperatures and reservoir pressures of the rhyolites between R1 and R2 are, however, very similar (within estimated errors of the used thermometers and geobarometers). Temperatures mostly range between 750-800 °C (e.g. Schmitz & Smith, 2004; Wilson et al., 2006; Shane et al., 2007; Allan et al., 2012; Chapter 2), and R1 and R2 rhyolites are stored at similarly shallow depths (~100 MPa; e.g. Liu et al., 2006; Johnson et al., 2011; Allan et al., 2012; Chapter 2). These pressures have been obtained with H_2O-CO_2 solubility models, and with other geobarometers independent of volatile saturation [i.e. amphibole geobarometry (e.g. Ridolfi et al., 2010), rhyolite-MELTS geobarometer (Gualda & Ghiorso, revised)].

The volatile and trace element data presented here separate the two rhyolite types. We observe large disparities in chlorine content (difference of ~1000 ppm; Fig. 3.5-3.6), and smaller differences in F contents (Fig. 3.5b and 3.6a). Carbon dioxide concentrations, however, are fairly similar (Fig. 3.6c), and water concentrations are on average slightly higher in the R1 magmas (Fig. 3.6b). These results show that there is a good correlation between the volatile concentrations of R1 and R2 rhyolites and the 'wet-oxidising' and 'dry-reducing' types as defined by Deering et al. (2008; 2010). However, it is counter-intuitive that the 'wet' R1 magmas have a lower volatile

concentration (i.e. Cl and F) compared to the 'dry' R2 magmas. These observations thus lead to several questions: what is the origin of the volatile (especially chlorine) disparities? Why do water and CO_2 not show the same disparities between the R1 and R2 melt inclusions analysed here as Cl concentrations? And why do R2 magmas have a higher Cl concentration?

When comparing different rhyolites, one has to consider that the measured volatile concentration in the melt inclusions does not necessarily represent the bulk volatile content of the magma (i.e. volatiles dissolved in the melt, hydrous crystals, and exsolved volatile phase, if present), which is inherently what will dictate early magma evolution prior to a gas phase forming. Hence, it is important to consider the behaviour of these volatiles in these melts, and more importantly the 'saturation state' of these melts during crystallisation (i.e. the exsolution of a volatile phase prior to, or during crystallisation in the silicic magma chamber).

3.6.1.1. Volatile saturation during crystallisation

Many studies have established that silicic magmas often become saturated in a volatile phase during shallow ascent and eruption, and during the final stages of crystallisation. However, a volatile phase might also form during the earlier stages of crystallisation within crystal-poor melt bodies prior to eruption (e.g. Anderson et al., 1989; Lowenstern et al., 1991; Lowenstern, 1993; 1994; Wallace & Gerlach, 1994; Wallace et al., 1995). Once saturation is reached, volatile species dissolved in the melt will partition to a volatile phase proportional to their relative solubilities and concentrations.

Exsolution of a fluid phase(s) occurs because the solubilities of the volatile components in the melt are finite; and these are strongly dependent on composition, density, and number of fluid phases present, which vary with temperature, pressure, and melt composition in the system. Chlorine solubility is largely dependent on P-T-X conditions, and an added complexity is that below ~200 MPa, Cl saturated melts can exsolve two separate phases: a low-density vapour phase and a high-density hydrosaline fluid (e.g. Webster, 2004; Carroll, 2005). Experimental studies on

Cl behaviour in silicic magmas show that Cl solubility decreases with decreasing temperature, but it increases with decreasing pressure, and there is a strong dependence of the solubility with the composition on the melt and coexisting volatile phase (if present) (e.g. Webster & Holloway, 1988; Carroll & Webster, 1994; Webster, 1997; Signorelli & Carroll, 2000; Carroll, 2005). Therefore, the Cl solubility will be affected by the presence and amount of other volatiles, and water concentration in the melt will have an inversely proportional relationship with the Cl solubility (Webster, 1997). To date no experimental data exist on how the CO2 content will affect Cl solubility for rhyolitic melts. From experiments on andesites, it is suggested that added CO_2 has only a minor effect on the dissolved Cl concentration in the melt, however, CO_2 will increase the likelihood for phase separation to form a separate vapour phase and hydrosaline fluid (Botcharnikov et al., 2007). Carbon dioxide generally has a very different behaviour compared to Cl (e.g. Lowenstern, 2001) and has a very low solubility in rhyolitic melts (generally an order of magnitude lower than H2O). In silicic magmas, Cl will partition in favour of co-existing volatile phases (either as Cl_2 gas or a Cl^- ion). Experimentally determined fluid-melt distribution coefficients ($D_{Cl}^{fl/melt}$) range from 2 to 80 for evolved silicic compositions (Webster & Holloway, 1988; Métrich & Rutherford, 1992; Webster, 1992; Student & Bodnar, 1999). Fluorine, in contrast to Cl, is highly soluble in silicate melts, and will typically favour the melt phase relative to an exsolved fluid. As a result, F concentrations will increase with fractionation, as there is no phenocryst phase with a high and fixed F concentration. In general, its content has to exceed ~8 wt.% (on average) for the partition coefficient ($D_F^{fl/melt}$) to be >1 (Carroll & Webster, 1994). For the TVZ rhyolites, fluorine is more likely to partition into a volatile phase at a later stage in the magmatic history of a system (i.e. during cooling and crystallisation of an intrusion at depth), and this behaviour of F is considered to be independent of H_2O and Cl.

Different approaches have been used to assess the saturation state of rhyolitic melts based on the composition of mineral-hosted melt inclusions, including: 1) H_2O-CO_2 solubility models to

establish the saturation pressure (e.g. Newman & Lowenstern, 2002; Papale et al., 2006), 2) the analysis of volatile variations in the melt and, 3) a determination of how they evolve relative to other incompatible elements (e.g. Webster, 1997). Previous studies in the central TVZ assessed the volatile behaviour and saturation state for many of the youngest Okataina Volcanic Centre (OVC) magmas (Johnson et al., 2011) and the Oruanui magma (Taupo Volcanic Centre, TVC; Liu et al., 2006). From the application of H2O-CO2 solubility models for the OVC and Oruanui melts (TVC), Johnson et al. (2011) and Liu et al. (2006) deduced that these rhyolites crystallised in the presence of an exsolved volatile phase. Furthermore, Johnson et al. (2011) interpreted the Cl concentration from the OVC magmas, which plateaus at 0.2 wt.% (Fig. 3.5-3.6), to be associated with Cl partitioning into an exsolved phase. Hydrous mineral fractionation (e.g. hornblende and biotite, which are present mostly in R1 rhyolites) and trace amounts of apatite is suggested to have a negligible effect on the H_2O and Cl concentrations, as these minerals only compose a small proportion of the total crystal population (e.g. Schmitz & Smith, 2004; Shane et al., 2007; Johnson et al., 2011). The measured volatile content in melt inclusions of these R1 rhyolites, thus, represent melts that have experienced some volatile loss. To date there is no literature on the saturation state of R2 rhyolites (i.e. eruptives from the Rotorua-Ohakuri Volcanic Centres, RoOhVC), hence a detailed assessment of volatile behaviour for these melts will be addressed here.

Application of H_2O-CO_2 solubility models on the RoOhVC magmas (R2 rhyolites) result in estimated saturation pressures between 75-150 MPa (Fig. 3.3a; using 760°C as an average temperature of the TVZ magmas; Newman & Lowenstern, 2002). These pressures are consistent with the estimated pressures of ~100 MPa, determined independently of the volatile data (using rhyolite-MELTS; Chapter 2 and Chapter 4). On average, the RoOhVC rhyolites have a slightly lower water content compared to R1 magmas (Fig. 3.6b), which results in slightly lower saturation pressures. However, from these solubility models, which are calibrated for melt in equilibrium with H_2O-CO_2-bearing fluids only, the results suggest that the RoOhVC melts may well be

saturated with regard to a volatile phase at the time of melt inclusion entrapment. These results are, nonetheless, inconsistent with experimental studies for silicic melts in equilibrium with H_2O-Cl-bearing fluids (Webster et al., 1999). Based on the results of these solubility experiments, the ~0.3 wt.% Cl in the RoOhVC melts would require them to be over-saturated with respect to the 200 MPa isobaric line (Fig. 3.3b). These results show that the solubilities and saturation with regard to multicomponent volatile phases are complex and may be difficult to predict without some other independent assessment of saturation (i.e. presence of fluid).

Another approach to assess if a volatile phase exsolved from the melt is to compare volatile variations with other incompatible elements. Cl, H_2O and CO_2 are interdependent, and incompatible during volatile under-saturated crystallisation (if no hydrous phases are present), and their concentration will be strongly affected during crystallisation in the presence of a volatile phase. If the melt is volatile under-saturated, there should be a positive linear correlation of increasing Cl, H_2O and CO_2 with incompatible elements (Webster, 1997). For the RoOhVC (i.e. Mamaku and Ohakuri eruptions), the volatile variation for each individual magma type is treated separately, as they are suggested to represent distinct magma batches (Chapter 2). Chlorine concentrations increase slightly with the Y contents for Mamaku Type 1 and Ohakuri Type 1 and 3 magmas (Fig. 3.4), suggesting that Cl was possibly not saturated and/or not lost to a coexisting volatile phase during crystallisation. For the H_2O vs. Cl content, the data are very scattered and no clear trends can be identified (Fig. 3.3b). For the H_2O vs. CO_2 only the Ohakuri fall deposit plot along a positive trend (Fig. 3.3a), which may be indicative of crystallization in a volatile under-saturated melt. However, for the Mamaku ignimbrite CO_2 contents cluster around ~25-75 ppm, and the melt inclusions of the Ohakuri ignimbrite have no CO_2 at all (Fig. 3.3a). The lack of clear correlations in the volatile record may be explained by post-entrapment CO_2 diffusion, and to a lesser extent H diffusion, through the quartz host or formation of a vapour bubble, which have been suggested to affect melt inclusion volatile concentrations (e.g. Bodnar, 2003; Severs et al., 2007; Steele-McInnis

et al., 2011; Bucholz et al., 2013). Furthermore, these magmas are crystal-poor (Table 3.1; magma Type 1 has <1 vol.% crystals), and therefore, the record of changes in crystallisation with Y or other trace elements is limited compared to systems where changes in volatiles are tracked along a larger chemical spectrum involving more crystallisation. This could also be the reason why no clear positive, linear trends are observed between F and the Rb/Sr ratio (Fig. 3.5b). In addition, plagioclase and pyroxenes represent only a fraction of the crystal cargo, which further reduces the potential affect on the Y content. In comparison, the R1 magmas of the TVZ are crystal-moderate to -rich and variations of volatile contents with incompatible elements are more easily observed.

From the assessment of saturation state above, some of the Mamaku and Ohakuri magmas from the RoOhVC appear to be under-saturated while others remain inconclusive. Importantly, if we consider Cl variations with regard to other incompatible elements, then the RoOhVC melt inclusions unlikely record Cl-loss to a coexisting phase, and therefore some care needs to be taken when solely using the H_2O-CO_2 solubility models, which here would indicate saturation. We suggest that our results for R2 melt inclusions may reflect that these melts were either at, or very close to, saturation in a volatile phase during melt inclusion entrapment. However, regardless of volatile saturation, we can conclude that the R1 magmas experienced a higher amount of degassing prior to and /or during crystallisation.

3.6.1.2. Differences in bulk volatiles

Disparities in volatile saturation between R1 and R2 rhyolites is suggested here, with the OVC and Oruanui magmas (TVC) being saturated prior to quartz crystallisation (Liu et al., 2006; Johnson et al., 2011), compared to the RoOhVC melts, where saturation, if reached, would have occurred during or after crystallisation. Measured volatile concentrations in melt inclusions thus represent variously degassed melts.

R1 magmas show clear volatile exsolution, which initiated the partitioning of Cl in the co-existing phase, as $D_{Cl}^{fl/melt}$ is >>1 (Webster & Holloway, 1988; Métrich & Rutherford, 1992;

Webster, 1992; Student & Bodnar, 1999), and 'stabilised' the Cl content at its solubility value of ~0.2 wt.% (Fig. 3.5 and 3.6a). Therefore, bulk Cl contents in the OVC had to be much higher than the concentration measured in melt inclusions. Equally, most of the H_2O partitioned into the coexisting volatile phase (Fig. 3.6b-c), requiring a higher initial bulk water content. Chlorine solubility is negatively correlated with the water content and will be higher in rhyolites with lower H_2O. This may explain the high Cl content in the RoOhVC magmas (Fig. 3.5-3.6), and suggest that R2 magmas have a lower bulk water content.

The exsolution of a volatile phase is highly dependent on the initial water content, among other parameters. Here, similar H_2O concentrations in the OVC and RoOhVC magmas (~3-6 wt.%) can be explained by the similar water solubilities at storage conditions of these melts (similar pressures and temperatures), independent of the initial water content. The variability in initial water content is also in agreement with the suggested petrogenesis of R1 and R2 rhyolites and the ubiquitous presence of hornblende (± biotite) in the R1 type (absent or only sparse in R2, Table 3.1). Variations in temperature, fH_2O and fO_2 in the lower crust are shown to dictate the resulting mineral assemblage of the rhyolites (Deering et al., 2008), which are generated largely through fractional crystallisation (e.g. McCulloch et al., 1994; Deering et al., 2008; 2010).

Bulk Cl concentrations, along with water and other volatiles, are also suggested to be much higher in the R1 compared to the R2 rhyolites. Some rough estimations on the differences of bulk Cl can be made using a $D_{Cl}^{fl/melt}$ of 10 (for pressures of ~100 MPa, e.g. Signorelli & Carroll, 2000), and considering the coexistence of ~20 vol.% bubbles with the melt. With these assumptions, the bulk Cl content in R1 rhyolites may be at least twice as high (~0.6 wt.%) compared to the R2 magmas, which will have non negligible effects on the amount of mass and heat transfer from magmatic systems.

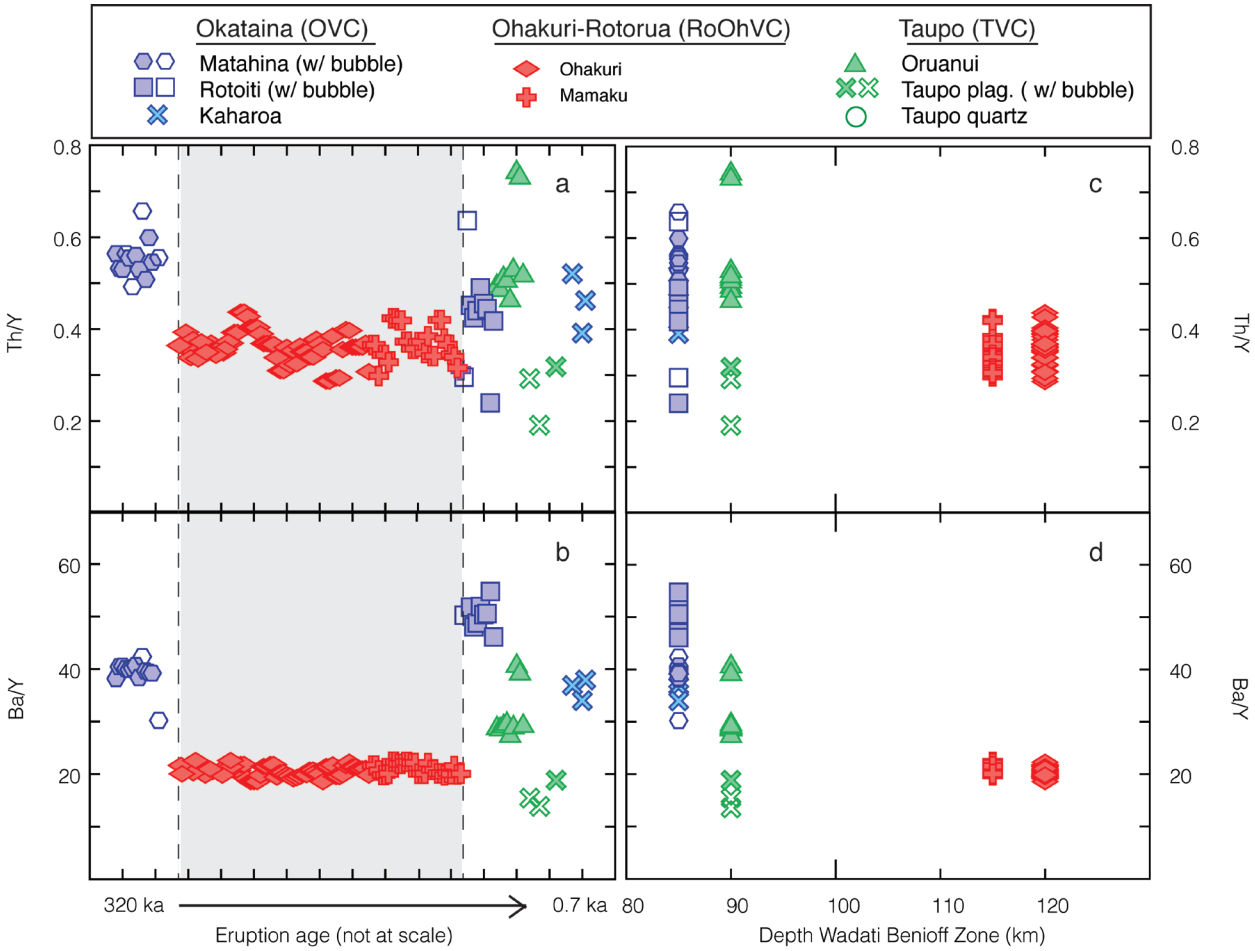

Figure 3.7: Variation Th/Y and Ba/Y in quartz-hosted melt inclusions from the central TVZ; (a-b) vs. time (data in chronological order, not to scale) starting with the 320 ka Matahina eruption (OVC) and ending with the 0.7 ka Kaharoa eruption (OVC), and (c-d) vs. depth of the Wadati Benioff Zone (after Reyners et al., 2006); open symbols correspond to melt inclusions containing a vapour bubble. The grey band represents the systems situated on the western border of the central TVZ (i.e. RoOhVC), compared to the other systems situated on the rift axis (i.e. OVC and TVC). Analytical error on these elements and ratios are smaller than the size of the symbol.

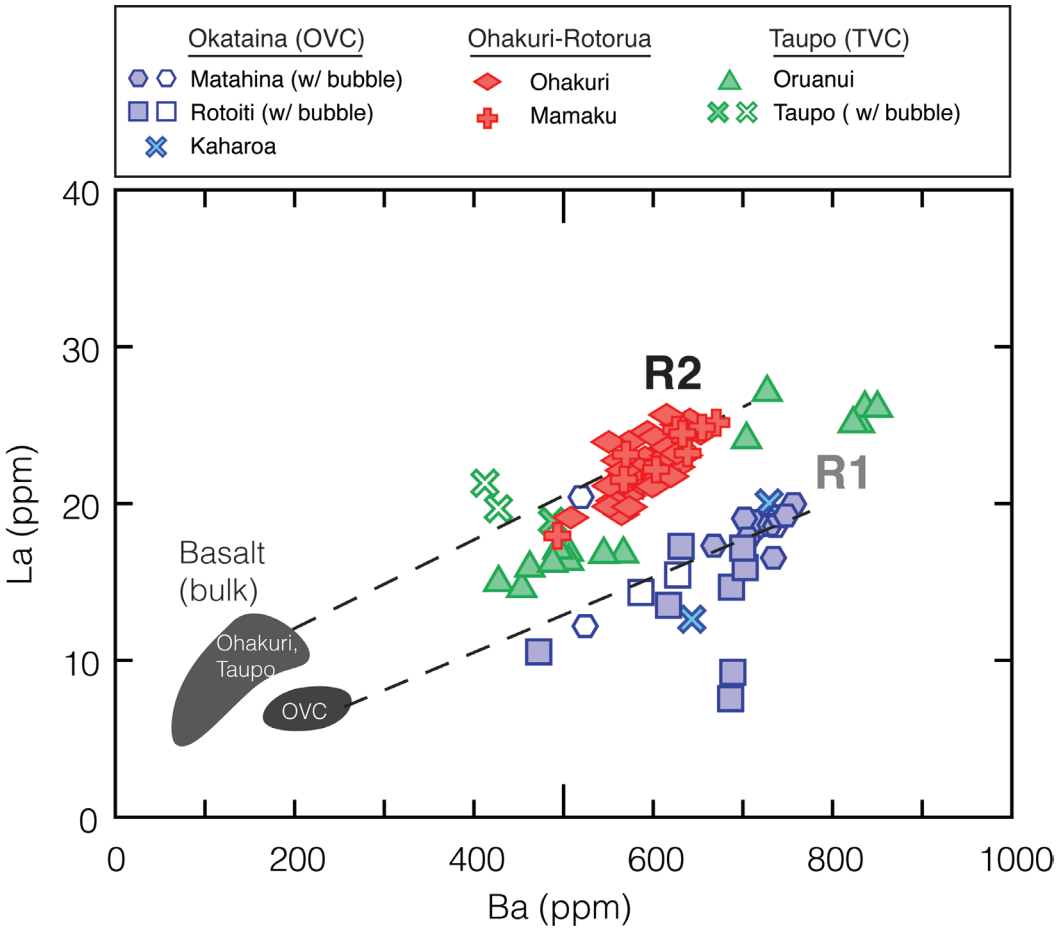

Figure 3.8: Ba-La variation in analysed rhyolitic melt inclusions, open symbols correspond to melt inclusions containing a vapour bubble. Black fields represent bulk data on basalts from the central TVZ, erupted in proximity of the OVC, or the TVC and Ohakuri volcano (Rooney & Deering, 2014). Analytical error is smaller than the size of the symbol.

3.6.1.3. Distribution of volatiles in the central TVZ

From the melt inclusion data, we suggest that the rhyolites form two groups based on their inferred bulk volatile content; R1 rhyolites having higher bulk volatile concentrations, corresponding to the 'wet-oxidising', compared to the 'dry-reducing' R2 magmas (after Deering et al., 2008; 2010). The distribution of the melt inclusion data, therefore, mirrors the variability in bulk-rock geochemistry and mineral assemblage indicated by the different rhyolite types. Deering et al. (2010) suggest that the last 550 kyrs in TVZ magmatism can be subdivided into two broad cycles each with R1 followed by R2 magmatism, and they suggest that the more buoyant R1 magmas, hence volatile-rich, are focused along the central rift axis in comparison to the volatile-poorer R2 magmas. The variability of these rhyolite types has previously been suggested to be associated with subduction zone processes and/or crustal level modulation induced by caldera collapse (Deering et al., 2008; 2010; Rooney & Deering, 2014). Therefore, our volatiles and trace element data from the melt inclusions appear to be consistent with differences originating from these processes as well.

3.6.2. Influence of slab-derived fluids?

The origin of the major volatiles in primary arc magmas is mainly the mantle wedge, the subducted altered oceanic crust and its overlying sediments (e.g. Wallace, 2005; Zelenski & Taran, 2011). It has long been established that these components of subduction zones play an important role in the generation of aqueous fluids and the transport of fluid-mobile elements, producing, ultimately, the typical arc signature in subduction zone volcanism (e.g. Kay, 1980; Hawkesworth & Ellam, 1989; McCulloch & Gamble, 1991).

In the TVZ, crystal fractionation and assimilation models (AFC) have been used to explain the rhyolite petrogenesis from a parental mafic magma (e.g. McCulloch et al., 1994; Graham et al., 1995; Price et al., 2005; Deering et al., 2011-a), and a significant mantle component in the silicic magmas has been suggested, with some assimilation (<25 %) in the lower crustal region

(e.g. McCulloch et al., 1994; Deering et al., 2008). The compositional and petrological variability present in the rhyolites has been suggested to reflect distinct zones of melting and magma generation in the mantle (Deering et al., 2008; 2011-a), and a recent study that utilized basalt bulk-rock geochemistry has provided a potential link between the 'wet' R1 and 'dry' R2 rhyolite types and the variability in the mafic parent (Rooney & Deering, 2014). The observed range of composition of these basalts suggests different sources for the primitive melt generation, with disparities in slab-derived components from the subduction zone (Rooney & Deering, 2014). A stronger petrogenetic connection between the basalts and the rhyolites has been established for the central TVZ (Rooney & Deering, 2014), which gives more confidence in using the rhyolite compositions to assess the slab-derived flux. Compared to the primitive basalts, the rhyolites are also much more abundant in the central TVZ, permitting a better evaluation of the fluid flux variability through time and space.

Volatiles and fluid-mobile elements are transported along with aqueous fluids from the subducting slab, and participate in melt generation processes. Thorium and Ba are such elements, representing components of the subduction zone, and Y represents a mantle component. Ba/Y and Th/Y ratios are thus independent of mantle source, partial melting or fractional crystallisation and represent a measure of the subduction input (Pearce & Peate, 1995; Pearce & Stern, 2006). This input seems to be distinct between the RoOhVC and OVC-TVC magmas (Fig. 3.7 a-d). With increasing distance from the trench (i.e. increasing depth of the Wadati Benioff Zone, after Reyners et al., 2006) there is decreasing input from slab-derived components, indicating that the contribution of slab-derived components were probably not as important for the RoOhVC as for the OVC. Similar patterns have been observed at numerous subduction zone systems on Earth [e.g. Izu-Bonin System (Hochstaedter et al., 2001); Tonga System (e.g. Jenner et al., 1987; Bach et al., 1998)]. These results thus indicate that trace element variations in the rhyolitic melt inclusions can be linked to the basalt bulk-rock data (Fig. 3.8), consistent with the findings of Rooney

& Deering (2014), showing that the variability in the TVZ rhyolites is a result of distinct sources for melt generation in the mantle region, and processes operational in the subduction zone. There is very little published volatile data for TVZ basalts, therefore, great caution should be applied in trying to establish a direct link in the volatile concentrations between the R1 and R2 rhyolites and the basalt distribution.

In most of the measurements of volatiles and trace elements from this study, the TVC magmas usually have compositions in between the OVC and the RoOhVC magmas (Fig. 3.7-3.8). These results are in agreement with the observations of Deering et al. (2008; 2010) suggesting that the TVC magma composition is less 'wet and oxidizing' than the OVC magmas (representing the R1 end-member composition). In Figure 3.8, the Oruanui rhyolite (TVC) plots along a trend above the OVC magmas, and has lower Ba/Y and Th/Y than the OVC, although the depth of the subducting slab beneath the volcanic centres is very similar (Fig. 3.7c-d). These results may be indicative of disparities in slab-derived fluid flux between the OVC and the TVC, as suggested by Reyners et al. (2006) and Eberhart-Phillips et al. (2008), and is also in agreement with the basalt study of Rooney & Deering (2014), suggesting a decrease in slab-derived contribution from north to south along the rift axis. Compositional differences between the Oruanui and the Taupo rhyolites from the TVC have been suggested to be unrelated to changes in fluid flux from the subduction zone (Deering et al., 2010).

3.7. Conclusion

In this study, we focused on the volatile and trace element composition of melt inclusions from seven major rhyolitic ignimbrites in the Taupo Volcanic Zone, to identify the spatial distribution of the major volatile species at the scale of the entire central TVZ, and to establish the importance of volatile saturation in these silicic systems. H_2O-CO_2 solubility models are combined with the study of chlorine variations along with incompatible elements to assess the saturation state of some of these rhyolitic melts, and to allow for comparison among the distinct volcanic centres. Some of the major conclusions are:

1. Rhyolites produced in the central TVZ over the past ~320 kyrs, have distinct volatile, fluid-mobile, and highly incompatible element compositions (e.g. Cl, F, Th, Ba), with the rhyolites from the Okataina Volcanic Centre (OVC) and the single Oruanui eruptive event and the Rotorua-Ohakuri Volcanic Centres (RoOhVC) and Taupo magmas forming two distinct types (R1 and R2 types respectively);
2. Water, CO_2, Cl and F concentrations from R1 and R2 rhyolites mirror the variability in bulk-rock geochemistry and petrology of the rhyolitic continuum between 'wet-oxidising' and 'dry-reducing' types established by Deering et al. (2008; 2010). However, the 'wet' R1 rhyolitic melt inclusions record a lower volatile concentration, compared to the 'dry' R2 melt inclusions. This emphasises the importance of considering the saturation state of these melts at the time of melt inclusion entrapment;
3. The origin of the disparities in volatile concentration between R1 and R2 is suggested to be related to differences in the bulk volatile concentration of the parental magmas, leading to differences in volatile saturation between R1 and R2 systems: R1 rhyolites were clearly saturated during crystallisation, whereas R2 rhyolic melt inclusions are suggested to record either less degassing than R1, or no degassing at all;

4. These results show that silicic systems with similar reservoir depths, eruption temperatures and major element compositions may exsolve a volatile phase at different stages in their magmatic history, and it can not always be assumed that all high-silica melts reached volatile saturation during crystallisation. The differences in volatile content will not only have an effect on the relative timing of exsolution of a volatile phase in a magmatic system, but the composition of this exsolved magmatic volatile phase as well.

Table 3.1: Summary of ignimbrites from the central TVZ, analysed in this study.

Eruption Name	Age (ka)	Volume (km3)	Source Caldera	Mineral Assemblage	Crystallinity (%)	No of analyzed pumice clasts	Rhyolite type
Kaharoa	0.7 ± 0.012	~ 5	Okataina	qtz + plg + bt ± hbl ± cum	~ 10	6	R1
Taupo	~ 1.8	35	Taupo	plg + opx ± qtz	< 5	5	R2
Oruanui	~ 26.5	~ 530	Taupo	qtz + plg + hbl+ opx	< 5	5	R1 + R2
Rotoiti	~ 61	~ 100	Okataina	qtz + plg + cum + hbl + opx ± bt	< 30	5	R1
Kaingaroa	230 ± 10	>100	Reporoa	plg + opx	~ 5	9	R2
Mamaku	240 ± 10	> 145	Rotorua	qtz + plg + opx ± hbl	< 10	9	R2
Ohakuri	240 ± 10	> 100	Ohakuri	qtz + plg + opx	< 10	14	R2
Matahina	322 ± 7	> 160	Okataina	qtz + plg + opx ± bt ± hbl	< 15	6	R1 + R2
Whakamaru Group	340 - 320	> 2000	Whakamaru	qtz + plg +san + opx + bt + hbl	35-40	3	R1

bt-biotite; cum-cumingtonite; hbl-hornblende; opx-orthopyroxene; plg-plagioclase; qtz-quartz; san-sanidine
Compilation from the following sources: Beresford (1997), Brown et al. (1998), Cole at al. (2010), Deering et al. (2008; 2010), Gravley (2004), Gravley et al. (2007), Milner et al. (2003), Nairn et al. (2004), Schmitz & Smith (2004), Smith et al. (2005), Sutton et al. (1995), Wilson et al. (2006, 2009).

Table 3.2: Average major element and volatile composition of melt inclusions for the analysed eruptive units.

	SiO_2 (wt%)	TiO_2 (wt%)	Al_2O_3 (wt%)	FeO (wt%)	MnO (wt%)	MgO (wt%)	CaO (wt%)	Na_2O (wt%)	K_2O (wt%)	P_2O_5 (wt%)	H_2O^a (wt%)	H_2O^b (wt%)	CO_2 (ppm)	Cl (wt%)	F (wt%)
Kaharoa (n = 64)															
avg.	77.78	0.10	12.37	0.89	0.05	0.07	0.62	3.58	4.06	0.01	na	na	na	0.21	0.04
1 σ	0.53	0.04	1.41	0.15	0.02	0.02	0.10	0.57	0.47	0.01				0.05	0.02
Taupo (n = 26)															
avg. (n = 4)	76.60	0.24	13.35	1.76	0.08	0.22	1.36	3.55	2.81	0.03	na	na	na		
1 σ	0.22	0.02	0.18	0.06	0.02	0.01	0.04	0.15	0.11	0.00					
avg.* (n = 22)	74.85	0.40	13.69	2.54	0.12	0.37	1.52	3.55	2.88	0.07	na	na	na	0.24	0.04
1 σ	1.32	0.18	0.27	0.70	0.03	0.20	0.17	0.55	0.11	0.06				0.07	0.02
Oruanui (n = 25)															
avg.	77.44	0.12	12.51	1.11	0.05	0.11	0.99	4.45	3.21	0.01	na	na	na	0.21	0.02
1 σ	0.27	0.02	0.13	0.12	0.01	0.02	0.12	0.25	0.13	0.01				0.02	0.01
Rotoiti (n = 25)															
avg.	77.92	0.13	12.45	0.94	0.06	0.15	0.89	4.23	3.22	0.02	na	na	na	0.20	0.02
1 σ	0.38	0.02	0.16	0.08	0.01	0.02	0.12	0.24	0.09	0.01				0.01	0.01
Mamaku (n = 73)															
Type 1 - avg.	78.37	0.13	11.94	0.99	0.04	0.05	0.53	3.80	4.14	0.00	4.06	4.11	53	0.31	0.06
1 σ	0.55	0.08	0.26	0.07	0.02	0.02	0.07	0.25	0.16	0.01	0.26	0.37	9	0.03	0.00
Type 2 - avg.	78.61	0.13	11.79	1.06	0.06	0.06	0.61	3.85	3.84	0.00	3.56	4.12	37	0.29	0.06
1 σ	0.41	0.06	0.21	0.07	0.02	0.02	0.08	0.31	0.23	0.00	0.28	0.28	12	0.02	0.01

Table 3.2: Average major element and volatile composition of melt inclusions for the analysed eruptive units (cont.).

	SiO_2 (wt%)	TiO_2 (wt%)	Al_2O_3 (wt%)	FeO (wt%)	MnO (wt%)	MgO (wt%)	CaO (wt%)	Na_2O (wt%)	K_2O (wt%)	P_2O_5 (wt%)	H_2O^a (wt%)	H_2O^b (wt%)	CO_2 (ppm)	Cl (wt%)	F (wt%)
Ohakuri (n = 97)															
Fall deposit - avg.	77.99	0.08	12.15	0.95	0.05	0.06	0.55	4.05	4.12	0.00	4.63	4.16	53	0.27	0.06
1 σ	0.23	0.04	0.12	0.07	0.02	0.01	0.05	0.06	0.09	0.00	0.84	0.42	19	0.01	0.00
Type 1 - avg.	78.56	0.09	11.76	1.01	0.04	0.06	0.54	3.87	4.10	0.01	4.05	4.20	1	0.31	0.05
1 σ	0.21	0.05	0.09	0.08	0.02	0.02	0.05	0.07	0.09	0.01	0.08	0.21	3	0.01	0.00
Type 2 - avg.	78.89	0.11	11.62	1.07	0.04	0.07	0.61	4.00	3.65	0.01	4.23	3.95	2	0.29	0.05
1 σ	0.30	0.06	0.13	0.11	0.03	0.02	0.05	0.07	0.14	0.01	0.56	0.23	3	0.01	0.00
Type 3 - avg.	79.47	0.14	11.37	0.96	0.03	0.05	0.54	3.87	3.61	0.01	na	4.02	na		
1 σ	0.59	0.06	0.36	0.09	0.01	0.02	0.05	0.18	0.18	0.01		0.68			
Kaingaroa (n = 22) *															
avg.	76.49	0.16	12.76	1.39	0.05	0.12	0.98	4.07	3.97	0.01	na	na	na	0.19	0.02
1 σ	0.87	0.03	0.34	0.43	0.02	0.04	0.09	0.26	0.25	0.01				0.01	0.01
Matahina (n = 36)															
avg.	77.84	0.09	12.58	0.99	0.05	0.08	0.80	3.82	3.72	0.01	na	na	na	0.19	0.03
1 σ	0.27	0.01	0.16	0.08	0.01	0.01	0.04	0.27	0.17	0.01				0.01	0.01

Analyses are normalised to anhydrous conditions.

* plagioclase-hosted melt inclusions

na - not analysed

Major elements for the Mamaku and Ohakuri eruptive deposits are after Bégué *et al.*, in review).

Major elements, and Cl and F analysed by electron microprobe (EMPA) at the University of Washington and Oregon State University. Analytical conditions for major elements: acceleration voltage 15kV, beam current 5nA, beam size 10µm. Cl and F analysed using a beam blanking technique (Witter & Kuehner, 2004) with an acceleration voltage of 10kV, beam current of 100nA, and beam size 10µm, and with standard analytical conditions at Oregon State University. Analytical error for Cl <3%, and ~10% for F.

[a] transmission FTIR, and [b] reflectance FTIR for CO_2 and H_2O analyses (analysed at Oregon State University). Uncertainties in measuring inclusion thickness and fitting the background are typically <0.3 wt.% for H_20 and <5 % for CO_2 using the transmission FTIR, and estimated error on H_2O using the reflectance FTIR is ±0.5 wt.%.

Table 3.3: Average trace element composition of melt inclusions for the analysed eruptive units.

	Li (ppm)	B (ppm)	Rb (ppm)	Sr (ppm)	Y (ppm)	Cs (ppm)	Ba (ppm)	La (ppm)	Ce (ppm)	Pr (ppm)	Nd (ppm)	Sm (ppm)	Th (ppm)	U (ppm)
Kaharoa (n = 12)														
avg.	76	25	113	36	19	5	694	17	34	4	12	3	9	1
1 σ	4	2	5	11	1	1	45	4	7	1	2	0	1	0
Taupo (n = 8)														
avg. (n = 1)	41	24	na	na	na	na	na	na	na	na	na	na	na	na
avg.* (n = 7)	48	21	90	117	28	3	456	21	44	0	19	4	8	6
1 σ	1	2	5	20	4	0	39	3	6	0	3	0	2	2
Oruanui (n = 9)														
avg.	72	28	102	60	16	3	494	16	32	0	11	2	9	3
1 σ	21	3	12	8	1	1	44	1	2	0	2	0	1	3
Rotoiti (n = 9)														
avg.	60	22	74	54	13	2	659	14	29	13	9	2	5	3
1 σ	13	2	8	15	2	0	43	3	4	3	2	0	1	2
Mamaku (n = 28)														
Type 1 - avg.	75	16	123	24	30	5	628	24	49	6	20	5	11	1
1 σ	9	2	6	6	1	1	23	1	2	0	1	0	1	0
Type 2 - avg.	72	16	112	28	28	5	565	21	45	5	18	4	9	0
1 σ	4	1	13	8	2	1	34	2	3	0	1	0	1	0
Ohakuri (n = 51)														
Airfall - avg.	63	18	123	24	30	6	619	23	48	5	19	4	11	2
1 σ	9	1	4	3	1	1	9	1	2	0	1	1	1	1
Type - avg.	53	17	124	26	30	4	615	24	49	5	19	4	11	3
1 σ	3	1	11	5	1	1	29	1	2	0	1	1	1	0
Type 2 - avg.	40	16	106	31	28	4	576	22	45	5	18	4	10	2
1 σ	7	1	8	4	2	0	24	2	3	0	2	1	1	1
Type 3 - avg.	41	17	132	24	30	4	616	23	49	5	19	4	10	3
1 σ	4	1	10	3	1	1	29	1	2	1	1	0	1	0

Table 3.3: Average trace element composition of melt inclusions for the analysed eruptive units (cont.).

	Li (ppm)	B (ppm)	Rb (ppm)	Sr (ppm)	Y (ppm)	Cs (ppm)	Ba (ppm)	La (ppm)	Ce (ppm)	Pr (ppm)	Nd (ppm)	Sm (ppm)	Th (ppm)	U (ppm)
Kaingaroa (n = 6) *														
avg.	27	23	119	52	19	4	474	19	37	0	14	3	9	3
1 σ	8	3	17	12	2	1	106	2	4	0	2	0	1	1
Matahina (n = 9)														
avg.	69	27	108	48	17	3	654	17	34	17	11	2	9	2
1 σ	10	1	26	11	4	1	163	4	8	4	3	1	2	1

* *plagioclase-hosted melt inclusions*

na - not analysed

Some trace elements for the Mamaku and Ohakuri eruptive deposits are after Bégué *et al.*, in review).

SIMS analyses with a IMS Cameca 6f (Arizona State University); 10 nA beam intensity, 10-20 μm spot size.

Analytical error: < 3 % for all elements, and ~10 % for Th and U.

Chapter 4

Phase-equilibrium geobarometers for silicic rocks based on rhyolite-MELTS. Part 2: Application to TVZ rhyolites

4.1. Abstract

Constraining the pressure of large silicic magma bodies gives important insight into the depth and vertical extent of magmatic plumbing systems and reservoirs. Pressure is an essential parameter influencing phase assemblage, volatile exsolution, and, hence, the eruptive potential of these magmas. In this study a new geobarometer based on phase assemblages calculated with rhyolite-MELTS is applied to glass compositions (matrix glass and melt inclusions) of seven eruptive deposits dated between ~320 and 0.7 ka from four distinct calderas in the central Taupo Volcanic Zone (TVZ). In this study we also discuss the utility of the rhyolite-MELTS geobarometer and assess advantages and limitations of the method in comparison with other geobarometers applied to the same eruptive deposits. Overall, there is good agreement with other pressure estimates from the literature. One of the main advantages of this new geobarometer is that it can be applied to both matrix glass and melt inclusions – regardless of volatile saturation. Hence, it can enhance our understanding of pre-eruptive and eruptive processes. Our examples also emphasise the utility of this method to filter out spurious glass compositions. Pressure estimates obtained with the new rhyolite-MELTS geobarometer range between ~250 to ~50 MPa, with a large majority at ~100 MPa. Small differences among the eruptive deposits can be observed and in comparison similar eruptions globally, these results confirm that the TVZ hosts some of the shallowest rhyolitic magma bodies on the planet, which is the result of the extensional tectonic regime and thinning of the crust. Distinct populations with different equilibration pressures are also recognised, which is

consistent with the idea that multiple batches of eruptible magma can be present in the crust at the same time, and can be tapped simultaneously by large eruptive events

4.2. Introduction

Significant effort has gone into determining the pressure under which silicic magma bodies reside in the crust and crystallise, as it is a crucial parameter influencing phase assemblage, volatile exsolution, and, hence, the eruptive potential of these magmas. Thus, finding the correct geobarometer and understanding its limits and potentials is essential in our attempts to understand the history and evolution of magmatic systems.

In Part 1 of this series, Gualda & Ghiorso (revised) present a new geobarometer based on phase equilibria calculations using rhyolite-MELTS (Gualda et al. 2012-a). This method uses major element compositions of rhyolitic glass (melt inclusions or matrix glass) as input, and seeks to find the pressure conditions at which the glass composition is in equilibrium with the coexisting mineral assemblage (for more details, see Gualda & Ghiorso, revised; 2013-b). This paper presents an application of this geobarometer to one of the best-studied silicic volcanic zones on Earth, the central Taupo Volcanic Zone (TVZ), New Zealand and includes a comparison with other geobarometers that have previously been applied.

The central TVZ is actively rifting and presents an exceptionally high rate of rhyolitic magma generation and eruption (e.g. Wilson 1996). Several studies have focused on constraining the residence depth of the rhyolitic magma bodies in the upper crust, mainly for the Okataina Volcanic Centre (OVC; Johnson et al. 2011; Shane et al. 2007; 2008-b; Shane & Smith 2013; Smith et al. 2010) and Taupo Volcanic Centre (TVC; Allan et al., 2012; Liu et al., 2006), where the most recent volcanic activity in the central TVZ focuses. In these studies amphibole geobarometry and H_2O-CO_2 solubility models are employed to estimate pressures. Deering et al. (2011-a) undertook a comparative pressure study using amphibole and clinopyroxene-liquid geobarometry on the TVZ's

central and southern segments to better understand the relationship between andesitic (southern TVZ) and rhyolitic (central TVZ) volcanism in the TVZ (Deering et al. 2011-a). However, little work has been done on the geobarometry of rhyolitic systems other than the OVC and TVC, particularly, for systems that lack amphibole in their mineral assemblage.

Here, we apply the rhyolite-MELTS geobarometer (Gualda & Ghiorso revised) to melt inclusion and matrix glass compositions of seven eruptive deposits, dated between ~320 and 0.7 ka, from four distinct caldera centres in the central TVZ (Fig. 4.1; Table 4.1). We focus on the utility of this geobarometer and compare it to other pressure estimates from the literature. This study also allows us to identify any temporal or spatial variations in pressures among the rhyolitic magma bodies, and to gain further insights into silicic magmatism in the central TVZ overall.

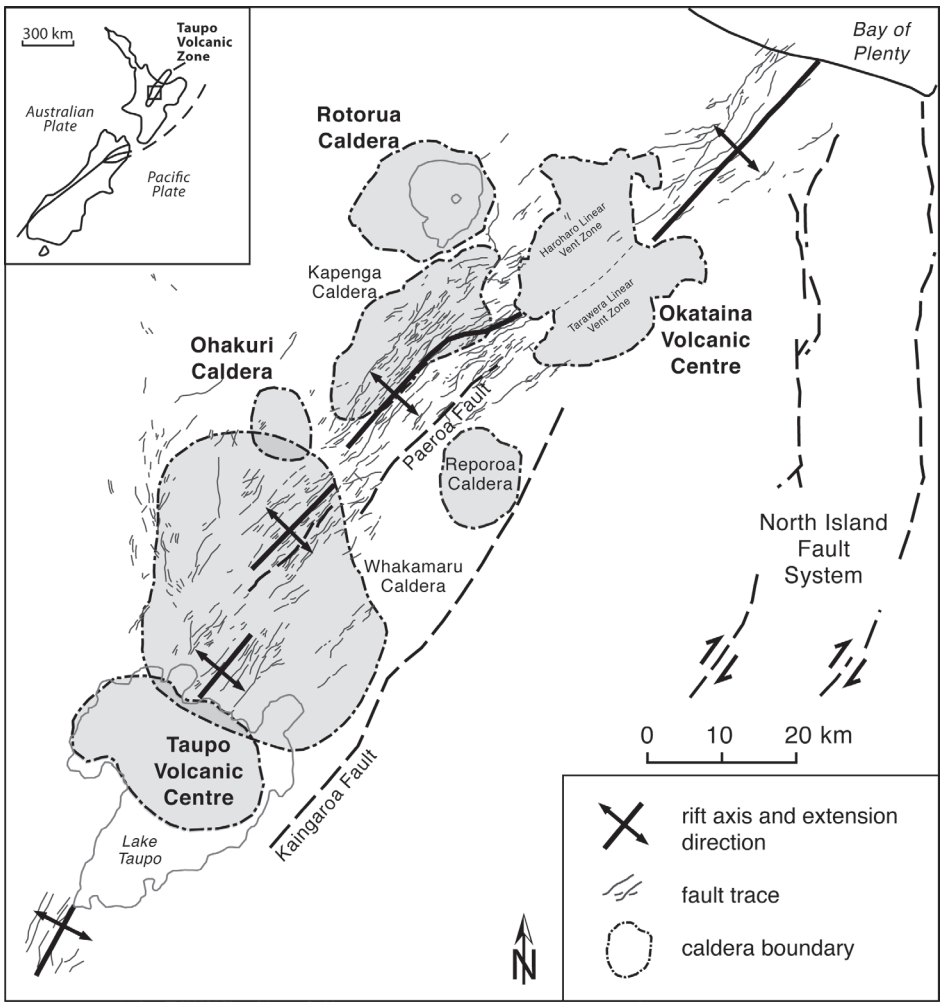

Figure 4.1: Map of structural boundaries of calderas in the central Taupo Volcanic Zone (TVZ) after Rowland et al. (2010).

4.3. Taupo Volcanic Zone

The TVZ is a rifted arc, with a NW-SE extension of 5-15 mm/yr (Darby & Meertens 1995; Wallace et al. 2004). It is volcanically and structurally segmented, with its northern and southern segments dominated by andesitic cone-building eruptions (e.g. Wilson et al. 1995). The central segment – which has been active since ~2 Ma – is dominated by explosive caldera-forming rhyolitic eruptions and effusive rhyolitic dome building, with minor andesites, dacites and basalts (Fig. 4.1; Eastwood et al. 2013; Houghton et al. 1995; Wilson et al. 1995; 2009). More than ~6,000 km3 of rhyolites have been evacuated from at least eight different caldera centres (Wilson et al. 2009). The age of rift initiation is poorly constrained; from interpretation of the TVZ's early history ~0.9 Ma has been suggested (Wilson et al. 1995); however, recent geochronology studies show that rhyolites erupted ~1.8 Ma, suggesting rifting may have been active for longer than initially thought (Eastwood et al. 2013).

The crustal structure has been characterised by seismic velocity contrasts at depth, with the upper crust dominated by volcanic deposits and the upper to mid-crust (3 to 11km) dominated by quartzo-feldspathic rocks (< 2Ma shallow igneous intrusives and Mesozoic basement; Harrison & White 2004; 2006; Stratford & Stern 2006). Controversy over the structure of the lower crust persists with the model of Stratford & Stern (2006) suggesting anomalous mantle at depths of ~16-30 km and the model of Harrison & White (2004; 2006) suggesting a heavily intruded lower crust (16-30 km) with the presence of at least 1% partial melt. Regardless of the model both ideas suggest that mafic rocks/melt dominate the region between 16 and 30 km. However, the Harrison & White (2004; 2006) model accounts best for the generation of rhyolitic melt and the proposed petrogenesis of the rhyolites from assimilation and fractionation related to lower crustal basaltic underplating in the central TVZ (Deering et al. 2008; 2011-a; McCulloch 1994). This is consistent with the ~35 km crustal thickness of the central TVZ inferred from seismic tomography (Reyners et al. 2006).

An abrupt change in magmatism, volcanism and tectonics occurred ~340 ka, with an ignimbrite flare-up event that lasted until ~240 ka, during which more than 3,000 km^3 of magma erupted from at least seven different calderas (Gravley et al. in preparation). A close relationship between rifting and accumulation and evacuation of large rhyolitic magma bodies has been inferred (e.g. Rowland et al. 2010). This regional extensional regime partly controls the geometry and structure of the caldera complexes (e.g. Cole et al. 2010; Seebeck et al. 2010; Spinks et al. 2005) and may also play an important role in magma migration in the upper crust and eruption (Allan et al. 2012; Chapter 2; Gravley et al. 2007). Detailed information on the different eruptive centres of the central TVZ can be found in Wilson et al. (1995; 2009) and Cole & Spinks (2009), among others. The main characteristics of the studied deposits here are summarised in Table 4.1.

4.4. Method and results

4.4.1. Dataset

We applied the rhyolite-MELTS geobarometer to glass analyses from seven eruptive deposits from the central TVZ (Fig. 4.1; Table 4.1), collected as part of studies of various volcanic centres in the TVZ (Chapter 2 and 3; Pamukcu et al. in preparation). A summary of the data with averaged compositions is provided in Table 4.2, and the extensive dataset is given as supplementary material. Major element compositions were determined by electron microprobe analysis in the University of Washington (JEOL Superprobe) and Oregon State University (Cameca S100) and with the analytical scanning electron microscope at Vanderbilt University (Tescan VEGA3 SEM with Oxford EDS detector). In the microprobe, we used an acceleration voltage of 15 kV, a beam current of 5nA, a defocused beam of ~10 μm in diameter, and measured Na and other major elements first to minimise the effects of analytical Na migration; detailed analytical conditions and standard errors are given in chapters 2 and 3. In the analytical SEM, we used an acceleration voltage of 15 kV, maximum beam intensity (BI=18, resulting in currents of ~2.5 nA), and we scanned

over rectangular or irregular areas over 30s of live time acquisition; quantification was performed using Oxford's AZtec software with oxygen calculated by stoichiometry and normalized oxide abundances. The quality of the results was checked by analysing the USGS reference material RGM-1 in the same session and under the same conditions, which resulted in errors <1 % for major elements and <5% for minor elements (Pamukcu et al. in preparation). We ran the rhyolite-MELTS geobarometer on a total of 567 glass compositions (404 from quartz-hosted melt inclusions, and 163 from matrix glass) from 48 different pumices (details are provided in Table 4.1).

The samples come from ignimbrites and fall deposits of several eruptive deposits from the Rotorua and Ohakuri Volcanic Centres (RoOhVC), the Okataina Volcanic Centre (OVC), and the Taupo Volcanic Centre (TVC; Fig. 4.1). For the RoOhVC, glass analyses from the paired Mamaku-Ohakuri eruptions (Gravley et al. 2007) have been used (ignimbrite and fall deposit). The geobarometer has been applied to matrix glass and melt inclusion analyses from different magma types of the paired eruption (the most evolved Type 1, with bulk-rock SiO_2 content of 74-78 wt. %, and Type 2 with SiO_2 contents of 70-75 wt. %), using the same terminology as Milner et al. (2003) and Gravley et al. (2004). From the OVC, melt inclusion analyses from the Matahina, Rotoiti and Kaharoa eruptions have been used (ignimbrites and fall deposit). For the Taupo Volcanic Centre (TVC); melt inclusion compositions from the Oruanui and the Taupo eruption have been used. The stratigraphy of the eruptive deposits for the Oruanui comprises ten phases (described in Wilson 2001); the samples used here are from phases 1, 2 and 10; for the Taupo eruption only three analyses could be used, as all other analyses were from plagioclase-hosted melt inclusions.

4.4.2. Rhyolite-MELTS phase-equilibrium geobarometry

We employ phase equilibria calculations using Rhyolite-MELTS (Gualda et al. 2012-a) to constrain crystallisation pressures (Gualda & Ghiorso revised), using major element glass compositions (melt inclusions and matrix glass) as data input. Simulations in rhyolite-MELTS are run at pressures of 25-500 MPa, in 25 MPa intervals, under water-saturated conditions, and with

oxygen fugacity fixed along the NNO buffer curve. These pressure estimates are independent of the water content, especially for the pressure range expected for the TVZ rhyolites (Gualda & Ghiorso 2013-b; revised). Melt inclusions are all quartz-hosted; as such, they are representative of melt in equilibrium with both quartz and plagioclase, given that bulk pumice compositions are invariably enriched in the plagioclase component relative to glass. Therefore, phase equilibria require that melt inclusions and matrix melt would be saturated in both quartz and plagioclase at their liquidii (e.g. Blundy & Cashman 2001; Tuttle & Bowen 1958). As sanidine phenocrysts are absent in the TVZ rhyolites studied here, pressure estimates using the quartz and two feldspars constraints cannot be addressed (Gualda & Ghiorso revised); the lack of intersection between sanidine saturation, and quartz and plagioclase saturation in figure 4.3 is expected. The pressure estimates for synchronous crystallisation of quartz and plagioclase is constrained by the intersection of the saturation curves for quartz and plagioclase. The exact pressure and acceptable range of residual temperature is determined by the difference in slope methodology outlined in Gualda & Ghiorso (revised; Fig. 4.2 a-b). The position of the crossover between the two saturation curves is determined by fitting a parabola to the curve describing the difference in saturation temperature between quartz and plagioclase (hereafter referred to as the residual temperature curve), whose minimum corresponds to the estimated pressure. The errors are estimated to be ±25 MPa for the quartz +1 feldspar constraint (Gualda & Ghiorso revised). In many cases, the saturation temperatures for quartz and plagioclase are never within 5 °C, and in these cases we conclude that no pressure estimation can be made (Fig. 4.2c). For some glass compositions (55 in total), the saturation curves for plagioclase and quartz become coincident or nearly so. This generally occurs below ~100 MPa and the parabola system in Gualda & Ghiorso (revised) is no longer suitable. In this case, we pick the highest pressure at which the coincidence within 5°C takes place (Fig. 4.3); these should be interpreted as maximum pressures.

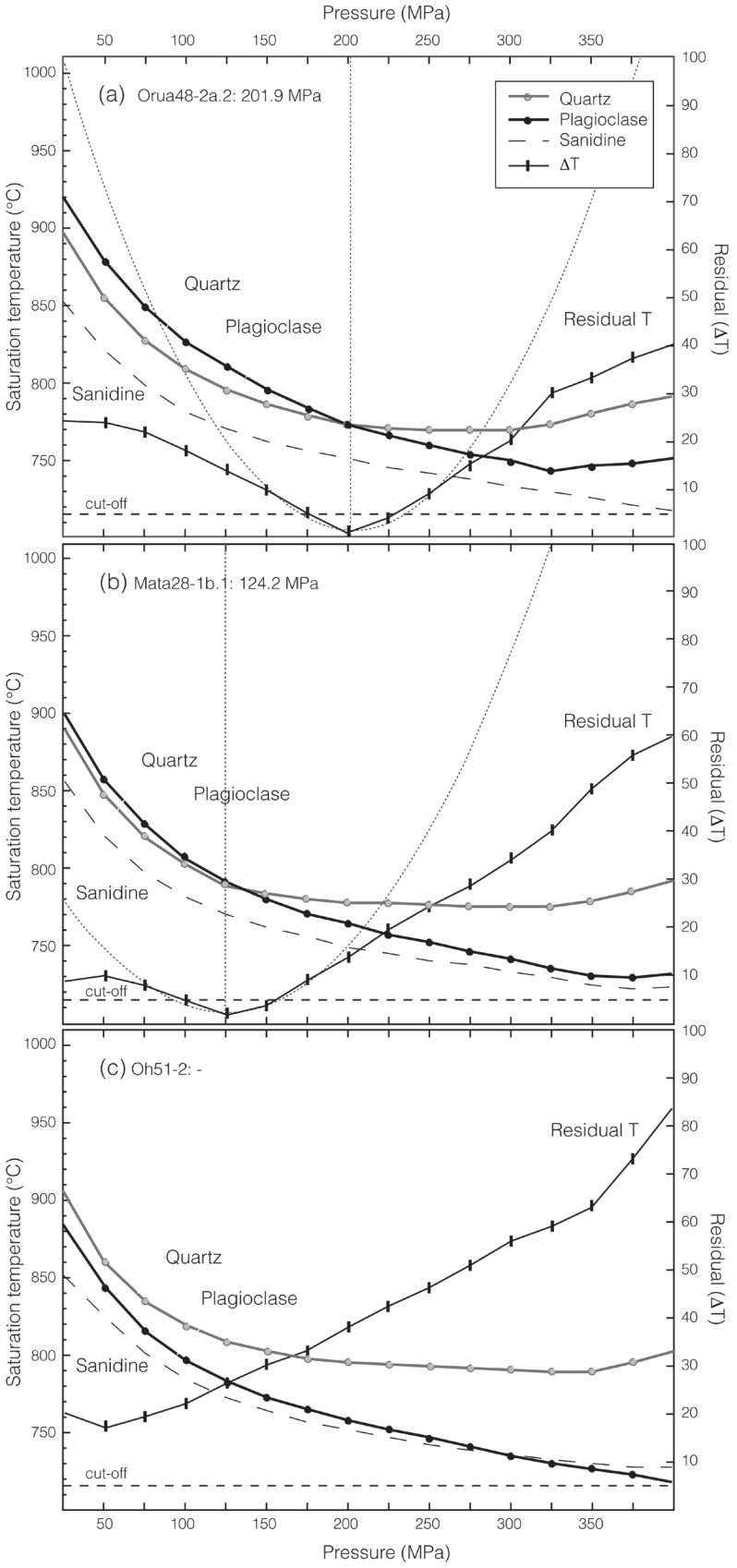

Figure 4.2: Application of the rhyolite-MELTS geobarometer to rhyolitic glass compositions from the TVZ. Diagrams show examples from (a) the Oruanui ignimbrite, Taupo Volcanic Centre, (b) the Matahina ignimbrite, Okataina Volcanic Centre, and (c) the Ohakuri fall deposit, Ohakuri Volcanic Centre for the quartz + 1 feldspar constraint, as there are no sanidine phenocrysts present. For (a) and (b), the estimated pressure corresponds to the minimum of the fitted parabola (dotted line) calculated for the residual temperature (ΔT) curve (difference between the quartz and plagioclase saturation curves). The glass composition in diagram (c) does not yield any pressure estimate, as there is no crossover between the quartz and plagioclase saturation curves.

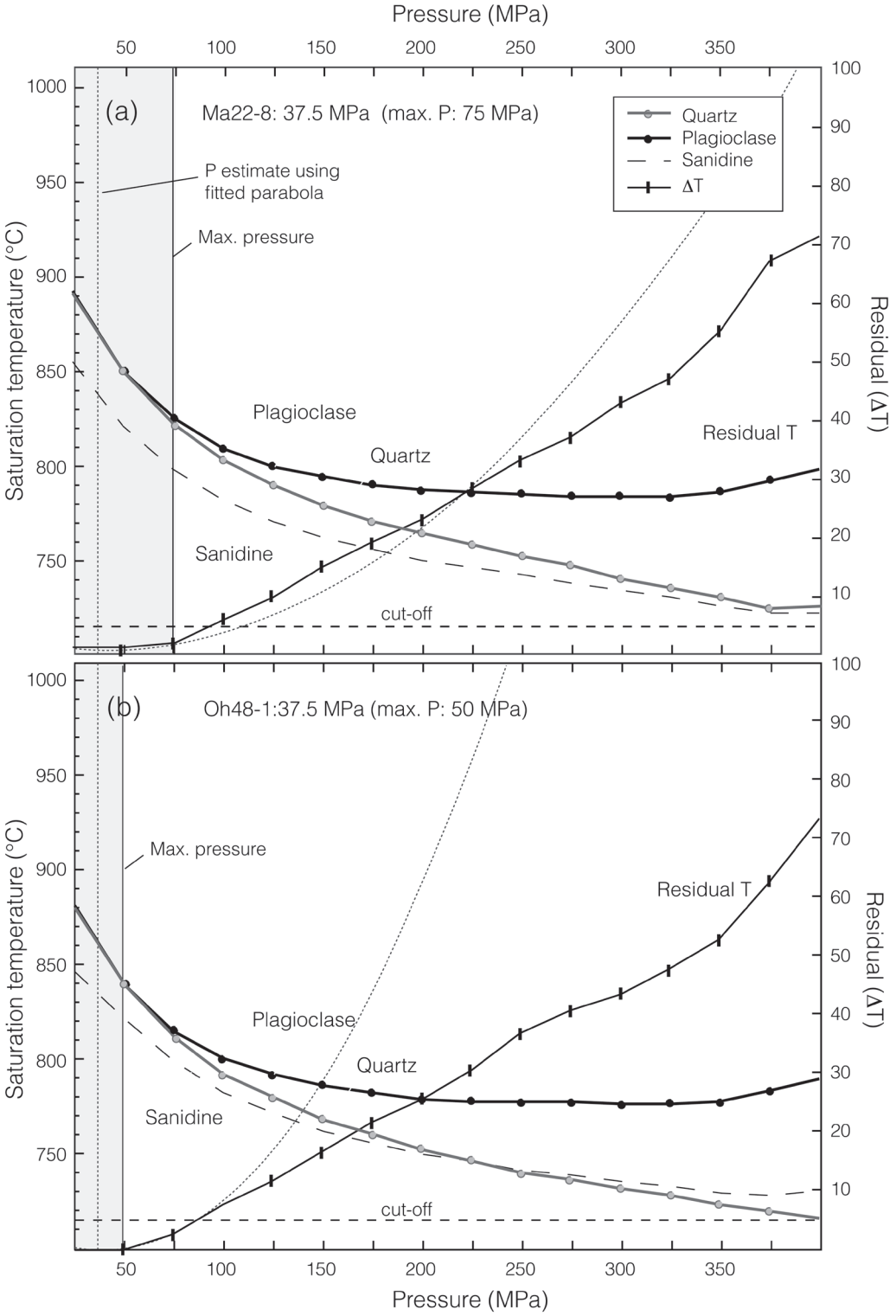

Figure 4.3: Application of the rhyolite-MELTS geobarometer to rhyolitic glass compositions from the TVZ. Diagrams show application examples from (a) the Mamaku ignimbrite, Rotorua caldera, and (b) the Ohakuri fall deposit, Ohakuri caldera for the quartz + 1 feldspar constraint. These diagrams show that the quartz and plagioclase saturation curves in some cases become nearly parallel for pressures below ~100 MPa. For these compositions, estimated pressures are manually adjusted to the maximum pressure at which there is a crossover between the two saturation curves (dashed line).

4.4.3. Pressure estimates

Application of the rhyolite-MELTS geobarometer leads to pressure estimates for 246 of 404 melt inclusions and 18 of 163 matrix glass compositions. A summary of the results is presented in Table 4.2 (for the entire dataset refer to the supplementary material). Some systematic differences between the eruptions and the volcanic centres can be observed (Fig. 4.4; Table 4.2). The distribution of the resulting pressures is displayed in figure 4.5 for the different volcanic centres. From figure 4.6, we observe that the pressure estimates from rhyolite-MELTS are positively correlated with Na_2O, and negatively with SiO2. All melt inclusion compositions with >78.5 wt. % SiO_2, and <3 wt. % Na_2O (Fig. 4.6 a and d) do not yield pressure estimations (i.e. no crossover between the plagioclase and quartz saturation curves in the pressure-temperature space, Fig. 4.2c). Matrix glass is the most affected and compositions with >78.5 wt. % SiO_2 and <3.5 wt. % Na_2O do not produce results (Fig. 4.7). Detailed study of matrix glass compositions from the RoOhVC show that these are likely affected by alkali mobility and secondary hydration (Chapter 2).

4.5. Rhyolite-MELTS geobarometry

The rhyolite-MELTS phase-equilibrium geobarometer has been applied in this study to numerous melt inclusion and matrix glass compositions from four distinct volcanic centres in the central TVZ (Table 4.1 and 4.2). Constraining the pressures of magma bodies in the crust is essential to gain insights into depths of storage and geometry of the magmatic systems. Before addressing the pressures and their implications for the TVZ, results obtained with the rhyolite-MELTS geobarometer are compared to other pressure estimates from the literature to assess the utility of this new geobarometer.

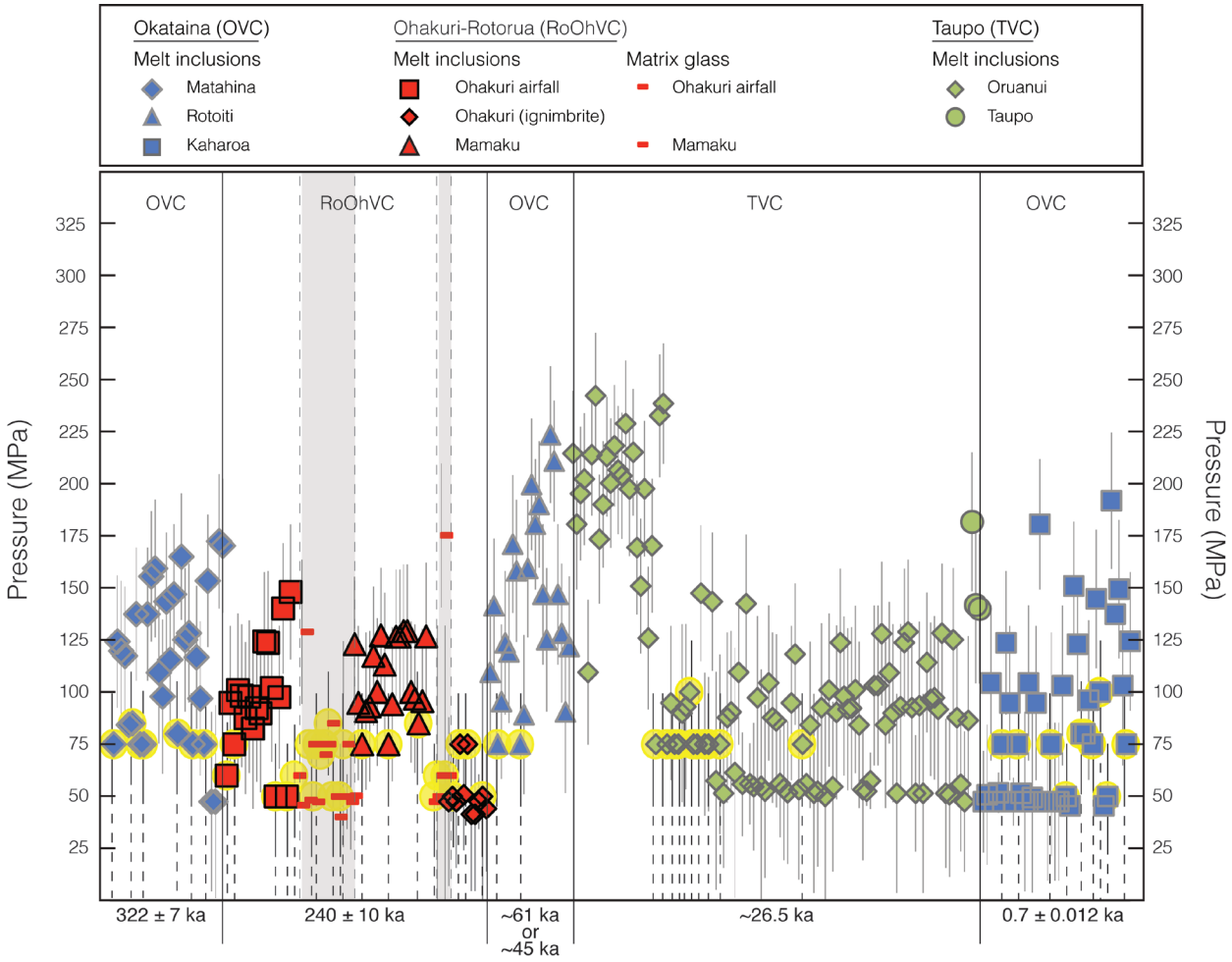

Figure 4.4: Pressure estimates derived from the rhyolite-MELTS geobarometer applied on rhyolitic glass compositions from the TVZ (references for eruption ages are in Table 4.1). The grey-shaded areas represent matrix glass compositions for the Rotorua and Ohakuri Volcanic Centres, the yellow areas around some data points represent compositions, which have manually adjusted pressures (maximum pressures). The compositions yielding no pressure have been removed to simplify the figure.

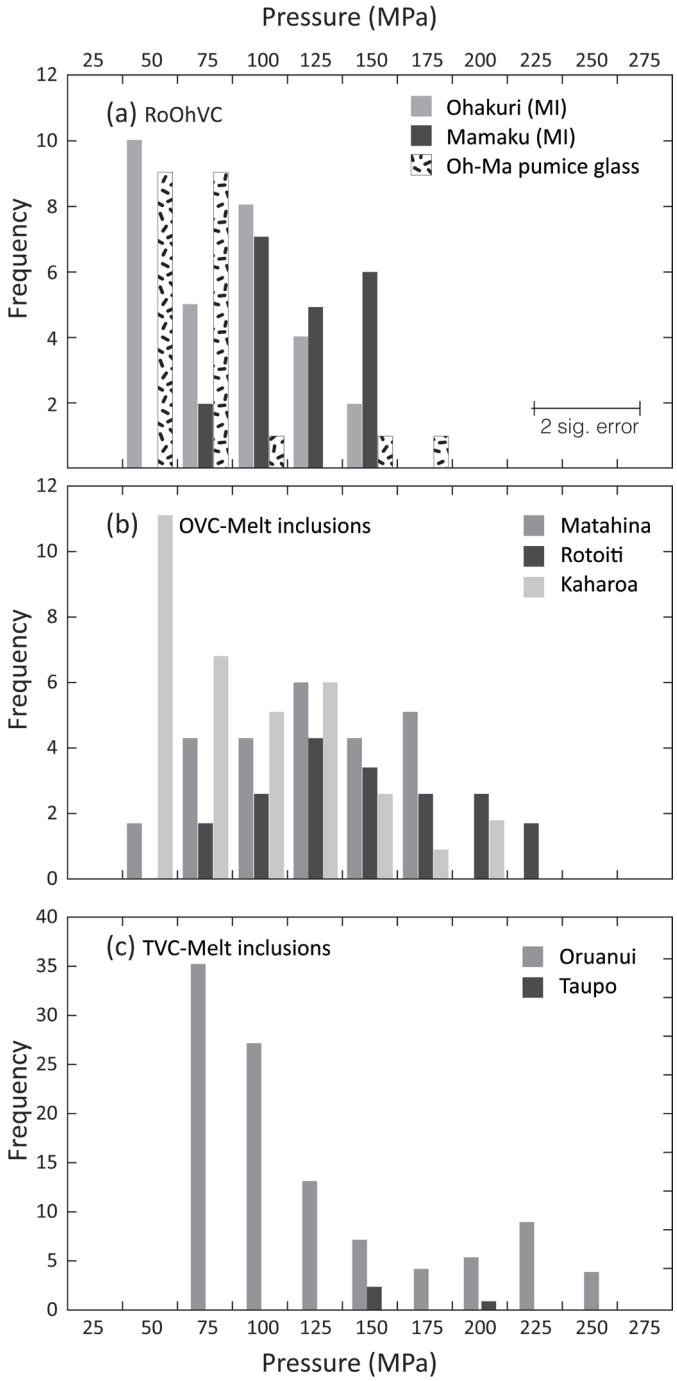

Figure 4.5: (a)-(c) Histograms showing the distribution of pressure estimates derived from the rhyolite-MELTS geobarometer applied to rhyolitic glass compositions from the central TVZ. Notice that matrix glass in the RoOhC rhyolites (a) gives lower pressures than melt inclusions, consistent with ascent-drive crystallization. Pressures in the OVC are a bit higher than in the other centres, with the exception of the Kaharoa eruption, which has been inferred to derive from a distinct vent than Matahina and Rotoiti. The Oruanui eruption yields a clearly bimodal distribution. All of these results are consistent with patchy distribution of independent magma bodies, often present at the same time and erupted during the same event.

4.5.1. Reliability of glass compositions

Unlike most geobarometers, which rely on exchange reactions involving minor phases, the rhyolite-MELTS geobarometer relies on the global minimisation of relevant thermodynamic potentials and consideration of the equilibration between the most abundant phases in the system (melt, plagioclase and quartz, in this case). As such, the rhyolite-MELTS geobarometer is very sensitive to glass compositions (Fig. 4.6-4.7; Gualda & Ghiorso revised), such that the quality of the glass, and to some extent the analytical procedure used to obtain glass compositions, will play a substantial role in obtaining viable pressure estimates.

It is well known that matrix glass is considerably affected by secondary hydration that involves alkali loss (i.e. hydrogen exchange for Na^+ and K^+ ions; Cerling et al. 1985). This effect is illustrated in figure 4.7 c-d, which shows that all the samples with low K_2O and Na_2O contents (<3.6 wt. % and <3.5 wt. % respectively) do not yield any pressure estimates. A result of secondary hydration is an apparent increase in SiO_2 concentrations (and to a lesser extent Al_2O_3) when normalised on an anhydrous basis, which explains why many compositions with very high SiO_2 do not yield pressure estimates.

Melt inclusions are, on the other hand, generally less affected by secondary processes than matrix glass, as the host mineral can potentially shield the melt inclusion from decompression and other post-entrapment changes (e.g. Schiano & Bourdon 1999). However, melt inclusion glass may also be affected by post-entrapment alteration, for instance through dissolution and re-precipitation on melt inclusion walls or diffusion of material through cracks within crystals (e.g. Bucholz et al. 2013; Gaetani et al. 2000; Severs et al. 2007; Steele-McInnis et al. 2011; Zajacz et al. 2009). Many studies on olivine-hosted inclusions (e.g. Bucholz et al. 2013), but also on quartz-hosted melt inclusions (e.g. Severs et al. 2007; Steele-McInnis et al. 2011), identify post-entrapment volatile loss through diffusion or formation of a vapour bubble. However, modification of the major elemental glass composition also occurs, and a recent study from Zajacz et al. (2009)

shows rapid diffusion of Na^+ (along with Li^+, Ag^+, Cu^+, and H^+) through the quartz host, leading to significant variation in concentrations within the melt inclusion at upper crustal P-T conditions. Another potential source of compositional complexity is the analysis of Na in glass: in electron-based analysis (e.g. electron microprobe), there is often a time-dependent observed reduction in intensity of the Na-Kα X-ray line intensity during electron-beam irradiation of the sample. Because SiO_2 is such an abundant component of rhyolite glasses, issues with analysis of any major element will be reflected in the resulting SiO_2 concentrations. While specific analytical settings can help minimise the problem, analytical Na-loss can remain an issue (Morgan & London, 1996).

Many melt inclusion compositions do not yield a pressure estimate using the rhyolite-MELTS geobarometer, which is correlated to the major element composition of the glass (Fig. 4.6). Compositions that yield no pressure estimate show either SiO_2 excess or a Na_2O deficit, and therefore, may be an effect of post-entrapment modification of the glass or a result of analytical problems. These results confirm the observation of Gualda & Ghiorso (revised), that the phase-equilibrium geobarometer is very sensitive to the glass composition. On one hand, this limits the applicability of the geobarometer to pristine glass and high quality analyses; on the other hand, the geobarometer may be effectively used to filter out spurious glass compositions.

4.5.2. Comparison with other pressure estimates in the TVZ

Other geobarometers have been applied to the TVZ eruptive deposits, and we compare the results obtained with those resulting from application of the rhyolite-MELTS geobarometer. Some of the early studies on pressure estimates for the TVZ rhyolites, include the use of mineral assemblage and Fe-Ti oxygen barometry, which yield a large range of results between ~100-400 MPa (Ghiorso & Sack, 1991). Other studies use experimental and thermodynamic data for cummingtonite, which is present in a number of the OVC rhyolites, to obtain crystallisation pressures of ~200 MPa (Ewart et al., 1975; Nicholls et al., 1992). Since, numerous more studies using different geobarometers have been applied to the TVZ eruptive deposits. The pressure estimates for the Okataina Volcanic

Centre (OVC) from the literature include: (1) amphibole geobarometry, with pressure ranges ~60-300 MPa (Deering et al. 2011-a; Shane & Smith 2013); (2) H_2O-CO_2 contents in quartz-hosted melt inclusions indicating pressures of ~90-260 MPa (Shane et al. 2007; 2008-b; Smith et al. 2010), and ~100-150 MPa (Johnson et al. 2011). For the Taupo Volcanic Centre (TVC), pressure estimates from the literature include: (1) amphibole geobarometry on the Oruanui biotite-bearing rhyolites indicating pressures of ~70-150 MPa (avg. ~140 MPa), and the biotite-free rhyolites of ~90-200 MPa (avg. ~140 MPa; Allan et al. 2012); (2) H_2O-CO_2 contents in melt inclusions from the Oruanui eruptive deposits yielding pressures of ~95-190 MPa (avg. ~140 Ma; Liu et al. 2006). For the Rotorua-Ohakuri Volcanic Centres (RoOhVC) pressures are compared to H_2O-CO_2 solubility models, yielding pressures between 75 and 200 MPa (avg. 100MPa; Chapter3).

Comparison between amphibole geobarometry with either the rhyolite-MELTS geobarometer or H_2O-CO_2 is problematic because it assumes equilibrium between quartz and amphiboles. Comparing pressures from the rhyolite-MELTS geobarometer with H_2O-CO_2 solubility models in quartz-hosted melt inclusions is more straightforward, as both correspond to quartz crystallisation and melt inclusion entrapment pressure conditions. However, H_2O-CO_2 solubility models assume fluid-saturation during melt inclusion entrapment, which is not always true for every silicic magma. Furthermore, at present these models do not consider the presence of other volatile phases in the melt, like chlorine for instance, which can reach high concentrations in the TVZ rhyolites (Chapter 3), and may cause an increase in the pressure estimates obtained with the H_2O-CO_2 solubility models (Botcharnikov et al. 2007). In contrast, no assumption regarding fluid saturation is necessary in rhyolite-MELTS geobarometry (Gualda & Ghiorso revised).

Small discrepancies can be observed for the Ohakuri eruption from the RoOhVC, where the H_2O-CO_2 solubility models generally yield slightly higher pressures (Fig. 4.8b). In chapter 3, we demonstrated that the magmas responsible for the Ohakuri ignimbrite may not have been saturated in volatiles at the time of quartz crystallisation, and that the chlorine content in these melts is

very high (~0.3 wt. %; Chapter 3). The pressures obtained with the H_2O-CO_2 solubility models may, therefore, be a slight over-estimation or represent maximum pressures. The composition of the melt inclusion glass in some cases may also be slightly affected by secondary processes; in general many of the compositions for the Ohakuri ignimbrite did not yield pressure estimates at all, indicating that the quality of the glass may be poor. Since the Ohakuri lacks hydrous phases in the mineral assemblage, it is also not possible to use amphibole geobarometry, making it difficult to assess uncertainties associated with the rhyolite-MELTS derived pressures. However, overall, the rhyolite-MELTS geobarometer compares well with other methods (Fig. 4.8), and yields similar pressure ranges.

4.5.3. Matrix glass vs. melt inclusions

Matrix glass and melt inclusions record different stages in magmatic evolution, so examining differences in the pressure estimates can reveal temporal trends in magmatic evolution. Matrix glass is representative of the melt composition at the last point of crystallisation prior to eruption, possibly including the effects of crystallization during ascent and eruptive decompression. Quartz and plagioclase crystals in the studied eruptive deposits do not display any features indicative of resorption or disequilibrium at their rims; it can thus be inferred that the crystals were in equilibrium with the melt until eruption. In this context, the resulting pressures from the matrix glass compositions may represent the evolution of the melt after inclusion entrapment, and may give insights into the syn-eruptive history and ascent of magma. Crystallisation as a result of eruptive decompression has been shown in crystal size distribution studies, where crystal nucleation events resulting from decompression just prior to and during eruption are suggested by large populations of tiny crystals (e.g. Cashman 1988; Pamukcu et al. 2012).

Here we compare the pressure estimates between matrix glass and melt inclusion compositions for the paired Mamaku-Ohakuri eruption from the RoOhVC (Fig. 4.7). The matrix glass compositions that yield pressure estimates (i.e. samples that are not as affected by secondary

processes) indicate lower pressures than the quartz-hosted melt inclusions from the same pumice (Fig. 4.7). These results are consistent with very shallow crystallisation as melt evolves during buoyant rise within a magma body or ascent towards eruption and/or eruptive decompression.

For the Ohakuri fall deposit, the melt inclusions show a large vertical extent of crystallisation pressures, and the lowest pressures include the lowest reliable pressure indicated by the matrix glass (some overlapping pressures at ~50 MPa; Fig. 4.7). This may indicate that the matrix glass did not significantly evolve or experienced significant pressure changes following melt inclusion entrapment. To date, no detailed textural study is available, however from petrographic observations and cathodoluminescence imaging (Chapter 2), no striking difference in crystal size or particular zoning pattern are associated to the quartz crystals and melt inclusions yielding these lower pressure estimates. The ability of deriving pressure estimates through the rhyolite-MELTS geobarometer using matrix glass compositions is an important advantage of this method, especially given the ability to filter out spurious data, which are more likely to occur for matrix glass analyses. The resulting pressure estimates may give useful information on the late stage evolution of silicic magmas especially in cases where syn-eruptive crystallisation is indicated.

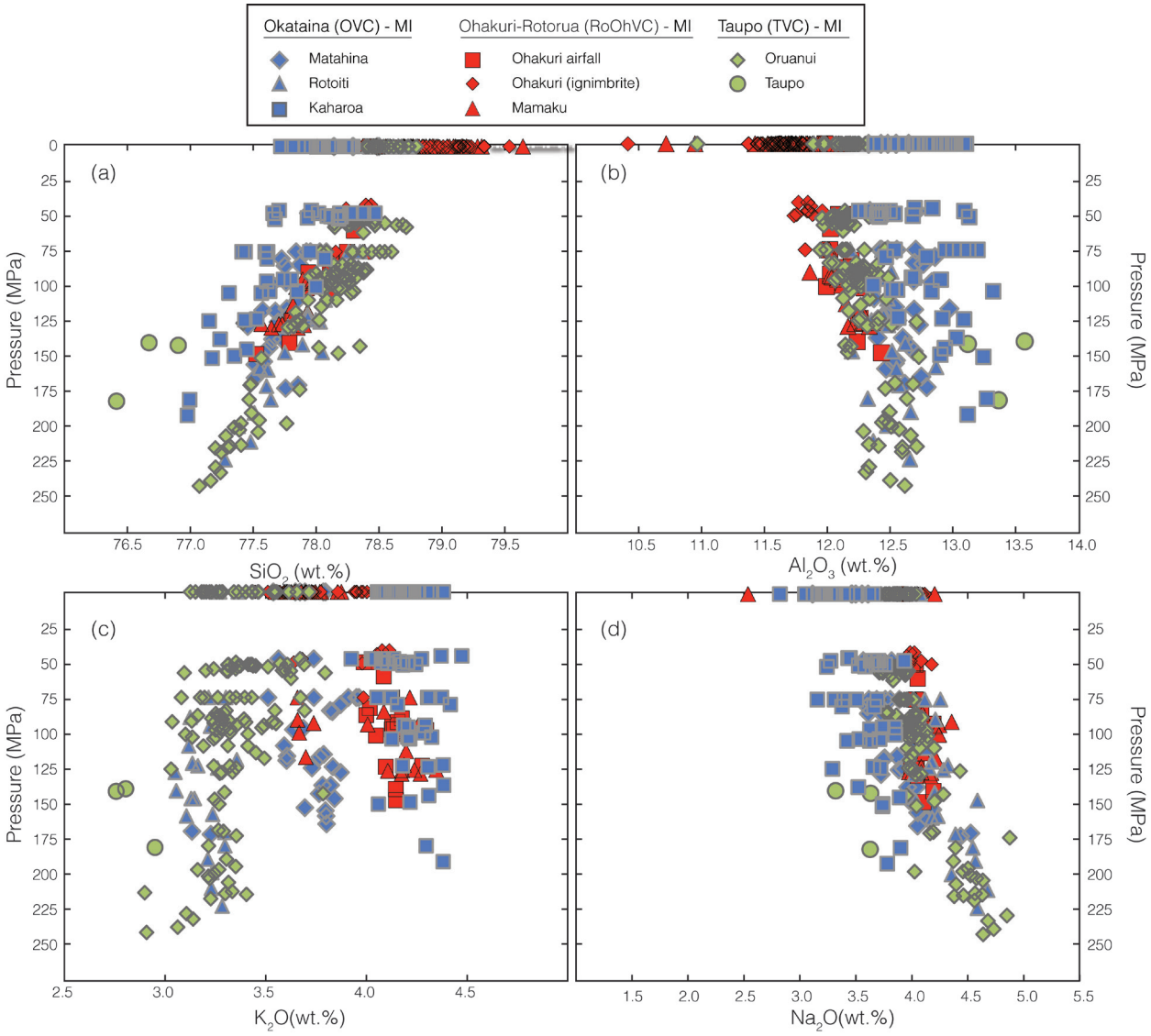

Figure 4.6: (a)-(d) Pressure estimates derived from the rhyolite-MELTS geobarometer vs. major oxides abundance (in wt.%, anhydrous basis) for all TVZ melt inclusion compositions. The results show strong correlation between glass composition and the calculated pressures; from (a) all compositions with SiO_2 contents >78.5 wt.% do not yield any results, suggesting that the highest SiO_2 values result from glass alteration. These results show that extreme compositions, very likely reflecting altered glass, can be effectively filtered out by the rhyolite-MELTS geobarometer.

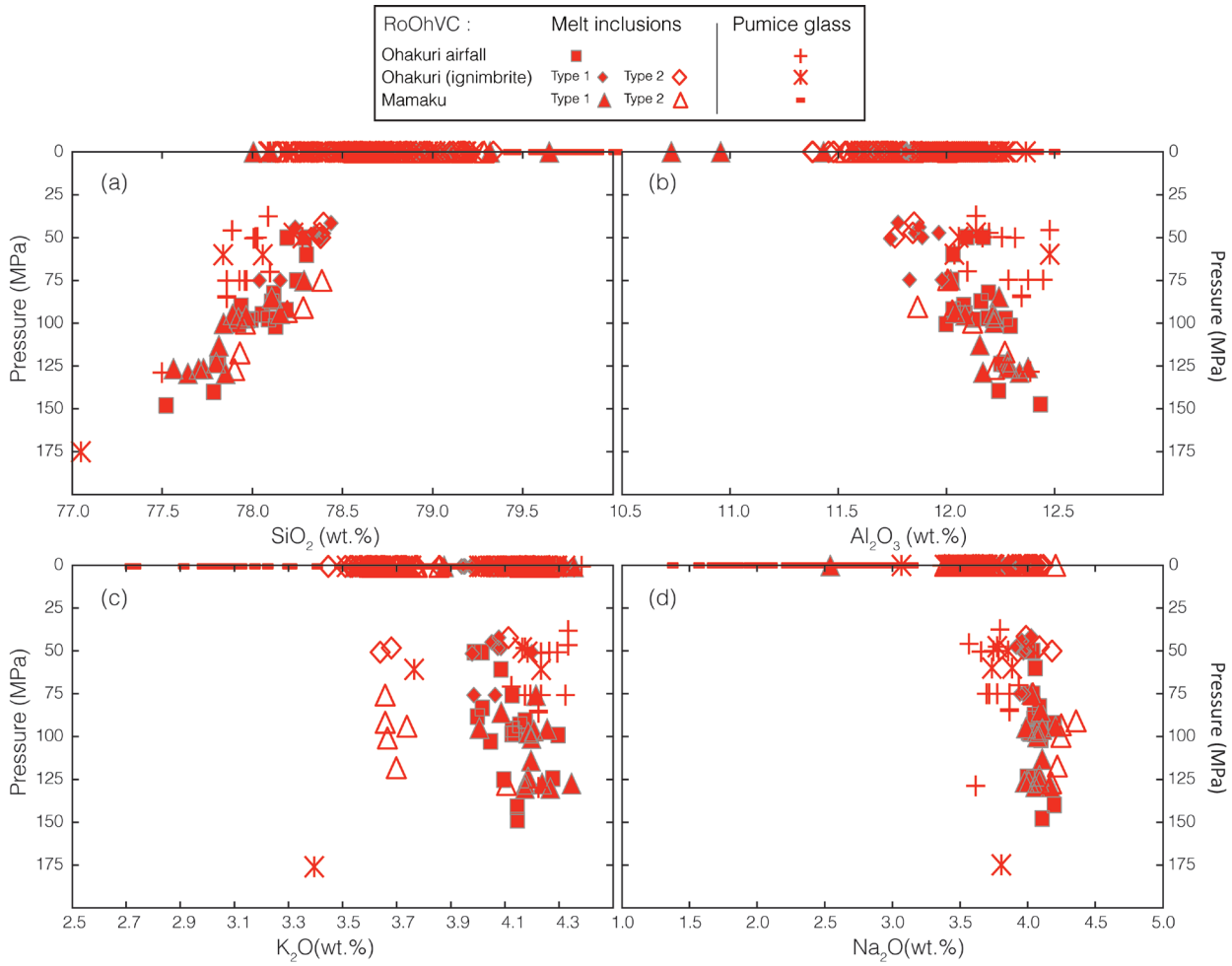

Figure 4.7: (a)-(d) Pressure estimates derived from the rhyolite-MELTS geobarometer vs. major oxides abundance (in wt.%, anhydrous basis) for the Mamaku and Ohakuri (RoOhVC) quartz-hosted melt inclusions and matrix glass compositions. This figure shows the strong correlation between calculated pressures and glass compositions. Most matrix glass compositions do not yield a pressure estimate; in diagram (d) all compositions (mostly matrix glass) with <3.5 wt.% Na_2O – which we infer to result from glass alteration – fail to yield pressure estimates. Matrix glass yields systematically lower pressures with this geobarometer, which is suggestive of decompression-driven crystallisation during syn-eruptive magma ascent.

4.6. Implications for the TVZ

The TVZ is a very active and productive volcanic zone, and its rhyolitic magmatism has predominated in the past ~1.6 Ma (Wilson et al. 1995; 2009) and possibly longer (i.e. ~2 Ma; Eastwood et al., 2013). Constraining the pressures, and hence the pre-eruptive storage depth, of silicic magma bodies in the TVZ is very important for understanding the vertical extent of these magmatic plumbing systems prior to eruption. The rhyolite-MELTS geobarometer is applicable to all the central TVZ rhyolites, such that we can compare different eruptive centres and eruptions, allowing us to further explore differences and similarities in residence depth among the central TVZ rhyolites.

The pressure estimates presented here confirm the shallow residence depth of the TVZ rhyolites (~2-10 km, majority ~4 km using a crustal density of 2.7 g/cm^3), concurring with previous estimates suggested in the literature with other geobarometers (e.g. Allan et al. 2012; Deering et al. 2011-a; Johnson et al. 2011; Liu et al. 2006; Shane et al. 2007; 2008-b; Shane & Smith 2013; Smith et al. 2010). We suggest that the main factor influencing the depth of the rhyolitic magma bodies in the central TVZ is active rifting, which along with magmatism, is ultimately responsible for the crustal and lithospheric architecture beneath the central TVZ (e.g. Harrison & White 2004, 2006; Rowland & Sibson 2001; Stratford & Stern 2006). The TVZ's present form (<350 ka) coincides with a structurally and magmatically segmented rift system with extension-related graben structures along the length of the central zone (Rowland & Sibson 2001; Rowland et al. 2010; Wilson et al. 1995). Active extension plays an essential role on the geometry and depth of the magmatic plumbing system in the central TVZ, and accommodation of rising magma may be enhanced in the upper crust. This is supported by an anomalously high thermal output at the surface of 4200±500 MW (estimations based on chloride fluxes in hot springs, Bibby et al. 1995). The thermal output at the surface largely exceeds that associated with volcanism in the central TVZ over the past ~350 ka, and it has been attributed to crustal magmatism (Bibby et al. 1995;

Hochstein 1995). Electrical resistivity surveys across the central TVZ show a high conductive zone at ~10 km depth, interpreted as plume-like structures of interconnected melt beneath the rift axis (Heise et al. 2007; 2010; Ogawa et al. 1999). The high heat flow from the lower intruded crust plays a significant role in the preconditioning of the mid to upper crust, and ultimately the shallow emplacement and residence depths of rhyolitic magma.

Rhyolite-MELTS yields particularly shallow pressures around 50 MPa (e.g. Ohakuri; Fig. 4.4). These pressures correspond to ~2 km depth, which are some of the shallowest pressures reported in the literature for caldera-forming silicic eruptions. The lack of shallow melt bodies detected by resistivity surveys in the central TVZ at these depths (Heise et al. 2007; 2010; Ogawa et al. 1999) makes it unlikely that these magmas have analogues in the present-day central TVZ crust (or limitations in resistivity at shallow depths). However, there is evidence for past silicic magmatism occurring at depths < 2km: the 0.71-0.65 Ma Ngatamariki intrusive complex (microdiorite, diorite, tonalite and mafic dykes) was intercepted by drilling (Browne et al. 1992; Chambefort et al. 2014-a). There is also evidence for such shallow magmatism at other volcanic centres outside the TVZ: in the Kumono caldera in Japan, drill-holes and geophysical surveys identified the top of the magma chamber being at ~1 km depth (Miura 1999). Alternatively, these shallow pressures may not correspond to shallow-level magma bodies, but rather they record the crystallization during ascent and eruption. In this context, the apparent lack of pressures below 50 MPa may simply reflect our inability to detect such pressures due to the similarity in the quartz and plagioclase saturation surfaces at very low pressures. Or, the limit of ~50 MPa represents the point at which crystallization largely stops due to kinetic effects.

Most of the central TVZ eruptive deposits record a wide range of pressures (~50-200 MPa; Fig. 4.4 and 4.5), corresponding to an apparent ~6-8 km depth variation recorded by melt inclusions, which implies a large vertical extent of the rhyolitic magma systems in TVZ. This could be in the form of continuous melt or, alternatively, distinct magma batches residing at different depths

through a dyke-sill complex. Multiple compositionally distinct magma batches are suggested to be present in the upper crust and co-erupt in large ignimbrite-forming eruptions (e.g. Cambray et al. 1995; Ellis & Wolff 2012; Gualda & Ghiorso 2013-b; Reubi & Nicholls 2005); this model has also been invoked for the TVZ magmatic systems (Chapter 2; Charlier et al. 2003; Shane et al. 2007, 2008-b). In the TVZ, most of these batches are likely to be shallow and at approximately the same level in the crust, however, there are some batches that are at higher pressure and have been erupted together with shallower batches, as exemplified by the Mamaku-Ohakuri eruption sequence. This will be discussed in more detail below.

A further possible explanation is that some of the quartz crystals may be of xeno- and /or antecrystic origin, representing assimilation of crystallised margins and/or relicts of the magmatic systems that fed previous eruptions. For the Mamaku and Ohakuri melt inclusions, inconsistencies in major and trace element compositions have led to the suggestion that antecrysts are present in most magma types (Chapter 2). Furthermore, evidence for interaction of some of the TVZ rhyolites with crystalline portions of the systems is shown by the presence of granodioritic lithics in the eruptive products (e.g. Kaharoa, Rotoiti, Ohakuri plutonic lithics; Brown et al. 1998-b; Burt et al. 1998; Shane et al. 2012). Similar pressure ranges have been observed for other large rhyolitic eruptions, for instance, the Kos-Plateau Tuff in Greece, where the pressure variations recorded by melt inclusions have been interpreted as crystal recycling in a long-lived and vertically extensive crystal-rich mush zone (Bachmann et al. 2009).

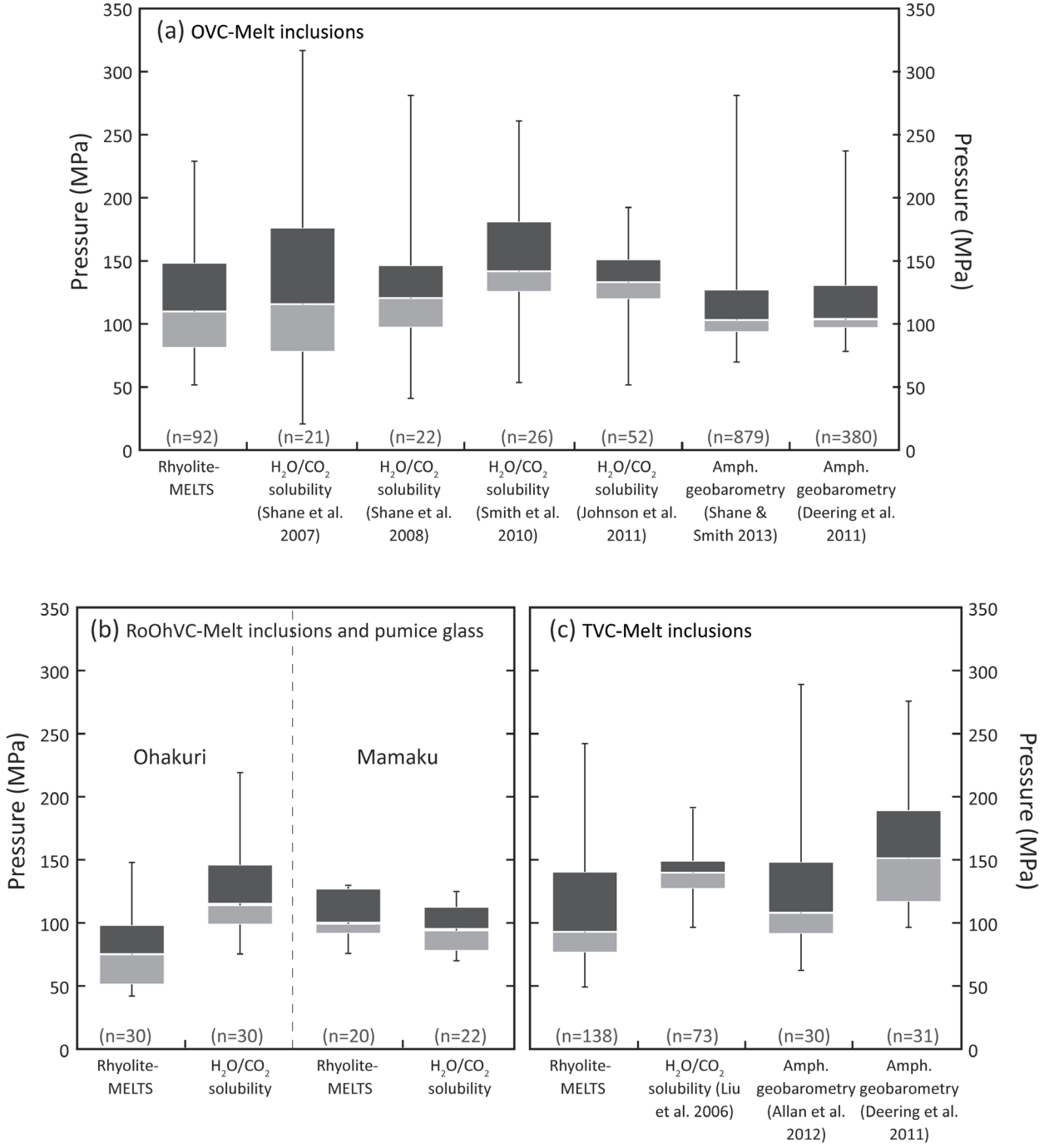

Figure 4.8: Box-whisker plots comparing the rhyolite-MELTS geobarometer with other geobarometers applied to TVZ rhyolites. Data for other geobarometers from Allan et al. (2012), Deering et al. (2011-a), Johnson et al. (2011), Liu et al. (2006), Shane et al. (2007, 2008-b), Shane & Smith (2013), and Smith et al. (2010). The white line represents the median of the dataset and the grey boxes the 25th and 75th percentiles; end of the whiskers represent the minimum and maximum of the dataset.

4.6.1. Pressure variations among the volcanic centres

Applying the same geobarometer to all the eruptive deposits allows for a more systematic comparison of storage and crystallisation pressures for the various volcanic centres and eruptions in the central TVZ. Overall most of the eruptive products studied here present similar pressure ranges, but some small and systematic differences among volcanic centres and eruptions are present (Fig. 4.4).

The Mamaku and Ohakuri eruptions, which occurred at the same time (~240 ka) from two distinct calderas (Fig. 4.1; Gravley et al. 2007), are associated with magmas characterised by distinct pressures and pressure ranges (Fig. 4.4 and 4.5a). Compared to the Mamaku ignimbrite, the Ohakuri fall magma shows a larger pressure range; the Ohakuri ignimbrite have a small range with systematically shallower pressures around 50 ± 25 MPa. Such differences are consistent with the existence of multiple magma bodies with variable residence depths and/or ascent histories that were co-erupted during the paired eruption (Chapter 2)

In contrast, glass from the Oruanui eruption yields a bimodal distribution, with a prevailing population recording shallow crystallisation pressures (~50-150 MPa), and a second population characterised by higher equilibration pressures (~200-250 MPa; Fig. 4.4 and 4.5c), with few compositions yielding pressures in between. The range of pressures presented here supports the mid to upper-crustal model for the Oruanui magmatic system (Wilson et al. 2006), but with crystallisation focussing at the bottom and top of this system. The extreme maximum pressures for the Oruanui correlate with the deepest geobarometric evidence for silicic magmatism in the TVZ and this may corroborate geophysical models where a transition from a thinner to a thicker crust occurs at the southern end of the central TVZ (e.g. Reyners et al. 2006). In addition, extension rates decrease from the central to southern parts of the TVZ (~10 to ~3 mm/a; Villamor & Berryman 2001; 2006) which may exert a control on the maximum depth of silicic magmatism at the southern end of the central TVZ (i.e. the Taupo Volcanic Centre).

Rhyolites from the OVC yield a similar distribution of pressures for the eruptions analysed in this paper. However, compositions for the Kaharoa eruption have a well-represented low-pressure population (~50 ± 25 MPa; Fig. 4.4 and 4.5b), which is not present in other OVC eruptions studied here. The vent location for the Kaharoa eruption is along the Tarawera volcanic complex and differs in location from the vent for the Matahina and Rotoiti eruption, which is along the Haroharo volcanic complex (Fig. 4.1; e.g. Leonard et al. 2002; Nairn et al. 2004). Similarly to the Rotorua-Ohakuri magmatic system, this indicates that magma body depths and geometries can vary considerably within a caldera. However, the Kaharoa is also considerably younger than the Matahina and the Rotoiti eruption (Table 4.1). Therefore, such changes may also reflect a shallow crustal structure that evolves through time following subsequent eruptions and crustal readjustments (e.g. Kennedy et al, 2012).

4.7. Conclusions

In this study we apply the phase equilibrium geobarometer (Gualda & Ghiorso revised) to TVZ rhyolitic glass compositions. Melt inclusion and matrix glass compositions of seven eruptions from four distinct eruptive centres (Chapter 2 and 3; Pamukcu et al. in preparation) are used as data input into rhyolite-MELTS, and the resulting pressures correspond to the pressure where the given melt is in equilibrium with quartz and plagioclase saturation (sanidine phenocrysts are absent in all of the analysed eruptive deposits here).

In general, the rhyolite-MELTS geobarometry compares well with other methods applied to the TVZ rhyolites, and we found that the rhyolite-MELTS geobarometer presents certain advantages in comparison to other methods: (1) it can be applied to amphibole-free rhyolites, as is the case for some of the TVZ eruptive deposits; (2) no assumption regarding volatile saturation is necessary, as needed in the case of fluid saturation pressures based on H_2O-CO_2 solubility models (Gualda & Ghiorso revised); and (3) both melt inclusion and matrix glass compositions can be used, which

makes it widely applicable for volcanic rocks. This geobarometer is also very sensitive to glass compositions and provides an objective criterion to detect spurious compositions. As a result, it shows that not only is matrix glass affected by secondary alteration, but also some of the melt inclusion glass has experienced post-entrapment modifications. Furthermore, sample preparation is less time consuming and easier, compared to H_2O and CO_2 analysis with transmission FTIR, and major element glass analysis with the electron microprobe is well-established and standard practice in many laboratories. On the downside, our study reveals that the rhyolite-MELTS geobarometer is less sensitive to pressures below ~100 MPa.

Overall there is good agreement between the rhyolite-MELTS geobarometer, amphibole geobarometry, and H_2O-CO_2 solubility models for the OVC and Mamaku ignimbrite (Fig. 4.8 a-b). However, some discrepancies are present (i.e. Ohakuri ignimbrite; Fig. 4.8c). It is somewhat difficult to assess to what extent these discrepancies correspond to limitations of rhyolite-MELTS or if they illustrate weaknesses in the assumptions or calibration of other geobarometers. The rhyolite-MELTS geobarometer is able to identify systematic differences between various volcanic centres and between different eruptions from the same volcanic centre.

The pressure estimates, obtained with the rhyolite-MELTS geobarometer, provide further evidence that the central TVZ magmas are stored in some of the shallowest reservoirs on Earth, which is suggested to be related to the extensional tectonic regime and an exceptionally high heat flux from depth. The recognition of various populations with different equilibration pressures is consistent with the idea that multiple batches of eruptible magma can be present in the crust at the same time, and they can be tapped simultaneously by large eruptive events (Chapter 2; Charlier et al. 2003; Ellis & Wolff 2012; Gualda & Ghiorso 2013-b; Reubi & Nicholls 2005; Shane et al. 2007, 2008-b). The challenge for the future is to combine geobarometric, chemical and textural data sets to constrain the geometries of magma bodies both vertically and horizontally. We suggest here that the rhyolite-MELTS geobarometer may provide further constraints not afforded by other

geobarometric techniques.

Explosive caldera-forming rhyolitic eruptions are devastating, and have significantly large impacts on populations. From a hazard perspective it is thus crucial to understand these systems and the depths at which they reside, which may give useful insights to the current state of dormant volcanoes.

Table 4.1: Summary of eruptive deposits from the central TVZ, analysed in this study.

Eruption Name	Age (ka)	Volume (km^3)	Source Caldera	Mineral Assemblage	No of analysed pumice clasts
Kaharoa	0.7 ± 0.012	~ 5	Okataina	qtz + plg + bt ± hbl ± cum	6
Taupo	~ 1.8	35	Taupo	plg + opx ± qtz	1
Oruanui	~ 26.5	~ 530	Taupo	qtz + plg + hbl+ opx	6
Rotoiti	~ 61[a] / ~45[b]	~ 100	Okataina	qtz + plg + cum + hbl + opx ± bt	5
Mamaku	240 ± 10	> 145	Rotorua	qtz + plg + opx ± hbl	9
Ohakuri	240 ± 10	> 100	Ohakuri	qtz + plg + opx	14
Matahina	322 ± 7	> 160	Okataina	qtz + plg + opx ± bt ± hbl	6

bt-biotite; cum-cumingtonite; hbl-hornblende; opx-orthopyroxene; plg-plagioclase; qtz-quartz; san-sanidine

Compilation from the following sources: Beresford (1997), Brown et al. (1998), Charlier et al. (2005); Danišic et al. (2012[b]), Deering et al. (2008; 2010), Gravley (2004), Leonard et al. (2010), Milner et al. (2003), Nairn (2002); Nairn et al. (2004), Schmitz & Smith (2004), Smith et al. (2005), Sutton et al. (1995), Wilson (2001); Wilson et al. (2006, 2007[a]).

Table 4.2: Average major element composition of quartz-hosted melt inclusions and matrix glass for the analysed eruptive units and summary of the pressure estimates resulting from the rhyolite-MELTS geobarometer.

	SiO_2 (wt%)	TiO_2 (wt%)	Al_2O_3 (wt%)	FeO (wt%)	MgO (wt%)	CaO (wt%)	Na_2O (wt%)	K_2O (wt%)	Pressure Rhyolite-MELTS (MPa) Avg.	P range
Quartz-hosted melt inclusions										
Kaharoa (n = 61)										
avg.	77.79	0.09	12.76	0.84	0.08	0.63	3.54	4.21	85	50-195
1 σ	0.54	0.03	0.28	0.06	0.02	0.09	0.48	0.12		
Taupo (n = 3)										
avg.	76.65	0.23	13.35	1.74	0.21	1.35	3.52	2.84	155	140-180
1 σ	0.20	0.01	0.18	0.04	0.01	0.03	0.15	0.08		
Oruanui (n = 135)										
avg.	77.44	0.12	12.51	1.11	0.11	0.99	4.45	3.21	110	50-245
1 σ	0.27	0.02	0.13	0.12	0.02	0.12	0.25	0.13	*85*	**Avg. P1*
									205	**Avg. P2*
Rotoiti (n = 25)										
avg.	77.92	0.13	12.45	0.94	0.15	0.89	4.23	3.22	140	75-225
1 σ	0.38	0.02	0.16	0.08	0.02	0.12	0.24	0.09		
Mamaku (n = 64)										
avg.	78.60	0.13	11.85	1.01	0.05	0.55	3.78	4.03	105	75-130
1 σ	0.60	0.07	0.30	0.08	0.02	0.08	0.31	0.24		
Ohakuri (n = 84)										
Fall deposit - avg.	78.04	0.08	12.15	0.95	0.06	0.55	4.05	4.12	95	50-150
1 σ	0.21	0.04	0.12	0.07	0.01	0.05	0.06	0.09		
Ignimbrite - avg.	78.75	0.11	11.67	1.03	0.06	0.56	3.92	3.89	50	45-75
1 σ	0.43	0.05	0.21	0.11	0.02	0.06	0.11	0.26		
Matahina (n = 36)										
avg.	77.84	0.09	12.58	0.99	0.08	0.80	3.82	3.72	115	50-175
1 σ	0.27	0.01	0.16	0.08	0.01	0.04	0.27	0.17		
Matrix glass										
Mamaku (n = 74)										
avg.	78.52	0.09	12.06	1.11	0.07	0.60	3.58	3.98	80.00	50-175
1 σ	0.30	0.05	0.18	0.12	0.02	0.10	0.13	0.25		
Ohakuri (n = 89)										
Fall deposit - avg.	78.13	0.08	12.22	1.06	0.06	0.57	3.68	4.21	65	40-130
1 σ	0.25	0.05	0.13	0.05	0.01	0.07	0.11	0.09		
Ignimbrite - avg.	79.86	0.13	12.17	1.20	0.08	0.65	2.28	3.63	-	-
1 σ	0.81	0.06	0.14	0.14	0.02	0.12	0.41	0.39		

Analyses are normalised to anhydrous conditions.
Major elements are from Bégué et al. (revised-a; revised-b) and Pamukcu et al. (in preparation), from electron microprobe (University of Washington and Oregon State University) and analytical scanning electron microscope (Vanderbuilt University).
n - number of analyses
** For the Oruanui eruption additional averages for the two pressure populations (P1 and P2) are given. The cut-off value between P1 and P2 is set at 150 Mpa.*

Chapter 5

Magmatic degassing and link with hydrothermal systems: Taupo Volcanic Zone, New Zealand

5.1. Abstract

The central segment of the Taupo Volcanic Zone (TVZ) is one of the world's most productive areas of silicic volcanism and geothermal activity. Rhyolites largely predominate the eruptive output in the central TVZ, with only minor basalts, andesites and dacites. Identifying the extent of the magmatic input into the hydrothermal systems is not straightforward, due to the strongly diluted nature of the hydrothermal fluids. The high temperature geothermal systems have been subdivided into two groups; 1) low-gas (i.e., CO_2), high Cl, low B and Li/Cs ratio systems suggested to have chemical affinities with basaltic (and rhyolitic) magmas related to back-arc fluids, or hereafter 'rift fluids', on the western side of the central TVZ, and 2) high-gas, low Cl, high B and Li/Cs ratio systems having chemical affinities with andesitic magmas, related to 'arc fluids' along the eastern border.

Here, we test this model using magmatic volatile and fluid-mobile element compositions (i.e. H_2O, Cl, F, Li, B, Cs) from rhyolitic melt inclusions of the central TVZ and andesitic melt inclusions from the southern TVZ. The rhyolites from the central TVZ are subdivided into two types (R1 and R2) that show significant differences in their volatile concentrations in melt inclusions. Based on differences in Cl/H_2O ratio, which is ~ 0.04 for R1 magmas, and ~0.075 for R2, exsolution of a predominant vapour phase is suggested for R1 melts, whereas R2 may be dominated by exsolution of a hydrosaline phase. These results will have a considerable effect on the magmatic fluid composition contributing to the hydrothermal systems depending on the type of rhyolite residing in the subsurface. Hydrothermal fluids in the central TVZ have maximum Cl concentrations

of ~2500 ppm (in geothermal wells), and there is only a small difference of a few hundred ppm between 'rift fluids' and 'arc fluids'. Considering their diluted nature (>90 % meteoric water) these fluids must have interacted with another Cl-rich fluid, most likely of magmatic origin. From calculated degassing trends for R1 and R2 melt compositions, we estimate Cl concentrations of the magmatic volatile phase (vapour and hydrosaline phase). Because the solubility and concentration of Cl in rhyolites is higher than in andesites, and there is an added potential effect of producing a highly concentrated exsolved hydrosaline fluid from R2 magmas; there is a strong likelihood that the hydrothermal systems have a significant rhyolitic fluid component (even in the 'arc' systems on the eastern border of the central TVZ).

The source of Boron in the hydrothermal fluids is less straightforward; however in some of the southern TVZ hot springs there is a significant B enrichment that is likely related to fluid-rock interaction with greywacke basement. In addition, southern TVZ melt inclusions from Mt. Ruapehu have two to four times more B than central TVZ melt inclusions. As a consequence, the B/Cl ratio in central TVZ hydrothermal fluids is somewhat ambiguous and we argue that it may not be an appropriate measure for distinguishing the effect of arc vs. back-arc magmatism. Here we demonstrate that the composition of the magmatic heat source may be difficult to trace in hydrothermal fluids and possibly veiled by degassing processes. More complex fluid distribution and mixing processes are likely, and along with fluid-rock interaction, are responsible for the end-member compositions of the two central TVZ hydrothermal fluid types.

5.2. Introduction

Magmatic degassing in volcanic hosted hydrothermal systems plays a key role in terms of hydrothermal alteration and mineralisation, and heat and mass transfer. Degassing may occur during several stages, from the initial establishment of a magmatic system (e.g. Anderson et al., 1989; Wallace & Gerlach, 1994; Wallace, 2005 for a review) to eruption and/or through the transition to pluton formation and intrusion-related ore-deposition (e.g. Hedenquist & Lowenstern, 1994; Lowenstern, 1994; Candela, 1997; Seedorf et al., 2005; Williams-Jones & Heinrich, 2005; Tosdal et al., 2009; Sillitoe, 2010). The exsolved volatiles associated with these different stages in the life of a magmatic system has variable compositions and phase relations, depending on pressure-temperature conditions, the solubility of the volatile species present and the composition of the magmatic system itself. Consequently, the magmatic component of the hydrothermal systems can be difficult to decipher in the fluid and gas compositions of geothermal wells, in particular in continental hosted geothermal systems (Henley & Ellis, 1983). Further complexity in characterising the magmatic component in hydrothermal fluids is related to processes that can significantly change the composition of the fluid such as dilution, boiling, mixing, pressure-temperature variations and fluid-rock interaction.

The rhyolite-dominated central Taupo Volcanic Zone (TVZ), New Zealand, is a good example of an active volcanic-hosted hydrothermal system where the precise contribution from magmatic degassing is difficult to detect. The TVZ has one of the highest heat fluxes measured globally, with a natural heat output of 4200±500 MW (Bibby et al., 1995). Large-scale fluid convective systems in the upper crust, dominated by meteoric water, are driven by an underlying magmatic heat source (e.g. Bibby et al., 1995; Hochstein, 1995). A small magmatic fluid contribution (~15% volume) has been suggested to be present in the hydrothermal fluids (e.g. Giggenbach, 1995; Christenson et al., 2002; Simmons & Brown, 2007; Bernal et al., 2014). Several studies have focused on the chemistry of discharge water including the pioneering research by Giggenbach (1995) who identified two

types of deep supply fluids: (1) a high gas and CO_2 content and geochemical affinities similar to andesitic fluids (high B/Cl, Li/Cs, CO_2/He and N_2/Ar ratios) related to arc magmatism, and (2) a low gas and CO_2, but a higher Cl content, which has chemical affinities with rhyolitic fluids related to back-arc magmatism. A spatial distribution of these two types of hydrothermal systems has been suggested, with the first type being mostly present along the eastern side of the TVZ, which is also where the heat flux appears to be more concentrated (Fig. 5.1; Bibby et al., 1995), and the second type focused around the western side of the central TVZ (Giggenbach, 1995). A simplified drawing of this model is presented in figure 5.2 (modified after Giggenbach, 1995; Bernal et al., 2014). Hereafter, we use the terminology of 'arc systems' vs. 'rift systems', as in Reyes and Trompetter (2012), to describe the high-gas, low Cl, and low-gas, high Cl hydrothermal systems, respectively. Importantly, this terminology should not be confused with the recognition that there is no magmatic-tectonic-volcanic distinction between arc and rift systems in the TVZ as clarified in the next section.

In this study, we test the Giggenbach (1995) model (Fig. 5.2) focusing on the magmatic composition and contribution to the hydrothermal systems. We use the volatile concentrations from melt inclusions in the rhyolites in the central TVZ (data from Chapter 3), which represent more than 90% of the eruptive deposits (Wilson et al., 1995; 2009) and andesites from the southern TVZ (data from Kilgour et al., 2013). These concentrations are used as analogues for the present day magmatic systems.

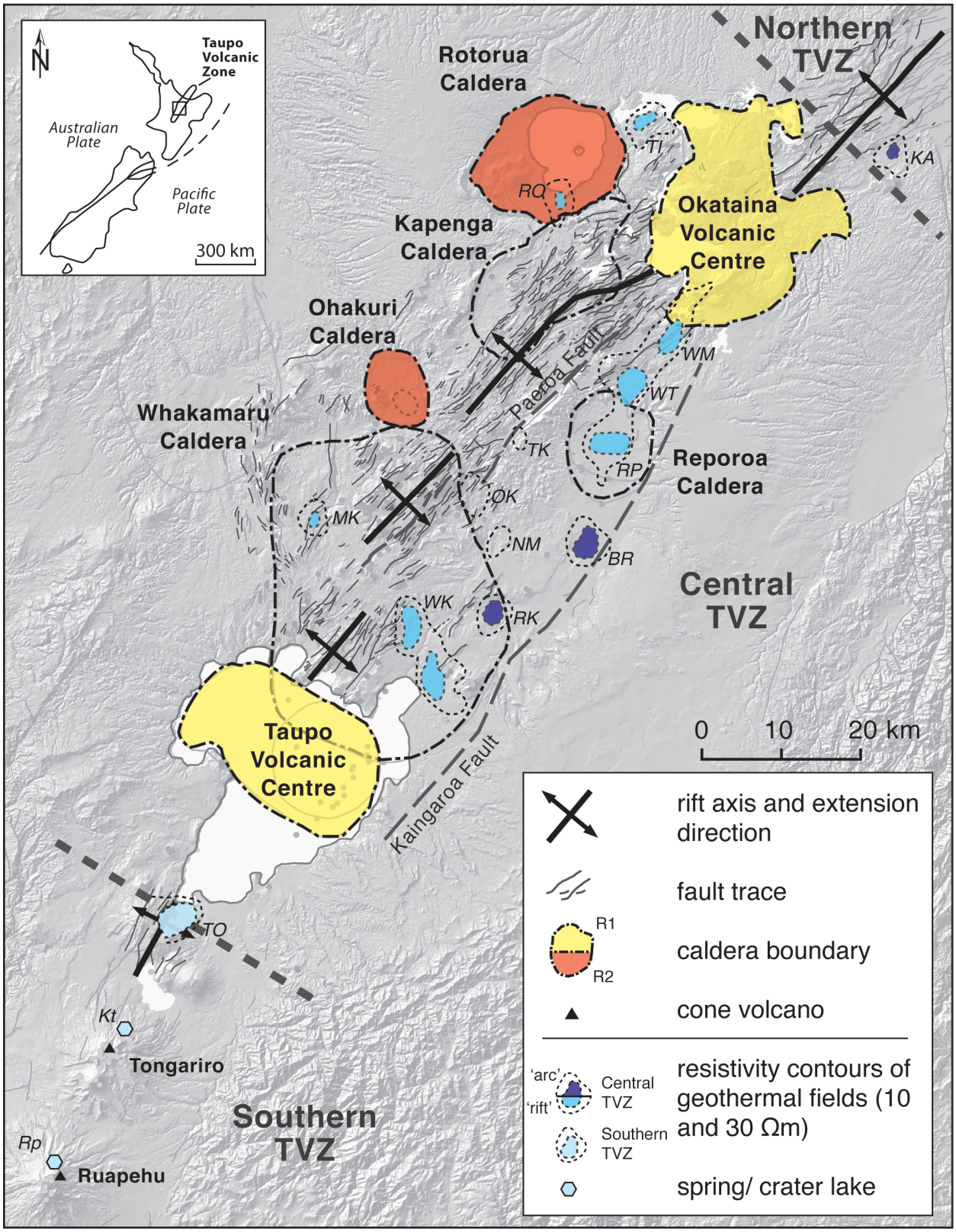

Figure 5.1: Map of the TVZ, New Zealand. Caldera boundaries and structures after Rowland et al., (2010), resistivity contours and geothermal fields after Bibby et al., (1995). Abbreviations geothermal fields: TO-Tokaanu, WK-Wairakei, RK-Rotokawa, MK-Mokai, NM-Ngatamariki, BR-Broadlands Ohaaki, OK-Orakei Korako, RP-Reporoa, TK-Te Kopia, WT-Waiotapu, WM-Waimangu, RO-Rotorua, TI-Tikitere, KA-Kawerau, Kt-Ketatahi, Rp-Ruapehu Crater Lake.

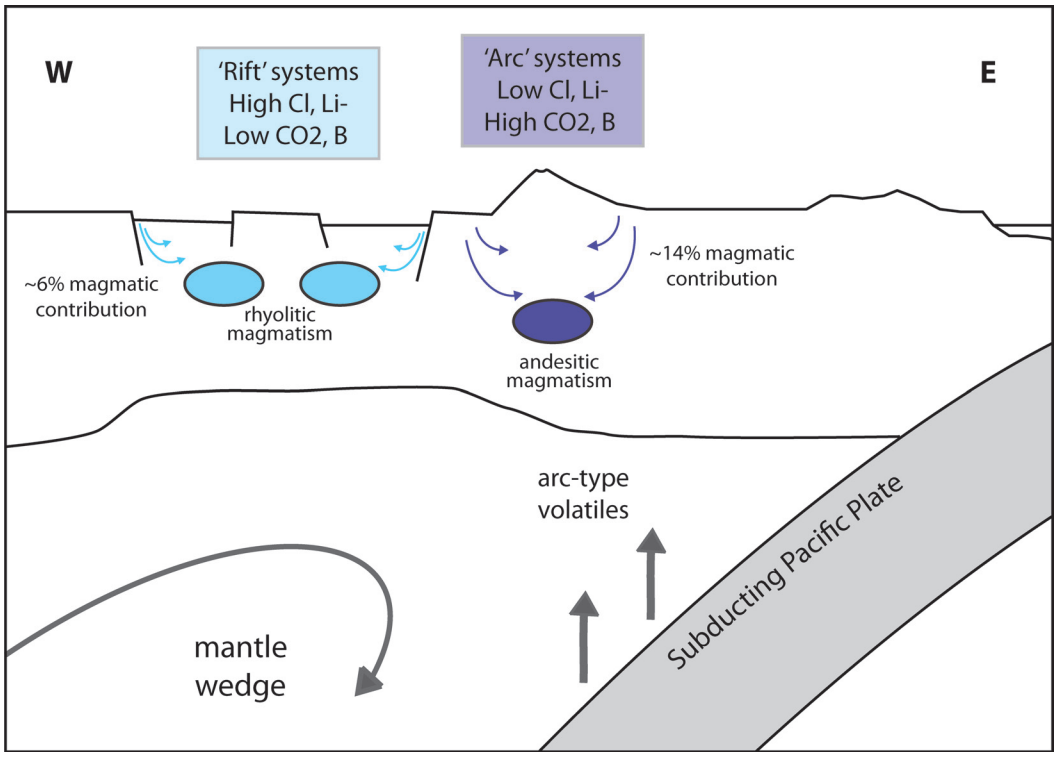

Figure 5.2: Schematic representation of the current model of the hydrothermal fluid distribution in the central TVZ (modified after Giggenbach, 1995; Bernal et al., 2014). Arc vs. back-arc (or 'rift') distribution is suggested to be related to andesitic and rhyolitic magmatic systems.

Table 5.1: Summary of the main characteristics of R1 and R2 rhyolites.

	Central TVZ rhyolites				**Southern TVZ andesites**	
	R1	*Std. Dev.*	**R2**	*Std. Dev.*	**Ruapehu**	*Std. Dev.*
Mineral assemblage	qtz + plg + opx ± bt ± hbl ± cum		qtz + plg + opx ± hbl		plg + cpx + opx	
Crystallinity (%)	~15-30		<10		25 - 40 %	
Melt inclusions (avg. in ppm)						
H_2O (wt.%)	4.8	*1*	4.2	*0.6*	1.4	*0.4*
Cl	2000	*130*	2900	*500*	715	*210*
F	255	*130*	550	*110*	1040	*260*
B	25	*3*	15	*2*	55	*9*
Li	68	*14*	58	*16*	42	*9*
Cs	3	*1*	5	*1*	-	-
Eruptive deposits (in this study)						
Okataina (OVC)	Matahina (~322 ka); Rotoiti (~65 ka); Kaharoa (~0.7 ka)					
Taupo (TVC)	Oruanui (~26 ka)					
Rotorua / Ohakuri (RoOhVC)			Mamaku (~240 ka); Ohakuri (~240 ka)			

bt-biotite; cum-cumingtonite; hbl-hornblende; opx-orthopyroxene; cpx-clinopyroxene; plg-plagioclase; qtz-quartz

Compilation from the following sources: Liu et al. (2006); Deering et al. (2008); Leonard et al. (2010); Johnson et al. (2011); Kilgour et al. (2013); Bégué et al. (in press).

5.3. Taupo Volcanic Zone

The Taupo Volcanic Zone (TVZ) is a rifted volcanic arc, which means that active rifting coexists in geographic space with arc volcanism and thus the tectonic setting is not the same as more 'classic' arc to back-arc subduction settings (Wilson et al., 1995). It is currently subject to a NW-SE extensional regime reflecting the subduction of the Pacific Plate beneath the Australian plate (e.g. Wallace et al., 2004; Reyners et al., 2006). It is magmatically and structurally segmented, with its northern and southern segments being dominated by andesitic cone-building volcanoes (Fig. 5.1; e.g. Wilson et al., 1995), and as mentioned above, caldera-forming eruptions and dome complexes of rhyolitic composition largely dominate the central segment of the TVZ (> 6,000 km^3 bulk volume of rhyolites over a period of ~1.8 Ma), with only minor dacites, andesites and basalts (e.g. Houghton et al., 1995; Wilson et al., 2009; Eastwood et al., 2013). Andesitic volcanism in the southern TVZ is persistent from ~0.34 Ma (Wilson et al., 1995); however, it still represents less than 10% in volume of the total erupted magma in the entire TVZ.

Extensive rifting in the central TVZ has lead to thinning of the crust, which allows for a heavily intruded lower crustal region (from ~16 to 30 km depth; e.g. Harrison and White, 2006), and for accommodation of significant volumes of silicic magma at shallow crustal levels (~4 km; Allan et al., 2012; Shane & Smith, 2013; Chapter 4). Regional tectonics related to the extensional regime is closely linked to magmatism and volcanism in the central TVZ (e.g. Wilson et al., 2009; Rowland et al., 2010), and plays a significant role in reservoir depth of the magmatic systems, magma transport, and eruptive processes (Gravley et al., 2007; Allan et al., 2012). These regional faults also form essential pathways for hydrothermal fluids, circulating in the upper crust (e.g. Rowland & Sibson, 2004; Rowland & Simmons, 2012).

5.3.1. TVZ Magmatism

Current models for the petrogenesis of voluminous rhyolites in the central TVZ involve multiple stages of crustal assimilation and fractional crystallisation processes (AFC) from a basaltic parent (e.g. McCulloch et al., 1994; Graham et al., 1995; Price et al., 2005; Deering et al., 2008; 2011-a). A significant mantle component in the silicic magmas has been suggested, with less than 25 % assimilation in the lower crustal region (e.g. McCulloch et al., 1994), based on Pb, Nd, Sr, and O isotopes. From recent bulk-rock data on the erupted basalts, Rooney & Deering (2014) established a strong genetic connection between two distinct types of basalt with two types of rhyolites. This link has been reinforced by melt inclusion data on the rhyolites (Chapter 3).

The two types of rhyolites represent two end-member compositions based on their relative bulk-rock and mineral chemistry and petrography (Deering et al., 2008; 2010). Hereafter the terminology R1 and R2 is used to distinguish between the two end-member rhyolite types; the main characteristics between R1 and R2 are summarized in Table 5.1 and a simplified spatial distribution of the main caldera centres producing these two rhyolite types is shown in figure 5.1. The compositional variability present in the rhyolites has been suggested to reflect differences in melting and magma generation. Consequently, changes in fH_2O, fO_2, and P-T conditions in the lower- to mid-crust (15-30 km), where the evolved magmas are generated through fractionation and melt extraction from crystal-rich residues from repeated basalt intrusions are present (Deering et al., 2008; 2011-a).

5.3.2. Magmatic volatile compositions in the TVZ

In Chapter 3, we show that R1 and R2 have significant variation in their volatile composition, based on quartz hosted melt inclusion data. The volatile content (i.e. H_2O, Cl, F, CO_2, S) are summarised in Table 5.1). R2 melt inclusions have high Cl and F concentrations (~3000 ppm and ~600 ppm respectively) and slightly lower H_2O concentration (~4 wt%) compared to R1 (~2000 ppm Cl, ~250 ppm F, and ~5 wt.% H_2O; Fig. 5.3; Table 5.1). CO_2 concentrations are low and share a similar range for R1 and R2, and S is below detection limit (Liu et al., 2006; Johnson et al., 2011; Chapter 3). R1 and R2 rhyolites also have distinct fluid-mobile element composition (Fig. 5.4-5.5; Chapter 3). These differences in volatile concentrations in the two rhyolite types originate from multiple processes including multiple igneous processes from a more primitive melt and subsequent degassing histories. Specifically, there is a genetic link between two basalt types intruding the lower crust (Rooney and Deering, 2014) and melt inclusion compositions from both rhyolite types (Chapter 3). Furthermore, prior to melt inclusion entrapment, R1 rhyolites were saturated in Cl and H_2O, and R2 rhyolites were under-saturated or close to saturation (Chapter 3). These degassing histories/differentiation is developed and discussed more below but an important initial conclusion is that not all rhyolites (even within the same volcanic area) have the same bulk volatile concentration or degassing pathways. From this conclusion diverse compositions of magmatic volatile phases can be expected, which will affect the magmatic signature in the hydrothermal systems.

Kilgour et al. (2013) present the first volatile data from pyroxene- and plagioclase-hosted melt inclusions from andesites in the southern TVZ. This study focuses on the more recent small eruptions occurring between 1945 and 1996 from Ruapehu (Fig. 5.1). Volatile and fluid-mobile element concentrations are summarised in Table 5.1; overall, the analysed eruptives seem, to represent relatively dry melts (low average H_2O of ~1.5 wt.%, Fig. 5.3a) in comparison to other examples of arc andesitic magmatism (Kilgour et al., 2013). In comparison to the central TVZ

rhyolites, the andesites have lower Cl concentrations (Fig. 5.3). This is expected, as Cl is incompatible in these magmas and increases with the evolution of the melt. However, they also have a much higher B and F concentrations (Fig. 5.3). The high B concentrations in the melt inclusions may be a result of assimilation of greywacke basement, suggested to be an important contributor to the petrogenesis of these andesites from isotopic and trace element studies (e.g. Graham and Hackett, 1987; Price et al. 2012). Reyes & Trompetter (2012) also show that greywackes can have significant amounts of B (e.g. Fig. 5.6). Melt inclusions from larger Ruapehu eruptions are shown to have higher H_2O concentrations (~4.5 wt.%, Pardo Villaveces, 2012). However, other volatile and trace element concentrations are to date not available for these eruptions.

5.4. Magmatic volatile differentiation

Volatile degassing is an important process in magmatic systems, and influences the style of volcanic eruptions and contributions of chemical species to the atmosphere. Degassing is also a major control on hydrothermal alteration and mineralisation. In magmatic systems, volatile saturation can occur at different stages of the magmatic history, depending on pressure, temperature and composition of the system, either through decompression-driven or crystallisation-driven degassing. Exsolution of a volatile phase occurs when a volatile species (i.e. H_2O, CO_2, Cl, F, S) reaches saturation, which is strongly dependent on the solubility of each volatile element. An important outcome from studies on volatile solubility is the diversity in solubilities of different species (e.g. Webster, 1997; Lowenstern, 2001; Wallace, 2005; Shinohara, 2013). Volatile saturation can occur at considerable depth, especially for insoluble species such as CO_2 (Lowenstern, 2001; Wallace, 2005), and it is also possible for magmas to become volatile saturated (e.g. in CO_2) before and independently of H_2O-rich volatile saturation. Exsolution of a volatile phase(s) in natural systems has been recognised through fluid and melt inclusion studies in intrusive and extrusive rocks, intrusion related fossil hydrothermal systems, as well as surface gas flux surveys

in volcanic areas. Direct evidence of magmatic volatile exsolution is represented by greisens (i.e. autogenic alteration of plutonic rock as a result of interaction with magmatic fluids), and other intrusion related ore deposits. Pegmatites may also be related to crystallisation in the presence of magmatic volatile phases (e.g. Cerni et al., 2012; London & Morgan, 2012).

In parts of a silicic magma system, subsolidus conditions play an important role in allowing magma to remain in the upper crust to form plutons (e.g. Bachmann et al., 2007; Lipman 2007, and references therein). In the TVZ, evidence for this is recorded in plutonic lithics present in many ignimbrites (Brown et al., 1998-b; Burt et al., 1998; Shane et al., 2012). Further, the 0.71-0.65 Ma Ngatamariki intrusive complex (microdiorite, diorite, tonalite and mafic dykes) which was intercepted by three wells at ~2.5 km depth represents the only known occurrence of in-situ plutonic rocks in the TVZ (Browne et al., 1992; Chambefort et al., 2014-a), and is further evidence for emplacement of shallow plutons. The intrusive-extrusive ratio (i.e. non erupted vs. erupted melt) is poorly constrained for the central TVZ (Deering et al., 2011-a); commonly this ratio is suggested to be close to 5:1 for most magmatic systems associated with subduction zones (Crisp, 1984; White et al., 2006). Deering et al. (2011-a) proposed an intrusive-extrusive ratio of 3:1 to explain the rhyolite output in the central TVZ. Regardless of the exact ratio, we can assume that large portions of un-erupted magma and now crystalline rock reside in the upper crust, and their degassing history is part of the global volatile flux and contributes (mass and heat) to overlying hydrothermal systems.

Evidence for magmatic volatile exsolution in the central TVZ has been shown or invoked in many studies, with:

(1) pre-eruptive degassing from melt inclusion studies in the Okataina Volcanic Centre and Oruanui rhyolites (Taupo Volcanic Centre; Fig. 5.1) (R1 rhyolites; Liu et al., 2006; Johnson et al., 2011);

(2) hypersaline multiphase fluid inclusions in the Ngatamariki plutonic complex and related hydrothermal system (e.g. Christenson et al., 1998; Chambefort et al., 2013-b, 2014-b);

(3) high CO_2 soil gas flux (e.g. Rotorua area, Werner & Cardellini, 2006) with a significant magmatic $\delta^{13}C$ component (e.g. Rotokawa geothermal field, Bloomberg et al., in review) and calcite deposition with a $\delta^{13}C$ magmatic signature (e.g. Ngatamariki geothermal field; Horton et al., 2012);

(4) an anomalously high Au and Ag flux in the central TVZ hydrothermal systems requiring degassing of magma at depth (Simmons & Brown, 2007); and

(5) fluorine mineralisation (topaz and fluorite) and metal and rare-earth elements enrichment (greisen type) of the hydrothermal alteration halo above the Ngatamariki intrusive complex, indicating late-stage exsolution of the more soluble species (Lewis et al., in review).

R1 and R2 rhyolites have distinct bulk volatile concentrations, and the melt inclusions represent distinct degassing histories. Pressure conditions for these two types (~100 MPa; e.g. Allan et al., 2012; Shane & Smith, 2013; Chapter 4) are below critical pressure. Therefore, instead of exsolving one single aqueous phase, fluid immiscibility is suggested to occur (e.g. Metrich & Rutherford, 1992, Shinohara, 1994; Webster, 2004), and the relative concentrations of Cl and H_2O in the melt and coexisting volatile phase will be a determining factor for the phase(s) exsolving from the melt (e.g. Shinohara, 1994). The TVZ rhyolites show distinct Cl/H_2O ratios with R1 being ~0.04 (Johnson et al., 2013) and R2 being ~0.075; (Chapter 3; Fig. 5.3a). Experimental studies on granitic melts (at 200 MPa) demonstrate that exsolution of a vapour phase only occurs if Cl/H_2O is less than 0.05, whereas exsolution of a vapour and co-existing hydrosaline fluid is more likely with Cl/H_2O higher than 0.05 (Webster, 2004). This ratio likely increases at lower pressure conditions and for andesitic melt compositions (0.35; Fig. 5.3a; Metrich & Rutherford, 1992; Webster, 2004). As already suggested by Johnson et al. (2013), for the OVC rhyolites, these results show that R1

rhyolites (which are volatile saturated; Liu et al., 2006; Johnson et al., 2011) would more likely just exsolve a vapour phase. Whereas, R2 rhyolites, with their higher Cl/H_2O ratio, are likely to exsolve an immiscible low density vapour, and a high density hydrosaline fluid phase (Fig. 5.3a). Many studies on the genesis of magmatic-hydrothermal ore deposits focus on the phase relations of the exsolved magmatic phase(s), as it plays an essential role in the partitioning of metals and other fluid-mobile elements (e.g.Hedenquist & Lowenstern, 1994; Harris et al., 2003; William-Jones & Heinrich, 2005; Audétat et al., 2008; Zajacz et al., 2008). Hence, the results presented here may have significant implications for metal transport and deposition in silicic environments.

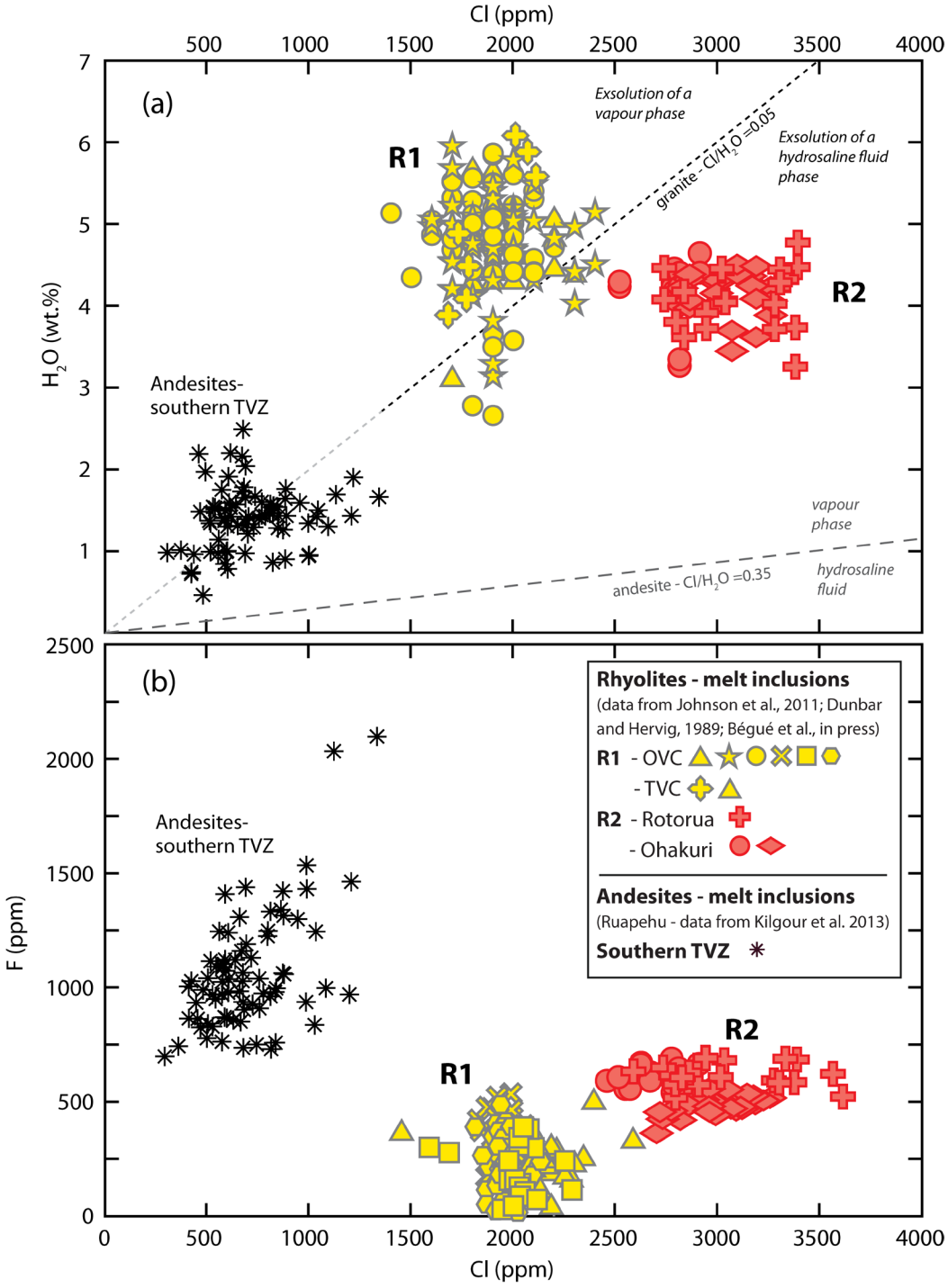

Figure 5.3: Summary of volatile disparities between R1 and R2 rhyolitic melt inclusions (data from Chapter 3; H_2O data for R1 from Dunbar and Hervig, 1989-b; Liu et al. 2006; Johnson et al., 2011) and andesitic melt inclusions (southern TVZ; Kilgour et al., 2013) – (A) H_2O vs. Cl, and (B) F vs. Cl. The black dashed line in (A) represents a Cl/H_2O ratio of 0.05 (from experimental studies on granitic compositions at 200 MPa; Webster, 2004), and the grey dashed line is a Cl/H2O ratio of 0.35 (andesitic melt compositions at 200 MPa); for compositions above the line, exsolution of a vapour phase only is suggested, and below the line a hydrosaline fluid phase (e.g. Webster, 2004).

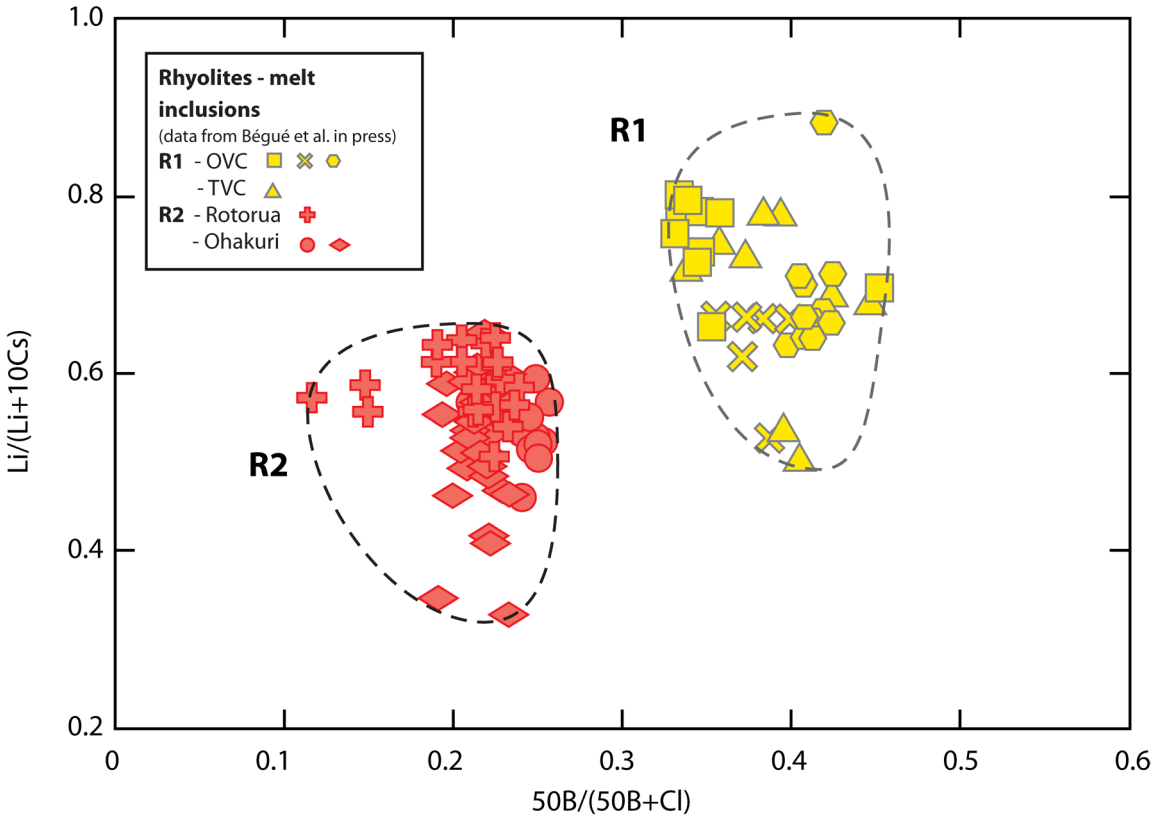

Figure 5.4. 50B/(50B+Cl) vs Li/(Li+10Cs) for rhyolitic melt inclusions, showing the variability in volatiles and fluid-mobile elements between R1 and R2 melts.

5.5. Link between magmatic degassing and hydrothermal systems

The hydrothermal systems in the central TVZ have been previously subdivided into two distinct groups; the 'arc' (andesite) and 'rift' (rhyolite) systems, based on differences in composition and stable isotopes of fumaroles, hot springs and pools (e.g. Giggenbach 1995; Bernal et al., 2014); here, we focus on Cl and B concentrations (Fig. 5.4-5.6). Data on hydrothermal fluids used in this study come from the following sources: Christenson & Wood (1993), Giggenbach (1995), Christenson (2000), Christenson et al. (2002), REGEMP II (2013) and Bernal et al. (2014). In a bivariate plot illustrating Cl vs. B (Fig. 5.5), hydrothermal fluids plot along linear trends radiating from the origin (i.e. the meteoric water composition). Four groups are discernible from the difference in slope of the trend line (Fig. 5.5):

(1) the Ketatahi springs (southern TVZ), have almost no Cl and follow the y-axis,

(2) the 'arc systems' of the central TVZ and the Tokaanu geothermal field, which is at the boundary between central and southern TVZ,

(3) the 'rift systems' from the central TVZ, and

(4) waters from the Ruapehu crater lake-hosted hydrothermal system (southern TVZ), with very low B and high Cl concentrations.

These trends indicate mixing between meteoric water and another end-member composition having diverse B and Cl concentrations. From the current knowledge on the TVZ, the other potential end-member compositions for these hydrothermal systems are magmatic fluids and chemical constituents leached from greywacke basement and /or other host-rocks in the geothermal fields.

The volatile compositions of melt inclusions represent a starting point in inferring the composition of primary magmatic fluids; however, as mentioned earlier, the compositions may reflect already degassed melt (e.g. R1; Fig. 5.5a). We can predict the composition of the volatile phase based on calculations of degassing trends assuming exsolution of a vapour phase and/or a hydrosaline fluid (Fig. 5.5b). In our calculations (Fig. 5.5), we use a simple approach that assumes constant

partition coefficients, 100% incompatibility in crystallising minerals, and isobaric, isothermal and isocompositional conditions. The partition coefficients are from Webster et al. (1989), Schatz et al. (2004) and Zajacz et al. (2008). Importantly, closed-system degassing is also considered until the exsolved gas reaches ~20-30 vol%, representing the percolation threshold (i.e. sufficient gas is exsolved for bubble coalescence to create permeability in the melt, allowing the volatiles to escape the magmatic system; Candela, 1991; Huber et al., 2012). In the case of exsolution of a hydrosaline fluid (as suggested for R2 rhyolites, Fig. 5.3a), Cl concentrations of that fluid will be exceedingly high (e.g. 30-40 wt.% NaCl from fluid inclusion data from the Ngatamariki geothermal field; Christenson et al., 1998; Chambefort et al., 2013-b; 2014-b) and will plot completely off the diagram in figure 5.5. The results from the degassing trends support the premise that melt inclusion data and accounting for volatile degassing histories cannot be underestimated when characterising and quantifying the magmatic component in hydrothermal fluids.

Fluids from the Ruapehu hydrothermal system have an anomalously high Cl and very low B (Christenson & Wood, 1993; Christenson, 2000), which is unexpected in comparison to the Cl content in the andesitic melt inclusions (Fig. 5.5-5.6; Kilgour et al., 2013). The high H2O/Cl ratio of the andesitic magmas requires that the Cl will more likely be partitioned into the vapour phase (Fig. 5.3a; e.g. Webster, 2004; Zajacz et al., 2012), however, there is not sufficient Cl in the melt to explain a contribution of ~7000 ppm to the Ruapehu crater lake. These results may thus indicate hydrothermal processes (e.g. shallow boiling) concentrating Cl in the lake; alternatively there may be another source for Cl in these systems, and may eventually suggest compositionally different magma types than those sampled for melt inclusion studies from Ruapehu eruptions between 1945 and 1996 (c.f. Kilgour et al., 2013). Mixing processes have been recognised in the eruptive products from the Ruapehu (1995-1996 eruptions; Nakagawa et al., 1999; 2012), and comparing the composition of the discharge fluids with the melt composition may provide further insights on the processes involved in the andesite genesis. However, the plagioclase- and pyroxene- hosted

melt inclusion data from Kilgour et al. (2013) does not represent all andesites in the southern TVZ and additional data would be needed on other volcanoes and also larger eruptions to better constrain the magmatic volatile composition. Similarly, some of the high Cl concentrations in the Ruapehu hydrothermal system used in this study are associated with the 1995–1996 eruption sequence (Christenson, 2000) and may not only represent a period of high magmatic activity but also a period when the crater lake water levels were particularly low and consequently less diluted.

Hydrothermal fluids from the southern TVZ show a very large diversity in B and Cl (Fig. 5.5 and 5.6). In contrast to the Ruapehu hydrothermal system, Ketatahi springs (Tongariro) follow a very different trend, with a very low Cl and high B concentrations, which exemplifies the effect of fluid-rock interaction. Fluid-rock interaction is an important contributor to hydrothermal fluid chemistry in the TVZ (see Ellis & Mahon, 1964; 1967; 1977; Giggenbach, 1989; Reyes & Trompetter, 2012). Dissolution and leaching from volcanic host rocks significantly affects boron, leading to increases in B concentrations in hydrothermal fluids (Fig. 5.6; Reyes & Trompetter, 2012). Additionally, greywacke, which has been encountered in deep wells in almost every high-enthalpy geothermal field explored in the central TVZ (i.e. Kawerau, Broadlands-Ohaaki, Rotokawa, Ngatamariki, Tauhara; e.g. Alcaraz et al., 2012) can have considerable B concentrations (e.g. Reyes & Trompetter, 2012). Chlorine can also be affected by fluid-rock interaction. However, neither greywacke, nor volcanic host rocks have a high enough Cl concentration to explain the measured contents in the hydrothermal systems (Fig. 5.5), supporting a magmatic origin for Cl.

In the central TVZ, the ‘arc’ and ‘rift’ systems plot along two distinct linear trends, representing different B/Cl ratios (Fig. 5.5); the ‘arc’ systems have up to ~1800 ppm, and the ‘rift’ systems up to ~2500 ppm Cl concentrations. These concentrations are high considering that these fluids are strongly diluted with meteoric waters, with the magmatic contribution suggested to be only ~14 % for the ‘arc’ and ~6 % for the ‘rift’ systems (Giggenbach, 1995). Hence, these results suggest mixing with a fluid of high Cl concentration. Considering the Cl content in the melt inclusions

(Fig. 5.3-5.6), such high-Cl fluids would less likely be produced from an andesitic magma, with similar composition to the melt erupted from Ruapehu the past ~50 years, compared to a rhyolitic magma, as Cl is less soluble and has a higher partition coefficient between the vapour phase and the melt in rhyolites (e.g Metrich & Rutherford, 1992; Shinohara, 1994; Webster, 1997; Zajacz et al., 2012). Additionally, exsolution of hydrosaline fluids are likely to be associated with rhyolitic magmatism, particularly with R2 magmas (Fig. 5.3a).

From the spatial distribution of the hydrothermal systems in the central TVZ (Fig. 5.1, same colour coding is used in the map as in the figures 5.3 to 5.6), the 'arc' systems are concentrated along the eastern boundary of the TVZ, as suggested by Giggenbach (1995). However, the 'rift' systems are not strictly limited to the western boundary, as shown in figure 5.1. The magmatic fluids do not seem to follow a simple distribution pattern as may be expected in other subduction zones, where the arc and the back-arc are clearly spatially separated (e.g. Fischer & Marty, 2005, Fischer, 2008), and which has been suggested in the original models (Fig. 5.2, Giggenbach, 1995). In the rifted-arc setting of the TVZ (i.e. no delineated difference in an arc and back-arc) the magmatic and subduction zone-related fluid/melt distribution may be controlled by different processes. From geophysical studies of the TVZ subduction system, Reyners et al. (2006) suggest that fluid/melt is focused along the actively rifting portion of the central TVZ, where rhyolitic magmatism predominates. This interpretation contrasts with conventional models on fluid/melt distribution in subduction zones, where the slab-derived fluids/melts are more concentrated along the volcanic arcs (e.g. Fig. 5.2). Additionally, the subducting slab in the New Zealand subduction system is twice as thick as a normal oceanic crust (subduction of the Hikurangi Plateau, 17km; e.g. Davy & Wood, 1994), which is suggested to cause more dehydration and releasing of water into the mantle wedge, and eventually at up to greater depth in the mantle (Reyners et al., 2006). The location of the hydrothermal systems, which have not changed in the past 0.3 Ma at least (Browne, 1979; Arehart et al., 2002), and has not been significantly disrupted by volcanic eruptions, so is,

therefore, more likely controlled by upper-crustal regional tectonics and fault permeability (e.g. Rowland & Sibson, 2004; Rowland & Simmons, 2012). The east-west distribution representing arc back-arc fluids (Fig. 5.1 and 5.2) is, thus, not an appropriate model for the central TVZ.

The differentiation among the two groups of hydrothermal systems in the central TVZ has also been based on the CO_2 concentrations, with the high-gas 'arc' systems suggested to be andesite related, and low-gas 'rift' systems rhyolite-related (Giggenbach, 1995). CO_2 concentrations in the rhyolitic melt inclusions are low to absent in both R1 and R2 melts (Liu et al., 2006; Johnson et al., 2011; Chapter 3). CO_2 solubility is very low compared to other volatile species (i.e. H_2O, Cl, F), and it has been shown in numerous studies that CO_2 exsolution and degassing can readily occur in mafic systems in the lower crust (e.g. Lowenstern 2001; Wallace, 2005). To date there are no published data on the volatile concentration of the TVZ basalts, but the CO_2 degassing may occur in the deeper-seated magmas. Similar conclusions have been made for Yellowstone, where the high CO_2 is suggested to be derived from large volumes of mafic magma intruding the lower crust (Lowenstern & Hurwitz, 2008). We also suggest that Cl and CO_2 are decoupled during degassing, and are very likely related to distinct magma compositions. Therefore, their degassing will likely reflect distinct stages in the life of the magmatic systems, and combining Cl and CO_2 to characterise the magmatic input into the hydrothermal systems may lead to erroneous observations regarding the heat source. A similar interpretation may extend to sulfur, which is below detection limit in rhyolites, as it may exsolve at the same time as the CO_2. These issues will remain unresolved until melt inclusions from erupted basalts are examined across the TVZ.

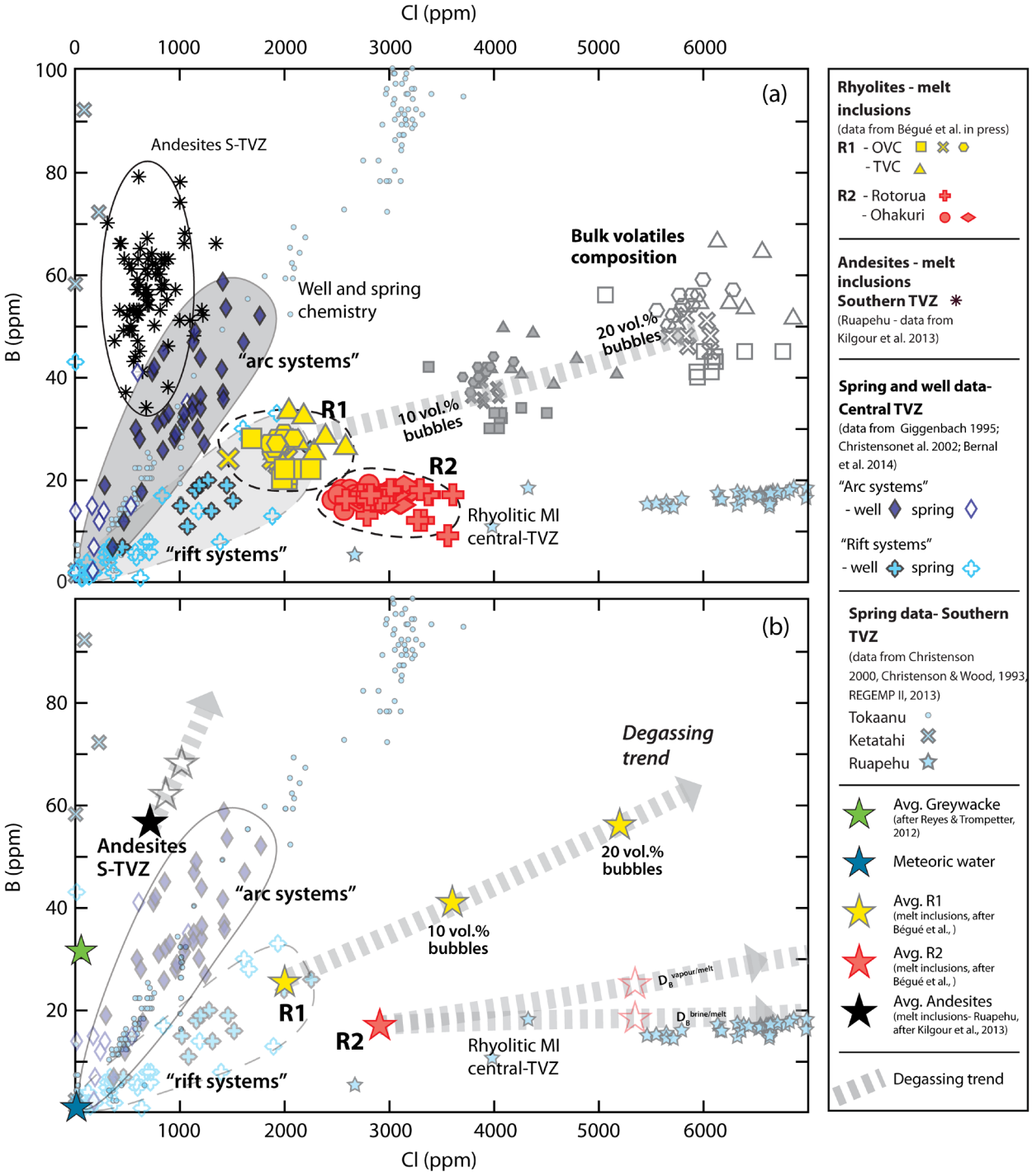

Figure 5.5: Variations of Cl vs B (in ppm) for hydrothermal fluids and rhyolitic and andesitic melt inclusions (Kilgour et al., 2013; Chapter 3); average greywacke composition after Reyes and Trompetter (2012). Bulk volatile concentration of R1 magma are calculated using a simplified degassing trend for 20 vol.% exsolved volatile phase; partitioning coefficients after Webster et al. (1989), Schatz et al. (2004) and Zajacz et al. (2008; 2012) (rhyolites: $D_{Cl}^{volatile/melt} \sim 8$; $D_{B}^{volatile/melt} \sim 6$; $D_{B}^{brine/melt} \sim 1.4$; andesites $D_{Cl}^{volatile/melt} \sim 2.1$; $D_{B}^{volatile/melt} \sim 1.2$). Chlorine concentrations for R2 melts and 20 vol.% bubbles are off the chart.

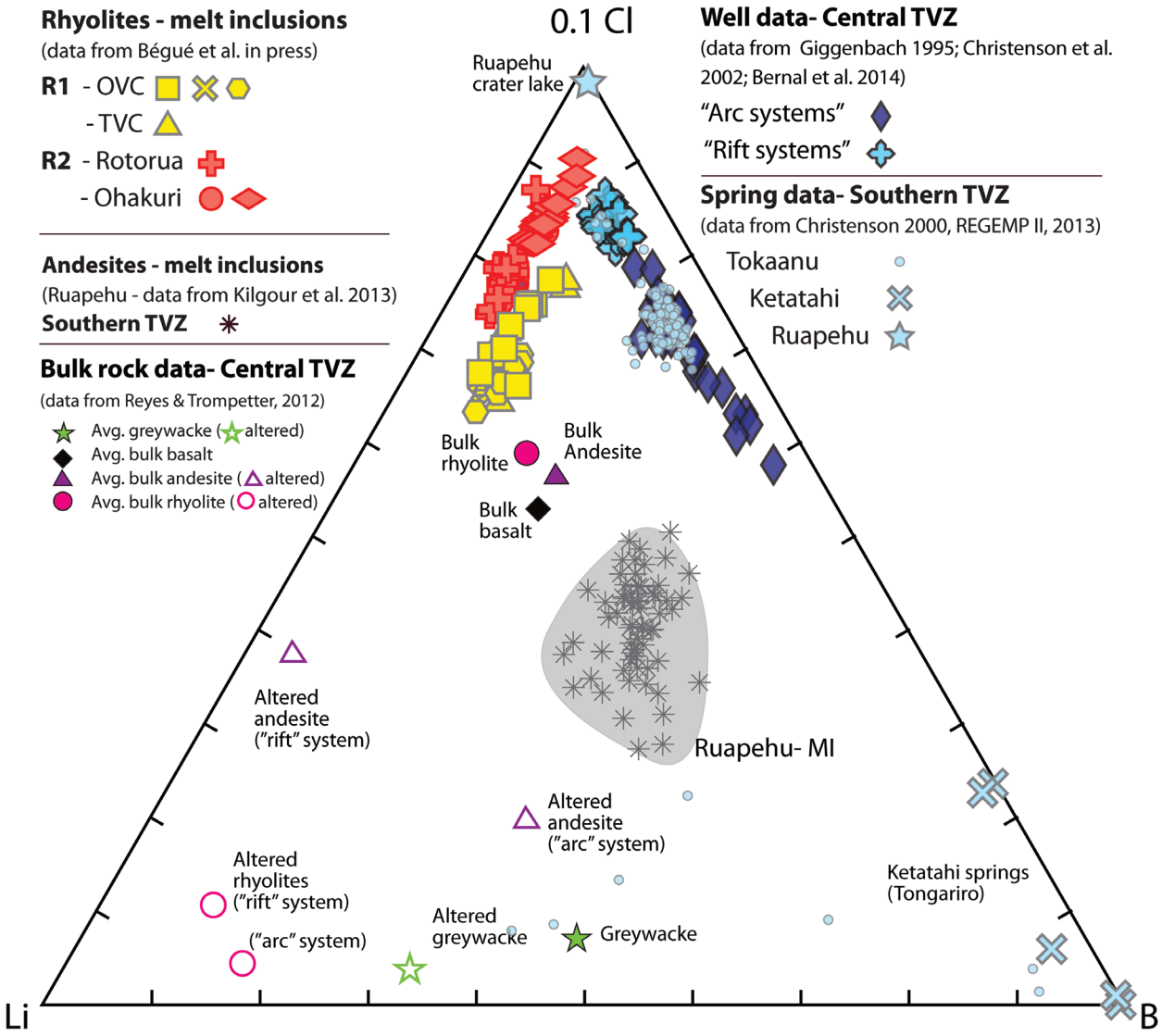

Figure 5.6: Summary of concentrations of Cl, Li, and B for well and spring data; rhyolitic and andesitic melt inclusions, and bulk-rock chemistry (fresh and altered) of rhyolites, andesites, basalts and greywacke (modified after Reyes and Trompetter, 2012).

5.6. Conclusions

Identifying the magmatic input into the hydrothermal systems in the central TVZ is not straightforward due to: 1) the strong dilution from meteoric water, 2) multiple types of magmatic compositions, and 3) the complex tectonic environment, and 4) the potential contribution from leached continental crust. Over the past few decades several studies have focused on interpreting the type of magmatic contribution to the hydrothermal system by measuring chemical species in surface fluids. The results of these studies, summarized by Giggenbach (1995), led to the suggestion that there are two distinct contributions to the hydrothermal systems in the central TVZ. One represented the typical 'arc' system, had a geochemical affinity with andesitic fluids and was located along the eastern margin of the TVZ, and the second represented the typical 'rift' system, had a geochemical affinity with rhyolitic fluids and was located along the central and/or western region of the TVZ (Fig. 5.2). By utilizing melt inclusion compositions from the central TVZ rhyolites and southern TVZ andesites we re-evaluated the magmatic contribution into the hydrothermal systems, with a particular focus on B and Cl. The results of this study indicate a more diverse variety of contributions to the meteoric water in the TVZ hydrothermal systems.

Boron and Cl concentrations in the hydrothermal system plot along distinct trends, suggesting mixing between meteoric water and four end-member fluid compositions having diverse B and Cl concentrations. From the volatile concentration measured in the melt inclusions, three distinct magmatic fluids compositions are recognised: R1, R2 and andesitic fluids. Chemical constituents leached from the greywacke basement and/or other host-rocks in the geothermal fields also represent an end-member fluid composition.

In the central TVZ, Cl concentrations in the hydrothermal systems are as high up to 2500 ppm, and considering the degree of dilution with meteoric water (~90 vol.%), mixing with a Cl-rich fluid is suggested, such as a hydrosaline fluid phase for instance. Volatile compositions of R2 melt inclusions reveal a likelihood for exsolution of such a hydrosaline phase. Importantly, the

Cl concentration of the current Ruapehu andesitic melt would not be high enough to explain the Cl concentrations in the hydrothermal systems. However, the available data on the andesitic melt is limited and may not be representative of all TVZ andesites. These results also show that the current model with an east-west distribution of 'arc' and 'rift' fluids is not viable for the central TVZ. An important outcome is that melt inclusion data and their volatile degassing history cannot be underestimated when characterising and quantifying the magmatic component in hydrothermal fluids. For the assessment of a robust mixing model, the end-member fluid compositions contributing to the hydrothermal systems need to be better constrained.

Chlorine concentrations are widely used not only to assess the origin of the hydrothermal fluids, but also to calculate the heat flux in a given system. These calculations are based on the Cl concentration of the magma and the fraction of magmatic input to the hydrothermal fluids, using the values for heat capacity and heat released from crystallisation (e.g. Stern, 1987). Giggenbach (1995) demonstrated that the heat transfer from an andesitic vapour phase would be three times higher in comparison to a rhyolitic volatile phase. Considering that R1 and R2 magmas have distinct Cl concentrations, and distinct degassing histories, their 'heat equivalent' of Cl will also differ, which would have to be taken into account for heat flux calculations.

CHAPTER 6

Conclusions

Rhyolites in the central TVZ show diversity in composition and volatile concentration, which is shown in this study on quartz (and rare plagioclase)-hosted melt inclusions from R1 and R2 rhyolites. Here, I summarise some of the main findings from Chapters 2, 3, 4 and 5, provide some suggestions to future research considerations, and some ongoing work.

1. A detailed petrological study on R2 magmas, with the Mamaku and Ohakuri rhyolites (Rotorua and Ohakuri Volcanic Centres) show that the pre-eruptive magmatic plumbing system has multiple magma batches rather than one large zoned chamber. Extraction of these isolated batches is suggested to occur from the same source reservoir (i.e. a continuous intermediate mush zone beneath the Rotorua-Ohakuri area). Similar silicic plumbing systems with multiple magma batches have been documented for other eruptive centres in the TVZ (e.g. OVC; Shane et al., 2007; 2008-a) and may be symptomatic of the regional tectonic regime, further emphasising the inter-relationship between tectonics and magmatism. Tectonic activity may also play a role as a trigger for volcanic eruptions, and may be an efficient way to activate these isolated magma batches. The evacuation of one magma batch could adjust regional tectonics sufficiently to trigger and allow simultaneous eruption of an adjacent melt batch.
2. A comparative study of melt inclusions between the R1 and R2 magmas show distinct volatile, fluid-mobile, and highly incompatible element compositions. This diversity mirrors the variability in bulk-rock geochemistry and petrography as established by Deering et al. (2008; 2010). Differences in the bulk volatile concentration of the parental magmas (i.e. basalts intruding the lower crust) is the suggested origin of the volatile disparities in the rhyolites, leading to differences in volatile saturation between R1 and R2 systems. A main

outcome of this study is that it can not always be assumed that all high-silica melts reach volatile saturation during crystallisation; in the TVZ, R1 and R2 magmas exsolve a volatile phase at different stages in their magmatic history, and differences in the composition of the resulting volatile phase may be expected.

3. The geobarometry study provides further evidence that the central TVZ magmas are stored in very shallow reservoirs (~4 km), and there are no significant differences in pressure estimates between the R1 and R2 rhyolites. The extensional regional tectonic regime and exceptionally high heat flux from depth account for the pre-conditioning of the crust allowing for this shallow magmatism. A comparison among the different eruptive deposits and volcanic centres show slight variations in equilibration pressures. This is consistent with the idea that multiple batches of eruptible magma can be present in the crust at the same time, and that they can be tapped simultaneously by large eruptive events (e.g. Chapter 2).

4. The main outcome of this thesis is that current models for the interpretation of hydrothermal fluid chemistry in the central TVZ can be refined with the addition of the new data on the rhyolitic melt inclusions. From the Cl and H_2O concentrations in these rhyolites, R1 magmas may exsolve a vapour phase first in comparison to R2 rhyolites, which due to their low original H_2O concentration, may likely exsolve a hydrosaline fluid phase. This will largely affect the magmatic contribution into the hydrothermal systems. As a result, the two rhyolitic compositions (R1 and R2) provide further constraints on the magmatic end-member composition, and it clearly shows that a simple *andesitic arc fluid* vs. *rhyolitic back-arc fluid* distribution alone cannot explain the diversity in the TVZ hydrothermal systems. Complex mixing relationships between at least five end-members (meteoric water, basement, and andesitic, R1 and R2 fluids) may be at the origin of this diversity.

These findings regarding the hydrothermal fluid composition represent the first step in the establishment of a new comprehensive model of the fluid distribution in the central TVZ and more research is needed. Some of that research would include: (1) revising heat flux calculations using the new Cl data on the rhyolitic melt inclusions, (2) fluid inclusion work in co-erupted plutonic lithics to better constrain the primary magmatic volatile composition, and (3) further studies on the fluid-rock interaction in the hydrothermal systems.

Ongoing work

- **Origin of the Ohakuri fall deposit**

  The detailed melt inclusion work that has been undertaken on the Rotorua and Ohakuri Volcanic Centres (work presented in Chapter 2) has lead to numerous questions on the provenance of the Ohakuri fall deposit.

  This fall deposit is sourced from a vent within or close to the Ohakuri caldera (Gravley et al., 2007); however, the melt inclusion major and trace element compositions are very similar to the Mamaku ignimbrite, as shown in Chapter 2 (Fig. 2.7 and 2.8). Water-CO_2 data on these same melt inclusions, presented in Chapter 3 (Fig. 3.3), plot along a positive, linear trend, which cannot be explained by simple degassing. Preliminary interpretations of these results are either crystallisation under a range of conditions from volatile bereft to volatile enriched (i.e. CO_2 fluxing from a more primitive magma source at depth) or polybaric crystallisation (i.e. ascent must be slow enough to allow for ongoing quartz crystallisation). To fully understand these results, additional data is needed on the Ohakuri fall deposit. Furthermore, to establish a potential physical link between the magmas associated with the Ohakuri fall and the Mamaku ignimbrite, similar analyses on the Horohoro dome (located in between the Rotorua and Ohakuri calderas; Fig. 2.1) need to be completed.

- **Boron isotopes**

  I started to collect data on the boron isotopes in the rhyolitic melt inclusions to use as a potential tracer for magmatic input into the hydrothermal systems. The combination of boron and boron isotopes has also been used in the literature as an effective tracer for the contribution of slab-derived fluids into silicic magma systems (e.g. Ishikawa & Nakamura, 1994; Ishikawa & Tera, 1997; Rosner et al., 2003). Reasons for this are: (1) boron acts conservatively and will preferentially partition into the fluid phase (Schatz et al. 2004; Zajacz et al., 2008), (2) there is a high isotopic fractionation between the melt and the fluid ($\Delta^{11}B_{melt\text{-}fluid}$ = -6.5 ‰ at 700°C; Wunder et al., 2005), and (3) isotopes does not fractionate during magmatic differentiation (Ishikawa et al. 2001).

  Preliminary $\delta^{11}B$ data show different signatures between R1 and R2 magmas (Fig. 6.1). A possible explanation for these differences may be variations in the fluid flux derived from dehydration of the subducting slab, which would be in agreement with the findings in Chapter 3. This interpretation would also be in agreement with the suggested origin of volatile disparities between R1 and R2 (Chapter 3). However, further data on the greywacke isotopic signature is needed, and will be essential to discuss all the potential contributing sources for the isotopic signature in the rhyolites.

  Preliminary results from this work have been presented at the New Zealand Geothermal Workshop in 2012 (short proceedings paper in Appendix E).

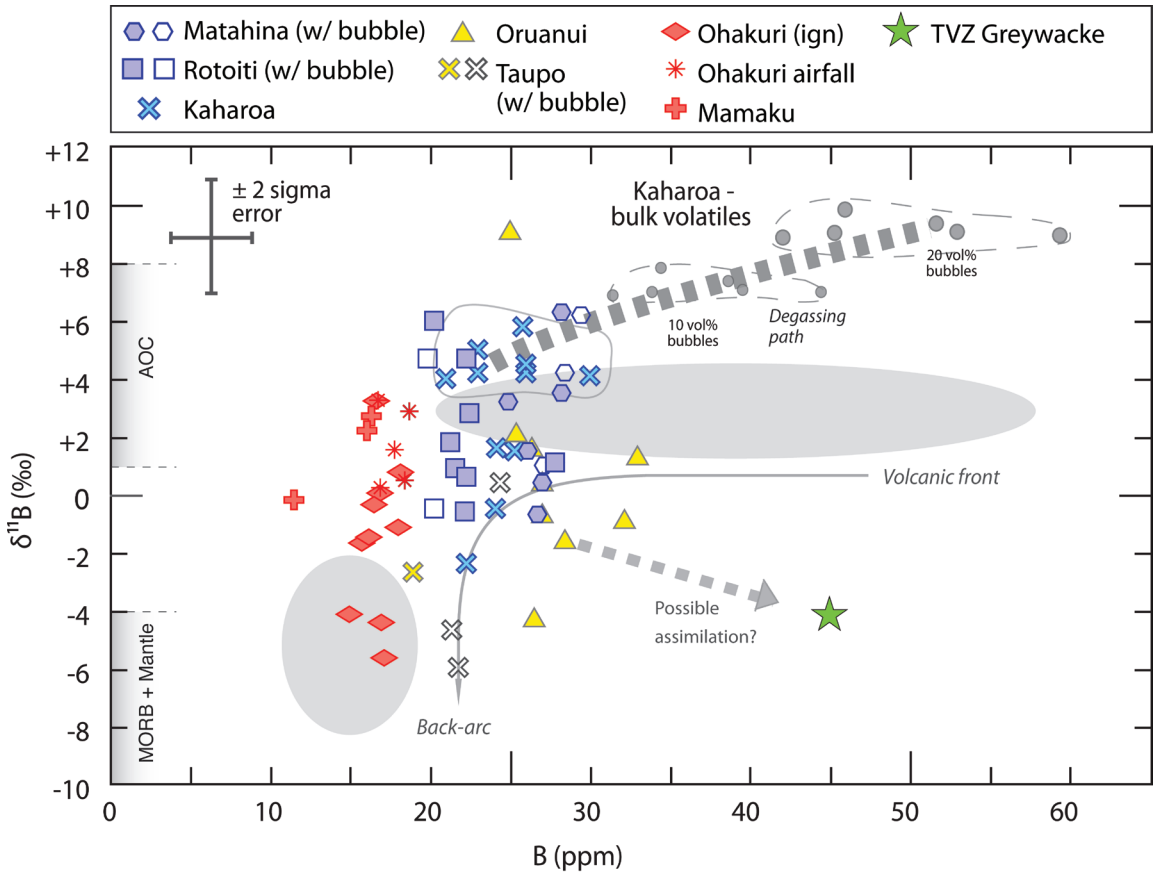

Figure 6.1: Plot of B (ppm) vs. $\delta^{11}B$ (‰) for the TVZ rhyolites. Bulk magma composition and degassing trend has been calculated for the Kaharoa rhyolites (OVC) for 10 and 20 vol% exsolved gas. $\delta^{11}B$ values for MORB, mantle and altered oceanic crust (AOC) after Chaussidon and Marty (1995) and Smith et al. (1995). Grey shaded fields represent across arc data in the Andes Central Volcanic Zone (after Rosner et al., 2003), with their interpretation of back-arc and volcanic front (text for explanations). (Error bars represent the analytical error of ±1 ‰).

Digital Appendix

The digital appendix contains the following files:

A **Declaration of Authorship Forms**

B **Supplementary material to Chapter 2**

B-1: Grid reference to the sample locations.

B-2: Matrix glass analyses of the Mamaku and Ohakuri ignimbrites and fall deposit.

B-3: Melt inclusion analyses of the Mamaku and Ohakuri ignimbrites and fall deposit.

C **Supplementary material to Chapter 3**

C-1: Major and volatile composition for the analysed central TVZ rhyolites.

C-2: Trace element composition for the analysed central TVZ rhyolites.

C-3: Comparison of H2O data between the transmission and reflectance FTIR.

D **Supplementary material to Chapter 4**

Complete dataset of all compositions used in this study (major element composition and pressure estimate).

E **New Zealand Geothermal Workshop 2012 Proceedings:**

"Volatile transfer from magma sources in the Taupo Volcanic Zone: A quartz-hosted melt inclusion study in rhyolites". (Auckland, 19-21 November, New Zealand)

References

Aiuppa, A., Federico, C., Paonita, A., Pecoraino, G. & Valenza, M. (2002). S, Cl and F degassing as an indicator of volcanic dynamics: The 2001 eruption of Mount Etna. Geophysical Research Letters, 29, 1–4.

Aiuppa, A., Baker, D. R. & Webster, J. D. (2009). Halogens in volcanic systems. Chemical Geology, 263, 1–18.

Alcaraz, S.A., Rattenbury, M.S., Soengkono, S., Bignall, G. & Lane, R. (2012). A 3D multi-disciplinary interpretation of the basement of the Taupo Volcanic Zone, New Zealand. In Proceedings, 37th workshop on geothermal reservoir engineering, Stanford, CA.

Allan, A.S.R., Wilson, C.J.N., Millet, M.-A. & Wysoczanski, R.J. (2012). The invisible hand: Tectonic triggering and modulation of a rhyolitic supereruption. Geology 40, 563–566.

Anderson, Jr. A.T., Newman, S., Williams, S.N., Druitt, T.H., Skirius, C. & Stolper, E. (1989). H_2O, CO_2, Cl, and gas in Plinian and ash-flow Bishop rhyolite. Geology, 17, 221–225.

Annen, C. & Sparks, R.S.J. (2002). Effects of repetitive emplacement of basaltic intrusions on thermal evolution and melt generation in the crust. Earth and Planetary Science Letters, 203(3-4), 937-955.

Annen, C., Blundy, J. D. & Sparks, R. S. J. (2006). The Genesis of Intermediate and Silicic Magmas in Deep Crustal Hot Zones. Journal of Petrology 47, 505–539.

Annen, C. (2009). From plutons to magma chambers: Thermal constraints on the accumulation of eruptible silicic magma in the upper crust. Earth and Planetary Science Letters 284, 409–416.

Arehart, G.B., Christenson, B.W., Wood, C.P., Foland, K.A. & Browne, P.R.L. (2002) Timing of volcanic, plutonic and geothermal activity at Ngatamariki, New Zealand. Journal of Volcanology Geothermal Research 116, 201–214.

Ashwell, P. A., Kennedy, B. M., Gravley, D. M., von Aulock, F. W. & Cole, J. W. (2013). Insights into caldera and regional structures and magma body distribution from lava domes at Rotorua Caldera, New Zealand. Journal of Volcanology and Geothermal Research 258, 87-202.

Audetat, A., Pettke, T., Heinrich, C.A. & Bodnar, R.J. (2008). The Composition of Magmatic-Hydrothermal Fluids in Barren and Mineralized Intrusions. Economic Geology 103, 877.

Bach, W., Hegner, E. & Erzinger, J. (1998). Chemical fluxes in the Tonga subduction zone : Evidence from the southern Lau Basin. Geophysical Research Letters, 25, 1467–1470.

Bachmann, O. & Bergantz, G. W. (2004). On the Origin of Crystal-poor Rhyolites: Extracted from Batholithic Crystal Mushes. Journal of Petrology 45, 1565–1582.

Bachmann O., Miller, C.F. & de Silva, S.L. (2007). The volcanic–plutonic connection as a stage for understanding crustal magmatism. Journal of Volcanology and Geothermal Research 167, 1–23.

Bachmann, O., Wallace, P.J. & Bourquin, J. (2009). The melt inclusion record from the rhyolitic Kos Plateau Tuff (Aegean Arc). Contributions to Mineralogy and Petrology 159, 187–202.

Bacon, C. R. & Hirschmann, M. M. (1988). Mg/Mn partitioning as a test for equilibrium between coexisting Fe-Ti oxides. American Mineralogist 73, 57–61.

Bacon, C.R. & Druitt, T.H. (1988). Compositional evolution of the zoned calcalkaline magma chamber of Mount Mazama, Crater Lake, Oregon. Contributions to Mineralogy and Petrology 98, 224–256.

Baer, G., Hamiel, Y., Shamir, G. & Nof, R. (2008). Evolution of a magma-driven earthquake swarm and triggering of the nearby Oldoinyo Lengai eruption, as resolved by InSAR, ground observations and elastic modeling, East African Rift, 2007. Earth and Planetary Science Letters 272, 339–352.

Behrens H., Tamic N. & Holtz F. (2004). Determination of the molar absorption coefficient for the infrared absorption band of CO2 in rhyolitic glasses. American Mineralogist, 89, 301–306.

Beresford, S.W. (1997). Volcanology and Geochemistry of the Kaingaroa Ignimbrite, Taupo Volcanic Zone, New Zealand. PhD Thesis, University of Canterbury, 363 pp.

Berlo, K., Blundy, J., Turner, S., Cashman, K., Hawkesworth, C. & Black, S. (2004). Geochemical precursors to volcanic activity at Mount St. Helens, USA. Science 306, 1167–1169.

Bernal, N.F., Gleeson, S.A., Dean, A.S., Liu, X. & Hoskin, P. (2014). The source of halogens in geothermal fluids from the Taupo Volcanic Zone, North Island, New Zealand. Geochimica et Cosmochimica Acta 126, 265–283.

Best, M.G. & Christiansen, E.H. (1991). Limited Extension During Peak Tertiary Volcanism, Great Basin of Nevada and Utah. Journal of Geophysical Research, 13,509–13,528.

Bibby, H.M., Caldwell, T.G., Davey, F.J. & Webb, T.H. (1995). Geophysical evidence on the structure of the Taupo Volcanic Zone and its hydrothermal circulation. Journal of Volcanology and Geothermal Research 68, 29–58.

Blake, S. (1981). Volcanism and the dynamics of open magma chambers. Nature 289, 783-785.

Bindeman, I. N., Ponomareva, V. V., Bailey, J. C. & Valley, J. W. (2004). Volcanic arc of Kamchatka: a province with high-$\delta^{18}O$ magma sources and large-scale $^{18}O/^{16}O$ depletion of the upper crust. Geochimica et Cosmochimica Acta, 68, 841–865.

Bloomberg, S., Werner, C., Rissmann, C., Mazot, A., Horton, T., Gravley, D., Kennedy, B. & Oze, C. (in review). Soil CO_2 emissions as a proxy for heat and mass flow assessment, Taupo Volcanic Zone, New Zealand. Geochemistry, Geophysics, Geosystems (Gcubed).

Blundy, J. & Cashman, K. (2001). Ascent-driven crystallisation of dacite magmas at Mount St Helens, 1980–1986. Contributions to Mineralogy and Petrology 140, 631–650.

Bodnar, R.J. (2003). Reequilibration of fluid inclusions. In: Samson, I., Anderson, A., Marshall, D. (Eds.), Fluid Inclusions: Analysis and Interpretation. Mineralogical Association of Canada, Short Course, vol. 32, 213–230.

Botcharnikov, R. E., Holtz, F. & Behrens, H. (2007). The effect of CO_2 on the solubility of H_2O-Cl fluids in andesitic melt. European Journal of Mineralogy 19, 671–680.

Brown, S.J.A., Wilson, C.J.N., Cole, J.W. & Wooden, J. (1998-a). The Whakamaru group ignimbrites, Taupo Volcanic Zone, New Zealand: evidence for reverse tapping of a zoneåd silicic magmatic system. Journal of Volcanology and Geothermal Research, 84, 1–37.

Brown, S.J.A., Burt, R.M., Cole, J.W., Krippner, S.J.P., Price, R.C. & Cartwright, I. (1998-b). Plutonic lithics in ignimbrites of Taupo Volcanic Zone, New Zealand; sources and conditions of crystallisation. Chemical Geology 148, 21–41.

Browne, P.R.L. (1979). Minimum age of the Kawerau geothermal field, North Island, New Zealand: Journal of Volcanology and Geothermal Research 6, 213-215.

Browne, P.R.L., Graham, I.J., Parker, R.J. & Wood, C.P. (1992). Subsurface andesite lavas and plutonic rocks in the Rotokawa and Ngatamariki geothermal systems, Taupo Volcanic Zone, New Zealand. Journal of Volcanology and Geothermal Research 51, 199–215.

Bucholz, C.E., Gaetani, G.A., Behn, M.D. & Shimizu, N. (2013). Post-entrapment modification of volatiles and oxygen fugacity in olivine-hosted melt inclusions. Earth and Planetary Science Letters, 374, 145–155.

Burnham, C. W. (1994). Development of the Burnham model for prediction of H_2O solubility in magmas. Reviews in Mineralogy 30, 123–130.

Burt, R.M., Brown, S.J.A., Cole, J.W., Shelley, D. & Waight, T.E. (1998). Glass-bearing plutonic fragments from ignimbrites of the Okataina caldera complex, Taupo Volcanic Zone, New Zealand: remnants of a partially molten intrusion associated with preceding eruptions. Journal of Volcanology and Geothermal Research 84, 209–237.

Cambray, F.W., Vogel, T.A. & Mills, J.G.J. (1995). Origin of compositional heterogeneities in tuffs of the Timber Mountain Group: The relationship between magma batches and magma transfer and emplacement in an extensional environment. Journal of Geophysical Research 100, 15793–15805.

Candela, P. (1991). Physics of aqueous phase evolution in plutonic environments. American Mineralogist 76, 1081–1091.

Candela, P. (1997). A Review of Shallow, Ore-related Granites: Textures, Volatiles, and Ore Metals. Journal of Petrology, 38,1619–1633.

Carroll, M.R. & Webster, J.D. (1994). Solubilities of sulfur, noble gases, nitrogen, chlorine, and fluorine in magmas. Reviews in Mineralogy, 30, 231–279.

Carroll, M. (2005). Chlorine solubility in evolved alkaline magmas. Annals of Geophysics, 48, 619–631.

Cashman K.V. (1988). Crystallisation of Mount St.Helens 1980-1986 dacite: A quantitative textural approach. Bulletin of Volcanology 50, 194–209.

Cerling, T.E., Brown, F.H. & Bowman, J. R. (1985). Low-temperature alteration of volcanic glass: hydration, Na, K, 18O and Ar mobility. Chemical Geology 52, 281–293.

Chambefort, I., Dilles, J.H. & Kent, A.J.R. (2008). Anhydrite-bearing andesite and dacite as a source for sulfur in magmatic-hydrothermal mineral deposits. Geology, 36, 719-722.

Chambefort, I., Dilles, J.H. & Longo, A.A. (2013-a). Amphibole chemistry of the Yanacocha Volcanics, Peru: Evidence for diverse sources of magmatic volatiles related to gold ores. Journal of Petrology 54, 1017-1046.

Chambefort, I.S., Dilles, J.H. & Heinrich, C. (2013-b). Hydrothermal mineralogy and fluid inclusions chemistry to understand the roots of active geothermal systems, Abstract presented at 2013 Fall Meeting, AGU, San Francisco, California, 9-13 December.

Chambefort, I., Lewis, B., Wilson, C.J.N., Rae, A.J., Bignall, G., Coutts, C. & Ireland, T.R. (2014-a). Stratigraphy and structure of the Ngatamariki geothermal system: New U-Pb geochronology and its implications for Taupo Volcanic Zone evolution. Journal of Volcanology and Geothermal Research 274, 51-70.

Chambefort, I., Bégué, F., Heinrich, C., Walle, M. & Dilles, J. (2014-b). From magma to mudpool: linking arc volatiles and active geothermal systems. Abstract presented at 2014 Goldschmidt, Sacramento California, 8-13 June.

Charlier, B.L.A., Peate, D.W., Wilson, C.J.N., Lowenstern, J.B., Storey, M. & Brown, S.J.A. (2003). Crystallisation ages in coeval silicic magma bodies: 238U–230Th disequilibrium evidence from the Rotoiti and Earthquake Flat eruption deposits, Taupo Volcanic Zone, New Zealand. Earth and Planetary Science Letters 206, 441–457.

Charlier, B.L.A., Wilson, C.J.N., Lowenstern, J.B., Blake, S., Van Calsteren, P.W. and Davidson, J.P. (2005). Magma Generation at a Large, Hyperactive Silicic Volcano (Taupo, New Zealand) Revealed by U-Th and U-Pb Systematics in Zircons. Journal of Petrology 46, 3–32.

Christenson, B.W. (2000). Geochemistry of fluids associated with the 1995–1996 eruption of Mt. Ruapehu, New Zealand: signatures and processes in the magmatic-hydrothermal system. Journal of Volcanology and Geothermal Research 97, 1–30.

Christenson, B.W., Mroczek, E.K., Kennedy, B.M., van Soest, M.C., Stewart, M.K. & Lyon, G. (2002). Ohaaki reservoir chemistry: characteristics of an arc-type hydrothermal system in the Taupo Volcanic Zone, New Zealand. Journal of Volcanology and Geothermal Research 115, 53–82.

Christenson, B.W., Wood, C.P. & Arehart, G.B. (1998). Shallow magmatig degassing: Processes and PTX constraints for paleo-fluids associated with the Ngatamariki diorite intrusion, New Zealand. Water-Rock Interaction.

Christenson, B. & Wood, C. (1993). Evolution of a vent-hosted hydrothermal system beneath Ruapehu Crater Lake, New Zealand. Bulletin of Volcanology 55, 547–565.

Chaussidon, M. & Marty, B., (1995). Primitive boron isotope composition of the mantle. Science, 269(5222), 383-386.

Cerny, P., London, D. & Novak, M. (2012). Granitic Pegmatites as Reflections of Their Sources. Elements 8, 289–294.

Crisp, J. A. (1984). Rates of magma emplacement and volcanic output. Journal of Volcanology and Geothermal Research 20, 177–211.

Cole, J.W., Spinks, K.D., Deering, C.D., Nairn, I. A. & Leonard, G.S. (2010). Volcanic and structural evolution of the Okataina Volcanic Centre; dominantly silicic volcanism associated with the Taupo Rift, New Zealand. Journal of Volcanology and Geothermal Research 190, 123–135.

Cole, J.W. & Spinks, K.D. (2009). Caldera volcanism and rift structure in the Taupo Volcanic Zone, New Zealand. Geological Society, London, Special Publications, 327, 9-29.

Cole, J.W., Deering, C.D., Burt, R.M., Sewell, S., Shane, P.A.R. and Matthews, N.E. (2014). Okataina Volcanic Centre, Taupo Volcanic Zone, New Zealand: A review of volcanism and synchronous pluton development in an active, dominantly silicic caldera system. Earth-Science Review 128, 1–17.

Danišík, M., Shane, P., Schmitt, A.K., Hogg, A., Santos, G.M., Storm, S., Evans, N.J., Fifield, L.K. & Lindsay, J.M. (2012). Re-anchoring the late Pleistocene tephrochronology of New Zealand based on concordant radiocarbon ages and combined 238U/230Th disequilibrium and (U–Th)/He zircon ages. Earth and Planetary Science Letters 349-350, 240–250.

Darby, D.J. & Meertens, C.M. (1995). Terrestrial and GPS measurments of deformation across the Taupo back arc and Hikurangi forearc regions in New Zealand. Journal of Geophysical Research 100, 8221–8232.

Davy, B. & Wood, R. (1994). Gravity and magnetic modelling of the Hikurangi Plateau. Marine Geology 118, 139–151

de Silva, S.L. & Gosnold, W.D. (2007). Episodic construction of batholiths: Insights from the spatiotemporal development of an ignimbrite flare-up. Journal of Volcanology and Geothermal Research 167, 320–335.

Deering, C.D. & Bachmann, O. (2010). Trace element indicators of crystal accumulation in silicic igneous rocks. Earth and Planetary Science Letters 297, 324–331.

Deering, C.D., Gravley, D.M., Vogel, T.A., Cole, J.W. & Leonard, G.S. (2010). Origins of cold-wet-oxidizing to hot-dry-reducing rhyolite magma cycles and distribution in the Taupo Volcanic Zone, New Zealand. Contributions to Mineralogy and Petrology 160, 609–629.

Deering, C.D., Cole, J.W. & Vogel, T. A. (2008). A Rhyolite Compositional Continuum Governed by Lower Crustal Source Conditions in the Taupo Volcanic Zone, New Zealand. Journal of Petrology 49, 2245–2276.

Deering, C.D., Bachmann, O., Dufek, J. & Gravley, D. M. (2011-a). Rift-Related Transition From Andesite to Rhyolite Volcanism in the Taupo Volcanic Zone (New Zealand) controlled by Crystal-Melt Dynamics in Mush Zones With Variable Mineral Assemblages. Journal of Petrology 52, 2243-2263.

Deering, C.D., Cole, J.W.J. & Vogel, T.A. (2011-b). Extraction of crystal-poor rhyolite from a hornblende-bearing intermediate mush: a case study of the caldera-forming Matahina eruption, Okataina volcanic complex. Contributions to Mineralogy and Petrology 161, 129–151.

Deering, C.D., Horton, T.W., Gravley, D.M. & Cole, J.W. (2012). Hornblende, cummingtonite, and biotite hydrogen isotopes: Direct evidence of slab-derived fluid flux in silicic magmas of the Taupo Volcanic Zone, New Zealand. Journal of Volcanology and Geothermal Research 233-234, 27–36.

Dilles, J.H., Einaudi, M.T., Proffett, J.M. & Barton, M.D. (2000). Overview of the Yerington porphyry copper district: Magmatic to non-magmatic sources of hydrothermal fluids: Their flow paths and alteration affects on rocks and Cu–Mo–Fe–Au ores. In: Thompson, T.B. (Ed.), Society Economic Geologists, Guidebook, United States, 32, 55–66.

Dufek, J. & Bachmann, O. (2010). Quantum magmatism: Magmatic compositional gaps generated by melt-crystal dynamics. Geology 38, 687–690.

Dunbar N.W., Kyle, P.R. & Wilson, C.J.N. (1989-a). Evidence for limited zonation in silicic magma systems, Taupo Volcanic Zone, New Zealand. Geology 17, 234–236.

Dunbar, N.W., Hervig, R.L. & Kyle, P.R. (1989-b). Determination of pre-eruptive H_2O, F and Cl contents of silicic magmas using melt inclusions: Examples from Taupo Volcanic Center, New Zealand. Bulletin of Volcanology 51, 177–184.

Eastwood, A.A., Gravley, D.M., Wilson, C.J.N., Chambefort, I., Oze, C., Cole, J.W. and Ireland, T.R. (2013). U-Pb dating of subsurface pyroclastic deposits (Tahorakuri Formation) at Ngatamariki and Rotokawa geothermal fields. 35th New Zealand Geothermal Workshop 2013 Proceedings Rotorua, New Zealand, pp 1–8.

Eberhart-Phillips, D., Reyners, M., Chadwick, M. & Stuart, G. (2008). Three-dimensional attenuation structure of the Hikurangi subduction zone in the central North Island, New Zealand. Geophysical Journal International 174, 418–434.

Edmonds, M., Oppenheimer, C., Pyle, D.M., Herd, R.A. & Thompson, G. (2003). SO_2 emissions from Soufrière Hills Volcano and their relationship to conduit permeability, hydrothermal interaction and degassing regime. Journal of Volcanology and Geothermal Research, 124(1-2), 23-43.

Edmonds, M., Gerlach, T.M. & Herd, R.A. (2009). Halogen degassing during ascent and eruption of water-poor basaltic magma. Chemical Geology 263, 122–130.

Elder, J.W. (1966). Heat and mass transfer in the earth, hydrothermal systems. New Zealand Department of Scientific and Industrial Research, Bulletin 169, 115.

Ellis, A.J. & Mahon, W.A.J. (1967). Natural hydrothermal systems and experimental hot water/rock interactions (Part II). Geochimica et Cosmochimica Acta 31, 519–538.

Ellis, A.J. & Mahon, W.A.J. (1977). Chemistry and Geothermal Systems. Academic Press, New York. 392 pp.

Ellis, A.J. & Mahon, W.A.J. (1964). Natural hydrothermal systems and experimental hot-water/rock interactions. Geochimica et Cosmochimica Acta 28, 1323–1357.

Ellis, B.S. & Wolff, J.A. (2012). Complex storage of rhyolite in the central Snake River Plain. Journal of Volcanology and Geothermal Research 211-212, 1–11.

Ewart, A. (1965). Review of mineralogy and chemistry of the acidic volcanic rocks of Taupo Volcanic Zone, New Zealand. IAV International Symposium on Volcanology (New Zealand).

Ewart, A., Hildreth, W. & Carmichael, I.S.E. (1975). Quaternary acid magma in New Zealand. Contributions to Mineralogy and Petrology 51, 1–27.

Fischer, T.P. & Marty, B. (2005). Volatile abundances in the sub-arc mantle: insights from volcanic and hydrothermal gas discharges. Journal of Volcanology and Geothermal Research 140, 205-216.

Fischer, T. (2008). Fluxes of volatiles (H_2O, CO_2, N_2, Cl, F) from arc volcanoes. Geochemical Journal, 42, 21–38.

Folch, A. & Martí, J. (1998). The generation of overpressure in felsic magma chambers by replenishment. Earth and Planetary Science Letters 163, 301–314.

Fridrich, C.J. & Mahood, G.A. (1987). Compositional layers in the zoned magma chamber of the Grizzly Peak Tuff. Geology 15, 299.

Gaetani, G.A. & Watson, E.B. (2000). Open system behavior of olivine-hosted melt inclusions. Earth and Planetary Science Letters 183, 27–41.

Gelman, S.E., Gutierrez, F.J. & Bachmann, O. (2013). On the longevity of large upper crustal silicic magma reservoirs. Geology 41, 759-762.

Geyer, A. & Martí, J. (2008). The new worldwide collapse caldera database (CCDB): A tool for studying and understanding caldera processes. Journal of Volcanology and Geothermal Research 175, 334–354.

Ghiorso MS, Sack RO (1991) Fe-Ti oxide geothermometry: thermodynamic formulation and the estimation of intensive variables in silicic magmas. Contrib to Mineral Petrol 108:485–510.

Ghiorso, M.S. & Evans, B.W. (2008). Thermodynamics of Rhombohedral Oxide Solid Solutions and a Revision of the Fe-Ti Two-Oxide Geothermometer and Oxygen-Barometer. American Journal of Science 308, 957–1039.

Giggenbach, W.F. (1989). Processes cotrolling CO_2- and Cl-contents of thermal discharges from the Taupo-Rotorua volcanic-magmatic hydrothermal system, New Zealand. Proceeding International Symposium Water-Rock Interaction 6, 259-262.

Giggenbach, W.F., Sheppard, D.S., Robinson, B.W., Stewart, M.K. & Lyon, G.L. (1994). Geochemical structure and position of the Waiotapu geothermal field, New Zealand. Geothermics 23, 599-644.

Giggenbach, W. F. (1995). Variations in the chemical and isotopic composition of fluids discharged from the Taupo Volcanic Zone, New Zealand. Journal of Volcanology and Geothermal Research 68, 89–116.

Giggenbach, W.F. (1996). Chemical composition of volcanic gases. In: Scarpa, R., Tilling H.I. (Eds.), Monitoring and Mitigation of Volcano Hazards. Springer, Berlin, 222–256.

Graham I.J & Hackett, W.R. (1987). Petrology of calc-alkaline lavas from Ruapehu volcano and related vents, Taupo volcanic zone, New Zealand. Journal of Petrology 28, 531-657.

Graham, I., Cole, J., Briggs, R., Gamble, J. & Smith, I. (1995). Petrology and petrogenesis of volcanic rocks from the Taupo Volcanic Zone: a review. Journal of Volcanology and Geothermal Research 68, 59–87.

Gravley, D.M., Wilson, C.J.N., Leonard, G.S. & Cole, J.W. (2007). Double trouble: Paired ignimbrite eruptions and collateral subsidence in the Taupo Volcanic Zone, New Zealand. Geological Society of America Bulletin 119, 18–30.

Gravley, D.M. (2004). The Ohakuri pyroclastic deposits and the evolution of the Rotorua- Ohakuri volcanotectonic depression. PhD Thesis, University of Canterbury, Christchurch, New Zealand, 245 pp.

Gravley, D.M., Wilson, C.J.N., Deering, C.D., Leonard, G.S. & Rowland, J.V. (in preparation). Scales of ignimbrite flare-ups and their drivers as exemplified by the central Taupo Volcanic Zone, New Zealand.

Gravley, D.M., Leonard, G.S., Wilson, C.J.N., Rowland, J.V. & Hikuroa, D.C.H. (2009). Build-up to an ignimbrite flare-up: Geologic evidence for magmatic-tectonic-volcanic interplay in the Central Taupo Volcanic Zone, New Zealand. Geological Society of America, Abstracts with Programs 41, 57p.

Gualda, G.A.R., Ghiorso, M.S., Lemons, R.V. & Carley, T.L. (2012a). Rhyolite-MELTS: a Modified Calibration of MELTS Optimized for Silica-rich, Fluid-bearing Magmatic Systems. Journal of Petrology 53, 875–890.

Gualda, G.A.R., Pamukcu, A.S., Ghiorso, M.S., Anderson, A.T., Sutton, S.R. & Rivers, M.L. (2012b). Timescales of quartz crystallization and the longevity of the Bishop giant magma body. PloS one 7, e37492.

Gualda, G.A.R. & Ghiorso, M.S. (Revised). Phase-equilibrium geobarometer for silicic rocks based on rhylite-MELTS. Part 1: Principles, procedures, and evaluation of the method. Contributions to Mineralogy and Petrology.

Gualda, G.A.R. & Ghiorso, M.S. (2013-a). Low pressure origin of high-silica rhyolites and granites. Journal of Geology 121, 537-545.

Gualda, G.A.R. & Ghiorso, M.S. (2013-b). The Bishop Tuff giant magma body: An alternative 1 to the Standard Model. Contributions to Mineralogy and Petrology 166, 755-775.

Harris, A.C., Kamenetsky, V.S, White, N.C., van Achterbergh, E. & Ryan, C.G. (2003). Melt inclusions in veins: linking magmas and porphyry Cu deposits. Science 302, 2109–2111.

Harrison, A. & White, R.S. (2006). Lithospheric structure of an active backarc basin: the Taupo Volcanic Zone, New Zealand. Geophysical Journal International 167, 968–990.

Harrison, A.J. & White, R.S. (2004) Crustal structure of the Taupo Volcanic Zone, New Zealand: Stretching and igneous intrusion. Geophysical Research Letters 31, 2–5.

Hawkesworth, C. & Ellam, R. (1989). Chemical fluxes and wedge replenishment rates along recent destructive plate margins. Geology 17, 46–49.

Hedenquist, J.W. & Lowenstern, J.B. (1994). The role of magmas in the formation of hydrothermal ore deposits. Nature 370, 519–527.

Heinrich, C.A., Driesner, T., Stefansson, A. & Seward, T.M. (2004). Magmatic vapor contraction and the transport of gold from the porphyry environment to epithermal ore deposits. Geology 32, 761–764.

Heise, W., Bibby, H.M., Caldwell, T.G., Bannister, S.C., Ogawa, Y., Takakura, S. & Uchida, T. (2007). Melt distribution beneath a young continental rift: The Taupo Volcanic Zone, New Zealand. Geophysical Research Letters 34, 1–6.

Heise, W., Caldwell, T.G., Bibby, H.M. & Bennie, S.L. (2010). Three-dimensional electrical resistivity image of magma beneath an active continental rift, Taupo Volcanic Zone, New Zealand. Geophysical Research Letters 37, 2–6.

Henley, R. & Ellis, A.J. (1983). Geothermal systems ancient and modern: a geochemical review. Earth-science Review 19, 1–50.

Hervig, R.L., Mazdab, F.K., Moore, G. & McMillan, P.F. (2003). Analyzing hydrogen (H_2O) in silicate glass by secondary ion mass spectrometry and reflectance Fourier transform infrared spectroscopy. In De Vivo, B., and Bodnar, R.J., eds., Melt inclusions in volcanic systems: Methods, applications and problems: Developments in Volcanology 5, 83–103.

Hildreth, W. (1981). Gradients in silicic magma chambers: implications for lithospheric magmatism. Journal of Geophysical Research 86, 10153–10192.

Hildreth, W. & Fierstein, J. (2000). Katmai volcanic cluster and the great eruption of 1912. Geological Society of America Bulletin 112, 1594–1620.

Hildreth, W. (2004). Volcanological perspectives on Long Valley, Mammoth Mountain, and Mono Craters: several contiguous but discrete systems. Journal of Volcanology and Geothermal Research 136, 169–198.

Hildreth, W. & Wilson, C.J.N. (2007). Compositional Zoning of the Bishop Tuff. Journal of Petrology 48, 951–999.

Hilton, D.R., Fischer, T.P. & Marty, B. (2002). Noble Gases and Volatile Recycling at Subduction Zones. Review in Mineralogy Geochemistry, 47, 319–370.

Hochstaedter, A., Gill, J., Peters, R., Broughton, P., Holden, P. & Taylor, B. (2001). Across-arc geochemical trends in the Izu-Bonin arc: Contributions from the subducting slab. Geochemistry, Geophysics, Geosystems, 2.

Hochstein, M. (1995). Crustal heat transfer in the Taupo Volcanic Zone (New Zealand): comparison with other volcanic arcs and explanatory heat source models. Journal of Volcanology and Geothermal Research 68, 117–151.

Holtz, F., Pichavant, M., Barbey, P. & Johannes, W. (1992). Effects of H_2O on liquidus phase relations in the haplogranite system at 2 and 5 kbar. American Mineralogist 77, 1223–1241.

Horton, T.W., Atkinson, L. & Oze, C. (2012). Hydrothermal carbonate geochemistry of the Ngatamariki subsurface reservoir, New Zealand. 37th Workshop Geothermal Reservoir Engineering Stanford University Stanford, California.

Houghton, B.F., Wilson, C.J.N., McWilliams, M.O., Lanphere, M.A., Weaver, S.D Briggs, R.M. & Pringle, M. S. (1995). Chronology and dynamics of a large silicic magmatic system: Central Taupo Volcanic Zone, New Zealand. Geology 23, 13-16.

Huang, R. & Audétat, A. (2012). The titanium-in-quartz (TitaniQ) thermobarometer: A critical examination and re-calibration. Geochimica et Cosmochimica Acta 84, 75–89.

Huber, C., Bachmann, O. & Manga, M. (2010). Two Competing Effects of Volatiles on Heat Transfer in Crystal-rich Magmas: Thermal Insulation vs Defrosting. Journal of Petrology 51, 847–867.

Huber, C., Bachmann, O., Vigneresse, J.L., Dufek, J. & Parmigiani, A. (2012). A physical model for metal extraction and transport in shallow magmatic systems. Geochemistry Geophysics Geosystems 13.

Ishikawa, T. & Nakamura, E. (1994). Origin of the slab component in arc lavas from across-arc variation of B and Pb isotopes. Nature, 370.

Ishikawa, T. & Tera, F. (1997). Source, composition and distribution of the fluid in the Kurile mantle wedge : Constraints from across-arc variations of Br, Nb and B isotopes. Earth and Planetary Science Letters 152, 123-138.

Ishikawa, T., Tera, F. & Nakazawa, T. (2001). Boron isotope and trace element systematics of the three volcanic zones in the Kamchatka arc. Geochimica et Cosmochimica Acta 65 (24), 4523-4537.

Jackson, M.D., Cheadle, M.J. & Atherton, M.P (2003). Quantitative modeling of granitic melt generation and segregation in the continental crust. Journal of Geophysical Research, 108.

Jarosewich, E., Nelen, J.A. & Norberg, J.A. (1980). Reference Samples for Electron Microprobe Analysis. Geostandards Newsletter 4, 43–47.

Jenner, G.A., Cawood, P.A., Rautenschlein, M. & White, W.M. (1987). Composition of back-arc basin volcanics, Valu Fa Ridge, Lau Basin: Evidence for a slab-derived component in their mantle source. Journal of Volcanology and Geothermal Research 32, 209–222.

Johnson, E.R., Kamenetsky, V.S., McPhie, J. & Wallace, P.J. (2011). Degassing of the H_2O-rich rhyolites of the Okataina Volcanic Center, Taupo Volcanic Zone, New Zealand. Geology 39, 311–314.

Johnson, E.R., Wallace, P.J., Cashman, K.V. & Delgado Granados, H. (2010). Degassing of volatiles (H_2O, CO_2, S, Cl) during ascent, crystallization, and eruption at mafic monogenetic volcanoes in central Mexico. Journal of Volcanology and Geothermal Research 197, 225–238.

Johnson, E.R., Kamenetsky, V.S. & McPhie, J. (2013). The Behavior of Metals (Pb, Zn, As, Mo, Cu) During Crystallization and Degassing of Rhyolites from the Okataina Volcanic Center, Taupo Volcanic Zone, New Zealand. Journal of Petrology 54, 1641–1659.

Karhunen, R.A. (1993). The Pokai and Chimp Ignimbrites of NW Taupo Volcanic Zone. Ph.D. Thesis, University of Canterbury, Christchurch, New Zealand, 356 pp.

Kay, R. (1980). Volcanic arc magmas: Implications of a melting-mixing model for element recycling in the crust-upper mantle system. The Journal of Geology 88, 497–522.

Kennedy, B.M. & Stix, J. (2007). Magmatic processes associated with caldera collapse at Ossipee ring dyke, New Hampshire. Geological Society of America Bulletin 119, 3–17.

Kennedy, B.M., Jellinek M.A. & Stix, J. (2008). Coupled caldera subsidence and stirring inferred from analogue models. Nature Geoscience 1, 385–389.

Kennedy B, Wilcock J, Stix J (2012) Caldera resurgence during magma replenishment and rejuvenation at Valles and Lake City calderas. Bull Volcanol 74:1833–1847.

Kilgour, G., Blundy, J., Cashman, K. & Mader, H.M. (2013). Small volume andesite magmas and melt–mush interactions at Ruapehu, New Zealand: evidence from melt inclusions. Contributions to Mineralogy and Petrology 166, 371–392.

Lahitte, P., Gillot, P. & Courtillot, V. (2003). Silicic central volcanoes as precursors to rift propagation: The Afar case. Earth and Planetary Science Letters 207, 103–116.

Landtwing, M.R. & Pettke, T. (2005). Relationships between SEM-cathodoluminescence response and trace-element composition of hydrothermal vein quartz. American Mineralogist 90, 122–131.

Lara, L.E., Naranjo, J.A. & Moreno, H. (2004). Rhyodacitic fissure eruption in Southern Andes (Cordón Caulle; 40.5°S) after the 1960 (Mw:9.5) Chilean earthquake: a structural interpretation. Journal of Volcanology and Geothermal Research 138, 127–138.

Leonard, G.S., Cole, J.W., Nairn, I.A. & Self, S. (2002). Basalt triggering of the c. AD 1305 Kaharoa rhyolite eruption, Tarawera Volcanic Complex, New Zealand. Journal of Volcanology and Geothermal Research 115, 461–486.

Leonard, G.S., Begg, J.G. & Wilson, C.J.N. (compilers) (2010). Geology of the Rotorua area. Institute of Geological & Nuclear Sciences 1:250,000 geological map 5. 102 p. + 1 folded map. Lower Hutt.

Lewis, B., Chambefort, I., Rae A., Bignall, G., & Ganefianto, N. (in review). Ngatamariki: the Porphyry-Epithermal Transition in the Taupo Volcanic Zone, New Zealand. Economic Geology.

Lindgren, W. (1907). The relation of ore-deposition to physical conditions. Economic Geology, 2, 105–127.

Lindsay, J., Schmitt, A.K., Trumbull, R.B., de Silva, S.L., Siebel, W. & Emmermann, R. (2001). Magmatic evolution of the La Pacana caldera system, Central Andes, Chile: Compositional variation of two cogenetic, large-volume felsic ignimbrites. Journal of Petrology 42, 459–486.

Lipman, P.W. (1967) Mineral and chemical variations within an ash-flow sheet from Aso caldera, South Western Japan. Contributions to Mineralogy and Petrology 16, 300-327.

Lipman, P.W. (2007). Incremental assembly and prolonged consolidation of Cordilleran magma chambers: Evidence from the Southern Rocky Mountain volcanic field. Geosphere 3, 1-29.

Liu, Y., Anderson, A.T., Wilson, C.J.N., Davis, A.M. & Steele, I.M. (2006). Mixing and differentiation in the Oruanui rhyolitic magma, Taupo, New Zealand: evidence from volatiles and trace elements in melt inclusions. Contributions to Mineralogy and Petrology 151, 71–87.

London, D., Hervig, R.L. & Morgan, G.B. (1988). Melt-vapor solubilities and elemental partitioning in peraluminous granite-pegmatite systems: experimental results with Macusani glass at 200 MPa. Contributions to Mineralogy and Petrology 99, 360–373.

London, D. & Morgan, G.B. (2012). The Pegmatite Puzzle. Elements 8, 263–268

Lowenstern, J.B., Mahood, G.A., Rivers, M.L. & Sutton, S.R. (1991). Evidence for extreme partitioning of copper into a magmatic vapor phase. Science 252, 1405-1409.

Lowenstern, J.B. (1994). Chlorine, fluid immiscibility, and degassing in peralkaline magmas from Pantelleria, Italy. American Mineralogy 79, 353–369.

Lowenstern, J.B. (1993). Evidence for a copper-bearing fluid in magma erupted at the Valley of ten thousand smokes, Alaska. Contributions to Mineralogy and Petrology 114, 409–421.

Lowenstern, J.B. (1994). Dissolved volatile concentrations in an ore-forming magma. Geology 22, 893–896.

Lowenstern, J.B. (2001). Carbon dioxide in magmas and implications for hydrothermal systems. Mineralium Deposita 36, 490–502.

Lowenstern, J. & Hurwitz, S. (2008). Monitoring a supervolcano in repose: Heat and volatile flux at the Yellowstone Caldera. Elements 4, 35–40.

Manga, M. & Brodsky, E. (2006). Seismic triggering of eruptions in the far field: Volcanoes and Geysers. Annual Review of Earth and Planetary Sciences 34, 263–291.

Matthews, N.E., Pyle, D.M., Smith, V.C., Wilson, C.J.N., Huber, C., Hinsberg, V. (2011). Quartz zoning and the pre-eruptive evolution of the ~340 ka Whakamaru magma systems, New Zealand. Contributions to Mineralogy and Petrology 163, 87–107.

McCulloch, M.T. & Gamble, J.A. (1991). Geochemical and geodynamical constraints on subduction zone magmatism. Earth and Planetary Science Letters 102, 358–374.

McCulloch, M.T., Kyser, T.K., Woodhead, J.D. & Kinsley, L. (1994). Pb-Sr-Nd-O isotopic constraints on the origin of rhyolites from the Taupo Volcanic Zone of New Zealand: evidence for assimilation followed by fractionation from basalt. Contributions to Mineralogy and Petrology 115, 303–312.

McMillan, P.F. & Holloway, J.R. (1987). Water solubility in aluminosilicate melts. Contributions to Mineralogy and Petrology 97, 320–332.

Métrich, N. & Rutherford, M.J. (1992). Experimental study of chlorine behavior in hydrous silicic melts. Geochimica et Cosmochimica Acta 56, 607–616.

Métrich, N. & Wallace, P.J. (2008). Volatile Abundances in Basaltic Magmas and Their Degassing Paths Tracked by Melt Inclusions. Reviews in Mineralogy and Geochemistry 69, 363–402.

Miller, C.F., Furbish, D.J., Walker, B.A., Claiborne, L.L., Koteas, G.C., Bleick, H.A. & Miller, J.S. (2011). Growth of plutons by incremental emplacement of sheets in crystal-rich host: Evidence from Miocene intrusions of the Colorado River region, Nevada, USA. Tectonophysics 500, 65–77.

Milner, D.M., Cole, J.W. & Wood, C.P. (2002). Asymmetric, multiple-block collapse at Rotorua Caldera, Taupo Volcanic Zone, New Zealand. Bulletin of Volcanology 64, 134–149.

Milner, D.M. (2001). The structure and eruptive history of Rotorua caldera, Taupo Volcanic Zone, New Zealand. Ph.D. Thesis, University of Canterbury, Christchurch, New Zealand, 434 pp.

Milner, D., Cole, J. & Wood, C. (2003). Mamaku Ignimbrite: a caldera-forming ignimbrite erupted from a compositionally zoned magma chamber in Taupo Volcanic Zone, New Zealand. Journal of Volcanology and Geothermal Research 122, 243–264.

Miura, D. (1999) Arcuate pyroclastic conduits, ring faults, and coherent floor at Kumano caldera, southwest Honshu, Japan. Journal of Volcanology and Geothermal Research 92, 271–294.

Morgan, G.B. & London, D. (1996). Optimizing the electron microprobe analysis of hydrous alkali aluminosilicate glasses. American Mineralogist 81, 1176–1185.

Mortimer, N. (2004). New Zealand's Geological Foundations. Gondwana Research, 7, 261-272.

Nakagawa, M., Wada, K., Thordarson, T., Wood, C.P. & Gamble, J.A. (1999). Petrologic investigations of the 1995 and 1996 eruptions of Ruapehu volcano, New Zealand: formation of discrete and small magma pockets and their intermittent discharge. Bulletin of Volcanology 61, 15–31.

Nakagawa, M., Wada, K. & Wood, C.P. (2002). Mixed Magmas, Mush Chambers and Eruption Triggers: Evidence from Zoned Clinopyroxene Phenocrysts in Andesitic Scoria from the 1995 Eruptions of Ruapehu Volcano, New Zealand. Journal of Petrology 43, 2279–2303.

Naruo, H. & Kobayashi, T. (2002). Two large-scale earthquakes triggered by a 6.5ka BP eruption from Kikai caldera, southern Kyushu, Japan. Quaternary Research Japan 41, 287-299.

Nairn, I.A. (2002). Geology of the Okataina Volcanic Centre. Institute of Geological and Nuclear Sciences Geological Map 25, 156p+map.

Nairn, I.A., Shane, P.R., Cole, J.W., Leonard, G.J., Self, S. & Pearson, N. (2004). Rhyolite magma processes of the AD 1315 Kaharoa eruption episode, Tarawera volcano, New Zealand. Journal of Volcanology and Geothermal Research 131, 265–294.

Newman, S. & Lowenstern, J.B. (2002). VolatileCalc: a silicate melt–H_2O–CO_2 solution model written in Visual Basic for excel. Computers & Geosciences 28, 597–604.

Nicholls, I.A., Oba, T. & Conrad, W.K. (1992). The nature of primary rhyolitic magmas involved in crustal evolution: Evidence from an experimental study of cummingtonite-bearing rhyolites, Taupo Volcanic Zone, New Zealand. Geochimica et Cosmochimica Acta 56, 955–962.

Norton, D. & Knight, J. (1977). Transport phenomena in hydrothermal systems: cooling plutons. American Journal of Science 277, 937–981.

Ogawa, Y., Bibby, H.M., Caldwell, T.G., Takakura, S., Matsushima, N., Bennie, S.L., Tosha, T. & Nishi, Y. (1999). Wide-band magnetotelluric measurements across the Taupo volcanic zone: Preliminary results, Geophysical Research Letters 26, 3673–3676.

Pallister, J., Hoblitt, R. & Reyes, A. (1992). A basalt trigger for the 1991 eruptions of Pinatubo volcano? Nature 356, 426–428.

Pamukcu, A.S., Gualda, G.A.R. & Anderson, A.T. (2012). Crystallization Stages of the Bishop Tuff Magma Body Recorded in Crystal Textures in Pumice Clasts. Journal of Petrology 53, 589–609.

Papale, P., Moretti, R. & Barbato, D. (2006). The compositional dependence of the saturation surface of H2O+CO2 fluids in silicate melts. Chemical Geology 229, 78–95.

Pearce, J.A. & Peate, D. (1995). Tectonic implications of the composition of volcanic arc magmas. Annual Review of Earth and Planetary Sciences 23, 251–285.

Pearce, J.A. & Stern, R.J. (2006). The origin of back-arc basin magmas: trace element and isotope perspectives. AGU Geophysical Monograph Series 166, 63–86.

Peppard, B.T., Steele, I.M., Davis, A.M., Wallace, P.J. & Anderson, A.T. (2001). Zoned quartz phenocrysts from the rhyolitic Bishop Tuff. American Mineralogist 86, 1034–1052.

Price, R.C., Gamble, J.A., Smith, I.E.M., Stewart, R.B., Eggins, S. & Wright, I.C. (2005). An integrated model for the temporal evolution of andesites and rhyolites and crustal development in New Zealand's North Island. Journal of Volcanology and Geothermal Research 140, 1–24.

Price, R.C., Gamble, J.A., Smith, I.E.M., Maas,R., Waight, T., Stewart, R.B. & Woodhead, J. (2012). The Anatomy of an Andesite Volcano: a Time-Stratigraphic Study of Andesite Petrogenesis and Crustal Evolution at Ruapehu Volcano, New Zealand. Journal of Petrology 53, 2139-2189.

Pardo Villaveces, N. (2012). Andesitic Plinian Eruptions at Mt. Ruapehu (New Zealand): From Lithofacies to Eruption Dynamics. PhD Thesis, Massey University, Palmerston North, 296 pp.

Reubi, O. & Nicholls, I.A. (2005). Structure and Dynamics of a Silicic Magmatic System Associated with Caldera-Forming Eruptions at Batur Volcanic Field, Bali, Indonesia. Journal of Petrology 46, 1367–1391.

Reubi, O., Blundy, J. & Varley, N.R. (2013). Volatiles contents, degassing and crystallisation of intermediate magmas at Volcan de Colima, Mexico, inferred from melt inclusions. Contributions to Mineralogy and Petrology 165, 1087–1106.

REGEMP II Regional Geothermal Geochemistry Monitoring Programme (2013) Interpretation of geochemical data. Waikato Regional Council, Report: TR 2013/30; Author: Golder Associates.

Reyes, A.G. & Trompetter, W.J. (2012). Hydrothermal water–rock interaction and the redistribution of Li, B and Cl in the Taupo Volcanic Zone, New Zealand. Chemical Geology 314-317, 96–112.

Reyners, M., Eberhart-Phillips, D., Stuart, G. & Nishimura, Y. (2006). Imaging subduction from the trench to 300 km depth beneath the central North Island, New Zealand, with Vp and Vp/Vs. Geophysical Journal International 165, 565–583.

Ridolfi, F., Renzulli, A. & Puerini, M. (2010). Stability and chemical equilibrium of amphibole in calc-alkaline magmas: an overview, new thermobarometric formulations and application to subduction-related volcanoes. Contributions to Mineralogy and Petrology 160, 45–66.

Roedder, E. (1984). Fluid Inclusions. Mineralogical Society of America, Reviews in Mineralogy 12, 644 pp.

Rogan, M. (1982). A geophysical study of the Taupo Volcanic Zon New Zealand. Journal of Geophysical Research 87, 4073–4088.

Rooney, T.O. & Deering, C.D. (2014). Conditions of melt generation beneath the Taupo Volcanic Zone: The influence of heterogeneous mantle inputs on large-volume silicic systems. Geology 42, 3–6.

Rosner, M., Erzinger, J., Franz, G. & Trumbull, R.B. (2003). Slab-derived boron isotope signatures in arc volcanic rocks from the Central Andes and evidence for boron isotope fractionation during progressive slab dehydration. Geochemistry Geophysics Geosystems 4.

Rowland, J.V. & Sibson, R.H. (2001). Extensional fault kinematics within the Taupo Volcanic Zone, New Zealand: soft-linked segmentation of a continental rift system. New Zealand Journal of Geology and Geophysics 44, 271–284.

Rowland, J.V. & Sibson, R.H. (2004). Structural controls on hydrothermal flow in a segmented rift system, Taupo Volcanic Zone, New Zealand. Geofluids 4, 259–283.

Rowland, J.V., Wilson, C.J.N. & Gravley, D.M. (2010). Spatial and temporal variations in magma-assisted rifting, Taupo Volcanic Zone, New Zealand. Journal of Volcanology and Geothermal Research 190, 89–108.

Rowland, J.V. & Simmons, S.F. (2012). Hydrologic, Magmatic, and Tectonic Controls on Hydrothermal Flow, Taupo Volcanic Zone, New Zealand: Implications for the Formation of Epithermal Vein Deposits. Economic Geology 107, 427–457.

Schatz, O.J., Dolejs, D., Stix, J., Williams-Jones, A.E. & Layne, G.D. (2004). Partitioning of boron among melt, brine and vapor in the system haplogranite-H_2O-NaCl at 800 °C and 100 MPa. Chemical Geology, 210(1-4), 135-147.

Schiano, P. & Bourdon, B. (1999). On the preservation of mantle information in ultramafic nodules: glass inclusions within minerals versus interstitial glasses. Earth and Planetary Science Letters 169, 173–188.

Schmitz, M.D. & Smith, I.E.M. (2004). The Petrology of the Rotoiti Eruption Sequence, Taupo Volcanic Zone: an Example of Fractionation and Mixing in a Rhyolitic System. Journal of Petrology 45, 2045–2066.

Seebeck, H., Nicol, A., Stern, T.A., Bibby, H.M. & Stagpoole, V. (2010). Fault controls on the geometry and location of the Okataina Caldera, Taupo Volcanic Zone, New Zealand. Journal of Volcanology and Geothermal Research 190, 136–151.

Seedorff, E., Dilles, J., Proffet, J., Einaudi, M., Zurcher, L., Stavast, W., Johnson, D. & Barton, M. (2005), Porphyry deposits: Characteristics and origin of hypogene features, Economic Geology 100th Anniversary Volume, 251-298.

Severs, M.J., Azbej, T., Thomas, J.B., Mandeville, C.W. & Bodnar, R.J. (2007). Experimental determination of H_2O loss from melt inclusions during laboratory heating: Evidence from Raman spectroscopy. Chemical Geology 237, 358–371.

Shane, P., Martin, S.B., Smith, V.C., Beggs, K.F., Darragh, M.B., Cole, J.W. & Nairn, I.A. (2007). Multiple rhyolite magmas and basalt injection in the 17.7 ka Rerewhakaaitu eruption episode from Tarawera volcanic complex, New Zealand. Journal of Volcanology and Geothermal Research 164, 1–26.

Shane, P., Nairn, I.A., Smith, V.C., Darragh, M., Beggs, K. & Cole, J.W. (2008-a). Silicic recharge of multiple rhyolite magmas by basaltic intrusion during the 22.6 ka Okareka 10 chambers. Bulletin of Volcanology 29, 83–103.

Shane, P., Smith, V.C. & Nairn, I.A. (2008-b). Millennial timescale resolution of rhyolite magma recharge at Tarawera volcano: insights from quartz chemistry and melt inclusions. Contributions to Mineralogy and Petrology 156, 397–411.

Shane, P., Storm, S., Schmitt, A. & Lindsay, J. (2012). Timing and conditions of formation of granitoid clasts erupted in recent pyroclastic deposits from Tarawera Volcano (New Zealand). Lithos 140-141, 1–10.

Shane, P. & Smith, V.C. (2013). Using amphibole crystals to reconstruct magma storage temperatures and pressures for the post-caldera collapse volcanism at Okataina volcano. Lithos 156-159, 159–170.

Shinohara, H. (1994). Exsolution of immiscible vapor and liquid phases from a crystallizing silicate melt: Implications for chlorine and metal transport. Geochimica et Cosmochimica Acta 58, 5215–5221.

Shinohara, H. (2013). Volatile flux from subduction zone volcanoes: Insights from a detailed evaluation of the fluxes from volcanoes in Japan. Journal of Volcanology and Geothermal Research 268, 46–63.

Signorelli, S. & Carroll, M.R. (2000). Solubility and fluid-melt partitioning of Cl in hydrous phonolitic melts. Geochimica et Cosmochimica Acta 64, 2851–2862.

Sillitoe, R.H. & Hedenquist, J.W. (2003). Linkages between Volcanotectonic Settings , Ore-Fluid Compositions , and Epithermal Precious Metal Deposits. Special Publication-Society of Economic Geologists 10, 315–343.

Sillitoe, R., (2010). Porphyry Copper Systems, Economic Geology 105, 3-41.

Simmons, S.F., Stewart, M.K., Robinson, B.W. & Glover, R.B. (1994). The chemical and isotopic compositions of thermal waters at Waimangu, New Zealand. Geothermics 23, 539–553.

Simmons, S.F., White, N.C. & John, D.A. (2005). Geologic characteristics of epithermal precious and base metal deposits. Economic Geology 100th Anniversary Volume, 485-522.

Simmons, S.F. & Brown, K.L. (2007). The flux of gold and related metals through a volcanic arc, Taupo Volcanic Zone, New Zealand. Geology 35, 1099.

Smith, V., Shane, P. & Nairn, I. (2010). Insights into silicic melt generation using plagioclase, quartz and melt inclusions from the caldera-forming Rotoiti eruption, Taupo volcanic zone, New Zealand. Contributions to Mineralogy and Petrology 160, 951–971.

Smith, V.C., Shane, P. & Smith, I. (2002). Tephrostratigraphy and geochemical fingerprinting of the Mangaone Subgroup tephra beds, Okataina Volcanic Centre, New Zealand. New Zealand Journal of Geology and Geophysics 45, 207–220.

Smith, V.C., Shane, P. & Nairn, I.A. (2004). Reactivation of a rhyolitic magma body by new rhyolitic intrusion before the 15.8 ka Rotorua eruptive episode: implications for magma storage in the Okataina Volcanic Centre, New Zealand. Journal of the Geological Society 161, 757–772.

Smith, V.C., Shane, P. & Nairn, I.A. (2005). Trends in rhyolite geochemistry, mineralogy, and magma storage during the last 50 kyr at Okataina and Taupo volcanic centres, Taupo Volcanic Zone, New Zealand. Journal of Volcanology and Geothermal Research 148, 372 – 406.

Smith, H.J., Spivack, A.J., Staudigel, H. & Hart, S.R. (1995). The boron isotopic composition of altered oceanic crust. Chemical Geology 126(2), 119–135.

Sparks, S.R.J., Sigurdsson, H. & Wilson, L. (1977). Magma mixing: a mechanism for triggering acid explosive eruptions. Nature 267, 315–318.

Spinks, K.D., Acocella, V., Cole, J.W. & Bassett, K.N. (2005). Structural control of volcanism and caldera development in the transtensional Taupo Volcanic Zone, New Zealand. Journal of Volcanololy and Geothermal Research 144, 7–22.

Steele-Macinnis, M., Esposito, R. & Bodnar, R.J. (2011). Thermodynamic Model for the Effect of Post-entrapment Crystallization on the H_2O-CO_2 Systematics of Vapor-saturated, Silicate Melt Inclusions. Journal of Petrology 52, 2461–2482.

Stern, A.T. (1987). Asymmetric back-arc spreading, heat flux and structure associated with the central volcanic region of New Zealand. Earth and Planetary Science Letters 85, 265–276.

Stolper E. (1982). Water in silicate glasses: An infrared spectroscopic study. Contributions to Mineralogy and Petrology 81, 1–17.

Storm, S., Shane, P., Schmitt, A.K. & Lindsay, J.M. (2011). Contrasting punctuated zircon growth in two syn-erupted rhyolite magmas from Tarawera volcano: Insights to crystal diversity in magmatic systems. Earth and Planetary Science Letters 301, 511–520.

Stratford, W.R. & Stern, T.A. (2006). Crust and upper mantle structure of a continental backarc: central North Island, New Zealand. Geophysical Journal International 166, 469–484.

Student, J. & Bodnar, R.J. (1999). Synthetic Fluid Inclusions XIV : Coexisting Silicate Melt and Aqueous Fluid Inclusions in the Haplogranite–H_2O–NaCl–KCl System. Journal of Petrology 40, 1509–1525.

Sutton, A.N., Blake, S. & Wilson, C.J.N. (1995). An outline geochemistry of rhyolite eruptives from Taupo volcanic centre, New Zealand. Journal of Volcanology and Geothermal Research 68, 153–175.

Symonds, R.B., Rose, W.I., Bluth, G.J.S. & Gerlach, T.M. (1994). Volcanic-gas studies: methods, results, and applications. Mineralogical Society of America, Reviews in Mineralogy 30, 1–66.

Taran, Y.A., Rozhkov, A.M., Serafimova, E.K. & Esikov, A.D. (1991). Chemical and isotopic composition of magmatic gases from the 1988 eruption of Klyuchevskoy volcano, Kamchatka. Journal of Volcanology and Geothermal Research 46, 255–263.

Thomas, J.B., Watson, E.B., Spear, F.S., Shemella, F.S., Nayak, S.K. & Lanzirotti, A. (2010). TitaniQ under pressure: the effect of pressure and temperature on the solubility of Ti in quartz. Contributions to Mineralogy and Petrology 160, 743–759.

Tosdal, R.M., Dilles, J.H. & Cooke, D.R. (2009). From Source to Sinks in Auriferous Magmatic-Hydrothermal Porphyry and Epithermal Deposits. Elements 5, 289–295.

Tuttle, O.F. & Bowen, N.L. (1958). Origin of Granite, in the Light of Experimental Studies in the System $NaAlSi_3O_8$-$KAlSi_3O_8$-SiO_2-H_2O. Geological Society of America, Memoirs 74,153 pp.

Villamor, P. & Berryman, K. (2001). A late Quaternary extension rate in the Taupo Volcanic Zone, New Zealand, derived from fault slip data. New Zealand Journal of Geology and Geophysics 44, 243–270.

Villamor, P. & Berryman, K. (2006). Late Quaternary geometry and kinematics of faults at the southern termination of the Taupo Volcanic Zone, New Zealand. New Zealand Journal of Geology and Geophysics 49, 1–21.

Wallace, P.J. (2005). Volatiles in subduction zone magmas: concentrations and fluxes based on melt inclusion and volcanic gas data. Journal of Volcanology and Geothermal Research 140, 217–240.

Wallace, P.J. & Gerlach, T.M. (1994). Magmatic vapor source for sulfur dioxide released during volcanic eruptions: evidence from Mount Pinatubo. Science 265, 497–9.

Wallace, P.J., Anderson, A.T. & Davis, A.M. (1995). Quantification of pre-eruptive exsolved gas contents in silicic magmas. Nature 377, 612–616.

Wallace, L.M., McCaffrey, R. & Desmond, D. (2004). Subduction zone coupling and tectonic block rotations in the North Island, New Zealand. Journal of Geophysical Research 109, 1–21.

Walter, T.R. & Amelung, F. (2007). Volcanic eruptions following $M \geq 9$ megathrust earthquakes: Implications for the Sumatra-Andaman volcanoes. Geology 35, 539.

Wardell, L.J., Kyle, P.R., Dunbar, N. & Christenson, B. (2001). White Island volcano, New Zealand: carbon dioxide and sulfur dioxide emission rates and melt inclusion studies. Chemical Geology, 177(1-2), 187-200.

Wark, D.A., Hildreth, W., Spear, F.S., Cherniak, D.J. & Watson, E.B. (2007). Pre-eruption recharge of the Bishop magma system. Geology 35, 235.

Wark, D.A. & Watson, E.B. (2006). TitaniQ: a titanium-in-quartz geothermometer. Contributions to Mineralogy and Petrology 152, 743–754.

Wark, D.A., & Spear, F.S. (2005). Ti in quartz: Cathodoluminescence and thermometry: Geochimica et Cosmochimica Acta 69, supplement, A592.

Webster, J.D. (1992). Water solubility and chlorine partitioning in Cl-rich granitic systems: effects of melt composition at 2 kbar and 800°C. Geochimica et Cosmochimica Acta 56, 679–687.

Webster, J.D. (1997). Chloride Solubility in Felsic Melts and the Role of Chloride in Magmatic Degassing. Journal of Petrology 38, 1793–1807.

Webster, J.D. (2004). The exsolution of magmatic hydrosaline chloride liquids. Chemical Geology 210, 33–48.

Webster, J.D. & Holloway, J.R. (1988). Experimental constraints on the partitioning of Cl between topaz rhyolite melt and H_20 and H_2O+CO_2 fluids : New implications for granitic differentiation and ore deposition. Geochimica et Cosmochimica Acta 52, 2091–2105.

Werner, C. & Cardellini, C. (2006). Comparison of carbon dioxide emissions with fluid upflow, chemistry, and geologic structures at the Rotorua geothermal system, New Zealand. Geothermics 35, 221–238.

White, S.M., Crisp, J.A. & Spera, F.J. (2006). Long-term volumetric eruption rates and magma budgets. Geochemistry Geophysics Geosystems 7, 968-990.

Wiebe, R.A., Wark, D.A. & Hawkins, D.P. (2007). Insights from quartz cathodoluminescence zoning into crystallization of the Vinalhaven granite, coastal Maine. Contributions to Mineralogy and Petrology 154, 439–453.

Wilcock, J., Goff, F., Minarik, W.G. & Stix, J. (2012). Magmatic Recharge during the Formation and Resurgence of the Valles Caldera, New Mexico, USA: Evidence from Quartz Compositional Zoning and Geothermometry. Journal of Petrology 54, 635–664.

Williams-Jones, A.E. & Heinrich, C.A. (2005). Vapor transport of metals and the formation of magmatic-hydrothermal ore deposits. Economic Geology 100, 1287-1312.

Wilson, C.J.N., Rogan, A.M., Smith, I.E.M., Northey, D.J., Nairn, I.A. & Houghton, B.F. (1984). Caldera Volcanoes of the Taupo Volcanic Zone, New Zealand. Journal of Geophysical Research 89, 8463–8484.

Wilson, C.J.N., Houghton, B.F., Mcwilliams, M.O., Lanphere, M.A., Weaver, S.D. & Briggs, R.M. (1995). Volcanic and structural evolution of Taupo Volcanic Zone, New Zealand: a review. Journal of Volcanology and Geothermal Research 68, 1–28.

Wilson, C.J.N., Blake, S., Charlier, B.L.A. & Sutton, A. (2006). The 26.5 ka Oruanui Eruption, Taupo Volcano, New Zealand: Development, Characteristics and Evacuation of a Large Rhyolitic Magma Body. Journal of Petrology 47, 35–69.

Wilson, C.J.N., Rhoades, D.A., Lanphere, M.A., Calvert, A.T., Houghton, B.F., Weaver, S.D. & Cole, J.W. (2007). A multiple-approach radiometric age estimate for the Rotoiti and Earthquake Flat eruptions, New Zealand, with implications for the MIS 4/3 boundary. Quaternary Science Review 26, 1861–1870.

Wilson, C.J.N. & Charlier, B.L.A. (2009). Rapid Rates of Magma Generation at Contemporaneous Magma Systems, Taupo Volcano, New Zealand: Insights from U-Th Model-age Spectra in Zircons. Journal of Petrology 50, 875–907.

Wilson, C.J.N., Gravley, D.M., Leonard, G.S. & Rowland, J.V. (2009). Volcanism in the central Taupo Volcanic Zone, New Zealand: tempo styles and controls. In: Thordarson, T., Larsen, G., Rowland, S. K., Self, S. & Hoskuldsson (eds.), Studies in Volcanology: The Legacy of George Walker, Special publications of IAVCEI 2, 225–247. Geological Society, London.

Wilson, C.J.N. (2001). The 26.5ka Oruanui eruption, New Zealand: an introduction and overview. Journal of Volcanology and Geothermal Research 112, 133–174.

Wilson, C.J.N. (1996). Taupo's atypical arc. Nature 379, 27–28.

Witter, J.B. & Kuehner, S.M. (2004). A simple empirical method for high-quality electron microprobe analysis of fluorine at trace level in Fe-bearing minerals and glasses. American Mineralogist 89, 57–63.

Wunder, B., Meixner, A., Romer, R.L., Wirth, R. & Heinrich, W. (2005). The geochemical cycle of boron: Constraints from boron isotope partitioning experiments between mica and fluid. Lithos, 84(3-4), 206-216

Wysoczanski, R. & Tani, K. (2006). Spectroscopic FTIR imaging of water species in silicic volcanic glasses and melt inclusions: An example from the Izu-Bonin arc. Journal of Volcanology and Geothermal Research 156, 302–314.

Zajacz, Z., Halter, W.E., Pettke, T. & Guillong, M. (2008). Determination of fluid/melt partition coefficients by LA-ICPMS analysis of co-existing fluid and silicate melt inclusions: Controls on element partitioning. Geochimica et Cosmochimica Acta 72, 2169–2197.

Zajacz, Z., Hanley, J.J., Heinrich, C.A., Halter, W.E. & Guillong, M. (2009). Diffusive reequilibration of quartz-hosted silicate melt and fluid inclusions: Are all metal concentrations unmodified? Geochimica et Cosmochimica Acta 73, 3013–3027.

Zajacz, Z., Candela, P.A., Piccoli, P.M. & Sanchez-Valle, C. (2012). The partitioning of sulfur and chlorine between andesite melts and magmatic volatiles and the exchange coefficients of major cations. Geochimica et Cosmochimica Acta 89, 81–101.

Zhang, Y., Belcher, R., Ihinger, P.D., Wang, L., Xu, Z. & Newman, S. (1997). New calibration of infrared measurement of dissolved water in rhyolitic glasses. Geochimica et Cosmochimica Acta 61, 3089–3100.

Zelenski, M. & Taran, Y. (2011). Geochemistry of volcanic and hydrothermal gases of Mutnovsky volcano, Kamchatka: evidence for mantle, slab and atmosphere contributions to fluids of a typical arc volcano. Bulletin of Volcanology 73, 373–394.